

## ABSTRACT

HOLLINGSWORTH, BRANDON DAVIS. Evaluating *Aedes*-vectored Disease Control: Risks and New Approaches. (Under the direction of Drs. Alun L. Lloyd and Michael H. Reiskind).

*Aedes*-vectored diseases are some of the most widespread and fastest growing infectious diseases worldwide. Many of the mosquito control measures originally used to drive *Aedes aegypti* to near extinction in the Americas, e.g. mass spraying of DDT, are no longer viable, and there is debate about the effectiveness of ultra-low volume (ULV) spraying for reducing *Aedes* populations and their associated disease risks. The recent reemergence of dengue and outbreaks of Zika and chikungunya have resulted in renewed interest in controlling both *Aedes (Stegomyia) aegypti* (Say) and *Aedes (Stegomyia) albopictus* (Skuse). In response to this, there have been numerous technologies and strategies proposed to target *Aedes* mosquitoes, but many of the strategies are not tested and, even for well-studied strategies, the dynamics during and following treatments are not fully understood. Mathematical models have proven to be an important tool for providing insights about *Aedes* population and *Aedes*-vectored disease dynamics, particularly in the absence of experimental data. In this dissertation, I used a combination of mathematical models, field experiments, and statistical analysis to elucidate the population and disease dynamics associated with the control of *Aedes* mosquitoes.

Using mathematical models, I examined transmission dynamics following the cessation of control programs in various disease systems. These simulations showed that use of non-immunizing controls against endemic diseases, e.g. vector control against dengue, could result in increases in incidence over some time periods, a phenomenon I termed the divorce effect. In these situations, I found that using a non-immunizing control, even for a relatively short period, resulted in a reduction in herd immunity. Once control ended, reemergence of the disease resulted in large outbreaks that negated any benefit obtained during the period in which the

disease was suppressed. This is an important result for dengue control, which relies heavily on vector reduction, as the growing prevalence of insecticide resistance could render many control programs obsolete.

A field experiment I conducted in 2018, examined the population dynamics following the use of spraying and larval habitat management (LHM) in individual yards, and to quantify their effectiveness. Pairs of houses were monitored every 4 days over a 33-day period, with one yard in the pair receiving a single application of the assigned treatment. Individual houses treated using barrier sprays had significantly reduced mosquito population for the entire post-control period. LHM did not result in a significant reduction in the population density over the entire period but resulted in significant reduction after 21 days.

Data from the field experiment were then used to parameterize a model for barrier sprays and LHM applied to individual yards within a neighborhood. Parameter estimation provided an estimate of the average lifespan of *Ae. albopictus*, percentage increase in adult mortality due to barrier sprays, half-life of the barrier spray's effect, percentage of larval habitat removed by LHM, and movement between yards. I then used the model to examine the effect of nine different control strategies on the neighborhood-wide *Ae. albopictus* population. These simulations suggested that treating a quarter of the yards with a combination of barrier sprays and LHM could reduce the neighborhood-wide *Ae. albopictus* population by up to 80%, on average, using targeted treatments. Our results suggested that significant reductions in the neighborhood-wide population is possible with relatively few treatments, even without perfect knowledge of the mosquito's distribution.

The results presented in this dissertation help to better understand the effects of mosquito control on both *Aedes* population dynamics and *Aedes*-vectored disease dynamics. Both the

modeling and experimental results we have presented have implications for future *Aedes*, and *Aedes*-vectored disease, control and will hopefully help guide future control programs.

© Copyright 2020 by Brandon Davis Hollingsworth

All Rights Reserved



Evaluating *Aedes*-vectored Disease Control: Risks and New Approaches

by  
Brandon Davis Hollingsworth

A dissertation submitted to the Graduate Faculty of  
North Carolina State University  
in partial fulfillment of the  
requirements for the degree of  
Doctor of Philosophy

Biomathematics

Raleigh, North Carolina

2020

APPROVED BY:

---

Dr. Alun L. Lloyd  
Committee Co-Chair

---

Dr. Michael H. Reskind  
Committee Co-Chair

---

Dr. Kevin Gross

---

Dr. Fred Gould

---

Dr. Zachary Brown

## **DEDICATION**

To Mom and Grandma: without your reassurance and support, this never would have been possible.

To my grandfathers: you are responsible for making me the man I am today, I wish you could have been here to see this.

## **BIOGRAPHY**

Brandon Davis Hollingsworth was born in Natchez, Mississippi on February 6, 1986. After graduating from Murrah High School in Jackson, Mississippi, he attended the University of Mississippi, graduating with a Bachelor of Science in biology, with a mathematics minor. After graduation, Brandon moved to Wyoming, where he took a position as the Social Recreation Coordinator at the Boys & Girls Clubs of Central Wyoming. During this time, he discovered his love of working with children, something he still pursues through his outreach.

In 2013, Brandon decided to return to school and received a Bachelor of Science in mathematics from the University of Southern Mississippi in 2015. Looking for ways to combine his interest in mathematics and biology, he decided to attend North Carolina State University to work with Dr. Alun Lloyd. After taking a class in Medical and Veterinary Entomology under Dr. Michael Reiskind in his second year, Brandon discovered a fascination with vector-borne disease ecology and found a way to combine his skills and interests. Brandon hopes to continue his work using quantitative methods to help develop more efficient disease control strategies.

## ACKNOWLEDGMENTS

I am deeply thankful to my advisors and the rest of my committee for their guidance and support over the past five years. In particular, I would like to thank Dr. Alun Lloyd for his support of my varying academic interests and for encouraging me to continue my outreach efforts even when I was overwhelmed with research. I would also like to thank Dr. Michael Reiskind for his willingness to train a biomathematician to conduct field work. To the rest of my committee, thank you for sharing your expertise with me and for your invaluable guidance throughout my studies. A special thank you to Dr. Fred Gould, who always challenged me to think not only about the science, but about its implications and impacts. My conversations with each of you have fundamentally changed how I view both research and the world around me. I would also like to thank Dr. Gail Stratton at the University of Mississippi for pushing me towards biomathematics, even though it took me years to listen. To Mrs. Kimberly Van Uden and Mrs. Betty Lamb, thank you for all your support in high school and for believing in me, even if I did not give you much reason to.

I am also thankful for the wonderful support system I had while at North Carolina State University, both inside and outside the Biomathematics Program. I would like to thank the members of the Gould and Lloyd modeling group for the invaluable help and discussions over the year and members of the Reiskind Lab for helping to teach me the intricacies of field work and allowing me to tag along for collections. A big thank you to all my fellow graduate students who have talked through ideas and projects with me. Thank you to Jaye for being a wonderful first mentee and good friend and making me look good.

Thank you to all of my friends that have helped me keep some semblance of balance in my life. In particular, thank you to Annie for all of the adventures, big and small, over the last

three years and for your support through all of this. I honestly do not know if I would have made it without you. Also, thank you to my roommates Paul and Helen for helping me through the stressful times and understanding when I neglect my dishes to finish a project. Thank you to Marco for all the fun times, haircuts, and help over the years, especially during this final push. Thank you to Corey for all the long phone calls and venting sessions. Finally, thank you to Natalie, Maureiq, Amanda, John, and everyone else for being such good friends and providing much needed distractions over the years.

Most importantly, thank you to my family. You have supported me through everything and always pushed me to follow my dreams. Mom and Grandma, I will never be able to express how vital your support has been through all of this. Ken and Joe, thanks for all you have done to make this possible and for believing in me. Thank you to Clint, Alecia, and Zoe for keeping me grounded through all of this and reminding me what was important. Finally, thank you to both of my grandfathers. You did not get to see me finish, but I know you never doubted that I would.

## TABLE OF CONTENTS

LIST OF TABLES .....	viii
LIST OF FIGURES.....	ix
<b>Chapter 1: Introduction</b> .....	1
Background .....	2
Dissertation Outline .....	5
Related Work .....	6
References .....	7
<b>Chapter 2: After the Honeymoon, the Divorce: Unexpected Outcomes of Disease</b>	
<b>Control Measures Against Endemic</b> .....	13
Introduction.....	16
Models.....	19
Results .....	25
Discussion .....	31
References .....	36
Figures.....	39
Supplemental Information .....	46
Supplemental Figures.....	53
<b>Chapter 3: Efficacy and Spatial Extent of Yard-scale Control of <i>Aedes (Stegomyia)</i></b>	
<b><i>albopictus</i> (Skuse) (Diptera: Culicidae) using Barrier Sprays and Larval Habitat</b>	
<b>Management</b> .....	79
Introduction.....	82
Methods.....	84
Results .....	88
Discussion .....	90
References .....	95
Tables .....	101
Figures.....	103
Supplemental Tables.....	106

## **Chapter 4: Targeted Treatments Against *Aedes (Stegomyia) albopictus***

### **(Diptera: Culicidae) in Heterogeneous Landscapes: Insights from a Data-**

<b>Driven Model</b> .....	111
Introduction .....	114
Methods .....	118
Results .....	127
Discussion .....	130
References .....	135
Figures .....	146
Tables .....	152
Supplemental Information .....	157
Supplemental Figures .....	159
Supplemental Tables .....	164

## **Chapter 5: Conclusions** .....

## **Appendices** .....

### **Appendix A: Locally Fixed Alleles: A Method to Localize Gene Drive to Island**

<b>Populations</b> .....	171
Introduction .....	173
Methods .....	174
Results .....	176
Discussion .....	179
References .....	180
Supplemental Information .....	183

## LIST OF TABLES

### Chapter 3

Table 3.1: Mean count of <i>Ae. albopictus</i> on given day after treatment, aggregated for each trap location, yard, and treatment pair within each treatment group. ....	101
Table 3.2: Percent reduction in adult female <i>Ae. albopictus</i> population due to treatment and p-values. ....	102
Table S3.1: Percent reduction in adult female <i>Ae. albopictus</i> population in each treatment group, and 95% confidence intervals. ....	106
Table S3.2: Percent of reduction at the center trap location seen at the side and neighbor trap locations, along with associated p-values. ....	108
Table S3.4: Temporal trends of percent reduction due to treatment in treated and untreated yards. ....	109
Tables S3.5: Additional percent reduction on day 25 post-treatment compared to 1-day post-treatment. ....	110

### Chapter 4

Table 4.1: Equations for the dependence of the per capita juvenile mortality and emergence rates on the density of juveniles within a patch. ....	119
Table 4.2: Treatment plans. ....	152
Table 4.2: Best fit parameter estimates for the three models. ....	155
Table 4.4: AIC (and $\Delta$ AIC) values for each of the model fits. ....	156
Table S4.1: Equilibrium values. ....	164
Table S4.2: Initial guess for model parameterization and source. ....	165

### Appendix A

Table 1: List of parameters and their values. ....	175
Supplemental Table 1: Baseline values and assumed distributions for parametric sensitivity analysis. ....	189



## LIST OF FIGURES

### Chapter 2

Figure 2.1: The divorce effect in the SIR model. ....	39
Figure 2.2: The divorce effect in the seasonal SIR model. ....	41
Figure 2.3: Divorce effect in a seasonal host-vector model.....	43
Figure 2.4: Suggested techniques for mitigating the divorce effect with seasonal transmission .....	44
Figure S2.1: Divorce effect in terms of cases averted. ....	53
Figure S2.2: Heat map of divorce effect from a control that increases recovery rate. ....	54
Figure S2.3: Time-series showing the divorce effect in non-seasonal SIR model. ....	55
Figure S2.4: Long-term time-series for the divorce effect in an SIR model. ....	56
Figure S2.5: Heat maps of divorce effect in SIR model for different strengths of control .....	57
Figure S2.6: Maximum RCI for a given effectiveness of control and $R_0$ .....	58
Figure S2.7: Long-term time-series for the divorce effect in a seasonal SIR model.....	59
Figure S2.8: The divorce effect in the seasonal SIR model with higher seasonality.....	60
Figure S2.9: Maximum RCI for a given basic reproductive number and seasonality in the directly transmitted model. ....	62
Figure S2.10: Time0series of the divorce effect in a non-seasonal vector-borne infection. ....	63
Figure S2.11: Heat map for non-seasonal host-vector model.....	64
Figure S2.12: Long-term time-series for the divorce effect in a seasonal host-vector model ....	65
Figure S2.13: Maximum RCI for a given basic reproductive number and seasonality in the host-vector model.....	66
Figure S2.14: Suggested techniques for mitigating the divorce effect in the seasonal SIR model.....	67
Figure S2.15: Suggested techniques for mitigating the divorce effect in a seasonal host-vector model.....	68
Figure S2.16: The divorce effect in the SIR model with a growing and shrinking population ...	70
Figure S2.17: Cessation of a vaccination program. ....	71
Figure S2.18: Divorce Effect in a SIRS model.....	72
Figure S2.19: Divorce effect in the within-host virus dynamics (HIV) model. ....	73

Figure S2.20: Divorce effect in an age-structured SIR model with realistic mixing.....	74
Figure S2.21: Analytical approximation of the magnitude of the divorce effect. ....	75
Figure S2.22: Sensitivity of the magnitude of the divorce effect to the background force of infection in the non-seasonal and seasonal SIR models. ....	76
Figure S2.23: Interaction between background force of infection, seasonality, timing of control, and the magnitude of the divorce effect. ....	77

### Chapter 3

Figure 3.1: Trap locations within the treated and neighboring yards. ....	103
Figure 3.2: Mean number of female <i>Ae. albopictus</i> for each treatment and location combination.....	104
Figure 3.3: Estimated percent reduction in female <i>Ae. albopictus</i> count due to treatment and 95% confidence interval on individual days in the treated and neighbor yards. ....	105

### Chapter 4

Figure 4.1: Distribution of mean <i>Ae. albopictus</i> counts in yards during the study period. ....	146
Figure 4.2: Example simulation runs. ....	147
Figure 4.3: Cost-benefit curves.....	148
Figure 4.4: Cost-benefit analysis .....	150
Figure S4.1: Observed data (DV) vs individual prediction (IPRED) .....	159
Figure S4.2: QQ-plot for CWRES .....	160
Figure S4.3: VPC Plot.....	161
Figure S4.4: Cost-benefit curves for differing neighborhood sizes .....	162
Figure S4.5: Sensitivity of mean reduction to parameter values. ....	163

### Appendix A

Figure 1: Island population dynamics for the no invasion threshold and invasion threshold scenarios. ....	176
Figure 2: Island and mainland population dynamics (blue curves) and genetics (red curves) in the invasion threshold scenario ( $s=.08$ and $h=.08$ ), following an above-threshold release of drive individuals on the island. ....	176

Figure 3:	Island and mainland population dynamics and genetics in the no invasion threshold scenario ( $s=0.8$ and $h=0.3$ ).....	177
Figure 4:	Maximum level of transient suppression seen on the mainland following an island release of 100 homozygous drive individuals in the no invasion threshold scenario ( $s=.08$ and $h=0.3$ ) across combinations of different migration rates and initial frequencies of resistant alleles on the mainland .....	178
Figure 5:	Maximum drive frequency observed on the mainland following an island release .....	178
Supplemental Figure 1:	Dependence of the time until the mainland population achieves its minimum on the initial level of resistance on the mainland and the migration rate from the island .....	185
Supplemental Figure 2:	Dependence of the time until the drive frequency achieves its maximum on the mainland on the initial level of resistance on the mainland and the migration rate from the island .....	186
Supplemental Figure 3:	Frequency of the susceptible allele on the mainland 100 years after an island release in the no invasion threshold scenario ( $s=0.8$ and $h=.03$ ).....	187
Supplemental Figure 4:	Maximum level of transient suppression, time taken for this level of suppression to occur, and maximum level of gene drive seen on mainland following releases of various sizes on the island under the no invasion threshold scenario .....	188
Supplemental Figure 5:	Heatmaps showing the dependence of the maximum suppression observed on the mainland and the maximum level of drive seen on the mainland on the drive parameters $s$ and $h$ .....	191
Supplemental Figure 6:	Heatmaps showing the dependence of the maximum suppression observed on the mainland and the maximum level of drive seen on the mainland on the drive parameters $s$ and $h$ .....	192
Supplemental Figure 7:	Maximum population suppression seen on the mainland and maximum drive frequency seen on the mainland for various levels of mainland initial resistant allele frequency, and for different values of the homing probability.....	193

Supplemental Figure 8: Dependence of the maximum suppression observed on the mainland, the maximum drive frequency seen on the mainland as the intrinsic per-capita group rate of the population ( $\lambda$ ) is varied.....	195
Supplemental Figure 9: Dependence of the maximum suppression observed on the mainland and the maximum drive frequency seen on the mainland as the parameter $\beta$ that determines the strength of density dependence is varied.....	197
Supplemental Figure 10: Histograms showing maximum suppression seen on the mainland and maximum frequency reached by drive on the mainland across 10,000 realizations of the stochastic model .....	199
Supplemental Figure 11: Histograms showing maximum suppression seen on the mainland and maximum frequency reached by drive on the mainland across 10,000 realizations of the stochastic model .....	200
Supplemental Figure 12: Suppression/replacement dynamics .....	202
Supplemental Figure 13: Heatmaps showing the dependence of the maximum suppression observed on the mainland, the maximum level of drive seen on the mainland, and the drive frequency on the mainland after 100 years, on drive fitness parameters $s$ and $h$ over regions of parameter space for which the drive does not have an invasion probability and suppresses the island population, but does not lead to extinction .....	203
Supplemental Figure 14: Heatmaps showing the dependence of the maximum suppression observed on the mainland, the maximum level of drive seen on the mainland, and the drive frequency on the mainland after 100 years, on initial level of resistance on the mainland and the migration rate, for drive parameters $s=0.6$ and $h=0.3$ that lead to threshold-free suppression but not extinction of the island population.....	204

## **CHAPTER 1 – Introduction**

*Aedes* is a genus of mosquitoes found throughout the tropics and subtropics worldwide. The two most well studied species in the group, *Aedes aegypti* and *Aedes albopictus*, are known to be highly invasive and efficient vectors for several important human arboviruses, most notably dengue, Zika, and yellow fever (Powell et al., 2018). Both species prefer peridomestic environments and human hosts and oviposit in a variety of manmade containers. It is this ability to utilize a variety of containers for oviposition, along with the ability of those eggs to diapause for months at a time (Hawley, 1988), that enabled both species to invade the tropics and subtropics worldwide. *Ae. aegypti* was the first to do this, likely making use of water containers on slave ships in the sixteenth century and has been present in the Americas since (Powell et al., 2018), with the first confirmed yellow fever outbreak in 1648 (McNeill, 2010). *Ae. albopictus* spread more recently, transported worldwide through the tire trade, first arriving in the US in Texas in 1985 (Sprenger & Wuithiranyagool, 1986). Since then, *Ae. aegypti* has been largely displaced by *Ae. albopictus* in the contiguous US, with its current distribution restricted to the southern most parts of Florida and Texas, Arizona, and California. Meanwhile, *Ae. albopictus* is found throughout the southeastern US, from Texas to Florida and as far north as Virginia, in urban areas of Arizona, and has recently begun invading California (Hahn et al., 2017). While *Ae. albopictus* is thought to be a less efficient vector than *Ae. aegypti* (Lambrechts et al., 2010), it has been shown to be a capable vector in laboratory studies (Boromisa et al., 1987) and has been responsible for outbreaks of dengue (Luo et al., 2017) and chikungunya (Gérardin et al., 2008).

Most *Aedes*-vectored diseases are members of the genus *Flaviviridae*, including dengue, yellow fever, and Zika viruses. In addition to these flaviviruses, *Aedes* mosquitoes are the main vectors of chikungunya, an alphavirus, and a known vector of dirofilariasis, dog heartworm. Dengue virus is a reemerging disease transmitted primarily by *Ae. aegypti* throughout most of the

tropics. It accounts for the majority of the morbidity and mortality associated with *Aedes*-vectored diseases, with between 64 and 159 million cases of dengue in 2017 resulting in between 18 and 50 thousand deaths (James et al., 2018), and is undergoing rapid expansion with an increase of between 100-400 million cases each year, with further expansion expected in Europe and the US in the coming decades (Brady & Hay, 2020). Yellow fever was eliminated from much of the world, thanks to the development of a vaccine, but an estimated 97 thousand cases resulted in an estimated 4800 deaths in 2017 (James et al., 2018). Both Zika and chikungunya are considered emerging viruses, having undergone recent expansion outside of their historical ranges (Lowe et al., 2018). A highly publicized outbreak of Zika in the Americas resulted in between 1.6 million and 3.1 million cases of Zika in 2017 but resulted in less than 100 deaths (James et al., 2018). chikungunya, on the other hand, has not seen a large-scale outbreak, but a single mutation allowed for transmission by *Ae. albopictus* in the Reunion Islands (Tsetsarkin et al., 2007), resulting in the highest incidence rate of any recorded arbovirus outbreak (Gérardin et al., 2008), stoking fear of further outbreaks.

Following the elimination of malaria in the US and much of Central America, there was a push for the eradication of *Ae. aegypti*, and the diseases it vectored, throughout the Americas. This program implemented a combination of container inspections, oiling of aquatic habitats, and spraying of dichlorodiphenyltrichloroethane (DDT) and resulted in the elimination of *Ae. aegypti* in large portions of South America (Soper, 1963). However, the high cost and lack of public support resulted in the program being discontinued in the US before the complete elimination of *Ae. aegypti* (Wilson et al., 2020). With the more recent introduction and spread of *Ae. albopictus*, and only isolated *Aedes*-borne disease outbreaks, the priority for mosquito control programs shifted to reductions in mosquito nuisance in most of the US (Wilson et al., 2020). Unfortunately,

this shift in priorities, coupled with decreases in funding, resulted in the government agencies responsible for mosquito and mosquito-borne disease control, e.g. mosquito abatement districts, being underfunded and ill-prepared to respond to mosquito-borne disease outbreaks in many areas (National Association of County and City Health Officials, 2017; Rosario et al., 2014). In the absence of publicly funded mosquito control, private mosquito control companies have increased in popularity in the last decade (Specialty Consultants, 2017). In contrast to publicly funded mosquito-control, which often uses ultra-low volume (ULV) applications of insecticides along with large-scale habitat removal projects aimed at reducing mosquito populations over a large area, these private companies implement barrier sprays coupled with larval habitat management to manage mosquito populations within individual yards.

Despite the long history of *Aedes*-vectored diseases and the renewed interest caused by outbreaks in recent decades, we still lack efficient proven methods to control outbreaks in the absence of vaccines. There is debate over the efficacy of ULV applications of insecticides for *Aedes* control (Bonds, 2012; Bowman et al., 2016; Faraji & Unlu, 2016; Roiz et al., 2018; Wilson et al., 2015), despite its acceptance for use against other species, and studies with epidemiological endpoints are scarce (Bowman et al., 2016; Wilson et al., 2015). The effect of smaller-scale applications of treatments, similar to what is used by private control companies, on *Aedes* populations has only begun to be quantified (Hollingsworth et al., 2020; Hurst et al., 2012; Richards et al., 2017; Trout et al., 2007; Vandusen et al., 2016) and no work has been done on their effectiveness against outbreaks. New technologies such as gene drives and the use of *Wolbachia* have the potential to drastically reduce *Aedes*-borne disease (Flores & O'Neill, 2018) and ongoing trials using *Wolbachia* show promise (Anders et al., 2018; O'Neill et al., 2018), however it is still unknown how sustainable they will be.



Used effectively, any of these treatments, or a combination thereof, could potentially eliminate *Aedes*-borne disease in an area, but none are without drawbacks. The overuse of insecticides, either through ULV or barrier sprays, has resulted in the emergence of insecticide resistant *Aedes* in many areas (Dusfour et al., 2019; Moyes et al., 2017; Tancredi et al., 2020). Likewise, it has been suggested that a similar situation could occur following the introduction *Wolbachia* or gene drives (Esvelt et al., 2014) into populations. On the other hand, there is no simple evolutionary response to the physical reduction of larval habitat, but larval habitat reduction is costly, slow, and exceptionally difficult for *Aedes* mosquitoes (World Health Organization, 2009).

## **Dissertation Outline**

In this dissertation, I used a combination of modeling and field experiments to elucidate the effect of non-immunizing controls, particularly the use of insecticides, on *Aedes* population and disease dynamics. Chapter 2 discusses an ordinary differential equation (ODE) modeling study where I examined the transient dynamics following the end of non-immunizing controls, including the use of insecticides against vector-borne diseases, showing that these controls can have unintended consequences when not maintained. Chapter 3 discusses a field experiment conducted in July-Aug 2018 in which I quantified the effects of barrier sprays and larval habitat reduction on individual treated yards and untreated neighbors. The data collected in this experiment was then used to estimate parameters for a multi-patch ODE model of *Ae. albopictus* across a heterogeneous neighborhood, which is discussed in Chapter 4. Using this model, I examined the effectiveness of different plans for applications and evaluated the added benefit of using different amounts of knowledge to target areas with high densities. Chapter 5 ties together the results of these studies.

## **Related work**

Outside of the work presented in this dissertation, the author has co-authored two peer-reviewed papers and three other manuscripts at various stages of preparation. A follow-up to the field experiment presented in Chapter 2 examining the effectiveness of three traps for controlling *Aedes* mosquitoes was conducted the following year, for which the author designed and performed the statistical analysis (Figurski, et al., in prep). The author has also worked on projects to correlate *Aedes* population density to land-use variables measured using satellite or aerial observations (Reiskind, et al., 2020), which would allow for easy identification of high-density areas, and plans for the release of *Wolbachia* infected *Ae. aegypti* [Hollingsworth, et al., in prep] and genetically engineered mice (Appendix).

## References

- Anders, K. L., Indriani, C., Ahmad, R. A., Tantowijoyo, W., Arguni, E., Andari, B., Jewell, N. P., Rances, E., O'Neill, S. L., Simmons, C. P., & Utarini, A. (2018). The AWED trial (Applying Wolbachia to Eliminate Dengue) to assess the efficacy of Wolbachia-infected mosquito deployments to reduce dengue incidence in Yogyakarta, Indonesia: Study protocol for a cluster randomised controlled trial. *Trials*, 19(302). <https://doi.org/10.1186/s13063-018-2670-z>
- Bonds, J. A. S. (2012). Ultra-low-volume space sprays in mosquito control: A critical review. *Medical and Veterinary Entomology*, 26(2), 121–130. <https://doi.org/10.1111/j.1365-2915.2011.00992.x>
- Boromisa, R. D., Rai, K. S., & Grimstad, P. R. (1987). Variation in the vector competence of geographic strains of *Aedes albopictus* for dengue 1 virus. *Journal of the American Mosquito Control Association*, 3(3), 378–386.
- Bowman, L. R., Donegan, S., & McCall, P. J. (2016). Is Dengue Vector Control Deficient in Effectiveness or Evidence?: Systematic Review and Meta-analysis. *PLOS Neglected Tropical Diseases*, 10(3), e0004551. <https://doi.org/10.1371/journal.pntd.0004551>
- Brady, O. J., & Hay, S. I. (2020). The Global Expansion of Dengue: How *Aedes aegypti* Mosquitoes Enabled the First Pandemic Arbovirus. *Annual Review of Entomology*, 65, 191–208. <https://doi.org/10.1146/annurev-ento-011019-024918>
- Dusfour, I., Vontas, J., David, J.-P., Weetman, D., Fonseca, D. M., Corbel, V., Raghavendra, K., Coulibaly, M. B., Martins, A. J., Kasai, S., & Chandre, F. (2019). Management of insecticide resistance in the major *Aedes* vectors of arboviruses: Advances and challenges.

*PLoS Neglected Tropical Diseases*, 13(10), e0007615–e0007615.

<https://doi.org/10.1371/journal.pntd.0007615>

Esvelt, K. M., Smidler, A. L., Catteruccia, F., & Church, G. M. (2014). Concerning RNA-guided gene drives for the alteration of wild populations. *ELife*, 3(e03401).

<https://doi.org/10.7554/eLife.03401>

Faraji, A., & Unlu, I. (2016). The Eye of the Tiger, the Thrill of the Fight: Effective Larval and Adult Control Measures Against the Asian Tiger Mosquito, *Aedes albopictus* (Diptera: Culicidae), in North America. *Journal of Medical Entomology*, 53(5), 1029–1047.

<https://doi.org/10.1093/jme/tjw096>

Flores, H. A., & O'Neill, S. L. (2018). Controlling vector-borne diseases by releasing modified mosquitoes. *Nature Reviews Microbiology*, 16(8), 508–518. <https://doi.org/10.1038/s41579-018-0025-0>

Gérardin, P., Guernier, V., Perrau, J., Fianu, A., le Roux, K., Grivard, P., Michault, A., de Lamballerie, X., Flahault, A., & Favier, F. (2008). Estimating Chikungunya prevalence in La Réunion Island outbreak by serosurveys: Two methods for two critical times of the epidemic. *BMC Infectious Diseases*, 8, 99. <https://doi.org/10.1186/1471-2334-8-99>

Hahn, M. B., Eisen, L., McAllister, J., Savage, H. M., Mutebi, J. P., & Eisen, R. J. (2017). Updated reported distribution of *Aedes (stegomyia) aegypti* and *Aedes (stegomyia) albopictus* (diptera: Culicidae) in the United States, 1995–2016. *Journal of medical entomology*, 54(5), 1420-1424. <https://doi.org/10.1093/jme/tjx088>

Hawley, W. A. (1988). The biology of *Aedes albopictus*. *Journal of the American Mosquito Control Association. Supplement*, 1, 1–39.

- Hollingsworth, B., Hawkins, P., Lloyd, A. L., & Reiskind, M. H. (2020). Efficacy and Spatial Extent of Yard-Scale Control of *Aedes (Stegomyia) albopictus* (Diptera: Culicidae) Using Barrier Sprays and Larval Habitat Management. *Journal of Medical Entomology*, 57(4), 1104-1110. <https://doi.org/10.1093/jme/tjaa016>
- Hurst, T. P., Ryan, P. A., & Kay, B. H. (2012). Efficacy of Residual Insecticide Biflex AquaMax Applied as Barrier Treatments for Managing Mosquito Populations in Suburban Residential Properties in Southeast Queensland. *Journal of Medical Entomology*, 49(5), 1021-1026. <https://doi.org/10.1603/ME11278>
- James, S. L., Abate, D., Abate, K. H., Abay, S. M., Abbafati, C., Abbasi, N., Abbastabar, H., Abd-Allah, F., Abdela, J., Abdelalim, A., Abdollahpour, I., Abdulkader, R. S., Abebe, Z., Abera, S. F., Abil, O. Z., Abraha, H. N., Abu-Raddad, L. J., Abu-Rmeileh, N. M. E., Accrombessi, M. M. K., ... Murray, C. J. L. (2018). Global, regional, and national incidence, prevalence, and years lived with disability for 354 Diseases and Injuries for 195 countries and territories, 1990-2017: A systematic analysis for the Global Burden of Disease Study 2017. *The Lancet*, 392(10159), 1789–1858. [https://doi.org/10.1016/S0140-6736\(18\)32279-7](https://doi.org/10.1016/S0140-6736(18)32279-7)
- Lambrechts, L., Scott, T. W., & Gubler, D. J. (2010). Consequences of the expanding global distribution of *Aedes albopictus* for dengue virus transmission. *PLoS Neglected Tropical Diseases*, 4(5), e646. <https://doi.org/10.1371/journal.pntd.0000646>
- Lowe, R., Barcellos, C., Brasil, P., Cruz, O. G., Honório, N. A., Kuper, H., & Carvalho, M. S. (2018). The zika virus epidemic in brazil: From discovery to future implications. *International Journal of Environmental Research and Public Health*, 15(E96). <https://doi.org/10.3390/ijerph15010096>

- Luo, L., Jiang, L. Y., Xiao, X. C., Di, B., Jing, Q. L., Wang, S. Y., Tang, J. L., Wang, M., Tang, X. P., & Yang, Z. C. (2017). The dengue preface to endemic in mainland China: The historical largest outbreak by *Aedes albopictus* in Guangzhou, 2014. *Infectious Diseases of Poverty*, 6(1), 148. <https://doi.org/10.1186/s40249-017-0352-9>
- McNeill, J. (2010). *Mosquito Empires: Ecology and War in the Greater Caribbean, 1620–1914 (New Approaches to the Americas)*. Cambridge: Cambridge University Press.  
doi:10.1017/CBO9780511811623
- Moyes, C. L., Vontas, J., Martins, A. J., Ng, L. C., Koou, S. Y., Dusfour, I., ... & Weetman, D. (2017). Contemporary status of insecticide resistance in the major *Aedes* vectors of arboviruses infecting humans. *PLoS neglected tropical diseases*, 11(7), e0005625.  
<https://doi.org/10.1371/journal.pntd.0005625>
- National Association of County and City Health Officials. (2017). *Mosquito Control Capabilities in the U.S.*
- O'Neill, S. L., Ryan, P. A., Turley, A. P., Wilson, G., Retzki, K., Iturbe-Ormaetxe, I., Dong, Y., Kenny, N., Paton, C. J., Ritchie, S. A., Brown-Kenyon, J., Stanford, D., Wittmeier, N., Anders, K. L., & Simmons, C. P. (2018). Scaled deployment of *Wolbachia* to protect the community from dengue and other *Aedes* transmitted arboviruses. *Gates Open Research*, 1.  
<https://doi.org/10.12688/gatesopenres.12844.2>
- Powell, J. R., Gloria-Soria, A., & Kotsakiozi, P. (2018). Recent history of *Aedes aegypti*: Vector genomics and epidemiology records. *BioScience*, 68(11), 854–860.  
<https://doi.org/10.1093/biosci/biy119>

- Reiskind, Michael H., et al. "Short-Term, Large-Area Survey of Container *Aedes* spp. (Diptera: Culicidae): Presence and Abundance is Associated with Fine-scale Landscape Factors in North Carolina, USA." *Environmental Health Insights* 14 (2020): 1178630220952806.
- Richards, S. L., Volkan, J. K., Balanay, J. A. G., & Vandock, K. (2017). Evaluation of bifenthrin and deltamethrin barrier sprays for mosquito control in eastern North Carolina. *Journal of Medical Entomology*, 54(6), 1659-1665. <https://doi.org/10.1093/jme/tjx152>
- Roiz, D., Wilson, A. L., Scott, T. W., Fonseca, D. M., Jourdain, F., Müller, P., ... & Corbel, V. (2018). Integrated *Aedes* management for the control of *Aedes*-borne diseases. *PLoS neglected tropical diseases*, 12(12), e0006845. <https://doi.org/10.1371/journal.pntd.0006845>
- Del Rosario, K. L., Richards, S. L., Anderson, A. L., & Balanay, J. A. G. (2014). Current status of mosquito control programs in North Carolina: the need for cost-effectiveness analysis. *Journal of environmental health*, 76(8), 8-15.
- Soper, F. L. (1963). The elimination of urban yellow fever in the Americas through the eradication of *Aedes aegypti*. *American Journal of Public Health*, 53, 7–16. <https://doi.org/10.2105/ajph.53.1.7>
- Specialty Consultants, L. (2017). *A strategic analysis of the U.S. structural pest control industry*.
- Sprenger, D., & Wuithiranyagool, T. (1986). The discovery and distribution of *Aedes albopictus* in Harris County, Texas. *Journal of the American Mosquito Control Association*, 2(2), 217.
- Sudweeks, J., Hollingsworth, B., Blondel, D. v., Campbell, K. J., Dhole, S., Eisemann, J. D., Edwards, O., Godwin, J., Howald, G. R., Oh, K. P., Piaggio, A. J., Prowse, T. A. A., Ross, J. v., Saah, J. R., Shiels, A. B., Thomas, P. Q., Threadgill, D. W., Vella, M. R., Gould, F., & Lloyd, A. L. (2019). Locally Fixed Alleles: A method to localize gene drive to island populations. *Scientific Reports*, 9(1), 1–10. <https://doi.org/10.1038/s41598-019-51994-0>

- Tancredi, A., Papandrea, D., Marconcini, M., Carballar-Lejarazu, R., Casas-Martinez, M., Lo, E., Chen, X. G., Malacrida, A. R., & Bonizzoni, M. (2020). Tracing temporal and geographic distribution of resistance to pyrethroids in the arboviral vector *Aedes albopictus*. *PLoS Neglected Tropical Diseases*, 4(6), e0008350. <https://doi.org/10.1371/journal.pntd.0008350>
- Trout, R. T., Brown, G. C., Potter, M. F., & Hubbard, J. L. (2007). Efficacy of two pyrethroid insecticides applied as barrier treatments for managing mosquito (Diptera: Culicidae) populations in suburban residential properties. *Journal of medical entomology*, 44(3), 470-477. <https://doi.org/10.1093/jmedent/44.3.470>
- Tsetsarkin, K. A., Vanlandingham, D. L., McGee, C. E., & Higgs, S. (2007). A single mutation in Chikungunya virus affects vector specificity and epidemic potential. *PLoS Pathogens*, 3(12), e201. <https://doi.org/10.1371/journal.ppat.0030201>
- VanDusen, A. E., Richards, S. L., & Balanay, J. A. G. (2016). Evaluation of bifenthrin barrier spray on foliage in a suburban eastern North Carolina neighborhood. *Pest Management Science*, 72(5), 1004-1012. <https://doi.org/10.1002/ps.4081>
- Wilson, A. L., Boelaert, M., Kleinschmidt, I., Pinder, M., Scott, T. W., Tusting, L. S., & Lindsay, S. W. (2015). Evidence-based vector control? Improving the quality of vector control trials. *Trends in parasitology*, 31(8), 380-390. <https://doi.org/10.1016/j.pt.2015.04.015>
- Wilson, A. L., Courtenay, O., Kelly-Hope, L. A., Scott, T. W., Takken, W., Torr, S. J., & Lindsay, S. W. (2020). The importance of vector control for the control and elimination of vector-borne diseases. *PLoS Neglected Tropical Diseases*, 14(1), e0007831. <https://doi.org/10.1371/journal.pntd.0007831>
- World Health Organization, Special Programme for Research, Training in Tropical Diseases, World Health Organization. Department of Control of Neglected Tropical Diseases, World



Health Organization. Epidemic, & Pandemic Alert. (2009). *Dengue: guidelines for diagnosis, treatment, prevention and control*. World Health Organization.

## **CHAPTER 2 - After the Honeymoon, the Divorce: Unexpected Outcomes of Disease Control Measures Against Endemic Infections**

Brandon Hollingsworth, Kenichi W. Okamoto, Alun L. Lloyd.

\*This chapter is published in PLoS Computational Biology. Hollingsworth, Brandon, Kenichi W. Okamoto, and Alun L. Lloyd. "After the honeymoon, the divorce: unexpected outcomes of disease control measures against endemic infections." PLoS Computational Biology 16.10 (2020): e1008292.

## **CONTRIBUTION**

As first author on this publication, I was responsible for coding and running simulations of the models presented, analyzing the results, prepared the figures, and wrote the manuscript.

## ABSTRACT

The lack of effective vaccines for many endemic diseases often forces policymakers to enact control programs that rely on non-immunizing controls, such as vector control, in order to reduce the massive burden of these diseases. It is well known that controls can have counterintuitive effects, such as the honeymoon effect, in which partially effective controls cause not only a greater initial reduction in infection than expected for an infection near its endemic equilibrium, but also large outbreaks during control as a result of accumulation of susceptibles. Unfortunately, many control measures cannot be maintained indefinitely, and the results of cessation are not well understood. Here, we examine the results of stopped or failed non-immunizing control measures in endemic settings. By using a mathematical model to compare the cumulative number of cases expected with and without the control measures, we show that deployment of control can lead to a larger total number of infections, *counting from the time that control started*, than without any control – the *divorce effect*. This result is directly related to the population-level loss of immunity resulting from non-immunizing controls and is seen in model results from a number of settings when non-immunizing controls are used against an infection that confers immunity. Finally, we also examine three control plans for minimizing the magnitude of the divorce effect in seasonal infections and show that they are incapable of eliminating the divorce effect. While we do not suggest stopping control programs that rely on non-immunizing controls, our results strongly argue that the accumulation of susceptibility should be considered before deploying such controls against endemic infections when indefinite use of the control is unlikely. We highlight that our results are particularly germane to endemic mosquito-borne infections, such as dengue virus, both for routine management involving vector control and for field trials of novel control approaches.

## INTRODUCTION

An estimated 200 million cases of malaria, 390 million cases of dengue fever, and 9 million cases of measles occurred in 2016 [1,2], representing only a portion of the total impact of endemic disease that year. The burden that this places on local populations, both in terms of morbidity and mortality and both direct and indirect economic costs, often pressures policy makers to act to suppress these infections. However, the scientific rationale on which the implemented policies are based is not always clear, making it difficult to assess whether the risks associated with control have been adequately addressed.

Eradication—the permanent reduction of worldwide incidence to zero [3]—is the ideal aim of all control programs. This goal is unrealistic, with only two infections having been successfully eradicated to date: smallpox and rinderpest [4]. Often, a more realistic goal for a control program is either long-term suppression or local elimination of the infection. These goals hold their own challenges though, as they require long-term or even indefinite control programs, which can face budgetary and public support issues, not to mention the potential for some controls to fail due to evolution of resistance. Further, if there is a loss of herd immunity in the population due to the control lowering population exposure to the pathogen, there is the additional risk that when a control program ends the infection will re-emerge in a post-control epidemic and reestablish in the population [4].

Naively, one might imagine that lowering the incidence of infection will have no detrimental effects for the population. However, mathematical modeling has previously revealed numerous perverse outcomes of application of ineffective control measures (by which we mean ones that do not bring the basic reproductive number,  $R_0$ , below one) in endemic settings. Perhaps the most famous example is the increased age at infection that results when a population

is partially vaccinated for rubella, leading to more infections occurring in women of child-bearing age, where severe complications, such as congenital rubella syndrome, can result when pregnant women become infected [5–7]. While this certainly represents a potential downside of the control, the population sees a reduction in rubella prevalence. McLean and Anderson (1988) showed that when an ineffective control is used against an endemic infection it often results in an initial drop in prevalence to well below the endemic level, the “honeymoon effect”, but this is followed by outbreaks that periodically increase prevalence above the endemic level as a consequence of a build-up of susceptible individuals. Similarly, in a seasonally-forced setting, Pandey and Medlock [9] found that vaccination against dengue virus could result in a transient period with periodic outbreaks of larger peak prevalence than occurred before vaccination. These last two examples illustrate possible negative side effects of ineffective controls: they can cause transient increases in prevalence while still resulting in a decrease in total incidence.

In the results above, there is higher incidence than expected, but Okamoto et al.[10] described an even more troubling theoretical result while exploring a model of failed or stopped combined strategies aimed at controlling dengue virus, e.g. vaccination along with transgenic vector control. They observed that when control was only transient the **total** number of infections that occurred, counting from the time that control started, a quantity they called the cumulative incidence (CI), could exceed the number of cases that would have been observed had no control been deployed. Even in situations where control measures had a significant positive impact over a period of years, the outbreaks that ensued following the cessation, or failure, of control could lead to an outbreak that was large enough to outweigh the number of cases prevented during the control period.

While Okamoto et al. [10] showed that it was possible for transient transgenic controls to increase the total number of infections, here we demonstrate that this effect—which we call the *divorce effect*—is not an artifact of very specific complex models, but quite a general phenomenon that can occur across a range of models and parameter space when deploying a control measure that does not confer immunity. By exploring the dynamics of the divorce effect in the setting of several simple models we gain insights that were not obtainable using the previous complex models. Conversely, we find that for immunizing controls (e.g. vaccination) the divorce effect does not occur, even when the duration of protection is relatively short-lived.

We demonstrate the generality of this result for endemic infections by simulating cessation of control measures in three commonly-used models for pathogen transmission. Unlike the honeymoon effect, the divorce effect occurs for both ineffective and effective controls, provided that they are transient. As anticipated, control results in the accumulation of susceptible individuals resulting in the potential for a large outbreak following the cessation of control. This outbreak is either triggered by infective individuals that remain in the population or by reintroduction of infection from outside the control area, and its size increases asymptotically towards the size of a virgin-soil epidemic as the length of the control period is increased and herd immunity is lost. Counterintuitively, and comparable to results in Okamoto et al. [10], we see that the post-control outbreak often results in there being timeframes over which the cumulative incidence of infection since the start of control is higher than would have occurred in the absence of control. Further, these outbreaks are significantly larger than the endemic levels of the infection and would likely overwhelm healthcare providers in the area.

This paper is organized as follows. We first describe the three models we choose to illustrate the divorce effect: a non-seasonal SIR model, a seasonal SIR model, and a host-vector

model. We then demonstrate, in each setting, the occurrence of the divorce effect and its sensitivity to relevant parameters, namely  $R_0$  and the duration and strength of control. Further, for the seasonal SIR model, we explore the sensitivity of the strength of the divorce effect on the timing of the start and end of the control. Then for the seasonal SIR and seasonal host-vector model we look at three possible strategies for mitigating the divorce effect and show they are incapable of eliminating the divorce effect. A crude analytical approximation for the divorce effect and additional models are explored in the Supplemental Information, as is the impact of using immunizing controls.

## **MODELS**

To evaluate the magnitude of the Divorce Effect, we simulate the cessation of a short-term control affecting transmission in three infection systems: a SIR model, a seasonal SIR model, and a host-vector SIR model. While these are the only models we discuss in detail here, this result can be seen in most models that have a replenishment of the susceptible population, including the more general SIRS model, for which host immunity is not life-long, and an age-structured model with realistic mixing parameters (see Supplemental Information for exploration of additional forms of transmission models). These results are parameterized for a human population and mosquito vector, but the results are generalizable to other species.

### **SIR Model:**

We assume a well-mixed population of one million hosts and a non-fatal infection that is directly transmitted and confers complete life-long immunity. The numbers of susceptible, infective, and removed individuals are written as  $S$ ,  $I$  and  $R$ , respectively. We allow for replenishment of the susceptible population by births, but assume the population size is constant by taking per-capita birth and death rates,  $\mu$ , to be equal (this assumption is relaxed in the



supplemental information). This results in the standard two-dimensional representation of the SIR model, where the number of removed individuals is  $R = N - S - I$  (Equation 1).

$$\begin{aligned}\dot{S} &= \mu(N - S) - \beta \frac{S(I + I_b)}{N} \\ \dot{I} &= \beta \frac{S(I + I_b)}{N} - (\gamma + \mu)I\end{aligned}\tag{1}$$

For our simulations, we assume parameters resembling a short-lived infection in a human population, lasting on average 5 days (average recovery rate,  $\gamma = 73/\text{year}$ ) and that individuals live on average 60 years ( $\mu = .0167/\text{year}$ ), allowing the transmission parameter,  $\beta$ , to be adjusted to achieve the desired value of  $R_0$ . In order to reseed infection following cessation of control and to counter the well-known weakness of infective numbers falling to arbitrarily low levels in deterministic transmission models, we follow numerous authors in including a constant background force of infection [11,12] in the model. This represents infectious contacts made with other populations, and occurs at a rate that is equivalent to there being  $I_b$  additional infective individuals within our focal population. For our simulations, we take  $I_b = 1$  (sensitivity of our results to  $I_b$  can be found in the supplemental information).

### Seasonal SIR Model:

For the seasonal SIR model, we allow the transmission parameter to fluctuate seasonally (annually) around its mean,  $\beta_0$ , taking the form given in Equation 2. Seasonal oscillations in the parameter have relative amplitude  $\beta_1 = .02$  with maxima occurring at integer multiples of 365 days. Noting that seasonally forced models are particularly susceptible to having the number of infectives fall to unreasonably low numbers between outbreaks [13], we again take  $I_b = 2$  in the background force of infection term.

$$\beta(t) = \beta_0(1 + \beta_1 \cos(2\pi t))\tag{2}$$

### Host-Vector Model:

We model an infection with obligate vector transmission. As in other models, we assume that the host population size is held constant ( $R = N - S - I$ ), but we allow the vector population size to fluctuate—so that, for instance, we can model vector control. For simplicity, we only model the female adult vector population and assume density-dependent recruitment into the susceptible class ( $U$ ), with a logistic-type dependence on the total female adult population size. Infectious vectors ( $V$ ) arise from interactions with infected hosts (Equation 3).

$$\begin{aligned}\dot{S} &= \mu(N - S) - \beta_{VH} \frac{SV}{N} \\ \dot{I} &= \beta_{VH} \frac{SV}{N} - (\gamma + \mu)I \\ \dot{U} &= (U + V)(r - k(U + V)) - \beta_{HV} \frac{U(I + I_b)}{N} - \delta(t)U \\ \dot{V} &= \beta_{HV} \frac{U(I + I_b)}{N} - \delta I\end{aligned}\tag{3}$$

We assume that host demography and recovery rates are the same as in the SIR model, with a host population of one million individuals. We assume that the vector lives on average 10 days ( $\delta = 36.5/\text{year}$ ), the growth constant ( $r$ ) and density dependence parameter ( $k$ ) are parameterized as in Okamoto et al. (2016):  $r = 304.775/\text{year}$  and  $k = 1.341 \times 10^{-7}/(\text{vector} \cdot \text{year})$ , resulting in an equilibrium vector population of 2 million individuals. The transmission parameter from host to vector ( $\beta_{HV}$ ) is assumed to be 109.5/year and the parameter for vector to host ( $\beta_{VH}$ ) is changed to produce the desired  $R_0$ . We again assume a background force of infection (with  $I_b = 2$ ), representing reintroduction of infection from outside our focal population.

Seasonality plays a large role in vector-borne infections and affects many aspects of the infection and its vector. Temperature affects breeding rates, larval development, and death rates of the vector, the extrinsic incubation period and transmissibility of the infection itself, and host encounter rates, while precipitation can affect the availability of appropriate habitat and encounter rates [14–16]. However, most of these add a level of model complexity which is unnecessary for this study, so we choose to use a simple forcing term for mosquito recruitment that fluctuates seasonally with relative magnitude  $r_s$  ( $r_s = 0.02$ ) about its baseline ( $r_0 = 304.775$  /year) (Equation 4).

$$r(t) = r_0(1 + r_s \cos(2\pi t)) \quad (4)$$

### **Control:**

We model a control that is applied instantaneously and consistently from time  $t_0$  (which, for simplicity, we usually take to be equal to zero) to time  $t_{end}$  and is instantaneously removed at the end of the control period. In the SIR and seasonal SIR models, control reduces the transmission rate by some proportion,  $\varepsilon$ , and, in the host vector model, causes a proportional increase,  $\sigma$ , in the vector mortality rate. This results in the transmission parameter given in Equation 5 for directly transmitted infections and the vector death rate given in Equation 6 for the vector-borne infections.

$$\beta(t) = \begin{cases} (1 - \varepsilon)\beta_0 & t_0 < t < t_{end} \\ \beta_0 & \text{otherwise} \end{cases} \quad (5)$$

$$\delta(t) = \begin{cases} (1 + \sigma)\delta_0 & t_0 < t < t_{end} \\ \delta_0 & \text{otherwise} \end{cases} \quad (6)$$

While we only look at these control measures in the main text, other controls (such as an increase in the recovery rate,  $\gamma$ ) are explored in the Supplemental Information (Figure S2.2), and give similar results.

### **Measuring Effectiveness:**

There are a number of measures that can be used to quantify the effectiveness of a control. We want to characterize the total number of cases that occur from the start of control until a particular point in time, a quantity we call the cumulative incidence (CI). For a directly transmitted infection, this is calculated as follows

$$CI(t) = \int_{t_0}^t \frac{\beta(\tau)S(\tau)I(\tau)}{N} d\tau, \quad (7)$$

i.e. by integrating the transmission term over the time interval from the start of control until the time,  $t$ , of interest. This quantity could be calculated both in the presence of control and in the baseline, no-control, setting; we distinguish between these two by labeling quantities (e.g. state variables) in the latter case with a subscript B to denote baseline.

One commonly-used measure of effectiveness is the number of cases averted by control (CA),  $CI_B(t) - CI(t)$ . This has the disadvantage (particularly in terms of graphical depiction) that it can become arbitrarily large as  $t$  increases. Consequently, some authors choose to utilize a relative measure of cases averted, dividing by the baseline cumulative incidence (see, for instance, the work of Hladish et al. [17]). We instead follow our earlier work and use the relative cumulative incidence (RCI) measure employed by Okamoto *et al.* [10], calculating the

cumulative incidence of the model with the control program relative to the cumulative incidence of the model without the control program (Equation 8).

$$RCI(t) = \frac{\int_{t_0}^t \beta(\tau)S(\tau)I(\tau)d\tau}{\int_{t_0}^t \beta S_B(\tau)I_B(\tau)d\tau}. \quad (8)$$

$RCI(t)$  values above one imply that the control measure has resulted in an increase in the total number of cases compared to the baseline. Importantly, as time becomes larger,  $RCI$  becomes less sensitive to outbreaks in the system. For a transient control,  $RCI$  will approach 1 as  $t$  becomes larger.

We see that the relative cases averted measure employed by Hladish et al. [15] is simply  $1-RCI(t)$ . Both relative measures have properties that make them attractive for graphical depiction although it should be borne in mind that both involve a loss of information on the actual number of cases averted. For example, an  $RCI$  of 1.1 after one year is a much smaller increase in total cases than an  $RCI$  of 1.1 after 10 years, and an  $RCI$  of just below one after many years can represent a large reduction in total incidence. In cases where this information is pertinent, it may be more appropriate to use non-relative measures such as cases averted. The choice of measure does not impact the occurrence of the divorce effect; figures that show cases averted are included in the Supplemental Information (Figure S2.1).

Analogous expressions for  $CI$  and  $RCI$  can be written for the host-vector model using the appropriate transmission terms.

## RESULTS

### SIR Model

Simulations show the successful suppression of infection following the implementation of a control which reduces the transmission parameter,  $\beta$ , in the population. With infection at endemic equilibrium, the honeymoon effect [8] states that even a modest reduction in the transmission parameter will have a large effect on the incidence of the infection due to the effective reproductive number,  $R_t$ , the expected number of new infections each infectious individual causes, being one. After the control is stopped, the incidence of the infection remains low for some time as the number of infective individuals builds from very low numbers (Figure 2.1(a), curve). However, once control ends  $R_t$  immediately rises above one and continues to increase while prevalence is low, due to the buildup of the susceptible population (plots of  $R_t$  and  $S(t)$  are provided in the supplemental information: see Figure S2.3). This increased  $R_t$  eventually drives a large outbreak, quickly depleting the susceptible population, at which point incidence (Figure 2.1(a), black curve), and  $R_t$ , again fall to low numbers.

To evaluate the success of the control, we examine the RCI in the period following introduction of control and see that during and immediately following the control period, when incidence is low, the RCI decreases towards 0, suggesting a successful control program. However, once the post-control outbreak begins, RCI increases rapidly resulting in the divorce effect ( $RCI > 1$ ) before dropping back below one once the epidemic begins to wane and incidence falls below endemic levels (Figure 2.1(a)). During the period where  $RCI > 1$ , lasting approximately 2 years in our example, the control has not only failed to decrease the total incidence of infection but has resulted in an increase in total incidence, the divorce effect.

Following this initial outbreak and trough, RCI continues to oscillate around one, and approaches one in the long run (see Figure S2.4).

Exploring values of  $R_0$  and the duration and strength of control shows that the divorce effect is present over a wide region of parameter space. Figure 2.1(b) shows the magnitude of the divorce effect, quantified by the maximum RCI seen, as a function of  $R_0$  and duration of control for a perfect control measure ( $\beta = 0$  during the control period). Perfect control was employed here to eliminate any confounding effects from the honeymoon effect that could occur during an imperfect control. We find that for the most biologically relevant area of parameter space ( $R_0 < 20$ , control lasting less than 20 yrs) the divorce effect always occurs and will result in a 20-60% increase in cumulative incidence (RCI=1.2-1.6) at its peak. However, we also find that it is possible to avoid the divorce effect if controls are maintained long enough. For infections with a high  $R_0$ , this requires maintaining the control for decades, and the length of time needed grows as  $R_0$  is decreased. The non-monotonic relationship between the magnitude of the divorce effect and the length of the control seen here suggests that a control program should either be discontinued immediately, if  $R_0$  is small, or continued as long as possible to avoid the divorce effect (Figure 2.1(b); see also Figure S2.5 in Supplemental Information).

Relaxing our assumption of a completely effective control and focusing on a fixed  $R_0$  ( $R_0=5$ , Figure 2.1(c)), we see that the relationship between the magnitude of the divorce effect and the length of the control period varies with the strength of the control. A steep edge-like pattern is seen in Figure 2.1c when control is ineffective but carried out for a long period of time, a consequence of the honeymoon effect. For populations at endemic equilibrium, the honeymoon effect means that any reduction in transmission will be sufficient to significantly reduce transmission for a period of time. For controls that are relatively short lived, here

approximately 5 years, the control does not outlast the honeymoon period, resulting in the magnitude of the divorce effect being relatively insensitive to the effectiveness of the control in this region of parameter space. How the interaction between the effectiveness of control and  $R_0$  affects the magnitude of the divorce effect is explored in the supplemental information (Figure S2.6).

### **Seasonal SIR Model**

Temporary control measures in the seasonal SIR model show many of the same dynamics as in the non-seasonal model, namely that a successful control is followed by a period of low incidence and eventually a post-control outbreak leading to a divorce effect (Figure 2.2(a)) before settling back into regular seasonal outbreaks (Figure S2.7). However, the timing and size of the post-control epidemic, and thus the magnitude of the divorce effect, depend not only on  $R_0$  and the length of the control but also the timing of both the onset and end of the control (Figures 2.2(b) and 2.2(c)). This leads to a highly nonlinear dependence of the magnitude of the divorce effect on  $R_0$  and the duration of control (Figure 2.2(b)). However, the presence of ranges of parameter space with smaller magnitudes of the Divorce Effect at regular intervals could allow policy makers to determine optimal times to stop control. These effects become more apparent with an increase in seasonality (Figure S2.8). As seasonality increases, the differences due to timing become more pronounced, resulting in more potential for mitigating the divorce effect with a properly timed treatment. Conversely, this also means a larger divorce effect will be seen with a poorly timed treatment (Figure S2.8).

The oscillatory nature of the relationship between the maximum RCI and  $R_0$  (Figure 2.2(b)) implies a relationship between the timing of the control period and the severity of the divorce effect. While the magnitude is only highly sensitive to the start time for very short



control periods, lasting around a year, it is highly sensitive to the end time (Figure 2.2(c)). This means that controls of similar lengths can have significantly different outcomes depending on their timing, e.g. a 1 year control ending day 700 results in a maximum RCI around 1.4 while a control of the same length ending day 515 results in a maximum RCI near 1.7. This is a direct result of the seasonal forcing function and delaying the outbreak until a period in which  $R_0$  is larger, similar to results seen when controls are used against epidemics in seasonal settings [18,19]. Regardless of start time, the optimal end time occurs shortly after the peak in the transmission parameter,  $\beta(t)$ , (days 750 and 1155 in Figure 2.2(c)), suggesting this would be the best time to end control programs.

### **Host-Vector Model**

The non-seasonal host-vector model has broadly similar dynamics to the non-seasonal SIR model in terms of the divorce effect (Figures S2.10 and S2.11), so here we focus instead on the seasonal host-vector model. Following one year of insecticide treatment that reduces the average mosquito lifespan by a half (i.e. increases the mosquito death rate by 100%,  $\sigma = 1$ ) the infection is suppressed and there is no seasonal outbreak for the next two years (Figure 2.3). A major outbreak, with approximately eight times the peak prevalence of the pre-control seasonal outbreaks, occurs in the third year and results in a maximum RCI of around 1.50, before the epidemic fades and incidence again returns to low levels. The size of this outbreak would almost certainly risk overwhelming even the most well-funded medical services. RCI then remains above 1 until year 7. The population continues to see large periodic outbreaks, each bringing RCI back above 1, for decades until the endemic equilibrium is reached again (Figure S2.12).

## Mitigating the Divorce Effect

It is apparent from earlier results (e.g. Figure 2.1(b)) that avoiding the divorce effect in a non-seasonal setting is only possible with a non-immunizing control by maintaining suppression for decades, due to the inevitable build-up of susceptible individuals. Therefore, the goal in these situations should be to maintain the control as long as possible or until a vaccine becomes available, and we focus instead on the seasonal SIR and host-vector models. In this section, we look at three different treatment plans for deploying a set amount of treatment, twelve one-month treatments, and their ability to mitigate the divorce effect. The first relies on annual controls lasting one month when  $R_0$  is at its maximum, the second has a month-long control applied in response to the prevalence reaching some set level—which we might imagine corresponding to an outbreak becoming detectable or reaching a sufficient level to cause concern to local authorities—that we take here to be when two hundred individuals out of a million are infective, and the third chooses when to implement a month-long control based on minimizing the peak RCI. For comparison, all three use 12 total months of control.

With annual monthly control for a directly transmitted seasonal infection, the population sees a significant initial reduction in prevalence. However, as predicted by the honeymoon effect, the repeated use of controls results in a diminished effect on the prevalence and seasonal outbreaks begin to occur between control periods. The peak prevalence of these outbreaks quickly grows to be significantly larger than the seasonal outbreaks before the control program was begun, however they are blunted by the next control period before RCI rises above one. Once the program is ended, however, a post-control outbreak quickly brings RCI above one (Figure 2.4(a)).

The reactive control has a similar effect following the initial control period, however it results in ever more rapid need for control, exhausting all 12 months of treatment in the first four years for both the directly transmitted infection (Figure 2.4(b)). We see that while this results in a lower RCI during the control program, it results in an even larger post-control outbreak and a larger maximum RCI for both transmission pathways.

Intuitively, Figure 2.2(c) suggests choosing a time period to implement the control that will minimize the divorce effect. To do this, we implement a third method which optimally chooses the time at which to begin the next control period. For this, we simulate the first one month control period, beginning at time 0. Then we run simulations with the next one month control beginning on all possible days over the next 365 days after the control ends, choosing the day that results in the lowest maximum RCI over the next decade, simulating through that control period, and repeating. This plan results in implementing the first three control periods in rapid succession and the remainder after the peak of an outbreak, when the control will have the least effect on transmission (Figure 2.4(c)), minimizing the magnitude of the divorce effect albeit at the cost of not providing significant protection against the infection. This result, along with other earlier results, suggests that the divorce effect is unavoidable and the potential for a divorce effect will continue to grow in magnitude unless the control is maintained for decades, regardless of the timing of the treatments. While it may not be possible to eliminate the divorce effect for relatively short controls, it may be possible to extend programs without worsening the divorce effect and to minimize the divorce effect by carefully choosing the timing of the end of the control program once cessation becomes necessary.

In the case of host-vector transmission, the yearly control successfully suppresses the infection for the first 1.5 years, however the population begins to experience outbreaks during

what was traditionally the off-season. After the control program is ended, the population enters a period of larger outbreaks occurring every three years (Figure S2.15(a)). The reactive control sees a similar result as the directly transmitted disease, with all twelve treatments used in the first 4 years (Figure S2.15(b)). For the third method, the optimal plan was to wait the maximum amount of time to deploy the control (Figure S2.15(c)). This is likely due to the peak of an outbreak not occurring within a year of the end of treatment in the seasonal host-vector model.

### **Additional Results**

Results for additional models, along with an analytical approximation to the magnitude of the divorce effect are included in the supplemental information.

## **DISCUSSION**

It has long been appreciated that non-immunizing control measures deployed against endemic infections will result in a large short-term reduction in prevalence but will lead to a reduction in herd immunity, leaving the population at risk of large outbreaks after the cessation of control. Here we have shown, in quite general settings, that these outbreaks can be so large as to increase, counting from the time that control started, the total incidence of infection above what would have occurred if no control had been used—a result we call the divorce effect. This represents a failure for control of the worst kind, namely a control that increases the total incidence of the infection. Unfortunately, many commonly used disease control plans rely on temporary non-immunizing controls, meaning that populations may be left at risk of the divorce effect once the control measure is ended.

Controls that do not confer immunity—including isolation, use of drugs as a prophylaxis or to shorten duration of infectiousness or behavioral changes such as social distancing—are often deployed in epidemic settings, particularly for new pathogens for which a vaccine is

unavailable, but may also be used to blunt seasonal outbreaks of endemic diseases. In these endemic settings, we have shown that it is important to weigh any potential benefit from these controls against the risk of post-control outbreaks and the divorce effect. While there are timeframes over which a temporary non-immunizing control has benefits, the severity of the post-control outbreak that results in the divorce effect will risk overwhelming even well-maintained healthcare systems.

Vector-borne infections represent the most common situation in which non-immunizing controls are regularly used against endemic diseases, e.g. insecticide spraying to combat seasonal dengue outbreaks. The honeymoon effect predicts that insecticides can provide short-term benefits in endemic settings but that the additional benefit of continued spraying will decrease over time due to the accumulation of susceptibles (i.e. depletion of herd immunity) that results. Indeed, Hladish *et al.* [17] saw precisely these effects using a detailed agent-based model for dengue control that employs indoor residual spraying. Cessation of spraying will be expected to lead to large post-control outbreaks: again, Hladish *et al.*'s model exhibited annualized incidence of 400% compared to the uncontrolled baseline setting in certain years. Here, we examine the divorce effect directly and show that they are not specific to a host-vector model and that if the control is not maintained indefinitely, or at least for a few decades, the damage of the divorce effect can quickly outweigh the short-term benefits. Further, programs implementing insecticides may be intended to be indefinite, but the evolutionary pressure imposed can result in the rapid and unpredictable evolution of resistance. Without proper monitoring, this could result in an increase in total incidence due to the divorce effect before officials realize that resistance has developed. While insecticides, and other non-immunizing controls, will, and should,

continue to play an important role in epidemic settings, where herd immunity is negligible, the results of this study raise important questions about their use in combating endemic infections.

In some instances, control measures are deliberately transient in nature, such as field trials for assessing the impact of proposed novel control methods, e.g. a review of field trials of dengue vector control showed they lasted between 5 months and 10 years [20]. Multiple year field trials such as these can result in considerable build-up of the susceptible population, meaning consideration needs to be given to the consequences of this accumulation and the potential for large outbreaks to occur in the wake of cessation of the trial. If our results are validated, they must be factored not only into the design of such trials but also into the informed consent process for trial participation, with participants made aware of the risk of the divorce effect and plans put in place to provide a reasonable level of protection during and following the study. As we have shown, these outbreaks can occur months or even many years later, and while disease incidence would be observed closely during the trial, our results argue that monitoring should continue for an appropriate length of time following the cessation of control. Furthermore, we emphasize that the epidemiological consequences of the honeymoon effect—specifically the relative ease of reducing incidence for an infection near endemic equilibrium—must be kept in mind when interpreting the results of such trials. Together, these dynamical effects argue that susceptibility of the population to infection should be monitored together with incidence to fully assess the impact and effectiveness of the control.

Additional concerns are raised when an endemic and an epidemic infection share the same transmission pathway (e.g. *Aedes aegypti* vectoring both dengue and Zika). Emergency control against the epidemic infection also impacts the endemic infection, leading to the potential for the divorce effect to occur in the latter if the control is ceased once the epidemic has

subsided. It may be that policy makers have to choose to allow an epidemic of a highly publicized, but low risk, epidemic in order to maintain immunity levels of another lower profile, but more dangerous, disease. On the other hand, if the risk due to the epidemic is sufficiently high, it may still be advantageous to use the control, however the risks need to be carefully compared and an informed decision, that accounts for the divorce effect, needs to be made.

While transient non-immunizing controls are common and provide opportunities to observe the divorce effect, researchers tend to focus on prevalence or incidence over short periods of time and not cumulative measures such as CI or relative measures such as RCI or CA, which would expose the divorce effect. Even when relative measures are used, such as Hladish et al. [17], the time frame over which incidence is compared can have a drastic effect on the interpretation of the result. The divorce effect is an easily missed phenomenon, even when examining models that lack much of the real-world complexity, but real-world data comes with a myriad of other problems. Often the divorce effect may occur when the system is poorly monitored, as with field trials and unintentional control, in systems that, like dengue, have large year-to-year variation, or in systems where the failure is associated with other confounding socio-economic events such as war or natural disaster, resulting in data that is either scarce or difficult to interpret. The divorce effect may become more apparent in coming years, though, as mosquito control is lessened following the end of the Zika epidemic, allowing for a rebound in dengue in areas such as South America, and as insecticide resistance problems continue to grow.

Careful thought should be given to whether or not it is appropriate to begin new programs that rely on non-immunizing controls in endemic settings. This is an inherently complicated decision that must take into account numerous factors, both scientific and sociopolitical, but, in light of our results, policymakers should carefully weigh the risks of the divorce effect against

other factors, e.g. imminent approval of a new vaccine or political pressure, before implementing disease management plans that rely on non-immunizing controls. Further, it is important that when non-immunizing controls are included in these management plans that they are not considered possible solutions but instead stop-gaps, and emphasis is placed on the development of vaccination as opposed to the indefinite continuation of the program.

Currently, control of endemic diseases worldwide, especially vector-borne diseases, relies heavily on non-immunizing controls such as insecticide. Policy makers should begin developing exit plans for these disease management programs —guidelines for safely ending the program when it becomes clear that indefinite maintenance is unlikely, which should be designed to minimize the impact of the divorce effect. In this paper, we have shown three possible designs for exit plans that could minimize the divorce effect. However, none of these designs were capable of eliminating the divorce effect. Our results suggest there is an inherent cost associated with the loss of immunity resulting from these programs.



## REFERENCES

1. Abajobir AA, Abate KH, Abbafati C, Abbas KM, Abd-Allah F, Abdulkader RS, et al. Global, regional, and national disability-adjusted life-years (DALYs) for 333 diseases and injuries and healthy life expectancy (HALE) for 195 countries and territories, 1990–2016: a systematic analysis for the Global Burden of Disease Study 2016. *Lancet*. 2017;390: 1260–1344. doi:10.1016/S0140-6736(17)32130-X
2. Bhatt S, Gething PW, Brady OJ, Messina JP, Farlow AW, Moyes CL, et al. The global distribution and burden of dengue. *Nature*. 2013;496: 504–507. doi:10.1038/nature12060
3. Dowdle WR. The principles of disease elimination and eradication. *Bull World Health Organ*. 1998;76 Suppl 2: 22–5. Available: <http://www.ncbi.nlm.nih.gov/pubmed/10063669>
4. Klepac P, Funk S, Hollingsworth TD, Metcalf CJE, Hampson K. Six challenges in the eradication of infectious diseases. *Epidemics*. 2015;10: 97–101. doi:10.1016/j.epidem.2014.12.001
5. Anderson RM, May RM. Directly Transmitted Infectious Diseases: Control by Vaccination. *Science* (80- ). 1982;215: 1053–1060. doi:10.1126/science.7063839
6. Knox EG. Strategy for rubella vaccination. *Int J Epidemiol*. 1980;9: 13–23. doi:10.1093/ije/9.1.13
7. Heesterbeek H, Anderson RM, Andreasen V, Bansal S, De Angelis D, Dye C, et al. Modeling infectious disease dynamics in the complex landscape of global health. *Science* (80- ). 2015;347: aaa4339–aaa4339. doi:10.1126/science.aaa4339
8. Mclean AR, Anderson RM. Measles in developing countries. Part II. The predicted impact of mass vaccination. *Epidemiol Infect*. 1988;100: 419–442.

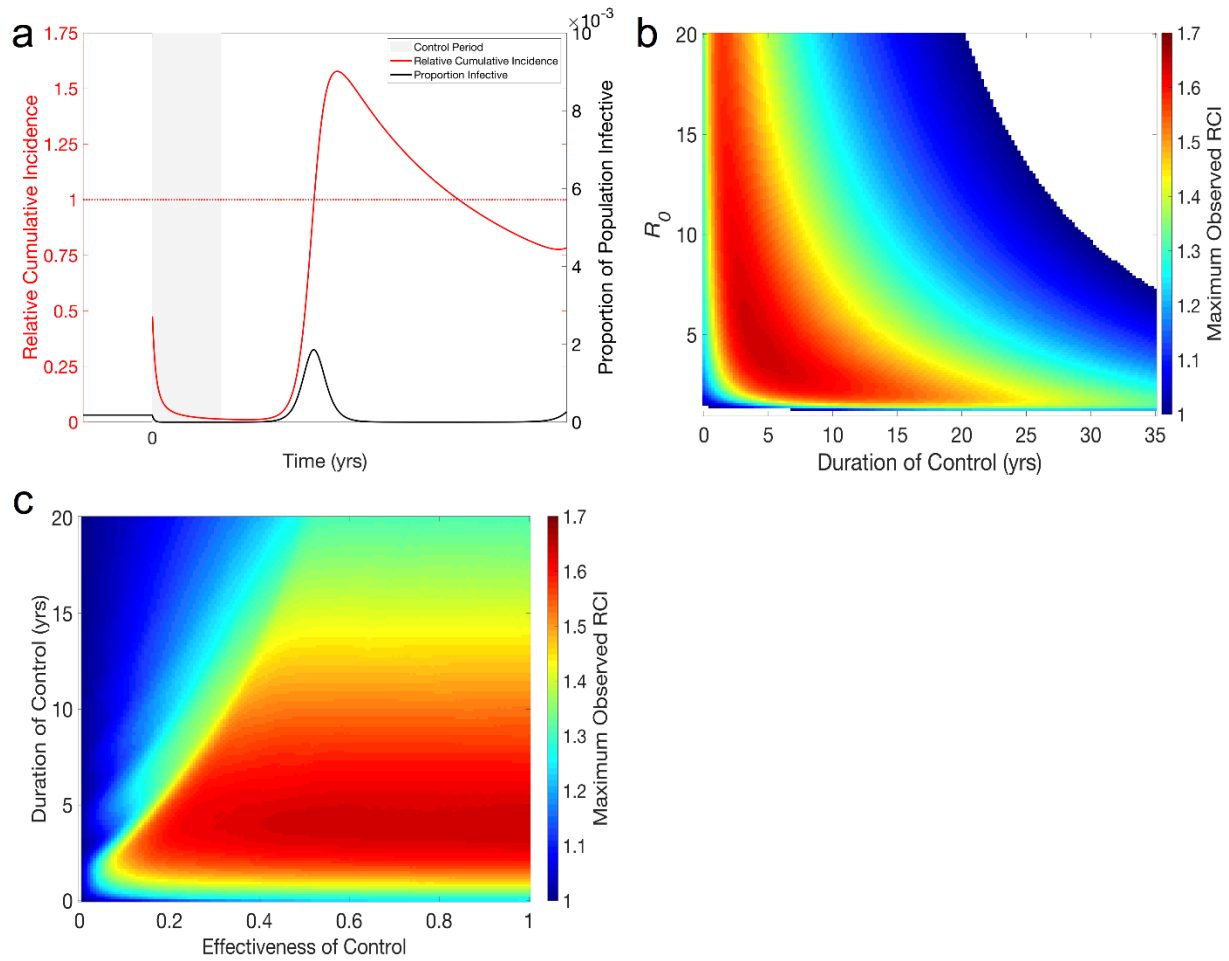
doi:10.1017/S0950268800067170

9. Pandey A, Medlock J. The introduction of dengue vaccine may temporarily cause large spikes in prevalence. *Epidemiol Infect.* 2015;143: 1276–1286.  
doi:10.1017/S0950268814001939
10. Okamoto KW, Gould F, Lloyd AL. Integrating Transgenic Vector Manipulation with Clinical Interventions to Manage Vector-Borne Diseases. *PLOS Comput Biol.* 2016;12: e1004695. doi:10.1371/journal.pcbi.1004695
11. Ferguson NM, Anderson RM, Garnett GP. Mass vaccination to control chickenpox: The influence of zoster. *Proc Natl Acad Sci USA.* 1996;93: 7231–7235.  
doi:10.1073/pnas.93.14.7231
12. Ferguson NM, Nokes DJ, Anderson RM. Dynamical complexity in age-structured models of the transmission of the measles virus: Epidemiological implications at high levels of vaccine uptake. *Math Biosci.* 1996; doi:10.1016/S0025-5564(96)00127-7
13. Grenfell BT. Chance and Chaos in Measles Dynamics. *J R Stat Soc Ser B.* 1992;  
doi:10.1111/j.2517-6161.1992.tb01888.x
14. Dell AI, Pawar S, Savage VM. Systematic variation in the temperature dependence of physiological and ecological traits. *Proc Natl Acad Sci.* 2011;108: 10591–10596.  
doi:10.1073/pnas.1015178108
15. Mordecai EA, Cohen JM, Evans M V., Gudapati P, Johnson LR, Lippi CA, et al. Detecting the impact of temperature on transmission of Zika, dengue, and chikungunya using mechanistic models. *PLoS Negl Trop Dis.* 2017;11: e0005568.  
doi:10.1371/journal.pntd.0005568
16. Mordecai EA, Paaijmans KP, Johnson LR, Balzer C, Ben-Horin T, de Moor E, et al.

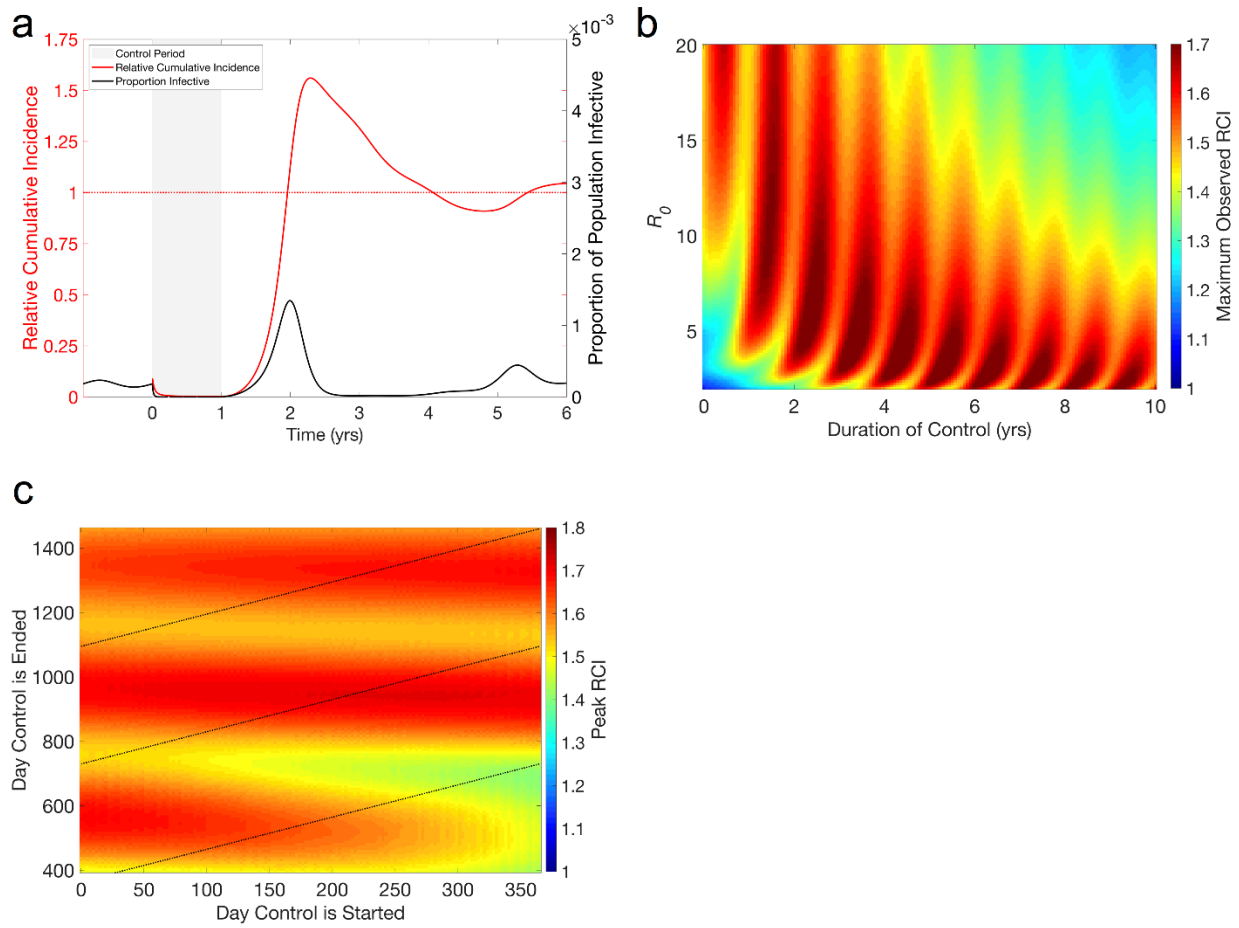
- Optimal temperature for malaria transmission is dramatically lower than previously predicted. *Ecol Lett.* 2013;16: 22–30. doi:10.1111/ele.12015
17. Hladish TJ, Pearson CAB, Patricia Rojas D, Gomez-Dantes H, Halloran ME, Vazquez-Prokopec GM, et al. Forecasting the effectiveness of indoor residual spraying for reducing dengue burden. *PLoS Negl Trop Dis.* 2018;12: e0006570. doi:10.1371/journal.pntd.0006570
  18. Bacaer N, Gomes G. On the Final Size of Epidemics with Seasonality. *Bull Math Biol.* 2009;71: 1954–1966. doi:10.1007/s11538-009-9433-7
  19. Towers S, Vogt Geisse K, Zheng Y, Feng Z. Antiviral treatment for pandemic influenza: Assessing potential repercussions using a seasonally forced SIR model. *J Theor Biol.* 2011;289: 259–268. doi:10.1016/j.jtbi.2011.08.011
  20. Bowman LR, Donegan S, McCall PJ. Is Dengue Vector Control Deficient in Effectiveness or Evidence?: Systematic Review and Meta-analysis. *PLoS Negl Trop Dis. Public Library of Science;* 2016;10: e0004551. doi:10.1371/journal.pntd.0004551

## FIGURES

**Figure 2.1: The divorce effect in the SIR model. (a) Typical time-series showing the divorce effect.** Beginning at time zero, a year-long 50% reduction in the transmission parameter of an endemic infection ( $R_0 = 5$ ,  $\beta = 365$  /year,  $\gamma = 73$  /year) reduces prevalence of the infection to near zero for the length of the control, where it remains until time 1.5 yrs, at which point a large post-control outbreak occurs. RCI falls towards zero as prevalence remains low, but the post-control outbreak is large enough to bring RCI well above 1 (peak RCI is approx. 1.4). **(b) Magnitude of divorce effect in terms of relative cumulative incidence (RCI).** Maximum RCI is found as the highest value of RCI observed within 25 yrs following a 100% effective control of an infection with  $1 < R_0 < 20$  and lasting between 1 month and 35 years.  $RCI > 1$  indicates the divorce effect and we see that the divorce effect occurs across a large portion of the parameter space, and ubiquitously for controls lasting less than 20 years.  $\beta$  is varied to attain the desired  $R_0$ , all other parameters as in (a). **(c) Maximum RCI for a given effectiveness and duration of control.** The maximum RCI is found as the maximum observed RCI within 25 yrs after the end of a control that is between 0% and 100% effective and lasts between 1 month and 20 years ( $R_0=5$ ). The ridge between areas of high and low maximum RCI results from ineffective controls being maintained long enough for outbreaks due to the honeymoon effect depleting the population of susceptible individuals before the control periods end. All other parameters as in (a).



**Figure 2.2: The divorce effect in the seasonal SIR model. (a) Typical time-series showing the divorce effect.** Beginning at time zero, when the transmission parameter is at its maximum, a year-long 90% reduction in the transmission parameter of an endemic infection ( $R_0 = 5$ ,  $\beta_0 = 365$  /year,  $\beta_1 = .02$ ,  $\gamma = 73$ /year) is implemented at the beginning of a seasonal outbreak and reduces prevalence of the infection to near zero for the length of the control. Following the end of the control, a large outbreak, many times the size of the regular seasonal outbreaks, occurs during the next season. RCI falls towards zero as prevalence remains low while the control is in effect and rises above 1 during the large outbreak the following year (Maximum RCI = 1.2). **(b) Magnitude of divorce effect in terms of relative cumulative incidence (RCI).** Maximum RCI is found as the highest value of RCI observed within 25 yrs following a 100% effective control of an infection with  $1 < R_0 < 20$  and lasting between 1 month and 35 years.  $RCI > 1$  indicates the divorce effect and we see that the divorce effect occurs in most of the parameter space.  $\beta_0$  is varied to attain the desired  $R_0$ , with all other parameters as in (a). **(c) Effect of timing on the magnitude of the divorce effect.** Maximum RCI is the highest RCI observed within 25 yrs following a 100% effective control of an infection with  $R_0 = 10$  ( $\beta = 730$  /year, all other parameters as in (a)) beginning and ending on specified days. Dashed lines represent controls lasting either 1, 2, or 3 years. Unlike the non-seasonal SIR model (Figure 2.1), the magnitude of the divorce effect is not solely dependent on  $R_0$  and the length of the control. Maximum RCI is most sensitive to the day the control is ended, moderately sensitive to the day it is started, and only slightly sensitive to the length of the control. This is due to the timing of the end of the control determining the timing of the outbreak. We also see that continuing the control for another year often has little impact on the magnitude of the divorce effect.



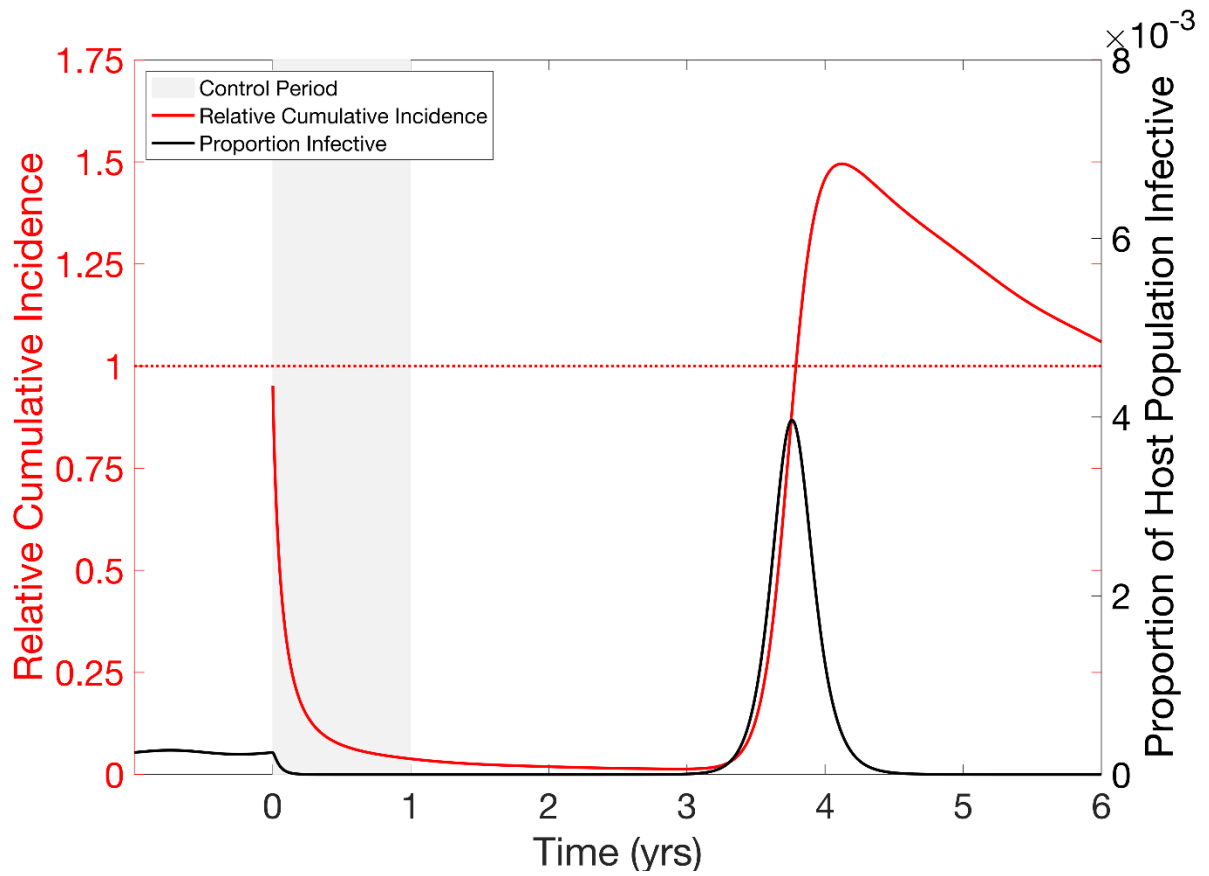
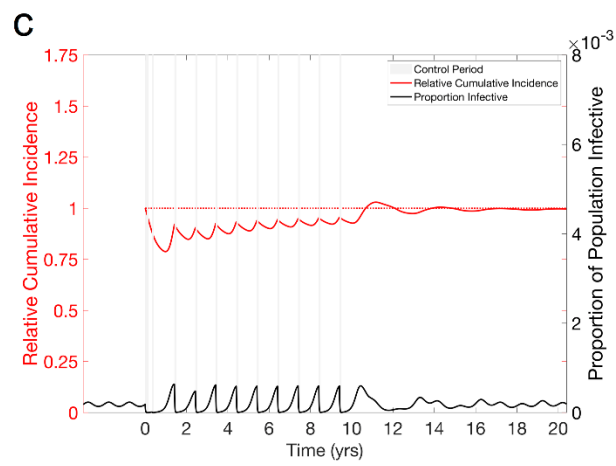
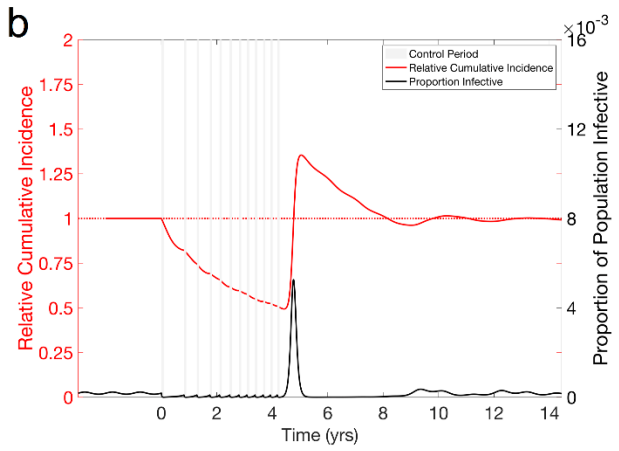
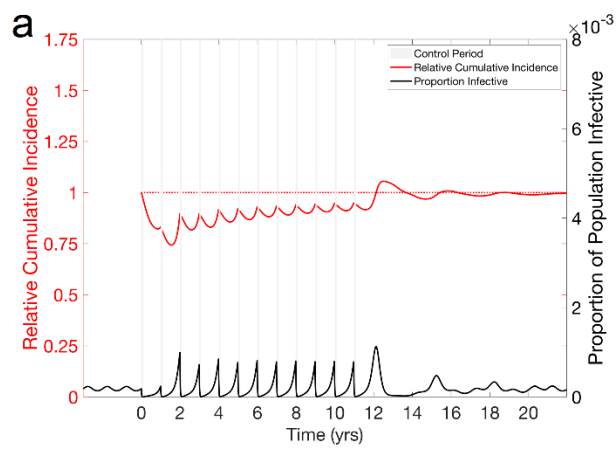


**Figure 2.3: Divorce Effect in a Seasonal Host-Vector model.** Control is shown in a seasonal ( $r_s = .02$ ) host-vector model with  $R_0 = 5$ . Beginning at time zero, a control is implemented that increases the vector mortality rate by 100% (corresponding to a 50% drop in vector life expectancy). This results in a reduction in prevalence (black curve) of the infection to near zero during the control period, where it remains until roughly time 3 yrs, at which point a large post-control outbreak occurs. RCI (red curve) falls towards zero during the control period and while prevalence remains low, but the post-control outbreak is large enough to bring RCI above 1 (peak of approx. 1.49).



**Figure 2.4: Suggested techniques for mitigating the divorce effect with seasonal transmission.** We consider an endemic disease, parameterized as in Figure 2.2(a). In all cases, twelve 1/12 yr. controls are used, to be consistent with the 1 yr. controls used in other figures, reducing the transmission parameter by 90% ( $\epsilon = .9$ ). **(a) Pulsed control for Seasonal SIR model.** Control occurs yearly at a fixed time (when  $R_0$  is highest) for a fixed time (1/12 yr.) to control an endemic disease (parameterized as in Figure 2.2(a)). The control is effective at stopping the outbreak the first year, but seasonal outbreaks in subsequent years are larger, driven by an increasing population of susceptible individuals. Stopping the control program still results in a large post-control outbreak and a divorce effect. **(b) Reactive Control for Seasonal SIR.** A fixed length (1/12 yr.) control is implemented to control an endemic disease (parameterized as in Figure 2.2(a)) once prevalence rises above a threshold (200 individuals in a population of 1 million). This stops the large early season outbreaks seen in the pulsed control, however the frequency of treatment increases as the susceptible population grows. Stopping the control program results in a large outbreak and divorce effect. **(c) Informed Control in seasonal SIR model.** The first control period occurs at time 0. The beginning of the next control period is decided at the end of the previous control period, and is the day (allowed to be up to a maximum of 365 days later) that will result in the smallest divorce effect if control was stopped after that period. This plan finds that it is optimal to perform the first few treatments relatively quickly, then to perform subsequent treatments during the peak in prevalence. We see that this is capable of nearly eliminating the Divorce Effect, but there is only a minimal benefit to the control, with large yearly outbreaks.



## SUPPLEMENTAL INFORMATION

### SIR Model with Changing Population Size

We assume a population similar to the SIR model in the main text, with the exception that the per capita birth and death rate are allowed to differ. We have

$$\begin{aligned}\dot{S} &= bN - \mu S - \beta \frac{S(I + I_b)}{N} \\ \dot{I} &= \beta \frac{S(I + I_b)}{N} - (\gamma + \mu)I \\ \dot{N} &= (b - \mu)N.\end{aligned}\tag{S1}$$

Here  $b$  is the per capita birth rate and  $\mu$  is the per capita death rate. For illustration, we take two values of  $b$ ,  $b = 1.25\mu$  and  $b = .75\mu$ , corresponding to 25% population growth or reduction per year. While this is an extreme case, we expect that any effect on the magnitude of the divorce effect would most likely be seen in the extremes. Since the endemic equilibrium is not well defined for a changing population, we simulate the population for a thousand years before starting control. Initial values of  $N$  were chosen so that at the end of the thousand years, the population size was  $1 \times 10^6$ . We see that the growth (Figure S2.16a), or decline (Figure S2.16b), of the population does not eliminate the divorce effect, but does affect the magnitude and timing of the post-control outbreak, with a larger and earlier post-control outbreak in the growing population due to a larger number of susceptible individuals being born.

### SIR Model with Vaccination

To model vaccination against infection, we assume that some portion,  $v$ , of births enter the recovered class instead of the susceptible class, while all other dynamics proceed similarly to the SIR model (Equations S2.2). For illustration, we take  $v = .5$  and assume the vaccination campaign lasts one year before being discontinued. We see that during the control period the proportion of the population that is infective falls significantly more slowly than with transmission reduction (Figure S2.17). Following the end of control, we see a series of post-control outbreaks that bring the infective proportion of the population above endemic levels, but they are not large enough to bring RCI above 1. This lack of divorce effect is due directly to the maintenance of population level immunity due to the vaccination, which keeps the susceptible

population from being able to build sufficiently. It is important to note that, as shown in Okamoto et al. [1], it is possible to see the divorce effect in combined controls that involve both immunizing and non-immunizing controls.

$$\begin{aligned}\dot{S} &= b(1 - v)(N - S) - \beta \frac{S(I + I_b)}{N} \\ \dot{I} &= \beta \frac{S(I + I_b)}{N} - (\gamma + \mu)I\end{aligned}\tag{S2}$$

### **SIRS Model**

We assume a well-mixed population with parameters defined as in the main text. However, instead of permanent immunity, we assume that immunity is lost at per-capita rate  $l$ , such that the average length of immunity following an infection is  $1/l$  (Equation S2.3). For the sake of illustration,  $l = 1/10 \text{ year}^{-1}$ , corresponding to an average of 10 years of immunity following recovery.

$$\begin{aligned}\dot{S} &= \mu(N - S) - \beta \frac{S(I + I_b)}{N} + lR \\ \dot{I} &= \beta \frac{S(I + I_b)}{N} - (\gamma + \mu)I \\ \dot{R} &= \gamma I - (\mu + l)R\end{aligned}\tag{S3}$$

Similar to the SIR model, we see suppression of the infection for a period of time during and immediately following the control (Figure S2.18). A large post-control outbreak is seen about 3 months after the end of treatment. This outbreak is sufficiently large to bring the RCI above 1, to about 1.45, before the outbreak subsides and prevalence and RCI fall again. As the immune period following infection shrinks towards zero, the SIRS model approaches the behavior of an SIS model. This results in the magnitude of the divorce effect being reduced as the immune period, and the population of immune individuals, becomes smaller.

### **Within-Host Virus Dynamics (HIV) Model**

We examine the divorce effect in the model for the within-host dynamics of HIV presented in Rong and Perelson [2], with all equations and parameters taken directly from their text (Equations 4 and Table 1). Here,  $T$  stands for the concentration of target cells,  $L$  for latently infected cells,  $T^*$  for actively infected cells,  $V_I$  for infectious virions, and  $V_{NI}$  for non-infectious

(defective) virions. Parameter names and values are given in Table 1. Here, cumulative incidence is in terms of actively infectious T cells. We see that the divorce effect does occur following a 25 day treatment that has both a protease inhibitor and reverse transcriptase inhibitor with efficacies of 50% (Figure S2.19).

$$\begin{aligned}
\dot{T} &= \lambda - d_T T - (1 - \epsilon_{RT}) k V_I T \\
\dot{L} &= \alpha_L (1 - \epsilon_{RT}) k V_I T - d_L L - a L \\
\dot{T}^* &= (1 - \alpha_L) (1 - \epsilon_{RT}) - \delta T^* + \alpha L \\
\dot{V}_I &= (1 - \epsilon_{PI}) N \delta T^* - c V_I \\
\dot{V}_{NI} &= \epsilon_{PI} N \delta T^* - c V_{NI}
\end{aligned} \tag{S4}$$

### Age-structured Model with Realistic Mixing

Here we show the presence of the divorce effect in an age-structured model with realistic mixing between groups. This model, and code, is from a tutorial given by Aaron King and Helen Wearing [3]. We assume that there 30 age-groups, with ages 0-19 occurring as single year age groups, 20-75 as 5 year age groups. Transitions between compartments occur according to Equation S5, note that we use  $\circ$  to denote elementwise multiplication. In which  $A$  is a matrix describing transitions between age classes, e.g. aging and deaths,  $b$  is a matrix describing births with a constant birth rate as its first element and zeros everywhere else. New-born susceptibles enter the youngest age class at a rate of  $b = 100/\text{year}$ , movement between the age classes takes on average 1 year for ages 0-20, 5 years for ages 21-75, and death occurs at a constant rate in the last age class, occurring on average after 15 years.  $S$ ,  $I$ , and  $R$  are vectors containing the numbers of individuals of each age class that are susceptible, infective, or immune, respectively.  $\beta$  is a matrix containing the transmission parameters for infection occurring within and between age classes, and is constructed by taking a matrix of age-specific contact rates and multiplying it by a constant rate of infection per contact. This contact network is based on [4] and freely available online, and the constant rate of infection per contact chosen so that  $R_0 = 5$ .  $\gamma$  is a vector containing the rate of recovery of individuals in each age class, but is assumed to be constant across all age classes and is the same as the main text ( $\gamma = 73/\text{year}$ ). Control works, as in the SIR model, by reducing the transmission parameter by 50% and lasts one year.

$$\begin{aligned}
\dot{S} &= -\beta I \circ S + AS + b \\
\dot{I} &= \beta I \circ S + AI - \gamma I \\
\dot{R} &= AR + \gamma I
\end{aligned} \tag{S5}$$

We see that, similar to the non-structured SIR model, there is a period of time, lasting about 4 years, in which RCI is falling, before a large outbreak brings RCI above 1 (Figure S2.20). Importantly, while the magnitude of the effect varies across groups, due to mixing, its presence does not.

## ANALYTICAL APPROXIMATION

Here we describe a crude analytical approximation for the magnitude of the divorce effect in the simplest setting of a non-seasonal directly transmitted infection (i.e. the SIR model), and based on the well-known analysis of the size of an outbreak in a closed population [5,6]. We assume that the post-control outbreak occurs immediately following the end of the control period and that the outbreak happens instantaneously. Further, we assume that control is perfect, so that there are no new cases of infection during the control period, and that all individuals that are infective before the control begins recover by the end of the control period. When control begins, the population can be subdivided into individuals that are susceptible and those that have previously been exposed and will be immune when the control is ended. Assuming  $R_0 > 1$ , the numbers in these two groups are determined by the endemic equilibrium, where  $S^* = N/R_0$  and  $R^* = N(1 - 1/R_0)$ . The number in the latter group decays exponentially due to mortality and the number of susceptibles grows at the same rate because of births (noting that the population size is taken to be constant). This gives the number of susceptible individuals at the time control ends,  $t_{\text{end}}$ , as

$$S = N \left( \frac{1}{R_0} + \left( 1 - \frac{1}{R_0} \right) (1 - e^{-\mu t_{\text{end}}}) \right) \tag{S6}$$

Once the control is ended, the infection is assumed to be reintroduced immediately by a small number of infectious individuals and occurs instantaneously, meaning that demography does not affect the final outbreak size. This means that the post-control outbreak size,  $Z$ , can be found by solving the familiar transcendental equation:

$$Z = S \left( 1 - e^{-R_0 \left( \frac{Z}{N} \right)} \right). \quad (S7)$$

The post-control outbreak size is then compared to the cumulative number of infections that would be expected in the endemic case to find the predicted RCI (Equation S8).

$$\text{RCI} = \frac{Z}{\mu N \left( 1 - \frac{1}{R_0} \right) t} \quad (S8)$$

### Results of Analytical Approximation

When compared to the simulations, our analytical approximation overestimates the magnitude of the divorce effect (Figure S2.21(a)). This is in direct contrast to simulations where the outbreak requires a long accumulation of infectives, often happens years later, and takes some time to occur. This approximation performs best in the most biologically relevant portion of parameter space ( $R_0 < 10$  and control lasting less than 20 years), where the error is generally below 20% (Figure S2.21(b)), however it performs very poorly for extremely short durations of control.

### Sensitivity to Background Force of Infection

Deterministic compartmental epidemiological models suffer from the well-known weakness that the numbers of infectives can fall to arbitrarily low levels. To combat this, a background force of infection is often included in such models, representing infections due to contact with populations outside the focal population [7]. In our model, this process is accounted for by adding  $I_b$  to the number of infectives in the transmission term. The background force of infection, which is taken to be small compared to the within-patch force of infection at the endemic state, ensures that there is a low level of transmission in the population, even as the number of infectives falls during the control period, and acts to reseed infection following control. In doing this, the background force of infection controls how quickly an outbreak will occur following the end of control, and hence can play an important role in determining the magnitude of the divorce effect. In general, a lower background force of infection means a later post-control outbreak, and often a larger divorce effect, while a higher background force of infection means an earlier post-control outbreak, less time for the build-up of the susceptible

population, and a smaller divorce effect. These effects are most noticeable for a short-lived control. At a sufficient level, the background force of infection is large enough to drive the overall dynamics of the system, eliminating the divorce effect. When this occurs, the dynamics become driven by exogenous factors, similar to a sylvatic infection, reducing the importance of local infections. In addition to affecting the magnitude of the divorce effect, increasing  $I_b$  increases the rate at which the system approaches its endemic equilibrium following the end of control. This results in subsequent outbreaks being increasingly diminished. For our manuscript, we choose to use a realistic value of  $I_b = 1$  for our models, compared to an endemic level of 183 infective individuals for these parameter values in the nonseasonal model. Figure S2.22 shows that for values of  $I_b$  that are sufficiently large to eliminate the divorce effect would require  $I_b$  to be roughly the same size as the endemic infection level.

It is well known that seasonally forced models are even more prone to having their numbers of infectives falling to low levels between outbreaks, with a background force of infection being commonly employed to counter this effect. Stronger seasonality magnifies this effect. Hence the background force of infection impacts the magnitude of the divorce effect, and given that the timing of control plays an important role in seasonal settings, there is an interaction between seasonality, the timing of the control, and the background force of infection in such cases. In general, as seasonality increases so does the difference between the maximum and minimum prevalence levels in the population. This results in an interaction between the background force of infection, the magnitude of seasonality, and the timing of the control determining the final magnitude of the divorce effect (Figures S2.8 and S2.23). This is important for predicting the magnitude of the divorce effect in real world situations, as there is a large amount of uncertainty associated with estimates of all three of these parameters. Importantly, below a specific background force of infection, the divorce effect is seen for all values of these parameters.



## References for Supplemental Information

1. Okamoto KW, Gould F, Lloyd AL. 2016 Integrating Transgenic Vector Manipulation with Clinical Interventions to Manage Vector-Borne Diseases. *PLOS Comput. Biol.* **12**, e1004695. (doi:10.1371/journal.pcbi.1004695)
2. Rong L, Perelson AS. 2009 Asymmetric division of activated latently infected cells may explain the decay kinetics of the HIV-1 latent reservoir and intermittent viral blips. *Math. Biosci.* **217**, 77–87. (doi:https://doi.org/10.1016/j.mbs.2008.10.006)
3. King AA, Wearing HJ. 2011 Age Structured Models.
4. Mossong J *et al.* 2008 Social contacts and mixing patterns relevant to the spread of infectious diseases. *PLoS Med* **5**. (doi:10.1371/journal.pmed.0050074)
5. Ma J, Earn DJD. 2006 Generality of the Final Size Formula for an Epidemic of a Newly Invading Infectious Disease. *Bull. Math. Biol.* **68**, 679–702. (doi:10.1007/s11538-005-9047-7)
6. Diekmann O, Heesterbeek JAP. 2000 *Mathematical Epidemiology of Infectious Diseases: Model Building, Analysis and Interpretation* - O. Diekmann, J. A. P. Heesterbeek.
7. Ferguson NM, Nokes DJ, Anderson RM. 1996 Dynamical complexity in age-structured models of the transmission of the measles virus: Epidemiological implications at high levels of vaccine uptake. *Math. Biosci.* (doi:10.1016/S0025-5564(96)00127-7)

## SUPPLEMENTAL FIGURES

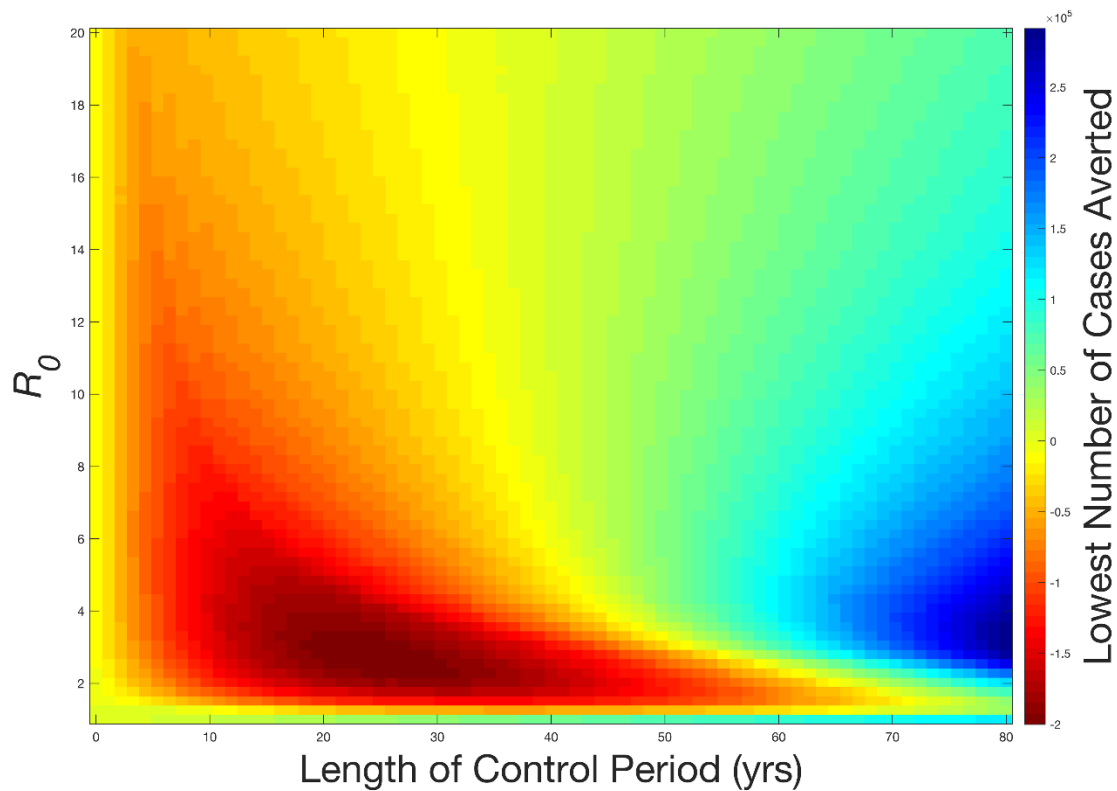


**Figure S2.1: Divorce effect in terms of cases averted.** All parameters the same as in Figure 2.1(b). When measuring the success of a control program in terms of Cases Averted as opposed to RCI, the overall results are retained, with negative values of cases averted corresponding to an  $RCI > 1$ . Parameters are as in Figure 2.1(b) for comparison.

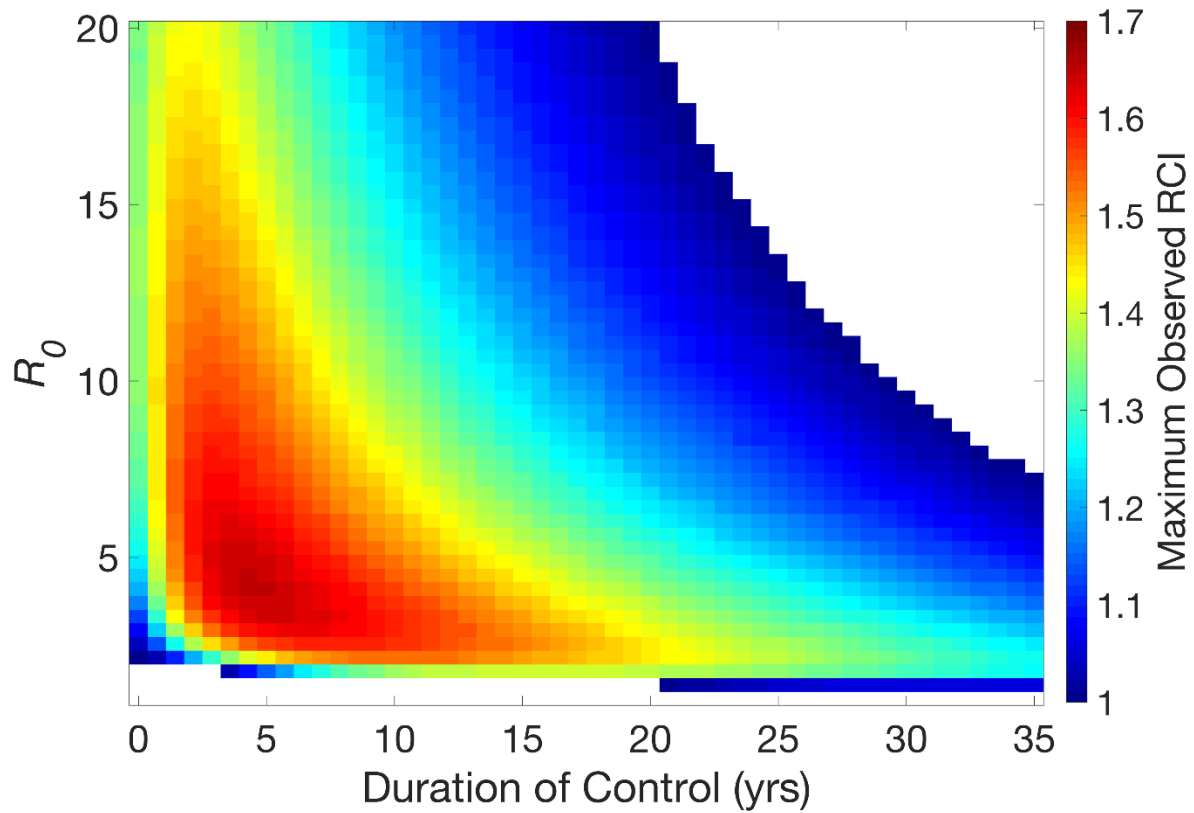


**Figure S2.2: Heat map of divorce effect from a control that increases recovery rate.** All parameters are as in Figure 2.1(b). The Divorce Effect is still observed if the control increases the recovery rate,  $\gamma$ , as opposed to decreasing the transmission parameter. All parameters the same as in Figure 2.1. Control increases  $\gamma$  to 730 (previously 73 /year).

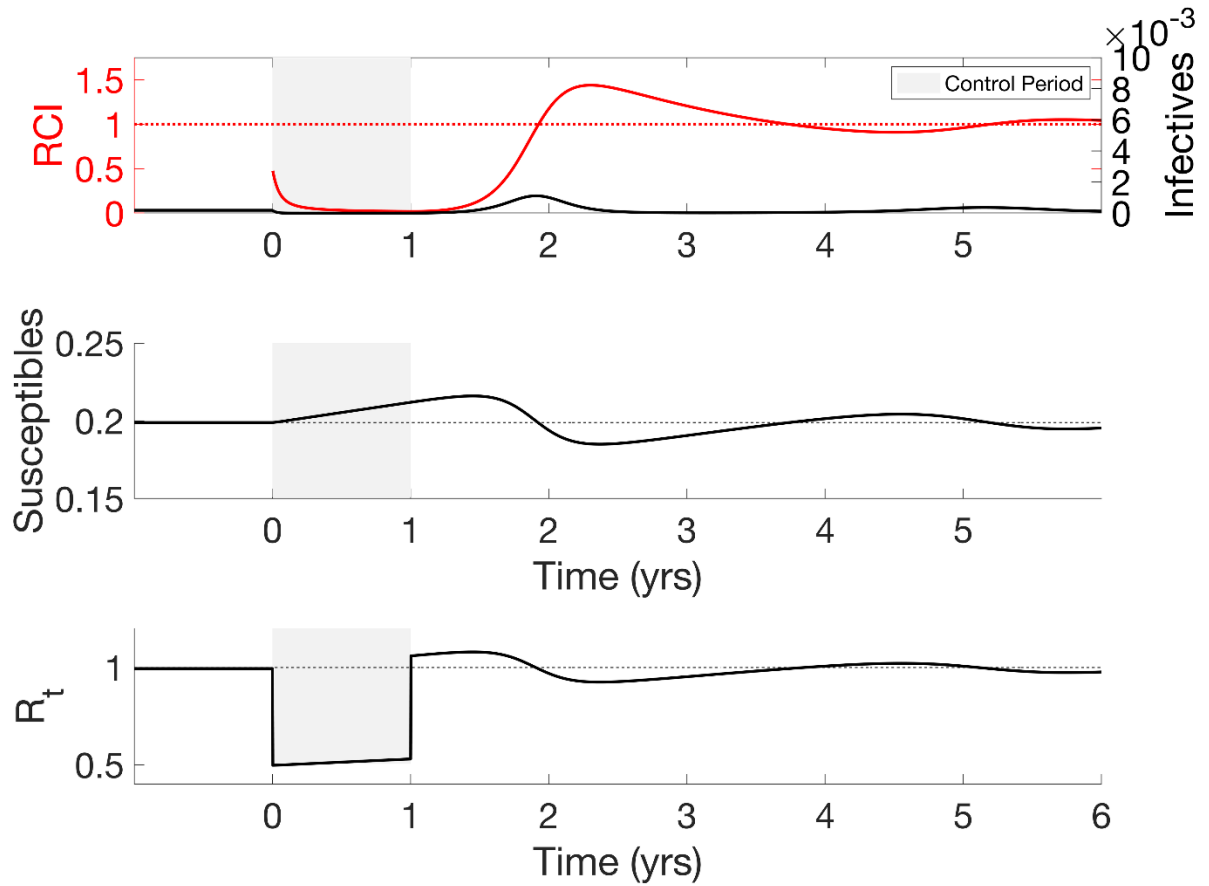


**Figure S2.3: Time-series showing the divorce effect in non-seasonal SIR model.** Figure corresponds to Figure 2.1(a) of the main text. Beginning at time zero, a year-long 50% reduction in the transmission parameter of an endemic infection ( $R_0=5$ ) reduces prevalence of the infection to near zero for the length of the control, where it remains until time 1.5 yrs, at which point a large post-control outbreak occurs. RCI falls towards zero as prevalence remains low, but the post-control outbreak is large enough to bring RCI well above 1 (approx. 1.6). Panel 2 shows that the susceptible population begins to rise during the control period and continues until the outbreak depletes the susceptible population. Likewise, the reproductive number at time  $t$ ,  $R_t$ , begins to rise during the control period. Once the control is released and the transmission rate retains its original value,  $R_t$  increases above one and continues to grow until an outbreak occurs.

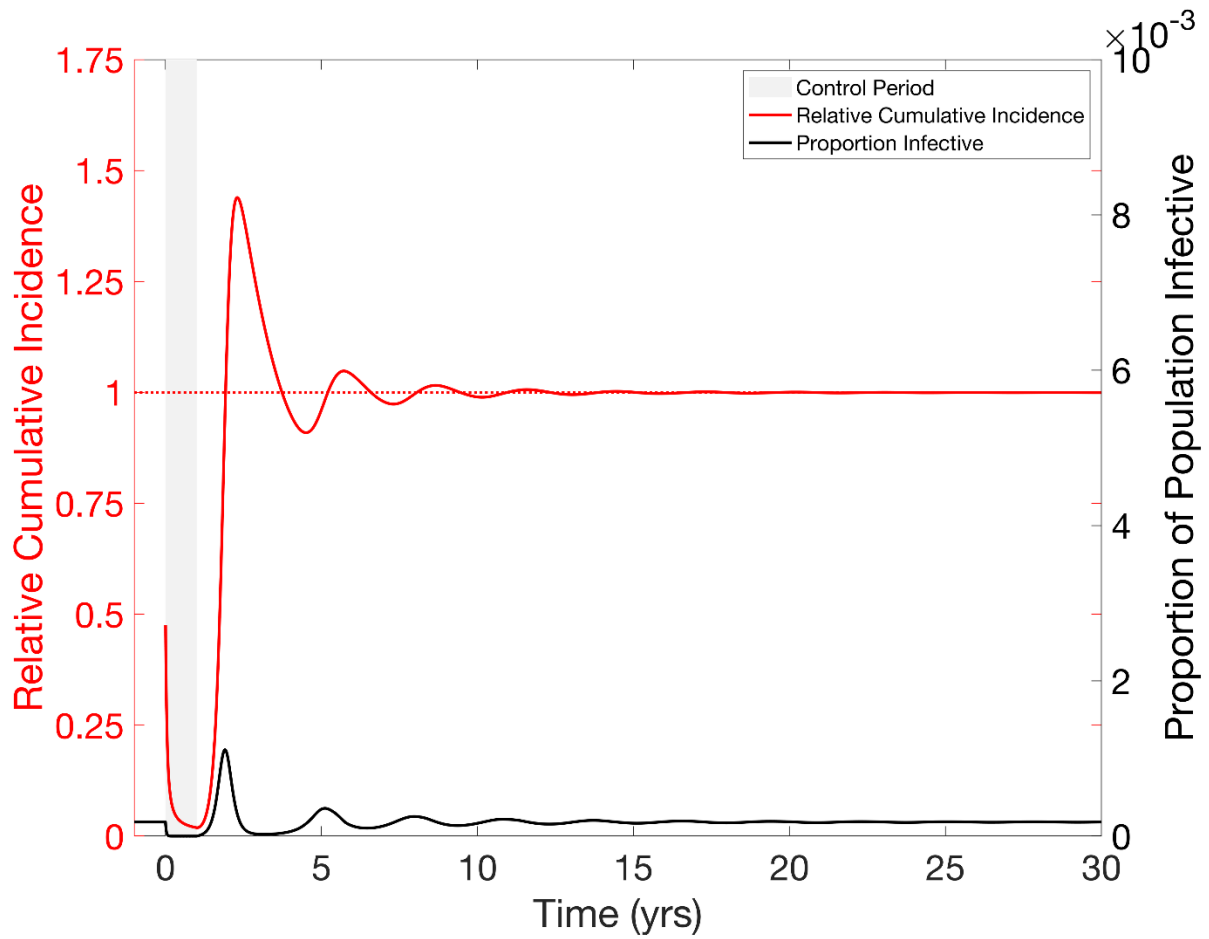


**Figure S2.4: Long-term time-series for the divorce effect in an SIR model.** Figure corresponds to Figure 2.1(a) of the main text. Following a one year control in which the transmission parameter is reduced by 50%, the host population continues to experience outbreaks that bring RCI above one until the infection approaches the endemic state and RCI approaches one.

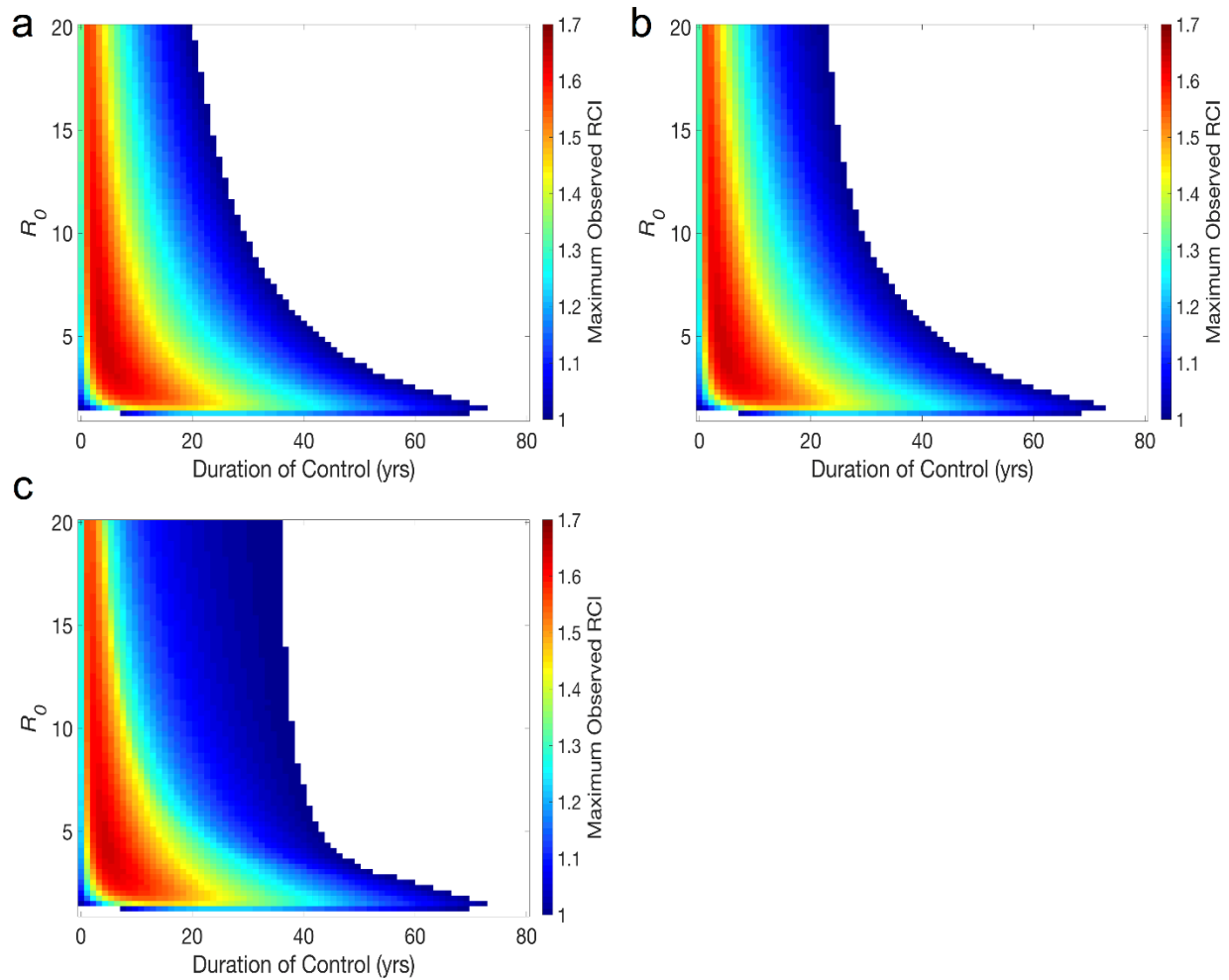


**Figure S2.5: Heat maps of divorce effect in SIR model for different strengths of control.**

We see that the Divorce Effect occurs in a significant area of the parameter space with controls that reduce the transmission parameter,  $\beta$ , by 100% (a), 75% (b), and 50% (c). In each case, the only way to avoid the divorce effect is to maintain control for more than 20 years (or approximately 40 years in the case of 50% control).

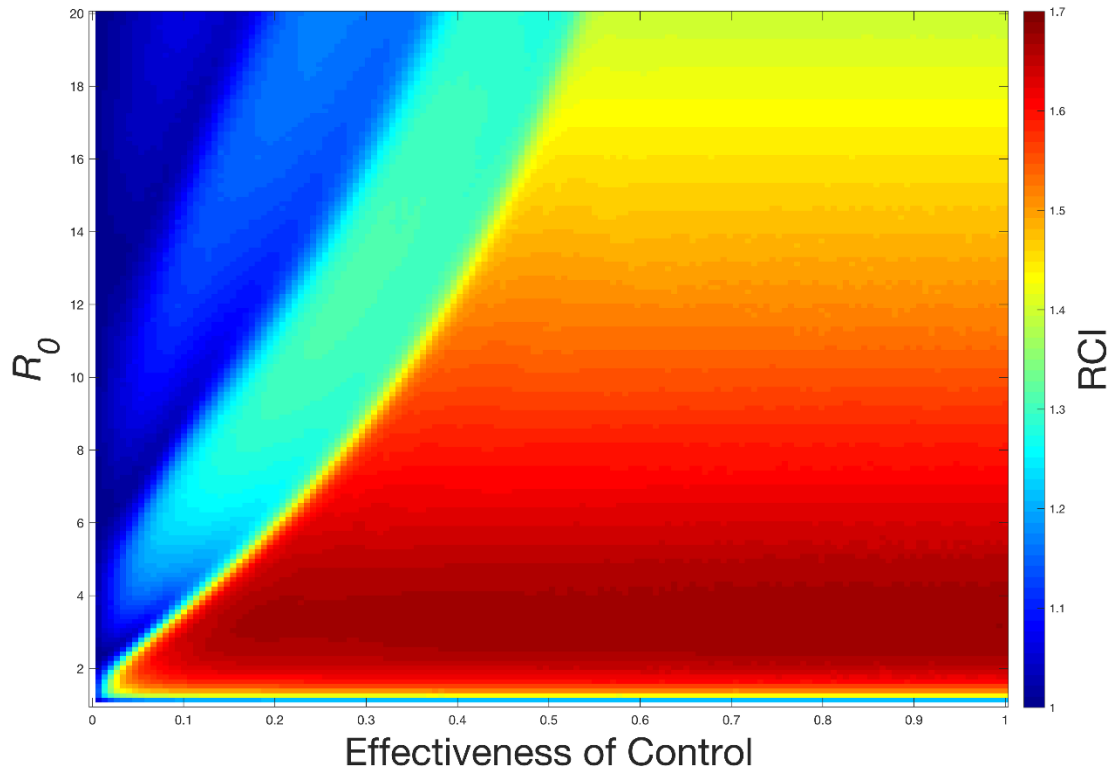


**Figure S2.6: Maximum RCI for a given effectiveness of control and  $R_0$ .** All controls are assumed to last for 1 year. The maximum RCI is found as the maximum observed RCI within 25 yrs after the end of a control that is between 0% and 100% effective for an infection with an  $R_0$  of between 0 and 20. The areas of lowered maximum RCI result from outbreaks due to honeymoon effect outbreaks depleting the population of susceptible individuals before the control periods end.

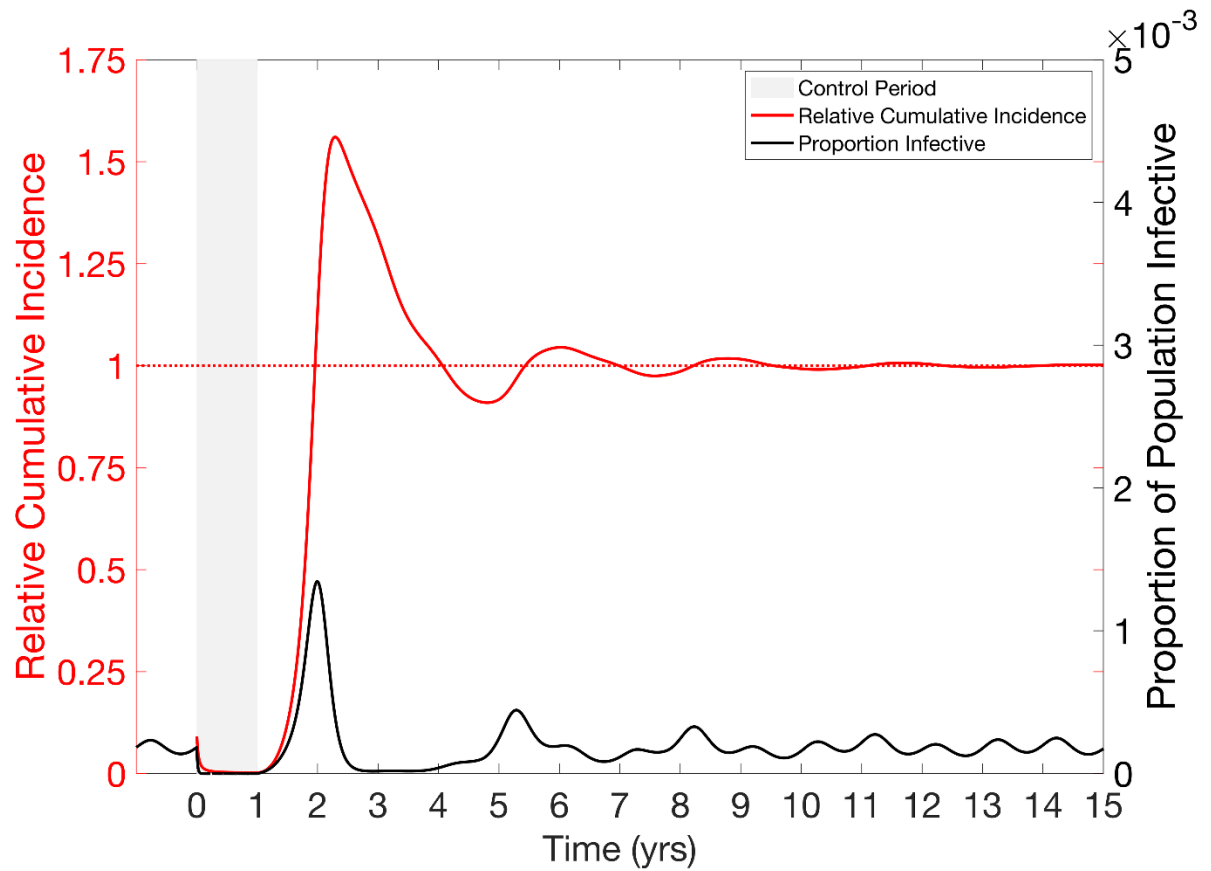
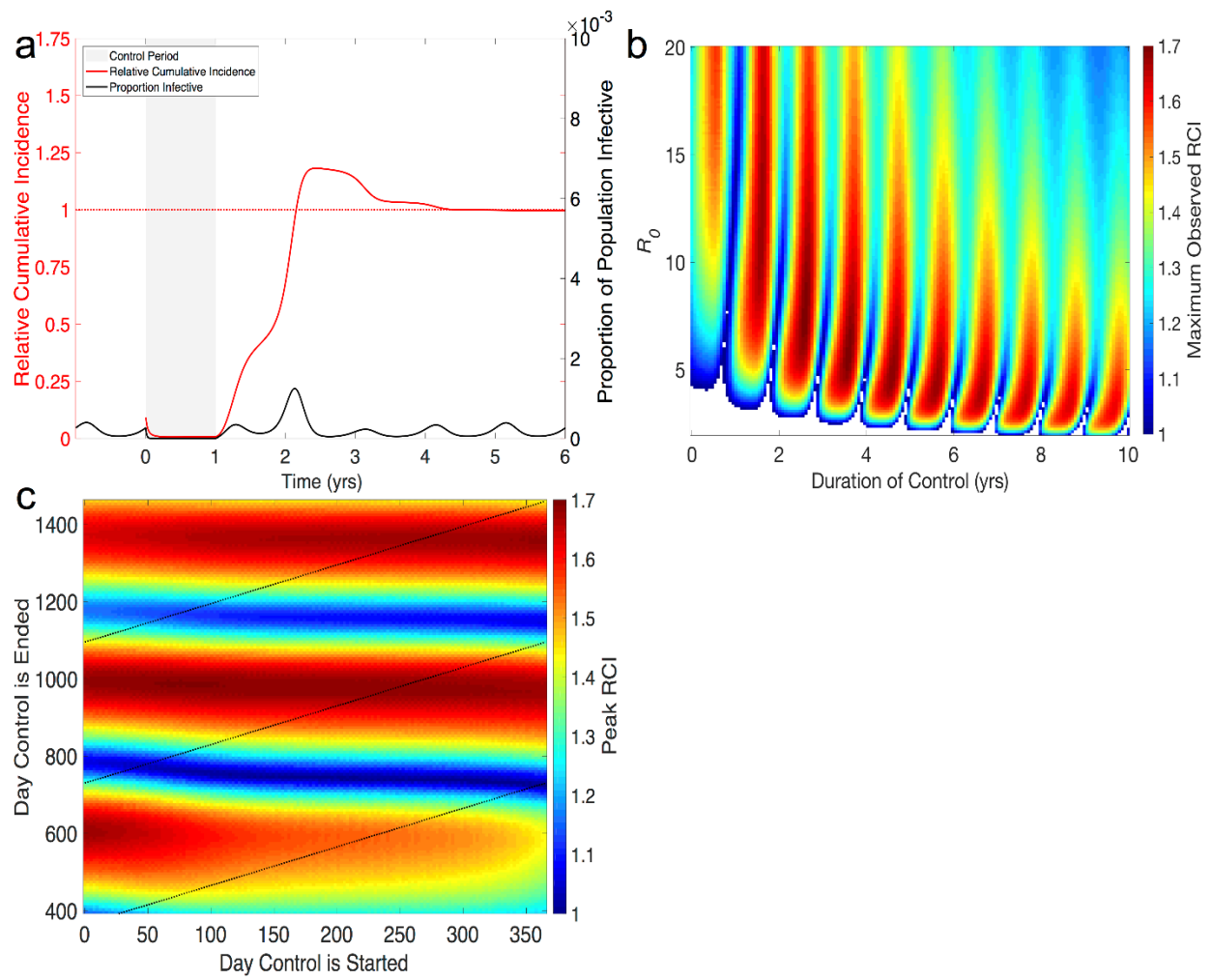


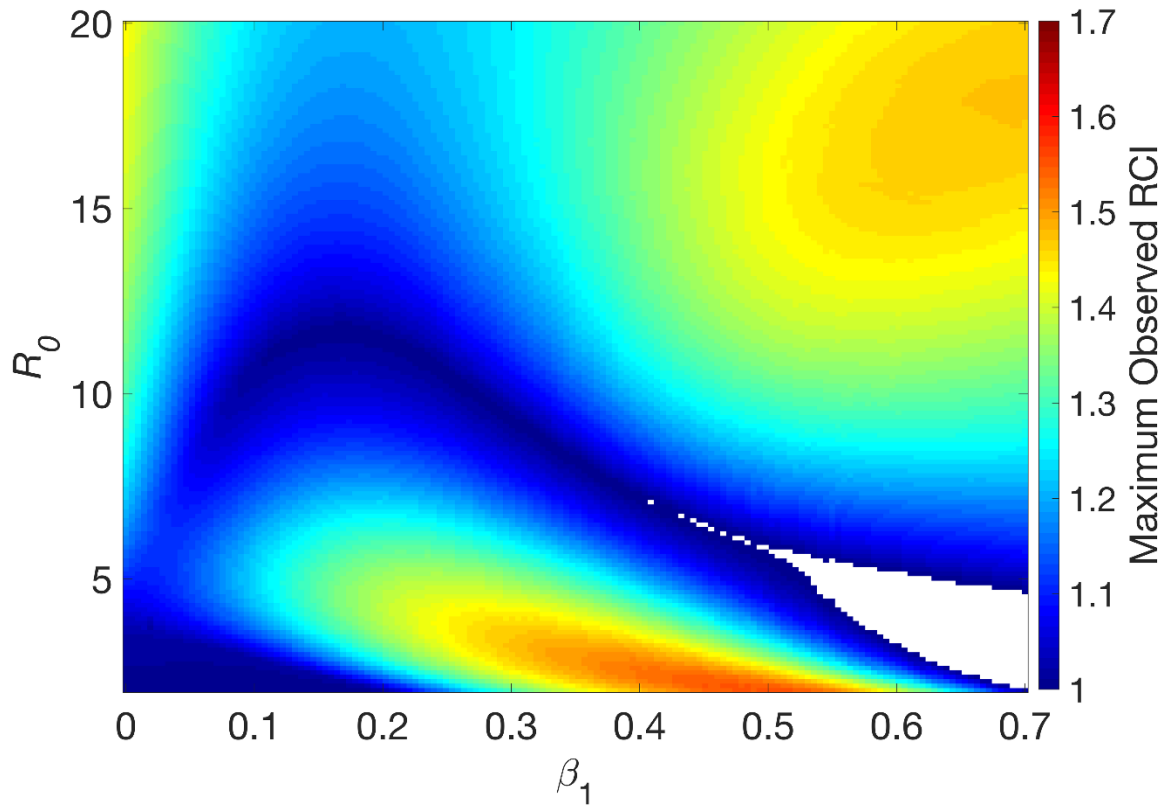
**Figure S2.7: Long-term time-series for the divorce effect in a seasonal SIR model.**

Following a one year control in which the transmission parameter is reduced by 50%, the host population continues to experience outbreaks that bring RCI above one until the infection approaches the endemic state and RCI approaches one.

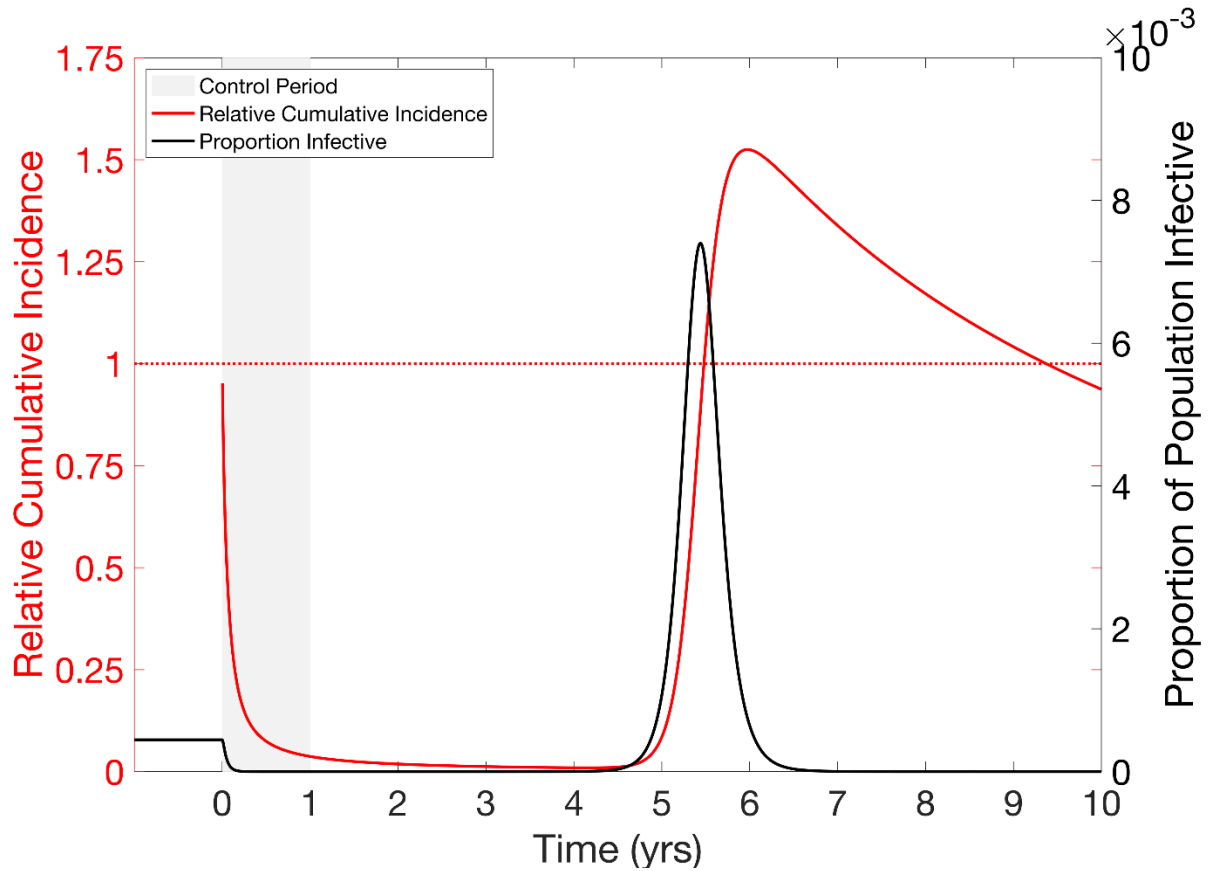


**Figure S2.8: The divorce effect in the seasonal SIR model with higher seasonality.**  $\beta_1 = .1$ ,  $I_b = 10$ , all other parameters as in Figure 2.2. Here a higher value of  $I_b$  is taken to adjust for the higher seasonality of the model. **(a) Typical time-series showing the divorce effect.** Beginning at time zero, when the transmission parameter is at its maximum, a year-long 90% reduction in the transmission rate of an endemic infection ( $R_0=5$ ) is implemented at the beginning of a seasonal outbreak and reduces prevalence of the infection to near zero for the length of the control. Following the end of the control, a small late season outbreak occurs, followed by a large outbreak during the next season. RCI falls towards zero as prevalence remains low while the control is in effect, rises slightly during the small late season outbreak, and rises above 1 during the large outbreak the following year. **(b) Magnitude of divorce effect in terms of relative cumulative incidence (RCI).** Maximum RCI is found as the highest value RCI observed within 25 yrs following a 100% effective control of an infection with  $1 < R_0 < 20$  and lasting between 1 month and 20 years.  $RCI > 1$  indicates the divorce effect and we see that divorce effect occurs in most of the parameter space. Unlike the SIR model (Figure 2.1), the magnitude of the divorce effect is not solely dependent on  $R_0$ . **(c) Effect of timing on the magnitude of the divorce effect.** Maximum RCI is the highest RCI observed within 25 yrs following a 100% effective control of an infection with  $R_0=10$  beginning and ending on specified days. Dashed lines represent controls lasting either 1, 2, or 3 years. Maximum RCI is most sensitive to the day the control is ended, moderately sensitive to the day it is started, and only slightly sensitive to the length of the control. This is due to the timing of the end of the control determining the timing of the outbreak. We also see that continuing the control for another year has little impact on the magnitude of the divorce effect.



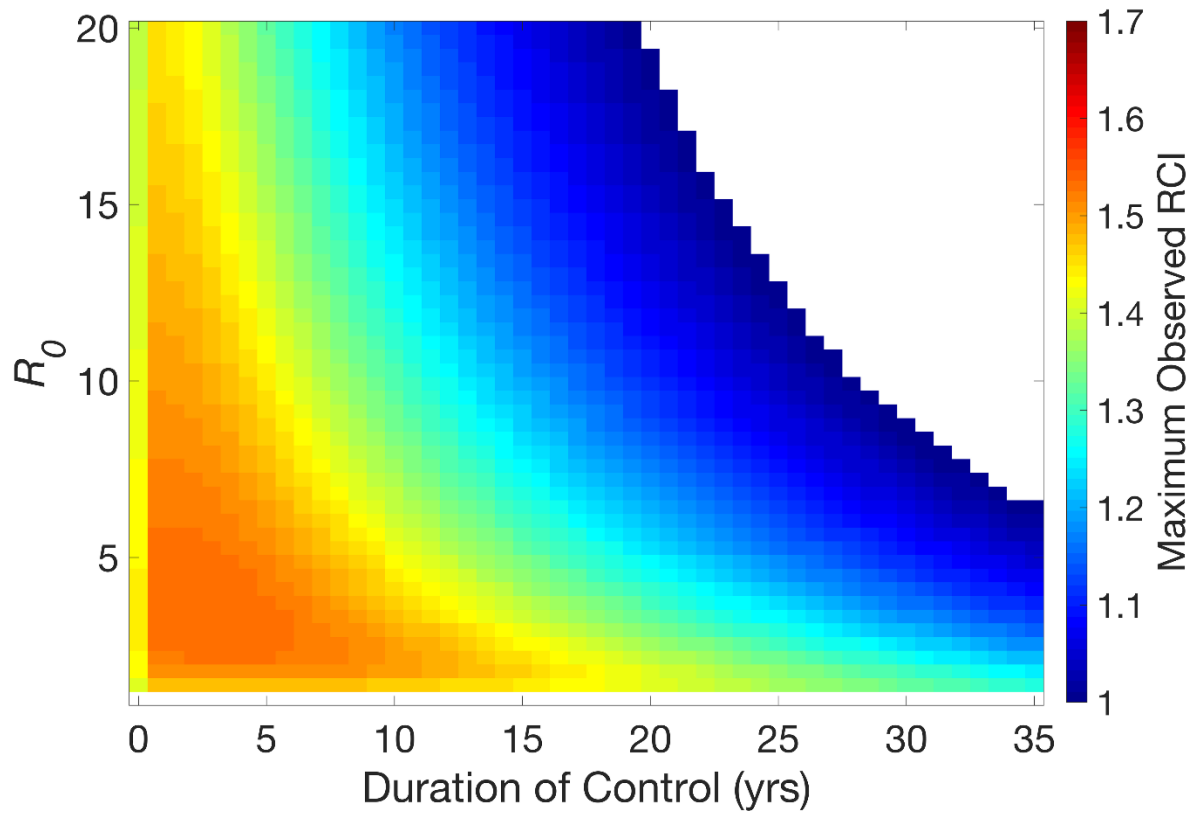


**Figure S2.9: Maximum RCI for a given basic reproductive number and seasonality in the directly transmitted model.** All controls are assumed to increase the vector mortality rate by 100% and to last for 1 year. The vector reproductive rate is assumed to have some average rate,  $r$ , and some level of seasonality ( $r_s$ ). The maximum RCI is found as the maximum observed RCI within 25 yrs after the end of a control. Here we see that the divorce effect is present throughout most of the parameter space.

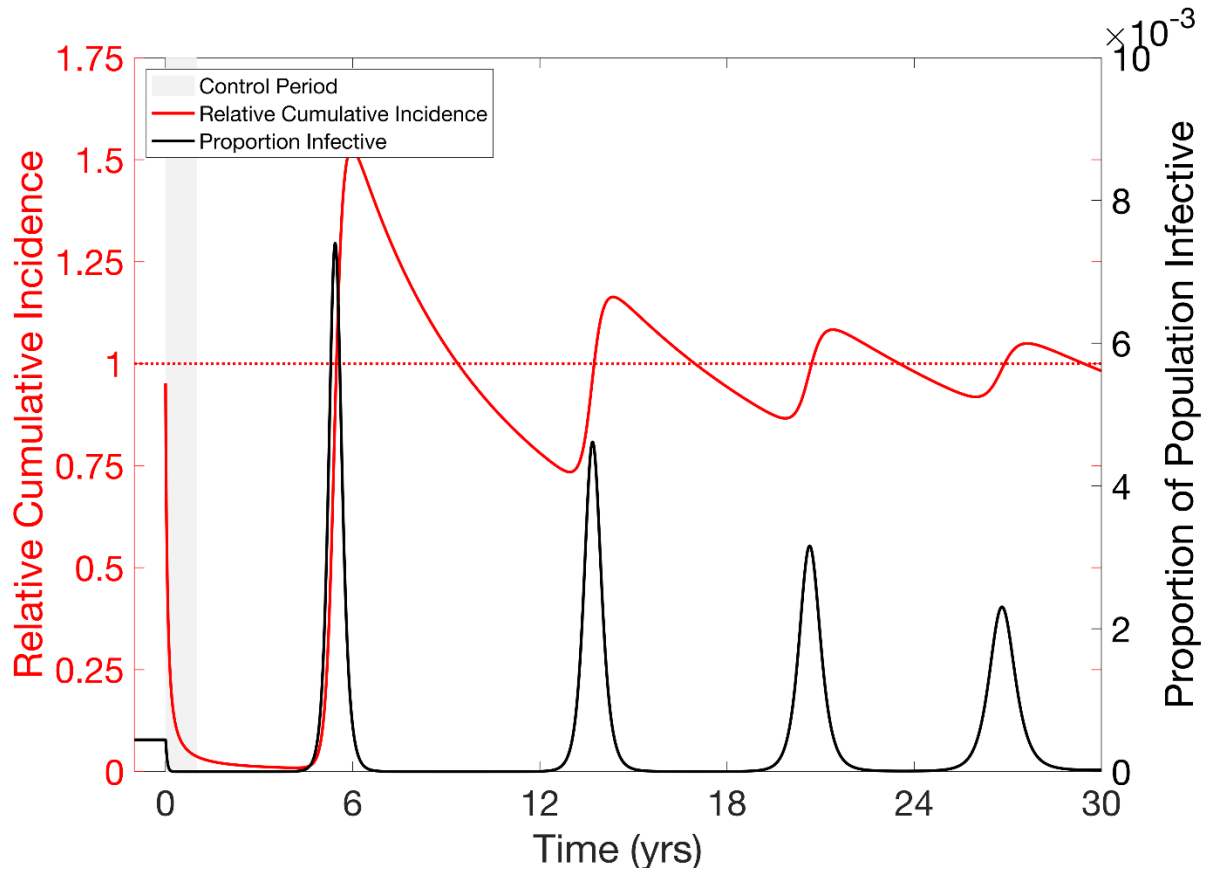


**Figure S2.10: Time-series of the divorce effect in a non-seasonal vector-borne infection.**

Figure shows the result of the non-seasonal host-vector model given in main text. Following a year of control, against an endemic infection ( $R_0 = 5$ ), in which the vector lifespan is reduced by 50% ( $\delta = 73/\text{year}$  increased from  $\delta = 36.5/\text{year}$ ) incidence is reduced to near zero. After the control is stopped, we see a post-control outbreak in year 3, resulting in the divorce effect (peak  $\text{RCI} \gg 1.5$ ).

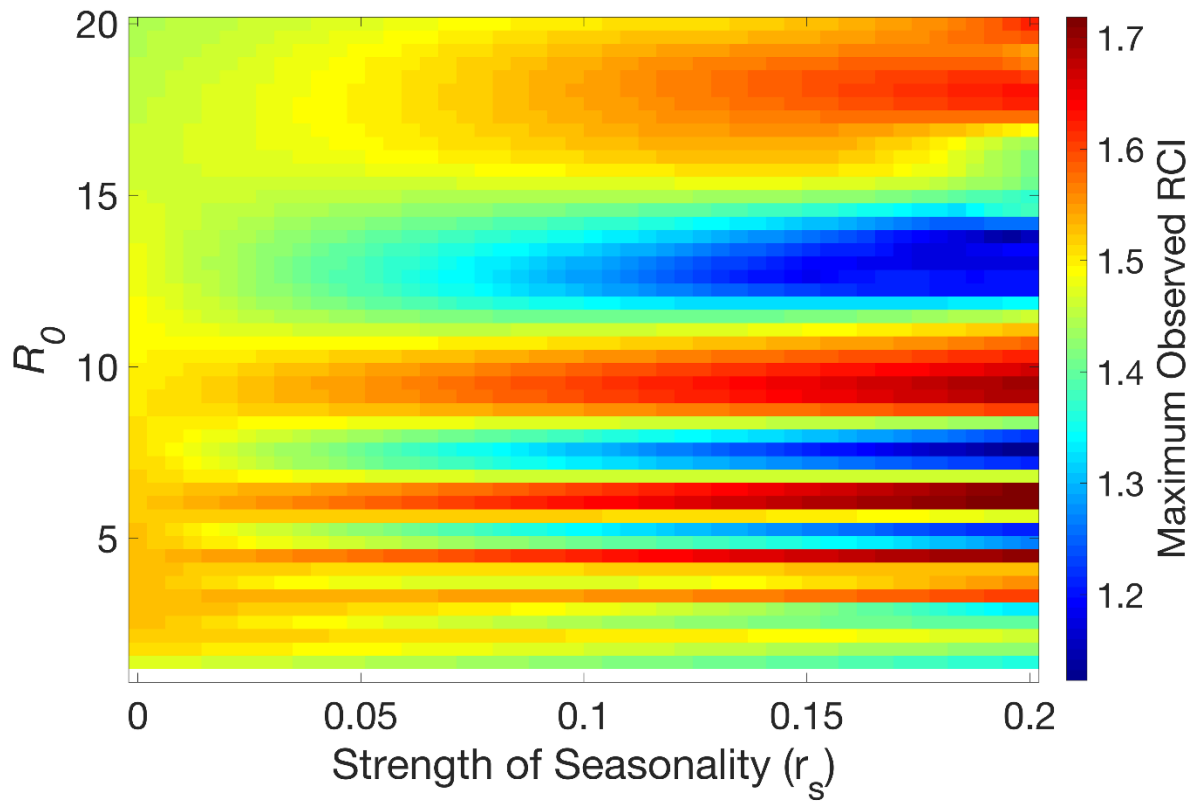


**Figure S2.11: Heat map for non-seasonal host-vector Model.** Maximum RCI is the highest RCI observed within 25 yrs following control of an infection with  $R_0 = 5$  beginning and ending on specified days. We see for the Host-Vector model that, much like the SIR model, the only way to avoid the divorce effect is to maintain control for more than 20 years. Parameters as given in the main text. Control decreases vector life-span by 50%.

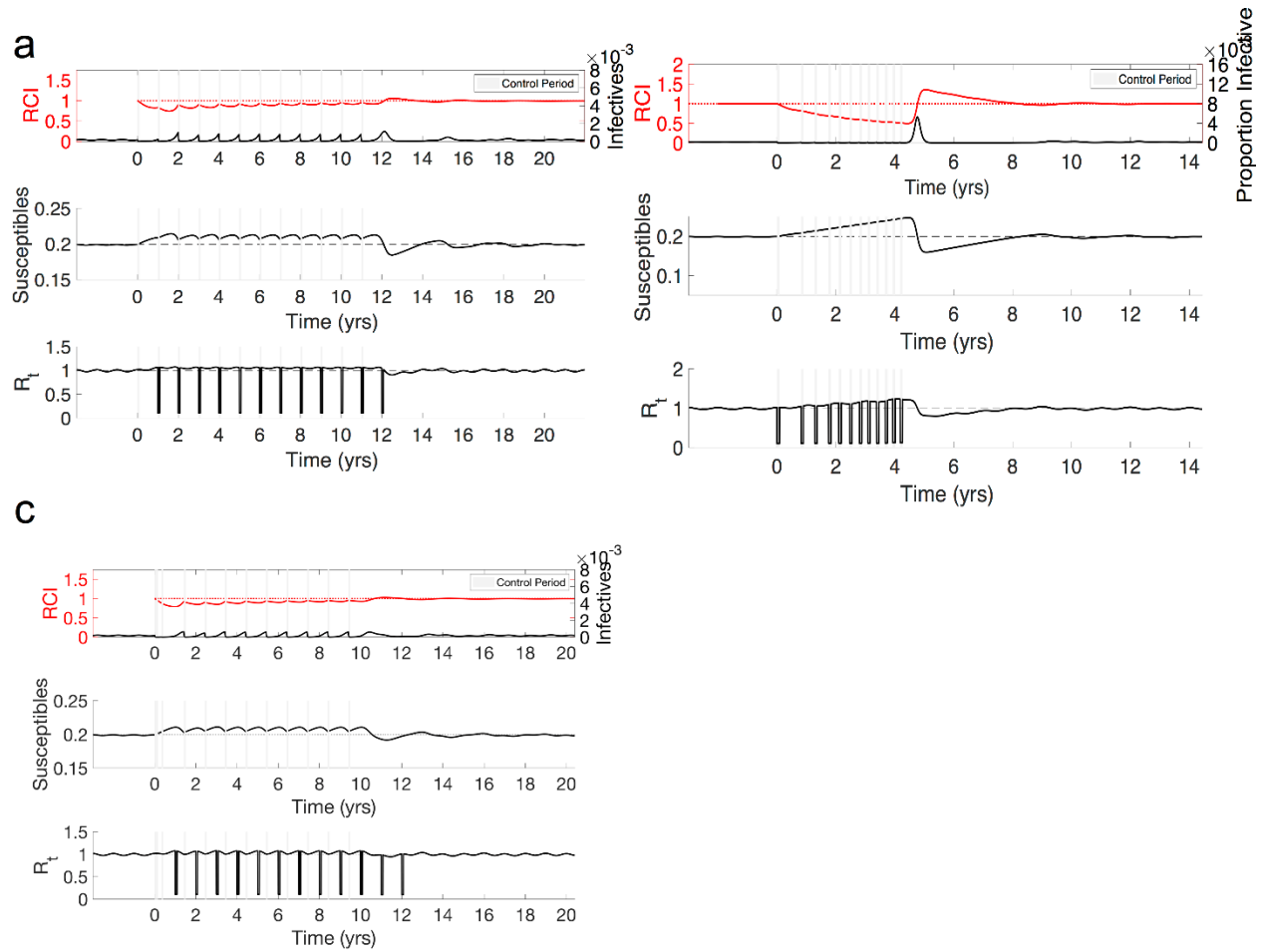


**Figure S2.12: Long-term time-series for the divorce effect in a seasonal host-vector model.**

All parameters are as in Figure 2.3 of the main text. Following a one-year control, a large outbreak occurs in year 3, that brings RCI above 1. This outbreak depletes the susceptible population, resulting in no outbreaks for the next five years. Each subsequent outbreak is sufficiently large to bring RCI above 1. Around year 30, the system is still experiencing larger than normal outbreaks, bringing RCI slightly above 1.



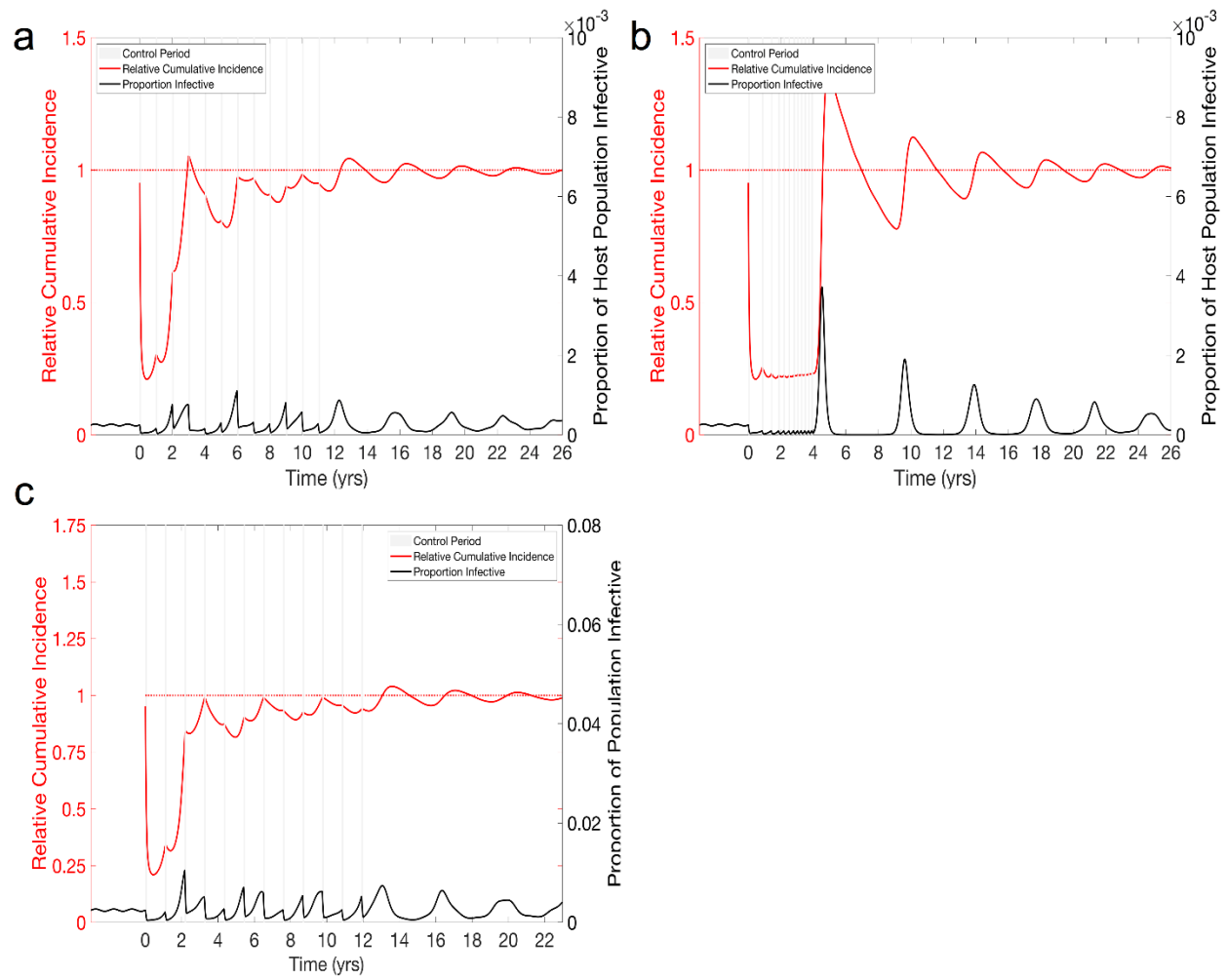
**Figure S2.13: Maximum RCI for a given basic reproductive number and seasonality in the host-vector model.** All controls are assumed to increase the vector mortality rate by 100% and to last for 1 year. The vector reproductive rate is assumed to have some average rate,  $r$ , and some level of seasonality ( $r_s$ ). The maximum RCI is found as the maximum observed RCI within 25 yrs after the end of a control. Here we see that the divorce effect is present throughout the parameter space.



**Figure S2.14: Suggested techniques for mitigating the divorce effect in the seasonal SIR model.** In the pulsed (a), reactive (b), and informed (c) techniques, we see the susceptible population begin growing with the first treatment and continue growing until the outbreak occurs after the 12<sup>th</sup> treatment, at which the susceptible population is quickly depleted. Likewise, the reproductive number,  $R_t$ , increases overall during this time with seasonal fluctuations, and reductions due to control periods.



**Figure S2.15: Suggested techniques for mitigating the divorce effect in a seasonal host-vector model.** (a) **Pulsed control for seasonal SIR model.** Control ( $\sigma = 1$ ) occurs yearly at a fixed time (when  $R_0$  is highest) for a fixed time (1 mo.). The control is effective at stopping the outbreak the first year, but seasonal outbreaks in subsequent years are of varied magnitudes due to the susceptible population being depleted in some years and replenished in others. An outbreak in year 2 is large enough to result in the divorce effect. Stopping the control program results in a large post-control outbreak and a divorce effect. (b) **Reactive control for seasonal SIR.** A fixed length (1 mo.) control is implemented once prevalence rises above a threshold (200 individuals in a population of 1 million). This stops the large outbreaks seen in the pulsed control, however the frequency of treatment increases as the susceptible population grows, and all treatments are depleted within the first four years. Stopping the control program results in a large outbreak and divorce effect. For all panels twelve 1 mo. controls are used to be consistent with the 1 yr. controls used in other figures. (c) **Informed Control in seasonal Host-Vector model.** Control works by increasing vector mortality by 100% for 1 month. The first control period occurs at time 0. The beginning of the next control period is decided at the end of the control period, and is the day that will result in the smallest Divorce Effect if control is stopped after that period (a maximum of 1 year between treatments). We see that this is capable of nearly eliminating the Divorce Effect, but there is only a negligible benefit to the control, with large yearly outbreaks. Importantly, this plan recommends waiting the full year, suggesting that the optimal timing of the next treatment may occur after this period.



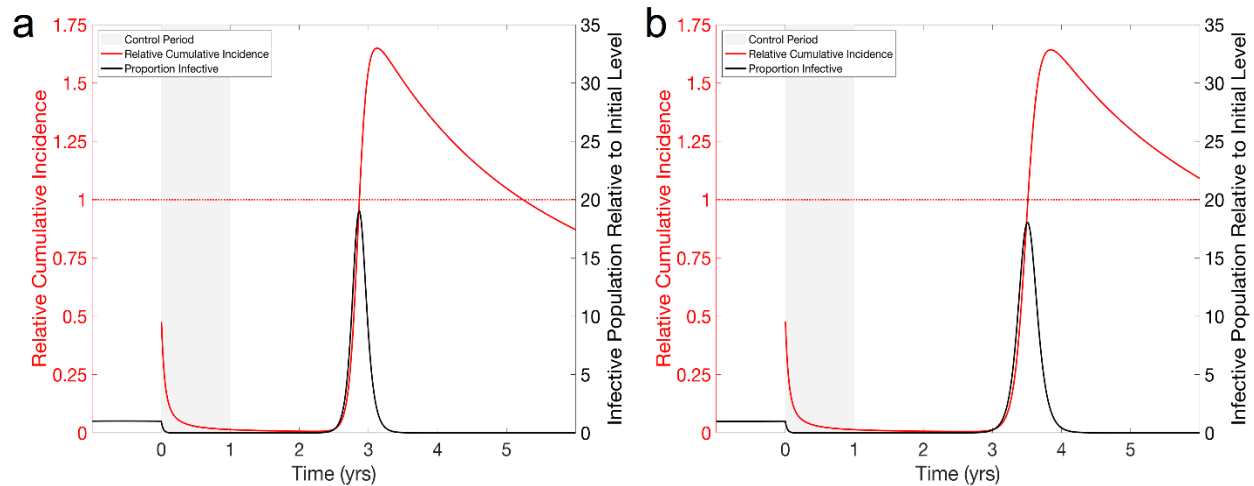


**Figure S2.16: The divorce effect in the SIR model with a (a) growing and (b) shrinking population.** The population is (a) growing or (b) shrinking during the simulation at a rate of 25% per year. Beginning at time zero, a year-long 50% reduction in the transmission parameter of an endemic infection ( $R_0=5$ ) reduces prevalence of the infection to near zero for the length of the control, where it remains until time 2.5 yrs (a) or 3 yrs (b), at which point a large post-control outbreak occurs. RCI falls towards zero as prevalence remains low, but the post-control outbreak is large enough to bring RCI well above 1 (peak RCI = 1.67 and 1.64 for the growing and shrinking population, respectively). Note that, because of the changing population sizes within and between graphs, prevalence of infection is plotted on a relative scale on both graphs.

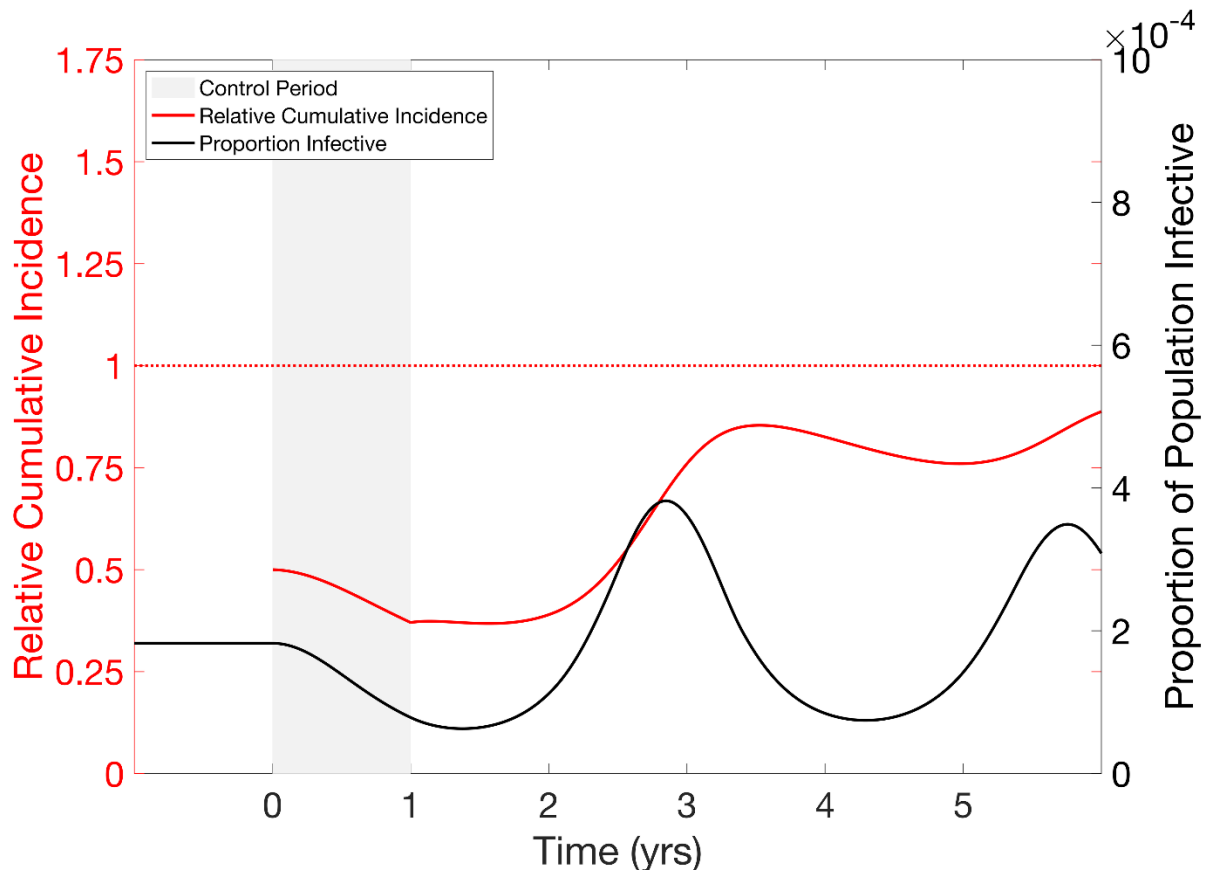


**Figure S2.17: Cessation of a vaccination program.** A vaccination program is put in place in which 50% of newborns are vaccinated for one year. All other parameters are as in Figure 2.1. The vaccination program is discontinued after the first year. While we see post-control outbreaks that bring incidence above the endemic level, they are not large enough to bring RCI above one, and RCI approaches 1 in the long run.

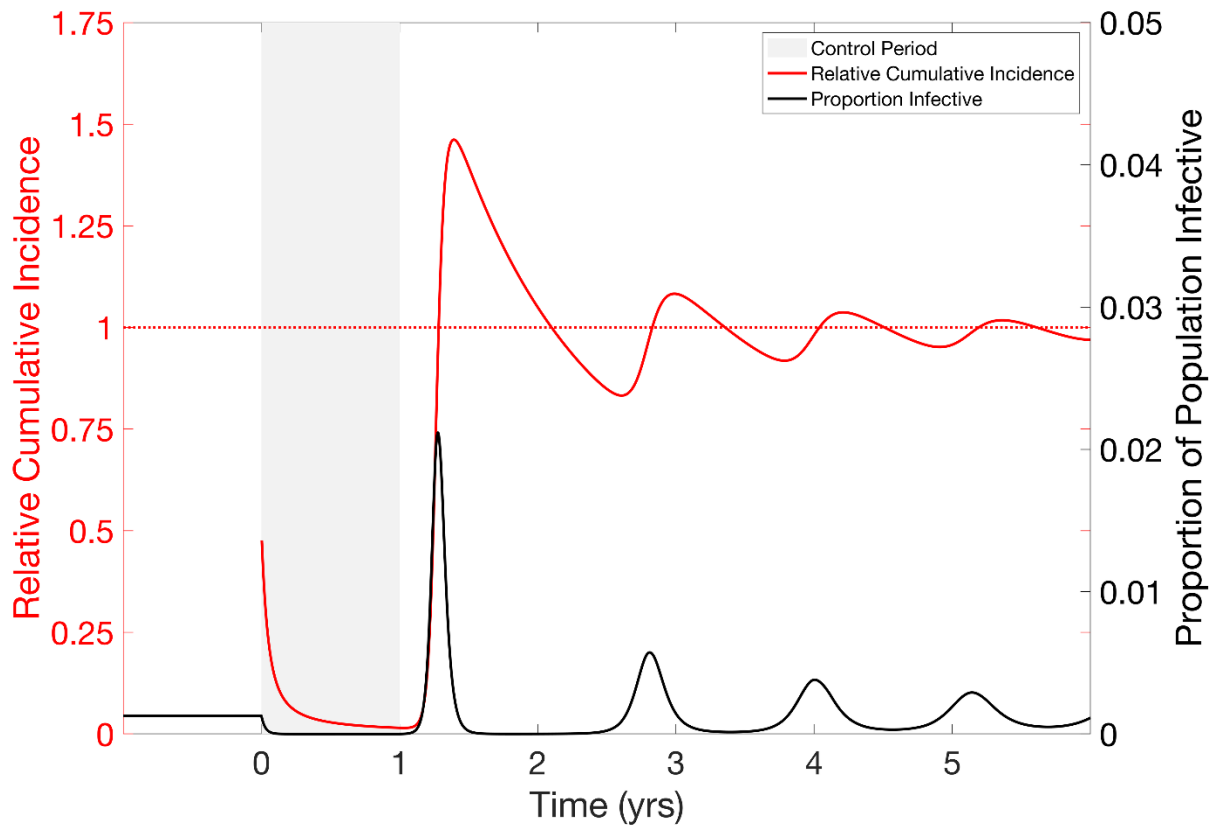


**Figure S2.18: Divorce effect in a SIRS model.** Beginning at time zero, a year-long 50% reduction in the transmission parameter of an endemic infection ( $R_0=5$ ) reduces prevalence of the infection to near zero for the length of the control, where it remains until time 1.5 yrs, at which point a large post-control outbreak occurs. RCI falls towards zero as prevalence remains low, but the post-control outbreak is large enough to bring RCI well above 1 (peak RCI is approx. 1.45).

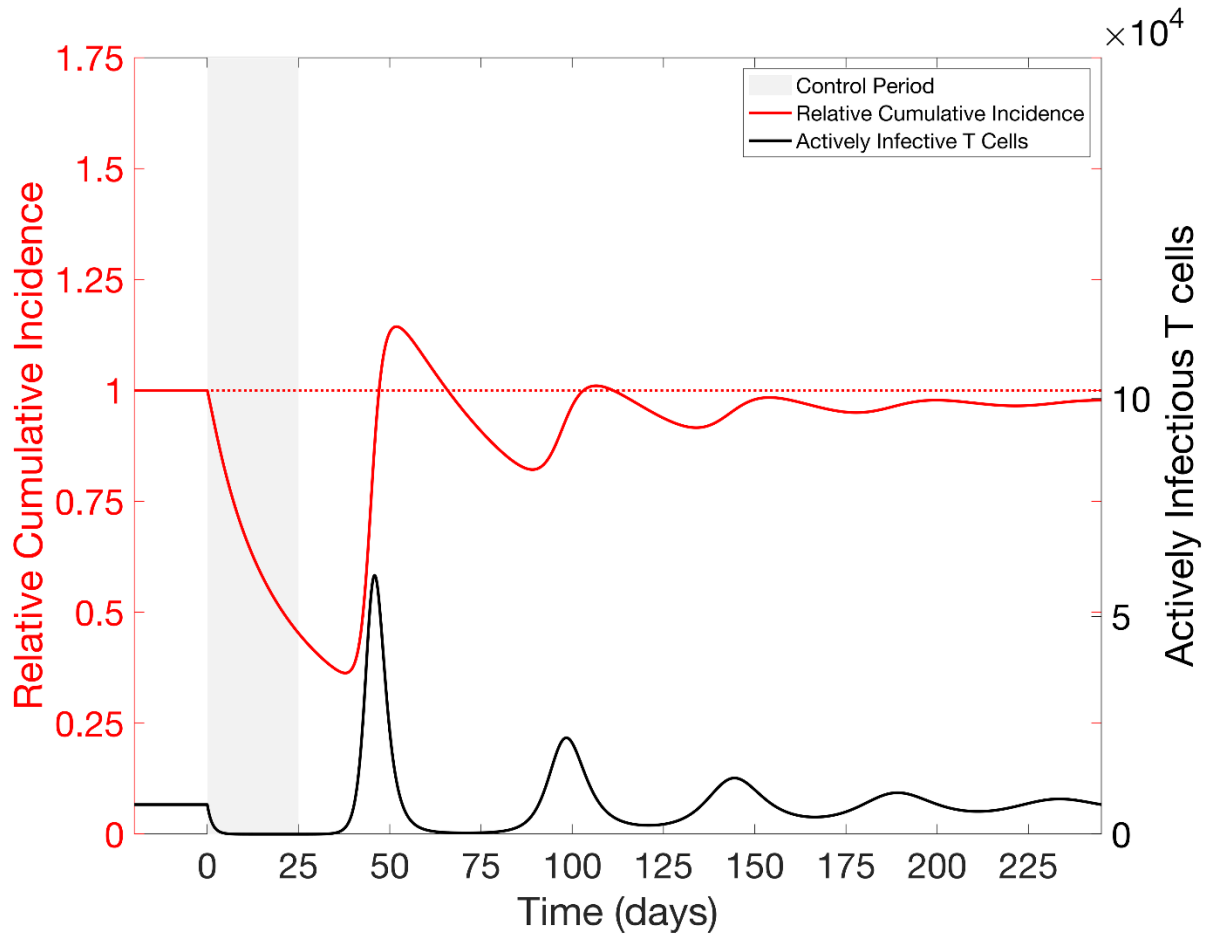


**Figure S2.19: Divorce effect in the within-host virus dynamics (HIV) model.** Beginning at time zero, a 25 day treatment occurs using a drug that combines a protease inhibitor and a reverse transcriptase inhibitor, both with 50% efficacy. This successfully reduces the infectious T cell count to near zero during and immediately following the treatment period. After the end of treatment, we see a transient increase in infectious T cells, bringing the relative cumulative incidence of T cell infection above one (max RCI»1.14). After years, RCI eventually approaches 1 from below.

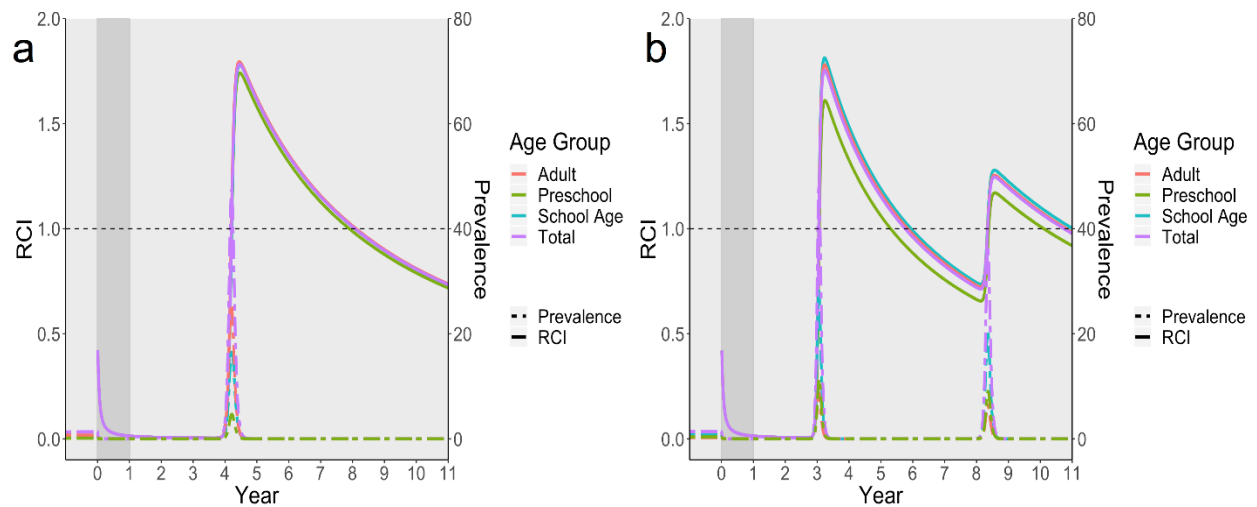


**Figure S2.20: Divorce effect in an age-structured SIR model with realistic mixing.** A control for a directly transmitted infection with  $R_0 = 5$  (a) and  $R_0 = 15$  (b) in a population of 9000 individuals is implemented at time 0, during which transmission is reduced by 50% for 1 year. At the end of the year, control is instantaneously removed. RCI quickly falls to 0 during the control period and remains there until a large outbreak in year 4 brings RCI up above 1 for all age groups. For the figure, prevalence, the number of individuals currently infective, (dashed lines) and RCI (solid lines) are shown for the total population, and age groups are shown aggregated into three groups: preschool (ages 0-5), school age (ages 6-18), and adult (ages 19+).

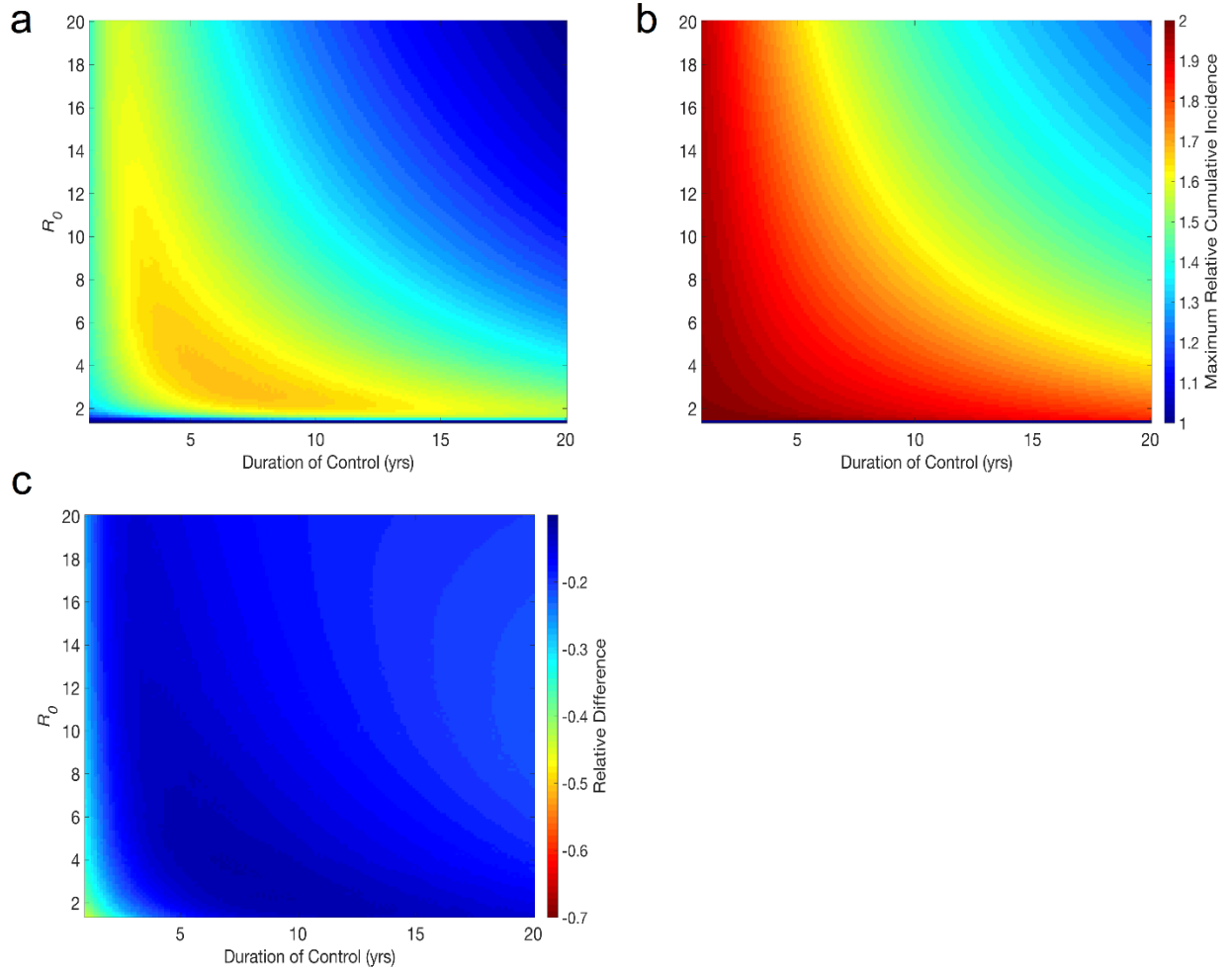


**Figure S2.21: Analytical approximation of the magnitude of the divorce effect. (a) Heat map of approximated and simulated magnitude of the Divorce Effect in terms of RCI.** The analytical approximation predicts the divorce effect for all controls lasting less than 20 years, similar to what is observed in the SIR model (Figure 2.1(b)). However, it overestimates the observed maximum RCI throughout the parameter space, and does so drastically for a short control in a system with  $R_0 < 3$ . **(b) Relative difference between the observed and predicted maximum RCI.** Calculated as (observed-predicted)/observed. The relative difference is small ( $< .25$ ) throughout most of the parameter space except for short controls in systems with  $R_0 < 3$ .



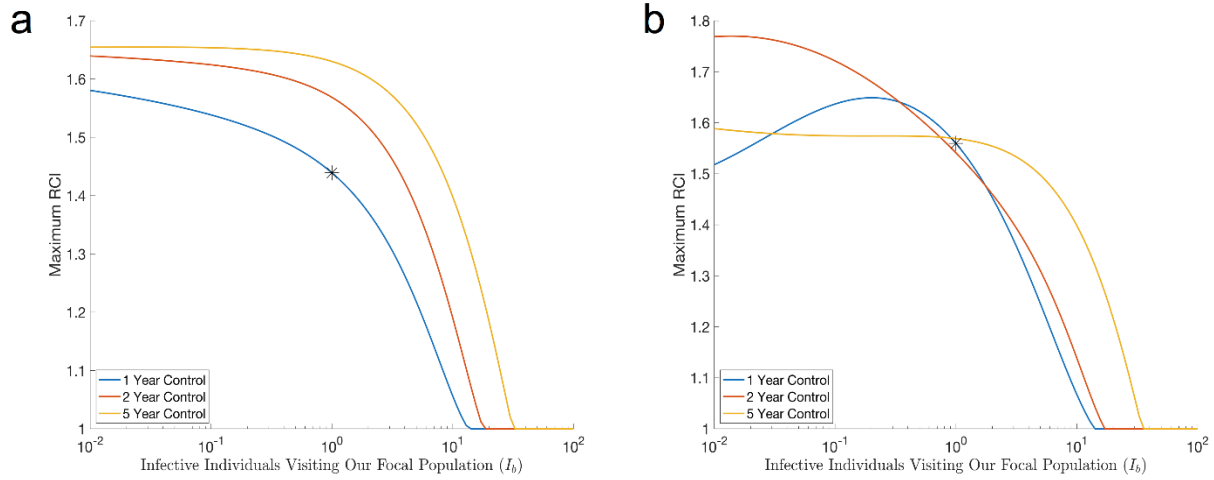


**Figure S2.22: Sensitivity of the magnitude of the divorce effect to the background force of Infection in the (a) non-seasonal and (b) seasonal SIR models.** Figure (a) is parameterized as in Figure 2.1(a) ( $R_0 = 5$ ) and (b) is parameterized as in Figure 2.2(a) ( $R_0 = 5$ ,  $\beta_1 = .02$ ). All controls are assumed to last one, two, or five years, beginning at  $t = 0$ . We see that for a sufficiently high number of infective individuals visiting our focal population ( $I_b$ ), the divorce effect is eliminated. We choose a seemingly realistic value of  $I_b = 1$  (stars) for our models, compared to an endemic level of 183 infective individuals for these parameter values in the nonseasonal model. This value will keep the number of infectives from falling to arbitrarily small values while not eliminating the divorce effect. We note that values of  $I_b$  that are sufficiently large to eliminate the divorce effect would require  $I_b$  to be roughly the same size as the endemic infection level.

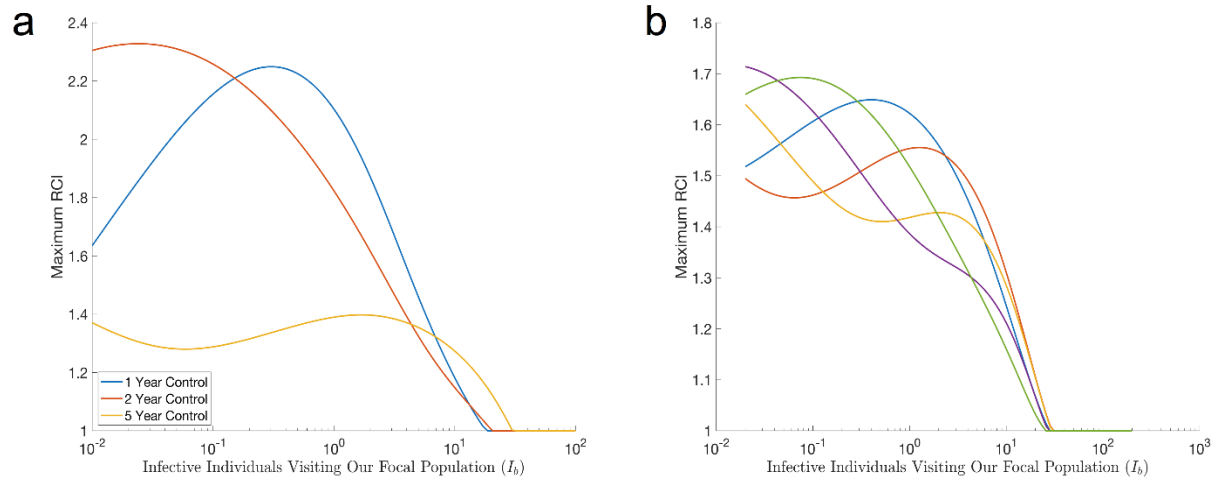


**Figure S2.23: Interaction between background force of infection, seasonality, timing of control, and the magnitude of the divorce effect.** (a) Increasing seasonality ( $\beta_1 = .1$  in contrast to  $\beta_1 = .02$  in Figure S2.22) increases the variation in the divorce effect seen at differing background force of infections. (b) Likewise, the timing of the start of the control (days 0, 73, 146, 219, 292) has a significant effect on the magnitude of the divorce effect seen at a particular background force of infection.

**CHAPTER 3 - Efficacy and Spatial Extent of Yard-scale Control of *Aedes (Stegomyia)*  
*albopictus* (Skuse) (Diptera: Culicidae) using Barrier Sprays and Larval Habitat**

**Management**

Brandon Hollingsworth, Pete Hawkins, Alun L. Lloyd, Michael H. Reiskind

\*This chapter is published in the Journal of Medical Entomology. Hollingsworth, B., Hawkins, P., Lloyd, A. L., & Reiskind, M. H. (2020). Efficacy and Spatial Extent of Yard-Scale Control of *Aedes (Stegomyia) albopictus* (Diptera: Culicidae) Using Barrier Sprays and Larval Habitat Management. *J. Med. Entomol.*  
<https://doi.org/10.1093/jme/tjaa016>

## **CONTRIBUTION**

As first author on this publication, I was responsible for designing and carrying out all aspects of the field experiment, except for performing treatments. I also performed all statistical analysis and wrote the manuscript.

## ABSTRACT

The Asian tiger mosquito, *Aedes (Stegomyia) albopictus* (Skuse), is a peridomestic, container-ovipositing mosquito commonly found throughout the southeastern United States. In the US, *Ae. albopictus* is typically considered a nuisance pest, however, it is capable of transmitting multiple pathogens. *Aedes albopictus* is an important pest species and the target of numerous mosquito-control efforts in the United States. Here, we evaluate the effectiveness and spatial extent of *Ae. albopictus* population reduction using a bifenthrin (AI Bifen IT, 7.9%) barrier spray and larval habitat management (LHM) in a temperate, suburban setting. Sixteen pairs of adjoining neighbors were randomly assigned to treatment groups with one neighbor receiving a treatment and the other monitored for evidence of a spill-over effect of the treatments. *Ae. albopictus* populations in both yards were monitored for 33 days, with treatments occurring on the 8<sup>th</sup> day. Barrier sprays, both alone and combined with LHM, resulted in a significant reduction in *Ae. albopictus* abundance post-treatment. While LHM alone did not result in a significant reduction over the entire post-treatment period, *Ae. albopictus* populations were observed to be in decline during this period. No treatments were observed to have any reduction in efficacy 25 days post-treatment, with treatments involving LHM having a significantly increased efficacy. Yards neighboring treated yards were also observed to have reduced population sizes post-treatment, but these differences were rarely significant. These results provide insights into the population dynamics of *Ae. albopictus* following two common treatments and will be useful for integrated pest management plans.

## INTRODUCTION

*Aedes (Stegomyia) albopictus* (Skuse) is a peridomestic container-ovipositing mosquito commonly found throughout the world. After its initial introduction in Texas in 1985 (Sprenger and Wuithiranyagool 1986), it quickly spread throughout the southeastern United States (US) and now has a range stretching from the Atlantic coast in the east to Texas in the west and from the southern tip of Florida up to New York in the north, along with areas of recent introduction in California on the west coast (Hahn et al. 2017). Its preference for ovipositing in artificial containers, along with its propensity for biting humans, makes it one of the most common nuisance mosquitoes in the US. Unfortunately, controlling *Ae. albopictus* using traditional methods such as ultra-low volume applications has proven difficult, suggesting a need for alternative control strategies (Roiz et al. 2018, Achee et al. 2019). Further, its ability to transmit dengue, Zika, and chikungunya viruses make it a potential public health threat, and the likely vector in the case of introduction of these pathogens into the US (Gostin and Hodge 2016, Messina et al. 2016, Moreno-Madriñán et al. 2018).

Traditionally, mosquito control in the US has been performed by mosquito abatement districts, with the aim of mitigating community-wide nuisance and risk of disease associated with mosquitoes. Abatement districts commonly deploy vehicle-based, ultra-low volume (ULV) application in order to treat large areas with insecticides. These ULV applications are often coupled with source reduction efforts to remove large oviposition sites, such as tire piles. However, recent budgetary cuts, including in North Carolina in 2011, have resulted in underfunded and underprepared mosquito control districts (Rosario et al. 2014).

Within North Carolina, 55% of mosquito control programs self-reported a barely functional budget (Rosario et al. 2014) and a recent survey of vector-control organizations

nationwide showed that 84% needed improvement in at least one of five core capacities: routine mosquito surveillance, surveillance based treatments, larviciding and/or adulticiding, routine vector control activities, and pesticide resistance testing (NACCHO 2017). These reports, combined with concerns about the effectiveness of ULV applications for reducing *Aedes* populations, and *Aedes*-vectored disease (Bonds 2012, Wilson et al. 2015, Bowman et al. 2016, Faraji and Unlu 2016, Roiz et al. 2018), suggest mosquito abatement districts may be ill-equipped to respond to vector-borne disease outbreaks and highlight a need for new plans for mosquito-borne disease response. The private mosquito control industry, in contrast, has grown significantly over the past decade (Specialty Consultants 2016). While this growth has been mostly driven by a high willingness to pay for mosquito nuisance control (Dickinson and Paskewitz 2012), fear of potential outbreaks of dengue and Zika virus in the US has likely also increased enrollment in their services. Unlike mosquito abatement districts, these companies deploy yard-scale mosquito treatments, the efficacy and spatial scale of which has not been fully quantified. It is possible that, if shown effective, these yard-scale treatments could provide a useful tool for precision mosquito control in the event of a mosquito-borne disease outbreak. In light of this, it is important to quantify the short-term effectiveness of yard-scale treatments and their effect on the dynamics of nearby mosquito population.

The yard-scale treatments employed by private mosquito control companies typically target nuisance mosquitoes, including *Ae. albopictus*, with treatments involving the use of a combination of an adulticidal barrier spray, most commonly a pyrethroid, and larval habitat management (LHM), tip-and-toss combined with a long acting larvicide, applied regularly during mosquito season. The success of these companies and the growth of the industry provides anecdotal evidence of their effectiveness. However, empirical studies of the effects of barrier

sprays (Muzari et al. 2014, Fulcher et al. 2015, Stoops et al. 2019), especially when applied to individual yards (Trout et al. 2007, Hurst et al. 2012, VanDusen et al. 2016, Richards, Balanay, et al. 2017) have focused on the long term effects of the treatments inside the treated area, and not on the short-term effects or the spill-over effects in the neighboring yard, which would likely play a major role in disease dynamics. Similarly, studies of the effect of larval habitat management, or larval source reduction, on *Ae. albopictus* have typically focused on neighborhood or city-wide efforts (Richards et al. 2008, Unlu et al. 2011, 2013, Fonseca et al. 2013, Faraji and Unlu 2016), with mixed results and further investigation about its effectiveness is needed (Faraji and Unlu 2016).

Here, we report on the efficacy of two standard mosquito control techniques, larval habitat management, through source reduction, and an adulticidal barrier spray, when applied to individual yards in the Wake County, NC area. Mosquito abundance from adjacent yards was also monitored to determine if there was a reduction outside of the treated area.

## **METHODS**

### **Participant Recruitment**

Households were recruited in Wake County, NC (35°47'24.00" N -78°39'0.00" W) beginning in May, 2018 using a combination of recruitment fliers placed at local community centers and recruitment emails sent through neighborhood listservs. Recruitment was limited to pairs of neighboring houses that had not received any professional mosquito treatment that year (since January 2018) and were willing to participate. Participating houses were enrolled on a first-come basis and adult residents for each house were met in person for the informed consent process. All participants received treatments free of charge, and participants not receiving a barrier spray treatment were offered a free treatment following the end of the study. Designation



of treatment and neighboring house for each pair was determined at time of informed consent. Typically, the house belonging to the primary contact for the pair, whoever initiated contact, was assigned to treatment unless residents preferred otherwise.

### **Ethical Clearance**

Informed consent was obtained from adult residents of all participating houses before the beginning of the study. All participants were informed about their rights and all risks associated with their inclusion in the study. Ethical approval was obtained from the North Carolina State University Institutional Review Board (Approved, NCSU Protocol # 12800, 5/14/2018).

### **Study Design**

We employed a split-split-plot design with sites, consisting of 16 house pairs, randomly assigned to a LHM by barrier spray (2x2) balanced factorial design and trap locations designated within each site. Each house pair was assigned to receive either LHM alone, the barrier spray alone, a combination of both LHM and barrier spray, or no treatment, with four replicates of each treatment. Three sampling locations were determined within each site (see Figure 3.1). Each location within a site was sampled concurrently every fourth day over a 33 day period.

After being assigned a treatment, each site was assigned to one of four groups for sampling, such that each group contained exactly one site assigned to each of the treatment levels. Sampling was conducted on a rotating basis, with all members of a group sampled on the same days, e.g. group 1 was sampled on days 1, 5, 9, etc. and group 2 on days 2, 6, 10, etc. Sampling consisted of 9 trap days at each location occurring on every 4<sup>th</sup> day, lasting 24 hours, and occurred over a period of 36 days, including the pretreatment period, from 6 August, 2018 – 10 September, 2018 due to rotating between groups.

During each sampling day, 3 BG-Sentinel 2 (Biogents, Regensburg, Germany) traps were set for 24 hours along a transect, with traps placed in the center and side (approx. 5m from the property line) of the treatment yard and adjacent neighboring yard (approx. 15m from the property line), all traps were baited using BG lures (Figure 3.1). Trap bags were collected at the end of the sampling period and collections frozen until sorted, with numbers of female *Ae. albopictus*, male *Ae. albopictus*, and other mosquitoes recorded for each trap day. Due to low count numbers of other mosquito species in collections, only female *Ae. albopictus* counts are reported here.

### **Insecticide Application**

Insecticide applications occurred the day before the third round of sampling at each site, e.g. day 8 for group 1 and day 9 for group 2, (13 August – 16 August, 2018), denoted Day 0 (grey dashed bar in Figure 3.1), and were performed between the hours of 1400 and 1700. Treatments were carried out by a trained, licensed applicator from a local mosquito control company. For houses receiving LHM or combined treatment, the yard was initially surveyed for larval habitat by the applicator and primary researcher. All containers with standing water were emptied and removed if possible and the larvicide, Altosid (AI 1.5% (S)-Methoprene, Zoecon, Schaumburg, IL), was applied to any standing bodies of water that could not be removed and did not contain fish, e.g. birdbaths. In yards that received the barrier spray or combined treatment, the applicator applied Bifen IT (AI 7.9% bifenthrin, Control Solutions, Pasadena, TX) as a barrier spray around the property and to any resting habitat, e.g. dense foliage, with care taken to avoid any flowering or fruiting plants and any ponds, consistent with the EPA/FIFRA pesticide label. Barrier sprays were performed throughout the front, back, and side of the yard and to any fences using a Stihl SR450 mist blower with the applicator walking approximately 3-4 km/hour,

applying approximately 1 gallon of mixed product, containing approximately 1 oz Bifen IT, per 1000 ft<sup>2</sup>. For houses assigned to the combined treatment group, LHM was performed before application of the barrier spray.

### **Statistical Model**

To evaluate the reduction in the female *Ae. albopictus* population due to the treatments, we modeled the number of female *Ae. albopictus* in the trap as a Poisson random variable using a generalized linear mixed model with a log-link function (Bolker et al. 2009, Zuur et al. 2010). All models included a random intercept for the study site, with correlation between traps at the same site, the trapping date, and an observation level random effect to account for overdispersion (Harrison 2014). Fixed effects were modeled as a LHM by barrier spray by location by days since treatment factorial design, with day taken as a covariate for comparisons between treatments and locations and as a factor for comparisons between days. The average pretreatment mosquito count was then used as a per location offset. All models were fit in R (R Development Core Team 2019) using the lme4 package (Bates et al. 2015), with means and contrasts calculated using the emmeans package (Lenth 2019).

The percent reduction in mosquito population due to treatment is found as the contrast between the treatment and control group  $((1 - \text{contrast}) * 100\%)$ . Multiple comparisons against a control, either the untreated yards or the first day post-control, were performed using a Dunnett adjustment. Pairwise multiple comparisons were conducted using a Tukey adjustment, while comparisons of individual days against the average of the days used a Bonferroni method (Longnecker and Ott 2015). Where not specifically noted, we test the contrast between a treatment and the untreated group using the appropriate adjustment. Confidence intervals for all estimates are given at the 95% level and contrasts are considered significant at the  $\alpha = .05$  level.

## RESULTS

*Aedes albopictus* counts for 429 trap-days were recorded (3 days, 1 of which was pretreatment, were lost due to trap failures) (Figure 3.2). There was no significant overall trend with regard to mosquito abundance for the control group (95% CI for slope (-.0311, .0010)) over the study period, suggesting that mosquito populations were not declining throughout the study period. However, counts in the post-treatment period were significantly lower than the pretreatment period for the control group (Table S3.1).

### Treatment Effects

Overall, we found that all treatment groups exhibited a decrease in the mosquito count during the entire post-treatment period. Compared to the pretreatment mean, pairs of houses in the LHM treatment group had a 63.9% (47.5%, 75.1%) mean reduction in the abundance of female *Ae. albopictus*, the barrier spray treatment group had a reduction of 77.1% (66.8%, 84.2%), and the combined treatment group had a reduction of 74.6% (62.8%, 84.2%) (Table S3.1). The application of LHM resulted in a 40.9% ( $p = .0866$ ) mean reduction in the abundance of female *Ae. albopictus* across the pair of yards over the post-treatment period, the barrier spray resulted in a 62.5% ( $p = 1.87 \times 10^{-4}$ ) mean reduction, and combining the treatments resulted in a 58.5% ( $p = .00123$ ) mean reduction.

Inside the treated yards, LHM resulted in a 33.3% ( $p = .457$ ) mean reduction in female *Ae. albopictus* abundance over the post-treatment period, the barrier spray in a 62.2% ( $p = .00808$ ) mean reduction, and the combined treatment in a 59.5% ( $p = .0176$ ) mean reduction. In the untreated neighboring yard, LHM resulted in a 54.6% ( $p = .209$ ) mean reduction over the post-treatment period, the barrier spray in a 62.5% ( $p = .0796$ ) mean reduction, and the combined treatment in a 58.6% ( $p = .143$ ) mean reduction (Table S3.2).

## Edge and Spill-over Effects

In general, *Ae. albopictus* counts were higher at the side and neighbor trap locations for the barrier spray group and lower for treatments that included LHM. However, we found no significant difference in the reduction of *Ae. albopictus* counts between the traps at the center, side, and neighboring locations, regardless of treatment (Table S3.2).

## Temporal Trends

The day immediately following treatment application, reduction due to treatment in the mean female *Ae. albopictus* abundance in treated yards was not significant for any treatment, with the largest reduction, 60.7% ( $p = .0717$ ), occurring when only the barrier spray was applied. Similarly, the reduction was not significant in the neighboring yards, despite the barrier spray resulting in a mean reduction of 68.9% ( $p = .0921$ ) and the combined treatment resulting in a 72.4% ( $p = .0865$ ) mean reduction.

In treated yards, the greatest reduction due to treatment was seen 17 days post-treatment when a barrier spray was applied, and 25 days post-treatment for LHM and combined treatments. Similar results were seen for neighboring yards, with the exception of when the combined treatment was implemented for which the greatest reduction occurred 9 days post-treatment (Figure 3.3). However, the reduction in abundance due to treatment was not significantly lower than the mean post-treatment reduction for any treatment in either the treated or neighboring houses (Table S3.3).

To determine if the *Ae. albopictus* population rebounded post-treatment, we examined four models for the change in treatment effectiveness over time. Based on AIC (Longnecker and Ott 2015), overall trends were best described using a linear fit for the time since treatment, compared to quadratic fits ( $\Delta AIC = 14.1$ ), cubic fits ( $\Delta AIC = 28$ ), or treating time as a factor

( $\Delta AIC = 62$ ). Within treated yards, estimates for trends in the *Ae. albopictus* reduction due to all treatments were positive, suggesting that treatments became increasingly effective during the post-treatment period. However, this trend was only significant for LHM ( $p=.0336$ ). Estimates of the trends for reduction due to the barrier spray and LHM in the neighboring yard were negative, but neither was significant (Table S3.4).

Contrasts between the effects 25 days post-treatment and the effects one day post-treatment also fail to show any evidence of a rebound in the *Ae. albopictus* population. 25 days post-treatment, treatment with LHM resulted in *Ae. albopictus* populations being reduced by 70.6% ( $p = .0123$ ) of its size one day post-treatment. The combined treatment and barrier spray also saw an increased reduction 25 days post-treatment compared to after one day, but neither was significant. *Ae. albopictus* populations in neighboring yards were lower 25 days post-treatment than one day post-treatment when the focal house was treated with LHM, showing a significant additional reduction 25 days post-treatment (73.2% reduction,  $p = .0361$ ) (Table S3.5). These results, combined with the overall trends provide no evidence that there is a loss in effectiveness of treatments 25 days post-treatment, and that there is significant evidence that *Ae. albopictus* populations in yards treated with, and neighboring to yards treated with, LHM are still declining 25 days post-treatment.

## DISCUSSION

The results of our study concur with previous studies that the yard-scale application of barrier sprays using the pyrethroid, bifenthrin, in conjunction with LHM can successfully suppress *Ae. albopictus* populations in yards in the temperate US (Trout et al. 2007, VanDusen et al. 2016, Richards, Volkan, et al. 2017) and our estimates of the overall effect of bifenthrin barrier sprays are in the range of previous studies. In addition to these estimates, the design of

this study allowed for the decoupling of the effects of LHM and barrier spray, and trapping repeatedly at short intervals allowed the estimation of how the effectiveness of treatments changed over the 25 days following treatment. Our study showed that bifenthrin barrier sprays quickly reduced the *Ae. albopictus* population by 60% and continued having an effect at 25 days, with little change in effectiveness over the 25 days post-treatment, while LHM effectiveness increased over the study period, having no effect immediately following treatment and only began to have an effect after about 21 days. While we did not find any evidence of an increased effect with combined treatments, the difference in timing of the effects suggest that there is an added benefit of using both treatments. In addition to measuring the effectiveness inside of treated yards, we were able to measure the effect of these treatments in untreated neighboring yards. Estimates in the untreated neighboring yards were on the same scale as in treated yards, suggestive of a spill-over effect of the treatments, but the differences were not significant. These estimates suggests that it may not be necessary to treat every yard to successfully reduce *Ae. albopictus* counts across a neighborhood, significantly reducing the risk posed by noncompliant houses.

While our results show that bifenthrin barrier sprays and LHM have an effect beyond 25 days post-treatment and may reduce *Aedes* populations beyond the perimeter of the treated yard, future studies need to maintain surveillance more than 25 days post-treatment and should monitor the mosquito populations further than 15m beyond the treated area. We also failed to see a significant decrease in numbers in the untreated neighboring yards, despite estimates of 50-60% reduction due, in part, to large variability in the results, something future studies should take into account. Previous studies of barrier sprays have also shown that the timing, with respect to the mosquito season, of treatments has an impact on the effectiveness of the control

(Williams et al. 2019), with increased effectiveness later in the season, suggesting that the effectiveness of the barrier sprays would be lessened earlier in the season, something that should be accounted for.

Our results show that it is possible to locally reduce *Ae. albopictus* populations using these treatments for significant periods of time. Applicators could deploy yard-scale treatments, such as barrier sprays and LHM, to target “hot-spot” yards containing large mosquito populations, which has been shown to be effective (Unlu et al. 2016), a strategy that could prove more effective than traditional neighborhood- and city-scale ULV applications. In addition, the estimated effects of the treatment on untreated neighboring yards, while not significant, suggests that an economically optimal strategy for deploying treatments may exist for temporarily reducing the mosquito population in a neighborhood or town in response to mosquito-borne disease outbreaks, e.g. spraying some proportion of yards. However, the efficacy and cost-effectiveness of such a plan would be highly dependent on the costs and accuracy of determining yards with consistently larger *Ae. albopictus* populations.

Control of *Ae. albopictus* populations using strategically deployed yard-scale treatments could also help prevent the emergence and spread of insecticide resistance in local populations when it is not necessary to suppress the entire population. Targeting specific yards and other habitats with large mosquito populations could mean that applicators are able to apply a higher concentration than what is possible from vehicle-based ULV applications. Fewer mosquitoes will be exposed to a sublethal dose, while leaving other areas untreated could serve as a natural refuge for susceptible populations. This would serve as a high-dose/refuge approach, similar to what is suggested for resistance management in crop pests (Gould 1998, Tabashnik et al. 2004,



Gould et al. 2018), and possibly creating a reservoir for genes beneficial for resistance management (Maino et al. 2019).

Yard-scale control of mosquitoes with a combination of a barrier spray and LHM successfully suppressed mosquito populations in treated and adjacently neighboring yards in our study. However, while we show an estimated reduction of 59.5% in the 25 days post-treatment, it is unclear if this would be sufficient to satisfy private customers. The use of LHM alone, with a longer effective period and an estimated 40.9% reduction over the initial 25 days post-treatment, may prove preferable for long-term reduction of nuisance due to *Ae. albopictus*. Barrier sprays provided an immediate reduction of the *Ae. albopictus*, an important addition for applications performed commercially or in response to an *Aedes*-borne disease outbreak. However, whether the additional reduction provided by barrier sprays would be sufficient for stopping an outbreak of an *Aedes*-vectored disease, e.g. dengue, would depend on the vectoral capacity of the local population (Fouet and Kamdem 2019). Yard-scale applications of barrier sprays could prove preferable to ULV spraying when used as part of a well-designed integrated vector management program as it allows for targeted “hot-spot” treatments. For instance, targeted barrier sprays could be used to supplement ongoing neighborhood-wide LHM, which has previously been shown to reduce *Ae. albopictus* populations (Fonseca et al. 2013), in response to a disease outbreak, or as part of ongoing activities (Roiz et al. 2018). While the results presented above show the potential of yard-scale treatments to reduce *Aedes* populations, much more information is needed to be able to optimally deploy yard-scale targeted controls as part of an integrated management plan. Key amongst this is the scale and magnitude of the spatial heterogeneity of the *Ae. albopictus* population, techniques to quickly and efficiently

identify “hot-spots”, and a framework for determining optimal treatment patterns (Baldacchino et al. 2015, Fouet and Kamdem 2019).

## REFERENCES

- (NACCHO) National Association of County and City Health Officials. 2017. Mosquito Control Capabilities in the U.S. Washington, DC.
- Achee, N. L., J. P. Grieco, H. Vatandoost, G. Seixas, J. Pinto, L. Ching-Ng, A. J. Martins, W. Juntarajumnong, V. Corbel, C. Gouagna, J. P. David, J. G. Logan, J. Orsborne, E. Marois, G. J. Devine, and J. Vontas. 2019. Alternative strategies for mosquito-borne arbovirus control. *PLoS Negl. Trop. Dis.* 13: e0006822.
- Baldacchino, F., B. Caputo, F. Chandre, A. Drago, A. della Torre, F. Montarsi, and A. Rizzoli. 2015. Control methods against invasive *Aedes* mosquitoes in Europe: A review. *Pest Manag. Sci.* 71: 1471–1485.
- Bates, D., M. Mächler, B. Bolker, and S. Walker. 2015. Fitting Linear Mixed-Effects Models Using lme4. *J. Stat. Softw.* 67: 1–48.
- Bolker, B. M., M. E. Brooks, C. J. Clark, S. W. Geange, J. R. Poulsen, M. H. H. Stevens, and J.-S. S. White. 2009. Generalized linear mixed models: a practical guide for ecology and evolution. *Trends Ecol. Evol.* 24: 127–35.
- Bonds, J. A. S. 2012. Ultra-low-volume space sprays in mosquito control: A critical review. *Med. Vet. Entomol.* 26: 121–130.
- Bowman, L. R., S. Donegan, and P. J. McCall. 2016. Is Dengue Vector Control Deficient in Effectiveness or Evidence?: Systematic Review and Meta-analysis. *PLoS Negl. Trop. Dis.* 10: e0004551.
- Dickinson, K., and S. Paskewitz. 2012. Willingness to Pay for Mosquito Control: How Important Is West Nile Virus Risk Compared to the Nuisance of Mosquitoes? *Vector-Borne Zoonotic Dis.* 12: 886–892.

- Faraji, A., and I. Unlu. 2016. The Eye of the Tiger, the Thrill of the Fight: Effective Larval and Adult Control Measures Against the Asian Tiger Mosquito, *Aedes albopictus* (Diptera: Culicidae), in North America. *J. Med. Entomol.* 53: 1029–1047.
- Fonseca, D. M., I. Unlu, T. Crepeau, A. Farajollahi, S. P. Healy, K. Bartlett-Healy, D. Strickman, R. Gaugler, G. Hamilton, D. Kline, and G. G. Clark. 2013. Area-wide management of *Aedes albopictus*. Part 2: Gauging the efficacy of traditional integrated pest control measures against urban container mosquitoes. *Pest Manag. Sci.* 69: 1351–1361.
- Fouet, C., and C. Kamdem. 2019. Integrated Mosquito Management: Is Precision Control a Luxury or Necessity? *Trends Parasitol.* 35: 85–95.
- Fulcher, A., M. L. Smith, J. M. Scott, E. Thomson, R.-D. Xue, M. Farooq, C.-X. Li, and P. E. Kaufman. 2015. Evaluation of a new spraying machine for barrier treatment and penetration of bifenthrin on vegetation against mosquitoes. *J. Am. Mosq. Control Assoc.* 31: 85–92.
- Gostin, L. O., and J. G. Hodge. 2016. Is the United States prepared for a major zika virus outbreak? *J. Am. Med. Assoc.* 315: 2395–2396.
- Gould, F. 1998. Sustainability of Transgenic Insecticidal Cultivars: Integrating Pest Genetics and Ecology. *Annu. Rev. Entomol.* 43: 701–726.
- Gould, F., Z. S. Brown, and J. Kuzma. 2018. Wicked evolution: Can we address the sociobiological dilemma of pesticide resistance? *Science.* 360: 728–732.
- Hahn, M. B., L. Eisen, J. McAllister, H. M. Savage, J. P. Mutebi, and R. J. Eisen. 2017. Updated reported distribution of *Aedes (Stegomyia) aegypti* and *Aedes (Stegomyia) albopictus* (Diptera: Culicidae) in the United States, 1995-2016. *J. Med. Entomol.* 54: 1420–1424.
- Harrison, X. A. 2014. Using observation-level random effects to model overdispersion in count data in ecology and evolution. *PeerJ.* 2: e616.

- Hurst, T. P., P. A. Ryan, and B. H. Kay. 2012. Efficacy of Residual Insecticide Biflex AquaMax Applied as Barrier Treatments for Managing Mosquito Populations in Suburban Residential Properties in Southeast Queensland. *J. Med. Entomol.* 49: 1021–1026.
- Lenth, R. 2019. emmeans: Estimated Marginal Means, aka Least-Squares Means.
- Longnecker, M., and R. Ott. 2015. An introduction to statistical methods and data analysis. Brooks/Cole, Belmont, CA.
- Maino, J. L., M. Renton, A. A. Hoffmann, and P. A. Umina. 2019. Field margins provide a refuge for pest genes beneficial to resistance management. *J. Pest Sci.* (2004). 92: 1017–1026.
- Messina, J. P., M. U. G. Kraemer, O. J. Brady, D. M. Pigott, F. M. Shearer, D. J. Weiss, N. Golding, C. W. Ruktanonchai, P. W. Gething, E. Cohn, J. S. Brownstein, K. Khan, A. J. Tatem, T. Jaenisch, C. J. L. Murray, F. Marinho, T. W. Scott, and S. I. Hay. 2016. Mapping global environmental suitability for Zika virus. *Elife.* 5: e15272.
- Moreno-Madriñán, M. J., M. Turell, and W. Reisen. 2018. Factors of concern regarding zika and other *Aedes aegypti*-transmitted viruses in the United States. *J. Med. Entomol.* 54: 251–257.
- Muzari, O. M., R. Adamczyk, J. Davis, S. Ritchie, and G. Devine. 2014. Residual Effectiveness of  $\lambda$ -Cyhalothrin Harbourage Sprays Against Foliage-Resting Mosquitoes in North Queensland. *J. Med. Entomol.* 51: 444–449.
- R Development Core Team. 2019. R: A language and environment for statistical computing. R Found. Stat. Comput. [www.r-project.org](http://www.r-project.org)
- Richards, S. L., J. A. G. Balanay, M. Fields, K. Vandock, and L. Eisen. 2017. Baseline insecticide susceptibility screening against six active ingredients for *Culex* and *Aedes* (Diptera: Culicidae) Mosquitoes in the United States. *J. Med. Entomol.* 54: 682–695.

- Richards, S. L., S. K. Ghosh, B. C. Zeichner, and C. S. Apperson. 2008. Impact of source reduction on the spatial distribution of larvae and pupae of *Aedes albopictus* (Diptera: Culicidae) in suburban neighborhoods of a Piedmont community in North Carolina. *J. Med. Entomol.* 45: 617–628.
- Richards, S. L., J. K. Volkan, J. A. G. Balanay, and K. Vandock. 2017. Evaluation of Bifenthrin and Deltamethrin Barrier Sprays for Mosquito Control in Eastern North Carolina. *J. Med. Entomol.* 54: 1659–1665.
- Roiz, D., A. L. Wilson, T. W. Scott, D. M. Fonseca, F. Jourdain, P. Müller, R. Velayudhan, and V. Corbel. 2018. Integrated *Aedes* management for the control of *Aedes*-borne diseases. *PLoS Negl. Trop. Dis.* 12: e0006845.
- Rosario, K. L. Del, S. L. Richards, A. L. Anderson, J. Anne, and G. Balanay. 2014. Current Status of Mosquito Control Programs in North Carolina: The Need for Cost- Effectiveness Analysis. *J. Environ. Health.* 76: 8–15.
- Specialty Consultants. 2016. A Strategic Analysis of the U.S. Structural Pest Control Industry. Jacksonville, FL.
- Sprenger, D., and T. Wuithiranyagool. 1986. The discovery and distribution of *Aedes albopictus* in Harris County, Texas. *J. Am. Mosq. Control Assoc.* 2: 217–9.
- Stoops, C. A., W. A. Qualls, T.-V. T. Nguyen, and S. L. Richards. 2019. A Review of Studies Evaluating Insecticide Barrier Treatments for Mosquito Control From 1944 to 2018. *Environ. Health Insights.* 13: 1178630219859004.
- Tabashnik, B. E., F. Gould, and Y. Carrière. 2004. Delaying evolution of insect resistance to transgenic crops by decreasing dominance and heritability. *J. Evol. Biol.* 17: 904–912.
- Trout, R. T., G. C. Brown, M. F. Potter, and J. L. Hubbard. 2007. Efficacy of two pyrethroid

- insecticides applied as barrier treatments for managing mosquito (Diptera: Culicidae) populations in suburban residential properties. *J. Med. Entomol.* 44: 470–477.
- Unlu, I., A. Farajollahi, S. P. Healy, T. Crepeau, K. Bartlett-Healy, E. Williges, D. Strickman, G. G. Clark, R. Gaugler, and D. M. Fonseca. 2011. Area-wide management of *Aedes albopictus*: Choice of study sites based on geospatial characteristics, socioeconomic factors and mosquito populations. *Pest Manag. Sci.* 67: 965–974.
- Unlu, I., A. Farajollahi, D. Strickman, and D. M. Fonseca. 2013. Crouching Tiger, Hidden Trouble: Urban Sources of *Aedes albopictus* (Diptera: Culicidae) Refractory to Source-Reduction. *PLoS One.* 8: e77999.
- Unlu, I., K. Klingler, N. Indelicato, A. Faraji, and D. Strickman. 2016. Suppression of *Aedes albopictus*, the Asian tiger mosquito, using a “hot spot” approach. *Pest Manag. Sci.* 72: 1427–1432.
- VanDusen, A. E., S. L. Richards, and J. A. G. Balanay. 2016. Evaluation of bifenthrin barrier spray on foliage in a suburban eastern North Carolina neighborhood. *Pest Manag. Sci.* 72: 1004–1012.
- Williams, G. M., I. Unlu, I. Rochlin, Y. Wang, and R. Gaugler. 2019. Timing of Lambda-Cyhalothrin and Pyriproxyfen Barrier Treatments for *Aedes albopictus* (Diptera: Culicidae) Management. *J. Econ. Entomol.* 112: 1337–1342.
- Wilson, A. L., M. Boelaert, I. Kleinschmidt, M. Pinder, T. W. Scott, L. S. Tusting, and S. W. Lindsay. 2015. Evidence-based vector control? Improving the quality of vector control trials. *Trends Parasitol.* 31: 380–390.
- Zuur, A. F., E. N. Ieno, and C. S. Elphick. 2010. A protocol for data exploration to avoid common statistical problems. *Methods Ecol. Evol.* 1: 3–14.

## TABLES

**Table 3.1: Mean count of *Ae. albopictus* on given day after treatment, aggregated for each trap location, yard, and treatment pair within each treatment group.**

		Day							
		<i>Pre-treatment</i>	<i>1</i>	<i>5</i>	<i>9</i>	<i>13</i>	<i>17</i>	<i>21</i>	<i>25</i>
Combined	<i>Total</i>	10.08	5.33	4.58	2.75	3.50	3.91	3.25	2.17
	<i>Treated</i>	10.625	6.25	4.75	3.25	3.75	4.5	3.38	1.75
	<i>Center</i>	12.12	8.00	8.25	5.00	4.25	7.00	4.00	1.25
	<i>Side</i>	9.13	4.50	1.25	1.50	3.25	2.00	2.75	2.25
	<i>Neighbor</i>	9	3.50	4.25	1.75	3.00	2.75	3.00	3.00
Barrier Spray	<i>Total</i>	20.63	7.00	5.92	6.75	6.67	5.58	6.83	5.08
	<i>Treated</i>	15.25	5.00	4.25	4.38	4.75	4.13	7.25	3.50
	<i>Center</i>	13.63	1.50	2.50	3.75	2.75	3.75	4.00	2.50
	<i>Side</i>	16.88	8.50	6.00	5.00	6.75	4.50	10.50	4.50
	<i>Neighbor</i>	31.38	11.00	9.25	11.50	10.50	8.50	6.00	8.25
LHM	<i>Total</i>	14.17	12.75	5.75	4.33	7.25	7.25	6.17	3.33
	<i>Treated</i>	13.88	10.88	6.00	4.50	8.13	7.75	5.38	3.13
	<i>Center</i>	9.38	8.50	5.25	4.50	6.50	5.75	6.50	3.00
	<i>Side</i>	18.38	13.25	6.75	4.50	9.75	9.75	4.25	3.25
	<i>Neighbor</i>	22.00	16.50	5.25	4.00	5.50	6.25	7.75	3.75
Control	<i>Total</i>	14.17	16.67	12.5	8.45	13.17	6.67	13.64	8.42
	<i>Treated</i>	13.75	12.00	11.25	6.86	13.00	6.13	13.86	9.00
	<i>Center</i>	11.13	10.75	6.75	4.00	6.25	7.50	5.33	4.50
	<i>Side</i>	16.38	13.25	15.75	9.00	19.75	4.75	20.25	13.5
	<i>Neighbor</i>	15.14	26.00	15.00	11.25	13.50	7.75	13.25	7.25



**Table 3.2: Percent reduction in adult female *Ae. albopictus* population due to treatment and p-values.** Percent reduction is found as the contrast between the reduction seen in the treated and control yards for each treatment and time period. Differences that are significant at the  $\alpha = .1$  (.) and  $\alpha = .05$  (\*) are denoted.

		<i>Pair</i>	<i>Treated</i>	<i>Neighbor</i>
<i>Combined</i>	Post-treatment	58.5 (.0012)*	59.5 (.0176)*	58.6 (.143)
	Day 1		37.6 (.534)	72.4 (.0865).
	Day 5		58.9 (.109)	58.1 (.330)
	Day 9		46.9 (.376)	82.8 (.133)
	Day 13		63.1 (.0539).	65.3 (.209)
	Day 17		40.0 (.527)	35.1 (.805)
	Day 21		69.2 (.0223)*	60.6 (.304)
	Day 25		81.2 (.00233)*	28.0 (.882)
<i>Barrier Spray</i>	Post-treatment	62.5 (1.88x10 <sup>-4</sup> )*	62.2 (.00808)*	62.5 (.0796).
	Day 1		60.7 (.0717).	68.9 (.0921).
	Day 5		65.4 (.0351)*	67.3 (.120)
	Day 9		47.0 (.351)	37.0 (.730)
	Day 13		73.4 (.00524)*	64.8 (.1626)
	Day 17		53.7 (.205)	49.3 (.514)
	Day 21		57.9 (.102)	77.9 (.0275)*
	Day 25		67.3 (.0288)*	53.9 (.412)
<i>LHM</i>	Post-treatment	40.9 (.0866).	33.3 (.457)	54.6 (.209)
	Day 1		-04.3 (.996)	35.1 (.754)
	Day 5		25.5 (.795)	63.8 (.202)
	Day 9		11.0 (.972)	53.9 (.431)
	Day 13		35.4 (.576)	66.3 (.168)
	Day 17		00.2 (1.00)	38.4 (.741)
	Day 21		60.8 (.0857).	59.2 (.304)
	Day 25		63.7 (.0668).	53.5 (.461)

## FIGURES

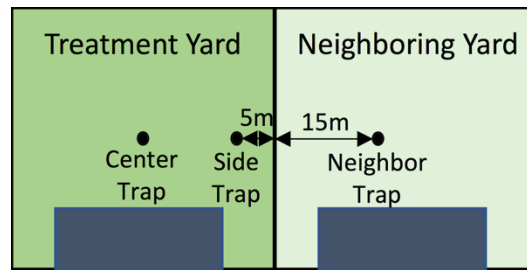


**Figure 3.1: Trap locations within the treated and neighboring yards.** The center trap was placed near the center of the treatment yard. The side trap was then set in the treatment yard, approximately 5m from the edge of the neighboring yard, and the neighbor trap was placed approximately 15m into the neighboring yard to form a transect.

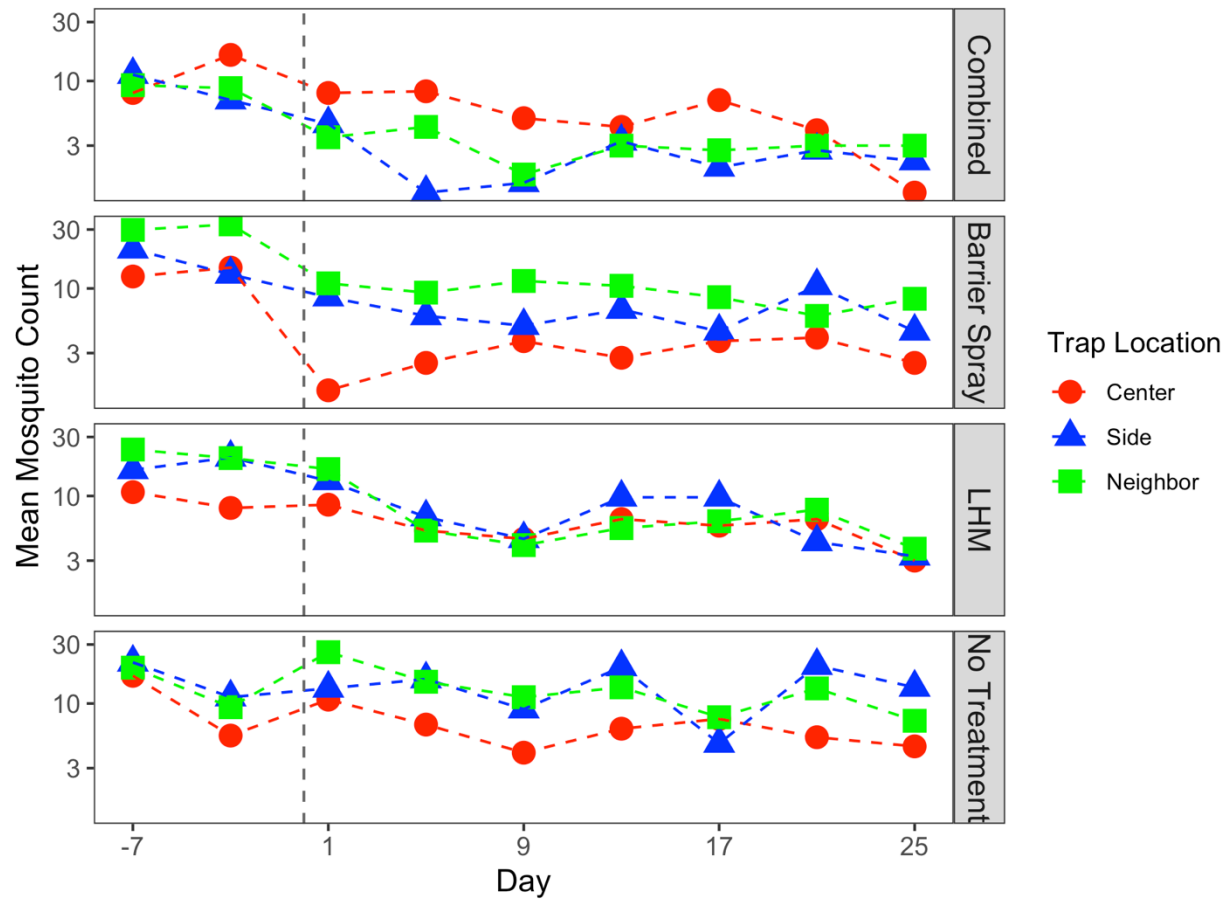


**Figure 3.2: Mean number of female *Ae. albopictus* for each treatment and location combination.** Treatment occurred on day 0 (grey dashed line). The average counts suggest an effect of the combined and barrier spray treatments.

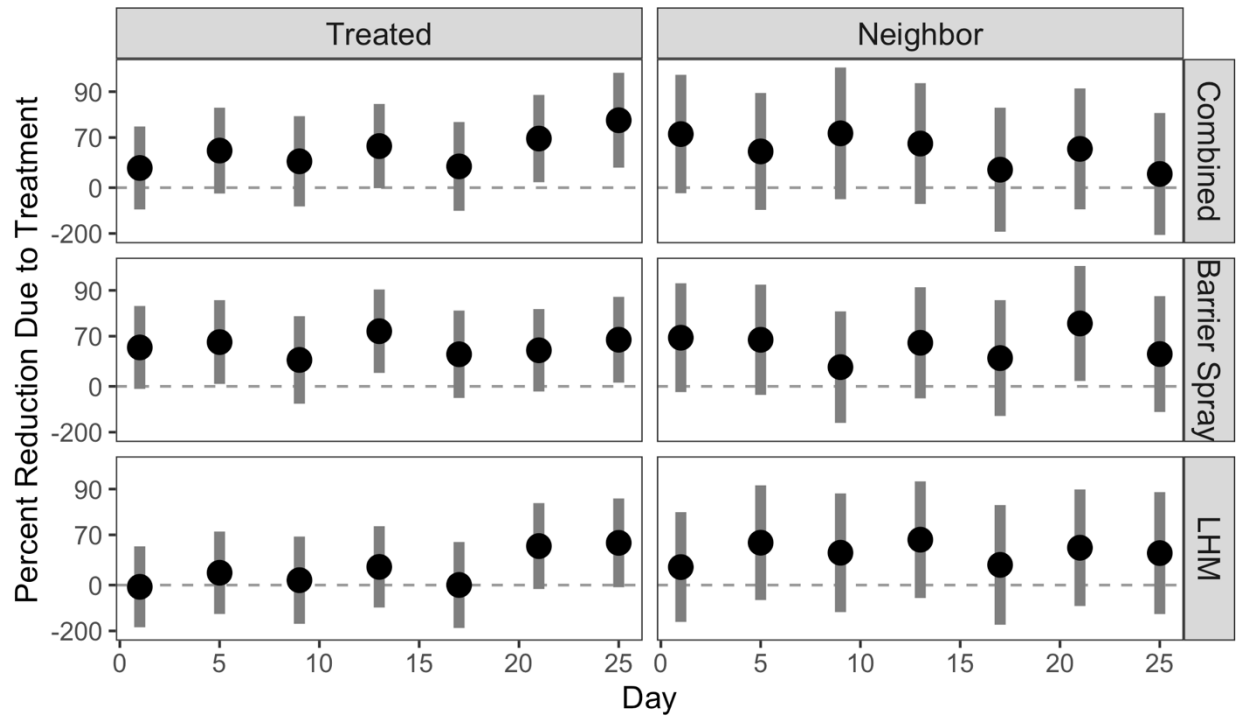


**Figure 3.3: Estimated percent reduction in female *Ae. albopictus* count due to treatment (dot) and 95% confidence interval (bars) on individual days in the treated and neighbor yards.** A value of 0 (dashed line) represents no difference from no treatment group. Only a few individual days differ significantly from the no treatment group. There is no overall trend showing a loss of effectiveness over 25 days, and treated yards that received LHM had reductions on day 25 that were significantly larger than the average reduction.

## SUPPLEMENTAL TABLES

**Table S3.1. Estimated percent reduction in adult female *Ae. albopictus* population in each treatment group, and 95% confidence intervals.**

		<i>Pair</i>	<i>Treated</i>	<i>Neighbor</i>
<i>Combined</i>	Post-treatment	74.6 (62.8, 82.7)	75.4 (60.8, 84.9)	73.9 (49.2, 86.6)
	Day 1		57.7 (16.3, 78.6)	69.9 (21.7, 88.5)
	Day 5		72.8 (44.1, 86.8)	64.9 (11.6, 86.2)
	Day 9		76.9 (53.8, 88.5)	85.8 (57.4, 95.2)
	Day 13		69.1 (38.9, 84.9)	74.1 (31.1, 90.3)
	Day 17		76.2 (50.4, 88.6)	74.8 (32.6, 90.6)
	Day 21		75.4 (49.1, 88.1)	73.1 (28.7, 89.9)
	Day 25		88.7 (74.2, 95.0)	70.7 (23.3, 88.8)
<i>Barrier Spray</i>	Post-treatment	77.1 (66.8, 84.2)	77.0 (63.0, 85.7)	76.4 (55.1, 87.6)
	Day 1		73.4 (47.3, 86.5)	66.2 (21.9, 85.3)
	Day 5		77.1 (54.2, 88.6)	72.6 (35.9, 88.3)
	Day 9		76.9 (53.8, 88.5)	66.9 (23.4, 85.8)
	Day 13		77.9 (55.6, 89.0)	73.8 (38.3, 88.9)
	Day 17		81.6 (62.5, 91.0)	80.3 (52.6, 91.9)
	Day 21		66.3 (34.2, 82.8)	84.9 (62.9, 93.9)
	Day 25		82.3 (61.9, 90.9)	81.1 (50.5, 92.8)

**Table S3.1 (Continued). Estimated percent reduction in adult female *Ae. albopictus* population in each treatment group, and 95% confidence intervals.**

		<i>Pair</i>	<i>Treated</i>	<i>Neighbor</i>
<i>LHM</i>	Post-treatment	63.9 (47.5, 75.1)	59.4 (34.6, 74.9)	71.4 (44.7, 85.2)
	Day 1		29.3 (-36.4, 63.4)	29.4 (-65.1, 69.8)
	Day 5		50.7 (3.3, 74.9)	69.7 (24.9, 87.8)
	Day 9		61.3 (22.6, 80.7)	75.8 (38.7, 90.5)
	Day 13		46.3 (-0.1, 72.6)	74.9 (36.6, 90.1)
	Day 17		60.4 (20.6, 80.2)	76.1 (39.3, 90.6)
	Day 21		68.6 (36.1, 84.5)	72.2 (30.2, 88.9)
	Day 25		79.2 (56.2, 90.1)	81.1 (54.7, 92.3)
<i>Control</i>	Post-treatment	38.9 (.122, 57.4)	39.2 (3.2, 62.8)	37.1 (-19.0, 66.7)
	Day 1		32.2 (-28.7, 64.3)	-8.8 (-147, 52.1)
	Day 5		33.8 (-25.6, 65.2)	16.3 (-90.7, 63.2)
	Day 9		56.5 (.14.6, 79.1)	47.5 (-22.8, 77.6)
	Day 13		16.9 (-56.2, 55.8)	25.4 (-70.7, 32.6)
	Day 17		60.3 (22.7, 79.6)	61.2 (7.4, 83.8)
	Day 21		19.9 (-53.4, 58.2)	31.9 (-56.9, 70.4)
	Day 25		42.8 (-9.1, 70.0)	59.3 (3.5, 82.8)

**Table S3.2. Percent of reduction at the center trap location seen at the side and neighbor trap locations, along with associated p-values.** An asterisk indicates differences that are significant at the  $p < .05$  level and a period indicates differences significant at the  $p < .1$  level. Dunnett adjustment for comparisons against a control is used to calculate p-values

	Combined	Barrier Spray	LHM
Side	150% (.5588)	49.0% (.1825)	97.4% (.9950)
Neighbor	117% (.8978)	66.5% (.5424)	140% (.6500)

**Table S3.3. Comparison of treatment effectiveness between given days and the post-treatment average.** An asterisk indicates differences that are significant at the  $p < .05$  level and a period indicates differences significant at the  $p < .1$  level. A Bonferroni-type adjustment for multiple comparisons used to calculate p-values.

		Treated			Neighboring		
		Combined	Barrier Spray	LHM	Combined	Barrier Spray	LHM
Day	1	.632 (.1179)	.163 (.9880)	.642 (.0755).	.176 (.9979)	.405 (.5815)	1.05 (.0140)*
	5	.117 (.9924)	-.0161 (.9880)	.221 (.6269)	.356 (.9979)	.158 (.7447)	.0606 (.9177)
	9	-.0710 (.9924)	-.00454 (.9880)	-.0602 (.9116)	-.695 (.9979)	.378 (.5815)	-.204 (.9177)
	13	.257 (.9592)	-.05518 (.9880)	.321 (.5663)	.00114 (.9979)	.108 (.7504)	-.1594 (.9177)
	17	-.0365 (.9924)	-.270 (.9793)	-.0333 (.9116)	-.0295 (.9979)	-.227 (.7281)	-.216 (.9177)
	21	.00307 (.9924)	.436 (.8972)	-.304 (.5663)	.0454 (.9979)	-.539 (.5815)	-.0392 (.9177)
	25	-.903 (.1105)	-.252 (.9793)	-.786 (.0755).	.146 (.9979)	-.284 (.7281)	-.490 (.7982)

**Table S3.4. Temporal trends of percent reduction due to treatment in treated and untreated yards.** An asterisk indicates differences that are significant at the  $p < .05$  level and a period indicates differences significant at the  $p < .1$  level.

	Treated	Neighboring
Combined	-3.24 (.1034)	3.03 (.3651)
Barrier Spray	-.119 (.9976)	.116 (.9986)
LHM	3.74 (.0336)*	-.856 (.9248)



**Table S3.5. Additional percent reduction on day 25 post-treatment compared to 1 day post-treatment.** An asterisk indicates differences that are significant at the  $p < .05$  level and a period indicates differences significant at the  $p < .1$  level. Dunnett adjustment for multiple comparisons against 1 day post-treatment used for comparisons.

	Treated	Untreated
Combined	73.2% (.0171)*	2.6% (1.000)
Barrier Spray	29.9% (.8298)	44.6% (.5747)
LHM	70.6% (.0123)*	73.2% (.0361)*

**CHAPTER 4 - Targeted treatments against *Aedes (Stegomyia) albopictus* (Diptera: Culicidae) in heterogeneous landscapes: insights from a data-driven model**

Brandon Hollingsworth, Michael H. Reiskind, Alun L. Lloyd.

## **CONTRIBUTION**

As first author on this publication, I was responsible for designing the model presented in this manuscript, along with performing the parameter estimation and simulations. I was also responsible for analyzing results, producing figures, and writing the manuscript.

## ABSTRACT

*Aedes (Stegomyia) albopictus* (Skuse) has become a ubiquitous nuisance and potential vector throughout much of the United States since its introduction in 1985. The emergence of new *Aedes*-vectored arboviruses, the reemergence of dengue and yellow fever, and uncertainty surrounding the effectiveness of ultra-low volume insecticide applications have led to interest in developing novel control plans for quickly and efficiently reducing *Aedes* populations in response to outbreaks of disease. However, spatial heterogeneity in the distribution of *Ae. albopictus* can make designing efficient control programs difficult. I parameterized a two-patch model of mosquito dynamics using data collected during a field experiment. Our best-fit model estimated that the mean adult lifespan was around 31 days, the barrier spray initially reduced the adult lifespan to 3 days with a 9 day half-life for its effectiveness, and that larval habitat management resulted in a reduction of larval habitat >50%. I then used our parameter estimates to simulate 9 different control plans across a synthetic neighborhood of 81 interconnected yards. These control plans vary in the level of knowledge of the mosquito distribution that is assumed and the proportion of houses that are treated. Using the best fit model, I predicted that treating 25% of houses is sufficient to reduce the neighborhood-wide mosquito population by 51.3%, even when houses are randomly selected. When I allowed for targeted control through imperfect or perfected knowledge of the mosquito distribution, the impact of treating 25% of houses increases to 71% and 82%, respectively. These predictions suggest that there is little added benefit of treating more than 25% to 50% of yards in a neighborhood, and that perfect knowledge of the population distribution is not necessary to achieve high levels of reduction.

## INTRODUCTION

Since its introduction into the United States (US) in Texas in 1985 (Sprenger & Wuithiranyagool, 1986), *Aedes (Stegomyia) albopictus* (Skuse) has spread throughout much of the US. Currently in the US, populations of *Ae. albopictus* are ubiquitous from Texas to Florida and as far north as Virginia and Washington, DC, and populations in heavily urbanized areas in Arizona and New York (Hahn et al., 2017). More recently, *Ae. albopictus* was introduced into California and is spreading rapidly (Hahn et al., 2017). This spread has been facilitated by the ability of *Ae. albopictus* to oviposit in a variety of man-made containers, e.g. tires and accumulated trash, and the ability of eggs to undergo diapause, lasting for months (Hawley, 1988). *Aedes albopictus* prefers peridomestic environments, where containers are plentiful, putting it in close contact with human populations. This proximity to humans, combined with high population densities and preference for human hosts, often results in high levels of nuisance and disease risk. Nuisance is often the main concern associated with *Ae. albopictus* populations in the US, as opposed to risk to public health (Lambrechts et al., 2010). However, it has been shown in laboratory settings to be a competent vector for dengue (Boromisa et al., 1987) and was the main vector in outbreaks of dengue in Hawaii in 2001 (Effler et al., 2005) and Guangzhou, China in 2014 (Luo et al., 2017) and chikungunya on Reunion Island from 2005-2006 (Gérardin et al., 2008). For these reasons, *Ae. albopictus* is considered a potential culprit for future arboviral outbreaks in the US (Gostin & Hodge, 2016; Messina et al., 2016; Moreno-Madriñán et al., 2018).

While *Ae. albopictus* exists across a large area of the US, its abundance can vary significantly across relatively small spatial scales, on the order of 10s of meters (Hollingsworth et al., 2020; Reiskind et al., 2017). This variation in abundance is due to the low vagility of *Ae.*

*albopictus* and the small size and heterogeneous distribution of its preferred oviposition and resting habitat. It has been estimated that most female *Ae. albopictus* move as little as 250m in their lifetime (Marini et al., 2019) and rarely more than 1km under their own volition (Medeiros et al., 2017). In Hollingsworth et al. (2020), traps set in suburban yards in the Raleigh, NC area recorded between 1 and 43 female *Ae. albopictus* per trap night, with counts per trap night differing by up to 27 female *Ae. albopictus* between adjacent neighbors and low levels of correlation,  $\rho = .212$ . This fine-scale spatial heterogeneity and low movement rates results in population structure that can have important implications for the effectiveness of control programs.

Mosquito control in the US has historically been performed by mosquito abatement districts and targeted species commonly responsible for disease in the region. Until the elimination of malaria in the US in 1951 (Williams, 1963), this was often the malaria vector, *Anopheles quadrimaculatus* Say. More recently, the focus has switched to controlling *Culex* mosquitoes following the introduction of West Nile virus (WNV) and the reemergence of eastern equine encephalitis (EEE) and St. Louis encephalitis (SLE) (Wilson et al., 2020). However, recent outbreaks of Zika and dengue in the Americas, a high willingness to pay for mosquito nuisance control (Dickinson & Paskewitz, 2012; Dupont, 2003), the continued spread of container *Aedes* (Hahn et al., 2017; Hopperstad & Reiskind, 2016), and the expected reemergence and spread of *Aedes*-vectored diseases (Wilson et al., 2020) have generated interest in developing plans for the control of *Aedes* mosquitoes. Recently, the focus of mosquito control in much of the US, performed by decentralized mosquito abatement districts and a rapidly growing private pest control industry, is minimizing nuisance as much as disease risk (Wilson et al., 2020). Mosquito abatement districts typically attempt to control mosquito populations over

large areas using a combination of ultra-low volume (ULV) sprays deployed from vehicle-based sprayers and removal or treatment of significant oviposition habitats, e.g. drainage areas and swamps. In contrast, private pest control companies, responsible for treatment of individual yards, have chosen to rely instead on barrier sprays, typically pyrethroid based, applied to private properties in conjunction with a reduction in oviposition habitat to control peridomestic, pest mosquito species (Hollingsworth et al., 2020).

While there is a growing body of literature supporting the effectiveness of barrier sprays for reducing *Aedes* populations within treated areas (Fulcher et al., 2015; Hollingsworth et al., 2020; Hurst et al., 2012; Muzari et al., 2014; Richards et al., 2017; Stoops et al., 2019; Trout et al., 2007; Vandusen et al., 2016), larger-scale chemical-based control of *Ae. albopictus* has proven more difficult, and there continues to be a significant debate about the effectiveness of ULV spraying against *Aedes* mosquitoes (Bonds, 2012; Bowman et al., 2016; Faraji & Unlu, 2016; Roiz et al., 2018; Wilson et al., 2015). In addition to questions about effectiveness, uniform treatments with ULV spraying over large areas presents an inherent risk for the emergence of resistant populations of *Ae. albopictus*, something that has been seen worldwide (Dusfour et al., 2019; Moyes et al., 2017; Tancredi et al., 2020) and to other insect populations, e.g. butterflies, in the area (Oberhauser et al., 2009). However, recent work on honeybees suggests that they may be unaffected by ULV spraying in field settings (Boyce et al., 2007; Pokhrel et al., 2018).

One approach that has been suggested to help mitigate many of these issues is the development of Integrated Vector Management (IVM) plans (Achee et al., 2019; Fouet & Kamdem, 2018; Roiz et al., 2018). These approaches follow the guidelines of Integrated Pest Management (IPM) plans that have been developed in previous decades for crop pests (Gould,

1998; Gould et al., 2018; Knipling, 1972; Tabashnik et al., 2004) and seek to integrate knowledge about the ecology and evolution of their targeted species to create more effective, sustainable plans. While IPM has been successful in reducing the costs associated with agricultural pests, the development of IVM for mosquito species, especially *Aedes* mosquitoes, has been much slower. Within the IVM framework, many have advocated for targeted treatments of areas with dense *Aedes* populations (Baldacchino et al., 2015; Fouet & Kamdem, 2018; Unlu et al., 2016), allowing areas with smaller populations to remain untreated. If targeted control can be accurately implemented across heterogeneous landscapes, it is expected that treatments will have an increased effect on the overall mosquito population compared to non-targeted treatments. This would allow IVMs to provide a cost-effective approach to managing *Aedes* populations across a large heterogeneous landscape (Roiz et al., 2018).

Empirical evidence for the effect of yard-based treatments outside of their treatment area is scarce, so I used data collected in Hollingsworth et al. (2020) to test the effectiveness of different control strategies deployed across a neighborhood. This experiment measured the effectiveness of two common treatments, larval habitat management (LHM) and barrier sprays, over a 25-day post-treatment period. LHM is a common mosquito control technique that aims to reduce the presence of oviposition and larval development habitat, most notably standing water, in an area. This is commonly done through “tip-and-toss”, where containers are emptied and removed so that they do not refill. Barrier-sprays are applications of chemical based adulticides, that are applied to foliage and other resting spots, along with the edge of the treated area. Hollingsworth et al. (2020) conducted a longitudinal study of 16 pairs of adjacent yards randomly assigned to a factorial, LHM by barrier spray, experimental design. They showed that



barrier sprays not only reduced the populations within treated yards, but likely reduced the population in untreated neighboring yards.

To explore the effectiveness of targeted controls implemented in heterogeneous neighborhoods, I used data collected in Hollingsworth (2020) to estimate parameters for a model of targeted yard-based treatments in suburban neighborhood settings. Using these parameters, I then simulated the mosquito population in the neighborhood under various theoretical control strategies to predict the neighborhood-wide reduction in the mosquito population. By examining how population reduction changes with the proportion of yards treated in the model, I assessed the benefit of targeted treatments with different levels of knowledge about the mosquito population's distribution across the neighborhood.

In the following sections of this chapter, I will (1) describe the formulation of the model for neighborhood-wide *Ae. albopictus* population dynamics, (2) describe how parameter estimation was performed using a modified version of this model, (3) present the results of parameter estimation and model simulations, and (4) discuss implications of the modeling results.

## METHODS

### Model Formulation

#### *Within Patch Dynamics*

Populations in each yard were modeled using a two life-stage model, representing the aquatic juvenile and terrestrial adult stages (Equations 1). Juvenile mosquitoes are recruited into the model at a constant per adult female rate,  $b$ , die at per capita rate  $d(J)$ , and emerge as adults at per capita rate  $e(J)$ , where both the per capita mortality and emergence rate can be a function of juvenile density. After emergence, adults die at per capita rate  $d_A$ .

$$\begin{aligned}
\dot{J} &= bA - d(J)J - e(J)J \\
\dot{A} &= e(J)J - d_A A
\end{aligned}
\tag{1}$$

Density dependence is assumed to only act on the aquatic juvenile stage where the population is constrained by intraspecific competition for resources. Density dependence is often modelled as only affecting the juvenile death rate, but experimental results suggest that density dependence affects both the mortality rate and the time to emergence (Alto et al., 2005; Hancock et al., 2016; Legros et al., 2009), and that the relationship is roughly linear in both cases (Hancock et al., 2016). However, others have made alternative assumptions (Legros et al., 2009; Walsh et al., 2012). I chose to model both the juvenile mortality rate and the time to emergence as linearly dependent on the juvenile density. To examine how these assumptions affect our results, I compared results for three different models, comprised of all combinations of functions given in Table 1 that include density dependence parameters either in the larval mortality rate ( $k_L$ ), emergence rate ( $k_E$ ), or both.

Baseline	Linear
$d(J) = d_J J$	$d(J) = d_J \left(1 + \frac{J}{k_L}\right)$
$e(J) = e$	$e(J) = e \left(1 + \frac{J}{k_E}\right)^{-1}$

**Table 4.1: Equations for the dependence of the per capita juvenile mortality and emergence rates on the density of juveniles within a patch.**

#### *Control*

Mosquito control is assumed to affect the population in two ways. Larval habitat management is assumed to reduce the density-dependence parameters,  $k_L$  and  $k_E$ , by some

proportion,  $R$ , e.g.  $\hat{k}_L = k_L(1 - R)$ , and barrier sprays are assumed to result in a proportional increase,  $C$ , in the adult mortality rate, i.e.  $\hat{d}_A = d_A(1 + C)$ . Each of these controls is temporary and their effectiveness is assumed to decay exponentially over time, with constants  $r_R$  and  $r_C$  respectively (Equation 2). In general, I use parameters denoted with carets, e.g.  $\hat{d}(J)$ , to represent parameters that have been modified by a control measure.

$$\begin{aligned}\dot{R} &= -r_R R \\ \dot{C} &= -r_C C\end{aligned}\tag{2}$$

### *Movement*

Mosquitoes are assumed to move between neighboring yards at an average per capita rate,  $m$ , that is biased by the presence of suitable habitat in the yards, which has been observed in *Ae. aegypti* (Edman et al., 1998). This assumes that individual mosquitoes will search in the general area for suitable habitat and will be more likely to move from a yard with very little habitat to a yard with more habitat than vice versa. I chose to use the equilibrium number of juveniles present (without movement) as a surrogate for the availability of habitat. This requires the additional assumption that larval habitat removal does not alter the environment in a way that affects what the adults perceive as appropriate habitat, e.g. it involves treating and removing containers, not landscaping. This may be the case if adults seek out resting habitat, e.g. bushes, as opposed to oviposition habitat, e.g. containers, as resting habitat would be less likely to be removed during LHM.

To do this, I assume that the average per capita movement rate between patch  $i$  and  $j$ , with equilibrium values of juveniles  $J_i^*$  and  $J_j^*$ , at per capita rate  $m \frac{J_j^*}{n J_i^*}$ , where  $n$  is the total number of yards neighboring patch  $i$ . This gives the total emigration rate from patch  $i$  as

$m \frac{\sum_K \tilde{C}_{j,k} J_k^*}{n J_i^*}$ , where  $\tilde{C}_{j,k}$  is the connectivity matrix for patches in the neighborhood. In the case of a homogeneous distribution of habitat in the neighborhood, in which  $J_i^* = J_j^*$ , this reduces to unbiased movement between yards at per capita rate  $m$ . Importantly, in heterogeneous neighborhoods,  $J_i^*$  are assumed independent random variables,  $J_i^* \sim \text{lognorm}(\mu, \sigma^2)$ . This means that in the heterogeneous neighborhood,  $\mathbb{E} \left[ m \frac{\sum_K \tilde{C}_{j,k} J_k^*}{n J_i^*} \right] = m$  and  $\mathbb{E} \left[ m \frac{J_j^*}{n J_i^*} \right] = \frac{m}{n}$ , giving an expected mean per capita movement rate  $m$ . This gives the full multi-patch model given in Equations 3, where  $M_{i,j}$  is the matrix of movement rates.

$$\begin{aligned}
 \dot{J}_i &= bA_i - d_L(J_i)J_i - \hat{e}(J_i)J_i \\
 \dot{A}_i &= \hat{e}(J_i)J_i - \hat{d}_A A_i + M_{i,j}A_j \\
 \dot{R}_i &= -r_R R_i \\
 \dot{C}_i &= -r_C C_i
 \end{aligned} \tag{3}$$

I note that the movement kernel results in heterogeneity in the equilibrium adult population size between patches, even if there is no heterogeneity in larval habitat. This is a result of patches along the boundary having less migration into them due to an assumption of no migration into or out of the neighborhood.

## Parameter Estimation

### *Model Modification*

For parameter estimation, I used a two-patch formulation of our model, corresponding to the experimental units which consist of one treated and one untreated yard. I denote dynamics occurring in the treated yard with a subscript T and neighboring yards with subscript N. Each patch was assumed to have density-dependence parameters taken from a distribution with means,

$\bar{\mu}_{k_E}$  or  $\bar{\mu}_{k_L}$ , and corresponding covariance matrices. This allows us to account for the possibility of neighboring yards being more similar than yards from different pairs. For movement, I replace biased movement based on the ratio of mosquito population sizes with biasing parameters,  $g_T$  and  $g_N$ . These parameters account for any increased (or decreased) movement, compared to the average movement rate, out of the treated yard or neighboring yard, respectively. For parameter estimation,  $g_T$  and  $g_N$  are assumed to be random effects that vary between pairs of yards with mean one and covariance matrix. This allows for the possibility that higher than average movement in one direction may correlate with below average movement in the other. These modifications give the two-patch formulation seen in Equations 4.

$$\begin{aligned}
\dot{J}_T &= bA_T - \hat{d}(J_T)J_T - \hat{e}(J_T)J_T \\
\dot{A}_T &= \hat{e}(J_T)J_T - \hat{d}_A A_T - m(g_T A_T - g_N A_N) \\
\dot{J}_N &= bA_N - d(J_N)J_N - e(J_N)J_N \\
\dot{A}_N &= e(J_N)J_N - d_A A_N + m(g_T A_T - g_N A_N) \\
\dot{R} &= -r_R R \\
\dot{C} &= -r_C C
\end{aligned} \tag{4}$$

### *Estimated Parameters*

In all model fits, I estimated fixed-effects parameter values for the initial effect of barrier spray treatments,  $C(0)$ , the proportional reduction in larval habitat due to LHM,  $R(0)$ , and the movement rate,  $m$ . A single density-dependence parameter per model, either  $k_L$  or  $k_E$ , along with the movement biasing parameters were estimated as random effects, with means and covariance matrices. In addition to these parameters, either (a)  $b$ ,  $d_A$ , and  $r_C$  (b)  $b$  and  $d_A$  or (c)

$d_A$  and  $r_C$  were estimated, giving a total of 6 model fits. AIC scores of the fits were then used to choose the best fit for each model. All other biological parameters, e.g.  $d_L$  and  $e$ , are fixed using the functions estimated in Mordecai et al (2018) and the average temperature over the study period taken from NOAA's Global Historical Climate Network for the Raleigh-Durham International Airport (Menne et al., 2012). I assumed the number of adults,  $A(0)$ , and juveniles,  $J(0)$ , present at the beginning of the experiment is at the equilibrium value for the patch in the absence of movement. Hollingsworth et al. (2020) found no evidence for a loss of effect for LHM,  $r_R$ , and initial parameter estimates agreed with this result, therefore I chose to fix  $r_R = 0$ .

#### *Parameter Estimation Method*

I estimated all parameters using a non-linear mixed-effects model, with variables treated as discussed in the previous section. Parameter estimation was done within the nlmixr package (Fidler et al., 2019) in R (R Development Core Team, 2019). This package implements multiple estimation methods, but I chose to use SAEM (Delyon et al., 1999), due to its wide use in nonlinear mixed-effects modeling and ability to incorporate multiple observation types, i.e. observations from both treated and neighboring yards, concurrently. Briefly, SAEM works by dividing the parameter estimation method into two stages, an exploration and smoothing stage. The exploration stage works by using the Markov Chain Monte Carlo (MCMC) algorithm to find the general neighborhood of the maximum likelihood estimate, defined by the log-likelihood function. Once the exploration stage has converged, the smoothing stage uses an iterative process of (1) using MCMC to calculate a set of individual parameters from the population parameters from the previous step and (2) calculating new population parameters as the mean of the individual parameters from all previous steps of the smoothing stage. Parameter estimates were initialized using parameters from literature (Mordecai et al., 2017) where possible and best

guesses where not. Initial estimates along with their sources are listed in Table S4.1. All parameters were constrained to biologically plausible values through transforms, either a log transform to maintain non-negativity or, in the case of the reduction in larval habitat due to LHM, a logit transform to constrain the parameter to [0,1]. Diagnostic plots from model fits were inspected for any violation of assumptions using the xpose package (Jonsson & Karlsson, 1998) and are discussed in the supplemental information.

## **Simulations**

### *Neighborhood Configuration*

I simulated an artificial neighborhood as 81 interconnected patches arranged in a 9x9 grid, with each patch representing a single yard in a suburban neighborhood. Movement was assumed to only happen between adjacent neighbors, with diagonal neighbors not considered adjacent. The system was assumed to be closed, i.e. no movement into or out of the neighborhood, a situation which may occur in neighborhoods surrounded by roads or other barriers to *Aedes* movement. Dynamics within yards, along with movement between yards, was parameterized using the estimates from our best fit model. Empirical data suggested that the number of mosquitoes per yard was well described by a log-normal distribution (Figure 4.1), so I estimated the mean,  $\mu$ , and variance,  $\sigma^2$ , associated with this distribution to use in our simulations. To explore the effects that heterogeneity in larval habitat across the neighborhood had on our results, I also examined situations in which larval habitat is homogeneous across all patches or has twice the variance. For the sake of comparison,  $\mu$  was fixed across all simulations. The population was assumed to be at equilibrium at the start of the simulation. Simulations were conducted using the deSolve package (Soetaert et al., 2010) and all figures

were produced using the ggplot2 package (Wickham, 2016) in R (R Development Core Team, 2019).

### *Control Strategies*

I evaluated nine different treatment plans, described below (Table 4.2). These plans vary in the scale at which decisions are made (household vs. neighborhood) and the amount of information that is used (naïve vs informed). I ran 100 simulations of 5 treatments occurring every 3 weeks (21 days) using each treatment plan in our simulated neighborhood and recorded the mean reduction in adult female mosquito numbers across the neighborhood for the post-control period (105 days) in each simulation. Within a simulation, yards in which control was implemented did not change over time but could change between simulations. For plans that can vary in the proportion of houses that are treated, as opposed to those that have a strict spatial pattern, I simulated the control across all possible numbers of treated houses (1 to 81).

Naïve plans are those that do not leverage any information about the distribution of the mosquito population in the neighborhood. Here, I tested seven naïve plans. Five of these plans used spatial patterns and would assume neighborhood-wide acceptance. They were (1) treating a grid of houses, (2) treating all yards around the perimeter of the neighborhood, (3) treating all yards **except** those along the perimeter of the neighborhood, i.e. interior yards, (4) treating the yards in such a way that every yard is either treated or neighbors exactly one treated yard, and (5) treating rings of yards, starting with yards along the neighborhood perimeter. The remaining two plans are a neighborhood-level decision to randomly choose a proportion of yards to be treated and a laissez-faire system, allowing individual homeowners to decide on treatment, that assumes all homeowners are equally likely to opt in. For both the neighborhood-level decision



and the laissez-faire system, I examined the effect of varying the percentage of yards in the neighborhood that are treated.

In addition to the naïve plans, I tested two informed plans. The first assumes perfect knowledge of the mosquito distribution and treats the given proportion of the yards with the largest populations. The second assumes that while we do not have perfect knowledge of the distribution, we have some imperfect knowledge, such that houses with higher mosquito densities are proportionally more likely to be chosen for treatment. This is done by randomly sampling from the yards, with the probability of being chosen weighted by their equilibrium mosquito density. For each of these, I examined the effect of varying the percentage of yards in the neighborhood that are treated. In actuality, treatment decisions made by homeowners are likely somewhere between the “laissez-faire” and partial knowledge strategies described here.

### *Sensitivity Analysis*

I examined the effects of our choice of neighborhood size and the uncertainty in parameter estimates on our prediction of the mean reduction in the neighborhood-wide mosquito population. Results were produced for neighborhoods of 49, 121, and 169 patches and were compared to those from our 81-patch neighborhood. Sensitivity of our results to the parameter estimates was done through simulation in the FME package (Soetaert & Petzoldt, 2010) using 100 sample parameter values drawn from their 95% confidence intervals using Latin hypercube sampling. Results of this analysis are discussed in the supplemental information.

### **Cost-Benefit Analysis**

I assumed a constant marginal cost for treatments,  $m_c$ , i.e. treating an additional yard always costs the same amount, and that there is a constant benefit,  $\eta$ , in monetary terms, of a reduction in mosquito population size, relative to the equilibrium population size. To determine

the proportion of yards to treat, I found when the marginal cost equaled the marginal benefit, i.e.  $m_c = \eta B(p)$ , where  $B(p)$ , the marginal benefits curve, is the additional reduction in the neighborhood-wide mosquito population size due to treating an additional yard past the current proportion of yards treated,  $p$ . The proportion of yards,  $p$ , that satisfies this occurs when  $p = B^{-1}\left(\frac{m_c}{\eta}\right)$ , and I refer to  $\frac{m_c}{\eta}$  as our cost-benefit ratio. However, a closed form solution to the marginal benefits curve does not exist, so I estimated it by approximating the slope of the cost-benefits curve obtained from our simulations using a first-order approximation.

## RESULTS

### Parameter Estimation

Best fit parameters for each model are provided in Table 4.3. Since the model incorporating linear density-dependence terms in both the mortality and emergence rates is most biologically tractable, the results focus on Model 3. The third set of estimated parameters provided the best overall fit, according to AIC (Table 4.4). The model fit estimated an adult mortality rate of .03 /day (95% CI of (.00891, .112)) and an initial increase in adult mortality of 1150% (95% CI of (232%, 5660%)) due to the barrier spray. This means that the barrier spray initially reduces the average lifespan of adult mosquitoes in the treated yard from 31.6 days to 2.75 days. This effect was estimated to decay at a rate of .0802 (95% CI of (.0218, .296)), giving a half-life of around 9 days. LHM is predicted by the model to be capable of reducing more than 50% (95% CI of (.500, 1.00)) of the available larval habitat. The mean movement rate of adult *Ae. albopictus* between yards was estimated to be 4.42 /day (95% CI of (2.18, 8.98)), however there was significant between yard variation (BSV) (Table 4.3).

### Simulations

I simulated the dynamics in the synthetic neighborhood using the best fit model and parameters. I note here that the 95% confidence intervals reported are a result of randomness in the simulations, e.g. the population distribution and treatment pattern, and not a result of parameter uncertainty. Within the parameter space given by the 95% confidence intervals, there was little variation in the mean reduction predicted by our model (Supplemental Information).

Figure 4.2 shows an example run for a 9x9 neighborhood, in which 25% of the houses are randomly assigned to receive treatment, using the neighborhood-level naïve decision plan. Under this plan, our model predicted that all yards in the neighborhood will see some level of suppression due to treatments. Spatial heterogeneity in carrying capacity did not directly affect this observation but did create variation in how much reduction was seen in the yards. Within the 95% confidence for the estimated movement rate (2.18, 8.98), changes in the movement rate had no discernable effect on the simulation results, and all yards saw a reduction in population numbers. This is a direct result of migration of mosquitoes from untreated yards into treated yards, where they experience an increase in mortality, and are unlikely to return or be replaced by migration out of the treated yard. This also suggests that our results are robust to uncertainty in the movement rate within this confidence interval.

### **Evaluating Control Plans**

Figure 4.3 shows how the reduction in the mosquito population, in percentage of equilibrium population size, changes with the percentage of the neighborhood that is treated. Our simulations suggest that near complete suppression of the *Ae. albopictus* population ( $\approx 97\%$  reduction) neighborhood-wide is possible through the treatment of all yards in the neighborhood (Figure 4.3: Central Panel). For the treatment plans where the number of treated yards can be varied, we see that most of the benefit is obtained by treating a relatively small number of yards.

The extent to which this occurs changes drastically with both the control plan implemented and the level of spatial heterogeneity present in the neighborhood.

None of the spatially patterned plans, nor the plan using naïve neighborhood-level decision to randomly treat a proportion of the yards, outperformed the laissez-faire strategy in any situation (Figure 4.3). These plans would require considerable effort compared to the laissez-faire strategy, with no additional benefit, so I choose not to discuss them in detail.

Under the assumption of homogeneous distribution of larval habitat in the neighborhood, simulations showed no difference in how treatment plans perform (Top Panel, Figure 4.3). However, the laissez-faire treatment plan had a significantly larger standard deviation than the others, due to uncertainty in the number of houses receiving treatment. All treatments plans saw large reductions in the neighborhood-wide population size occur with only a small percentage of the neighborhood treated. For instance, treating 25% of yards resulted in approximately a 60% reduction in the neighborhood-wide mosquito population (95% CI of (48.0%, 72.0%)) for laissez-faire control and in the range (58.2%, 61.8%) for all others.

Under the assumption that the spatial heterogeneity follows either the observed distribution or a distribution with double the observed variance, simulations clearly showed the benefit of using knowledge about the population's distribution. Under the observed level of between yard variation, the use of imperfect knowledge increased the reduction in the neighborhood-wide population from 51.3% (95% CI of (29.9%, 72.7%)) to 71.4% (95% CI of (61.5%, 81.3%)) when a quarter of the yards are treated. Using perfect knowledge increased this reduction to 82.4% (95% CI of (78.9%, 86.1%)). Likewise, with 50% of yards treated there was an increase in reduction from 75.0% (95% CI of (64.3%, 85.8%)) under the laissez-faire plan to 87.2% (95% CI of (83.2%, 91.3%)) and 91.4% (95% CI of (90.1%, 92.7%)) utilizing imperfect

and perfect knowledge, respectively. The benefit of using knowledge of the mosquito population distribution was seen to increase further with an increased heterogeneity in the carrying capacity between yards (Figure 4.3).

### **Cost-Benefit Analysis**

I used our estimates of the marginal benefit curve,  $B(p)$ , obtained from the first order approximation of the derivative of the cost-benefit curves (Figure 4.3), to numerically find the relation between the cost-benefit ratio and percentage of yards that should be treated so that the marginal benefit and cost are equal (Figure 4.4). As in the cost-benefit curves, there is no difference between plans under the assumption of a homogeneous distribution of larval habitat between yards. When heterogeneity in larval habitat was taken into account, plans taking advantage of perfect, and to a lesser extent imperfect, knowledge saw a steep drop in the percentage of yards treated until approximately 25%, at which point decrease slows. This suggests that it would rarely be beneficial, for the neighborhood as a whole, to treat more than 25% of yards in a neighborhood when information about the distribution is used to inform which yards to treat. This is similar to the results seen with the cost-benefit curve, where a 25% of the yards being treated resulted in a neighborhood-wide reduction of 71.4% or 82.4% (CIs given previously) depending on how much information is known.

## **DISCUSSION**

Our results suggested that the yard-scale population dynamics of *Ae. albopictus* were best described by a model that incorporated density dependence in both the larval mortality rate and the emergence rate. This concurs with experimental data that shows that both rates vary with larval density (Alto et al., 2005; Hancock et al., 2016). Our best fit parameter estimates for this model suggest that the average lifespan of *Ae. albopictus* in the Raleigh, NC area was around 31

days, which falls between the presumed lifespan of around 20 days (Hawley, 1988) used in other models of *Ae. albopictus* dynamics and the estimate of 104 days, taken from laboratory studies, from Mordecai et al. (2017), and is at the high end of previous estimates of between 4 and 32 days obtained from a review of mark-recapture studies (Brady et al., 2013). I also found that the use of barrier spray treatments resulted in an additional increase in adult mortality of around 1150%, which decreases by half every 9 days. In a single isolated patch, a 1150% increase in adult mortality would be expected to result in a much larger decrease in *Ae. albopictus* counts than was observed in Hollingsworth et al. (2020). However, the high movement rate suggests that the mosquitoes caught in yards post-barrier spray may be likely new immigrants from neighboring yards. Further, a half-life of 8.64 days would result in a decrease in the effect to 155% after 25 days, the length of post-control observation, which would be a sufficient reduction in impact to allow populations to begin to rebound. The movement rate I estimated suggests that *Ae. albopictus* routinely moves between yards multiple times a day. While this may seem contrary to their short dispersal range, it is not unexpected since study yards were often <30m across with much of the available resting habitat along the edge, meaning that it was only a short flight into neighboring yards. Our model also suggests that LHM is effective in removing the larval habitat within treated yards, with estimates suggesting it removes 50-100% (95% CI) of the habitat.

Using targeted applications of adulticides and LHM has been suggested as a possible alternative to ULV spraying for the control of *Aedes* mosquitoes (Baldacchino et al., 2015; Fouet & Kamdem, 2018; Unlu et al., 2016). Simulations suggest that it should be possible to achieve greater than a 70% reduction in the neighborhood-wide population while treating approximately 25% of yards with targeted barrier sprays and LHM, even without perfect knowledge about the

underlying spatial distribution of the population. This suggests that targeted controls, using a combination of barrier sprays and LHM, are a viable option for controlling *Aedes* mosquitoes in suburban areas and could prove preferential to ULV sprays under some situations.

The predicted reduction in the neighborhood-wide population density from our best fit model are robust to changes in parameter values within our estimated 95% confidence intervals (Supplemental Information). This suggests that the results will likely extend to models of *Ae. aegypti*, as well as container *Aedes* found in other regions, e.g. *Aedes notoscriptus* in California and *Aedes koreicus* in Europe, as life history traits (Mordecai et al., 2017) and movement (Juarez et al., 2020; Medeiros et al., 2017) have not been found to differ vastly between the species in the US. Other questions about the use of targeted controls can initially be addressed within the modeling framework developed here, including the probability of insecticide resistance emergence and the inclusion of epidemiological endpoints for viral disease. In addition, this model, and the parameter estimates I present, can be used to inform optimal treatment strategies for reducing either the disease risk or nuisance associated with *Ae. albopictus*.

Our analysis had several limitations, some of which reflect the experimental data on which it builds. Our estimate of the reduction in larval habitat due to LHM produced a large 95% confidence interval (50%, 100%) and I had insufficient information to estimate the rate at which larval habitat recovers following treatment. This was due to limitations of the experiment the data was taken from (Hollingsworth et al., 2020), which only trapped 25 days post-treatment. However, previous experiments measuring the reduction in larval habitat following mitigation have also estimated 43-98% reductions in habitat (Tun-Lin et al., 2009). As discussed in Hollingsworth et al. (2020), LHM only began to show a significant effect 21 days post-treatment and the effect was still increasing at 25 days. A delay in effect of this length is not surprising,

given our estimate of an average lifespan of 31 days for *Ae. albopictus* in the area. I also lacked any information about the mosquito population in yards surrounding those in the experiment. Because of this, I chose to assume a closed system during parameter estimation. It is also possible that the use of ordinary differential equation (ODE) models are inappropriate at this scale, as the populations within each yard are small, on the order of tens to hundreds or smaller following treatment. However, ODE models are often used to understand underlying dynamics before introducing the increased complexity of stochastic processes. Lastly, our model assumes that the spatial distribution of larval habitat does not change over time, i.e. “hot-spots” do not move. There is some disagreement in the literature as to the validity of this assumption, but at least two studies have suggested it is the case for *Ae. aegypti* (Barrera, 2011; Estallo et al., 2013). Future modeling efforts can relax this assumption and evaluate the impact of unstable “hot-spots” of larval habitat.

Decisions concerning where to treat are almost always informed, to some extent. These decisions are made either by homeowners who have experienced nuisance or by mosquito control professionals who have based their choices on observational data. For that reason, it is likely that a true laissez-faire system would be a combination of the laissez-faire strategy, as presented here, and the partial knowledge strategy. If homeowners are sufficiently knowledgeable about the mosquito population in their yard, a voucher program that lowers the cost of treatments, thus increasing the number of homeowners choosing treatment, may be more effective at increasing the neighborhood-wide reduction than extensive mosquito surveillance.

These models, parameterized using field data on the impact of controls, indicate the likely effectiveness of targeted controls and can provide guidelines for implementation of efficient mosquito control. However, models cannot replace field experiments to evaluate the



effectiveness of different strategies, and the results I present here should be experimentally tested. Experiments and control programs operating at the neighborhood-scale are expensive and require extensive coordination, and our results should be used as a starting point for these programs. Importantly, our models suggest that it is likely that neither detailed data on the distribution of *Aedes* in the area nor access to every yard is necessary for the treatment programs to successfully reduce the population density of *Ae. albopictus* neighborhood wide. However, the use of some information about the distribution of mosquitoes substantially improves control.

## REFERENCES

- Achee NL, Grieco JP, Vatandoost H, Seixas G, Pinto J, et al. (2019) Alternative strategies for mosquito-borne arbovirus control. *PLOS Neglected Tropical Diseases* 13(1): e0006822. <https://doi.org/10.1371/journal.pntd.0006822>
- Alto, B. W., Lounibos, L. P., Higgs, S., & Juliano, S. A. (2005). Larval competition differentially affects arbovirus infection in *Aedes* mosquitoes. *Ecology*, 86(12), 3279–3288. <https://doi.org/10.1890/05-0209>
- Baldacchino, F., Caputo, B., Chandre, F., Drago, A., della Torre, A., Montarsi, F., & Rizzoli, A. (2015). Control methods against invasive *Aedes* mosquitoes in Europe: a review. *Pest management science*, 71(11), 1471–1485. <https://doi.org/10.1002/ps.4044>
- Barrera, R. (2011). Spatial stability of adult *Aedes aegypti* populations. *American Journal of Tropical Medicine and Hygiene*, 85(6), 1087–1092. <https://doi.org/10.4269/ajtmh.2011.11-0381>
- Bonds, J. A. S. (2012). Ultra-low-volume space sprays in mosquito control: A critical review. *Medical and Veterinary Entomology*, 26(2), 121–130. <https://doi.org/10.1111/j.1365-2915.2011.00992.x>
- Boromisa, R. D., Rai, K. S., & Grimstad, P. R. (1987). Variation in the vector competence of geographic strains of *Aedes albopictus* for dengue 1 virus. *Journal of the American Mosquito Control Association*, 3(3), 378–386.
- Bowman, L. R., Donegan, S., & McCall, P. J. (2016). Is Dengue Vector Control Deficient in Effectiveness or Evidence?: Systematic Review and Meta-analysis. *PLOS Neglected Tropical Diseases*, 10(3), e0004551. <https://doi.org/10.1371/journal.pntd.0004551>
- Boyce, W. M., Lawler, S. P., Schultz, J. M., McCauley, S. J., Kimsey, L. S., Niemela, M. K., Nielsen, C. F., & Reisen, W. K. (2007). Nontarget effects of the mosquito adulticide

- pyrethrin applied aerially during a West Nile virus outbreak in an urban California environment. *Journal of the American Mosquito Control Association*, 23(3), 335–339.  
[https://doi.org/10.2987/8756-971X\(2007\)23\[335:NEOTMA\]2.0.CO;2](https://doi.org/10.2987/8756-971X(2007)23[335:NEOTMA]2.0.CO;2)
- Brady, O. J., Johansson, M. A., Guerra, C. A., Bhatt, S., Golding, N., Pigott, D. M., Delatte, H., Grech, M. G., Leishnam, P. T., Maciel-De-Freitas, R., Styer, L. M., Smith, D. L., Scott, T. W., Gething, P. W., & Hay, S. I. (2013). Modelling adult *Aedes aegypti* and *Aedes albopictus* survival at different temperatures in laboratory and field settings. *Parasites and Vectors*, 6(1), 1–12. <https://doi.org/10.1186/1756-3305-6-351>
- Delyon, B., Lavielle, M., & Moulines, E. (1999). Convergence of a stochastic approximation version of the EM algorithm. *Annals of Statistics*, 94–128.  
<https://doi.org/10.1214/aos/1018031103>
- Dickinson, K., & Paskewitz, S. (2012). Willingness to Pay for Mosquito Control: How Important Is West Nile Virus Risk Compared to the Nuisance of Mosquitoes? *Vector-Borne and Zoonotic Diseases*, 12(10), 886–892. <https://doi.org/10.1089/vbz.2011.0810>
- Dupont, D. P. (2003). Do children matter? An examination of gender differences in environmental valuation. *Working Paper - Centre for Social and Economic Research on the Global Environment*, 1, 1–30. <https://doi.org/10.1016/j.ecolecon.2004.01.013>
- Dusfour, I., Vontas, J., David, J.-P., Weetman, D., Fonseca, D. M., Corbel, V., Raghavendra, K., Coulibaly, M. B., Martins, A. J., Kasai, S., & Chandre, F. (2019). Management of insecticide resistance in the major *Aedes* vectors of arboviruses: Advances and challenges. *PLoS Neglected Tropical Diseases*, 13(10), e0007615.  
<https://doi.org/10.1371/journal.pntd.0007615>

- Edman, J. D., Scott, T. W., Costero, A., Morrison, A. C., Harrington, L. C., & Clark, G. G. (1998). *Aedes aegypti* (Diptera: Culicidae) Movement Influenced by Availability of Oviposition Sites. *Journal of Medical Entomology*, 35(4), 578–583. <https://doi.org/10.1093/jmedent/35.4.578>
- Effler, P. v., Pang, L., Kitsutani, P., Vorndam, V., Nakata, M., Ayers, T., Elm, J., Tom, T., Reiter, P., Rigau-Perez, J. G., Hayes, J. M., Mills, K., Napier, M., Clark, G. G., & Gubler, D. J. (2005). Dengue fever, Hawaii, 2001-2002. *Emerging Infectious Diseases*, 11(5), 742. <https://doi.org/10.3201/eid1105.041063>
- Estallo, E. L., Más, G., Vergara-Cid, C., Lanfri, M. A., Ludueña-Almeida, F., Scavuzzo, C. M., Introini, M. V., Zaidenberg, M., & Almirón, W. R. (2013). Spatial Patterns of High *Aedes aegypti* Oviposition Activity in Northwestern Argentina. *PLoS ONE*, 8(1), e54167. <https://doi.org/10.1371/journal.pone.0054167>
- Faraji, A., & Unlu, I. (2016). The Eye of the Tiger, the Thrill of the Fight: Effective Larval and Adult Control Measures Against the Asian Tiger Mosquito, *Aedes albopictus* (Diptera: Culicidae), in North America. *Journal of Medical Entomology*, 53(5), 1029–1047. <https://doi.org/10.1093/jme/tjw096>
- Fidler, M., Wilkins, J. J., Hooijmaijers, R., Post, T. M., Schoemaker, R., Trame, M. N., Xiong, Y., & Wang, W. (2019). Nonlinear Mixed-Effects Model Development and Simulation Using nlmixr and Related R Open-Source Packages. *CPT: Pharmacometrics and Systems Pharmacology*, 8(9), 621–633. <https://doi.org/10.1002/psp4.12445>
- Fouet, C., & Kamdem, C. (2019). Integrated mosquito management: is precision control a luxury or necessity?. *Trends in parasitology*, 35(1), 85-95. <https://doi.org/10.1016/j.pt.2018.10.004>

- Fulcher, A., Farooq, M., Smith, M. L., Li, C.-X., Scott, J. M., Thomson, E., Kaufman, P. E., & Xue, R.-D. (2015). Evaluation of a New Spraying Machine for Barrier Treatment and Penetration of Bifenthrin on Vegetation Against Mosquitoes. *Journal of the American Mosquito Control Association*. 31(1), 85-92. <https://doi.org/10.2987/14-6424R.1>
- Gérardin, P., Guernier, V., Perrau, J., Fianu, A., le Roux, K., Grivard, P., Michault, A., de Lamballerie, X., Flahault, A., & Favier, F. (2008). Estimating chikungunya prevalence in La Réunion Island outbreak by serosurveys: Two methods for two critical times of the epidemic. *BMC Infectious Diseases*, 8, 99. <https://doi.org/10.1186/1471-2334-8-99>
- Gostin LO, Hodge JG. (2016). Is the United States Prepared for a Major Zika Virus Outbreak? *JAMA*. 315(22), 2395–2396. doi:10.1001/jama.2016.4919
- Gould, F. (1998). Sustainability of Transgenic Insecticidal Cultivars: Integrating Pest Genetics and Ecology. *Annual Review of Entomology*. 43, 701-726. <https://doi.org/10.1146/annurev.ento.43.1.701>
- Gould, F., Brown, Z. S., & Kuzma, J. (2018). Wicked evolution: Can we address the sociobiological dilemma of pesticide resistance?. *Science*, 360(6390), 728-732. <https://doi.org/10.1126/science.aar3780>
- Hahn, M. B., Eisen, L., McAllister, J., Savage, H. M., Mutebi, J. P., & Eisen, R. J. (2017). Updated reported distribution of *Aedes (stegomyia) aegypti* and *Aedes (stegomyia) albopictus* (diptera: Culicidae) in the United States, 1995–2016. *Journal of medical entomology*, 54(5), 1420-1424. <https://doi.org/10.1093/jme/tjx088>
- Hancock, P. A., White, V. L., Callahan, A. G., Godfray, C. H. J., Hoffmann, A. A., & Ritchie, S. A. (2016). Density-dependent population dynamics in *Aedes aegypti* slow the spread of

- wMel Wolbachia. *Journal of Applied Ecology*, 53(3), 785–793.  
<https://doi.org/10.1111/1365-2664.12620>
- Hawley, W. A. (1988). The biology of *Aedes albopictus*. *Journal of the American Mosquito Control Association. Supplement*, 1, 1–39.
- Hollingsworth, B., Hawkins, P., Lloyd, A. L., & Reiskind, M. H. (2020). Efficacy and Spatial Extent of Yard-Scale Control of *Aedes (Stegomyia) albopictus* (Diptera: Culicidae) Using Barrier Sprays and Larval Habitat Management. *Journal of Medical Entomology*, 57(4), 1104–1110. <https://doi.org/10.1093/jme/tjaa016>
- Hopperstad, K. A., & Reiskind, M. H. (2016). Recent Changes in the Local Distribution of *Aedes aegypti* (Diptera: Culicidae) in South Florida, USA. *Journal of Medical Entomology*, 53(4), 836–842. <https://doi.org/10.1093/jme/tjw050>
- Hurst, T. P., Ryan, P. A., & Kay, B. H. (2014). Efficacy of residual insecticide Biflex AquaMax applied as barrier treatments for managing mosquito populations in suburban residential properties in southeast Queensland. *Journal of medical entomology*, 49(5), 1021–1026.  
<https://doi.org/10.1603/ME11278>
- Jonsson, E. N., & Karlsson, M. O. (1998). Xpose - An S-PLUS based population pharmacokinetic/pharmacodynamic model building aid for NONMEM. *Computer Methods and Programs in Biomedicine*, 58, 51–64. [https://doi.org/10.1016/S0169-2607\(98\)00067-4](https://doi.org/10.1016/S0169-2607(98)00067-4)
- Juarez, J. G., Garcia-Luna, S., Chaves, L. F., Carbajal, E., Valdez, E., Avila, C., Tang, W., Martin, E., Barrera, R., Hemme, R. R., Mutebi, J.-P., Vuong, N., Roark, E. B., Maupin, C. R., Badillo-Vargas, I. E., & Hamer, G. L. (2020). Dispersal of female and male *Aedes aegypti* from discarded container habitats using a stable isotope mark-capture study design in South Texas. *Scientific Reports*, 10(1), 6803. <https://doi.org/10.1038/s41598-020-63670-9>

- Knippling, E. F. (1972). ENTOMOLOGY AND THE MANAGEMENT OF MAN'S ENVIRONMENT. *Australian Journal of Entomology*, 11(3), 153–167.  
<https://doi.org/10.1111/j.1440-6055.1972.tb01618.x>
- Lambrechts, L., Scott, T. W., & Gubler, D. J. (2010). Consequences of the expanding global distribution of *Aedes albopictus* for dengue virus transmission. *PLoS Neglected Tropical Diseases*, 4(5), e646. <https://doi.org/10.1371/journal.pntd.0000646>
- Legros, M., Lloyd, A. L., Huang, Y., & Gould, F. (2009). Density-Dependent Intraspecific Competition in the Larval Stage of *Aedes aegypti* (Diptera: Culicidae): Revisiting the Current Paradigm. *Journal of Medical Entomology*, 46(3), 409–419.  
<https://doi.org/10.1603/033.046.0301>
- Luo, L., Jiang, L. Y., Xiao, X. C., Di, B., Jing, Q. L., Wang, S. Y., Tang, J. L., Wang, M., Tang, X. P., & Yang, Z. C. (2017). The dengue preface to endemic in mainland China: The historical largest outbreak by *Aedes albopictus* in Guangzhou, 2014. *Infectious Diseases of Poverty*, 6(1), 148. <https://doi.org/10.1186/s40249-017-0352-9>
- Marini, F., Caputo, B., Pombi, M., Travaglio, M., Montarsi, F., Drago, A., Rosà, R., Manica, M., & della Torre, A. (2019). Estimating Spatio-Temporal Dynamics of *Aedes Albopictus* Dispersal to Guide Control Interventions in Case of Exotic Arboviruses in Temperate Regions. *Scientific Reports*, 9(1), 10281. <https://doi.org/10.1038/s41598-019-46466-4>
- Medeiros, M. C. I., Boothe, E. C., Roark, E. B., & Hamer, G. L. (2017). Dispersal of male and female *Culex quinquefasciatus* and *Aedes albopictus* mosquitoes using stable isotope enrichment. *PLoS Neglected Tropical Diseases*, 11(1).  
<https://doi.org/10.1371/journal.pntd.0005347>

- Menne, M. J., Durre, I., Korzeniewski, B., McNeal, S., Thomas, K., Yin, X., Anthony, S., Ray, R., Vose, R. S., E. Gleason, B., & Houston, T. G. (2012). *Global Historical Climatology Network - Daily (GHCN-Daily), Version 3*. NOAA National Climate Data Center.  
<https://doi.org/10.7289/V5D21VHZ>
- Messina, J. P., Kraemer, M. U. G., Brady, O. J., Pigott, D. M., Shearer, F. M., Weiss, D. J., Golding, N., Ruktanonchai, C. W., Gething, P. W., Cohn, E., Brownstein, J. S., Khan, K., Tatem, A. J., Jaenisch, T., Murray, C. J. L., Marinho, F., Scott, T. W., & Hay, S. I. (2016). Mapping global environmental suitability for Zika virus. *ELife*, 5, e15272.  
<https://doi.org/10.7554/eLife.15272>
- Mordecai, E. A., Cohen, J. M., Evans, M. v., Gudapati, P., Johnson, L. R., Lippi, C. A., Miazgowicz, K., Murdock, C. C., Rohr, J. R., Ryan, S. J., Savage, V., Shocket, M. S., Stewart Ibarra, A., Thomas, M. B., & Weikel, D. P. (2017). Detecting the impact of temperature on transmission of Zika, dengue, and chikungunya using mechanistic models. *PLoS Neglected Tropical Diseases*, 11(4), e0005568.  
<https://doi.org/10.1371/journal.pntd.0005568>
- Moreno-Madriñán, M. J., & Turell, M. (2017). Factors of concern regarding Zika and other *Aedes aegypti*-transmitted viruses in the United States. *Journal of medical entomology*, 54(2), 251-257. <https://doi.org/10.1093/jme/tjw212>
- Moyes, C. L., Vontas, J., Martins, A. J., Ng, L. C., Koou, S. Y., Dusfour, I., ... & Weetman, D. (2017). Contemporary status of insecticide resistance in the major *Aedes* vectors of arboviruses infecting humans. *PLoS neglected tropical diseases*, 11(7), e0005625.  
<https://doi.org/10.1371/journal.pntd.0005625>



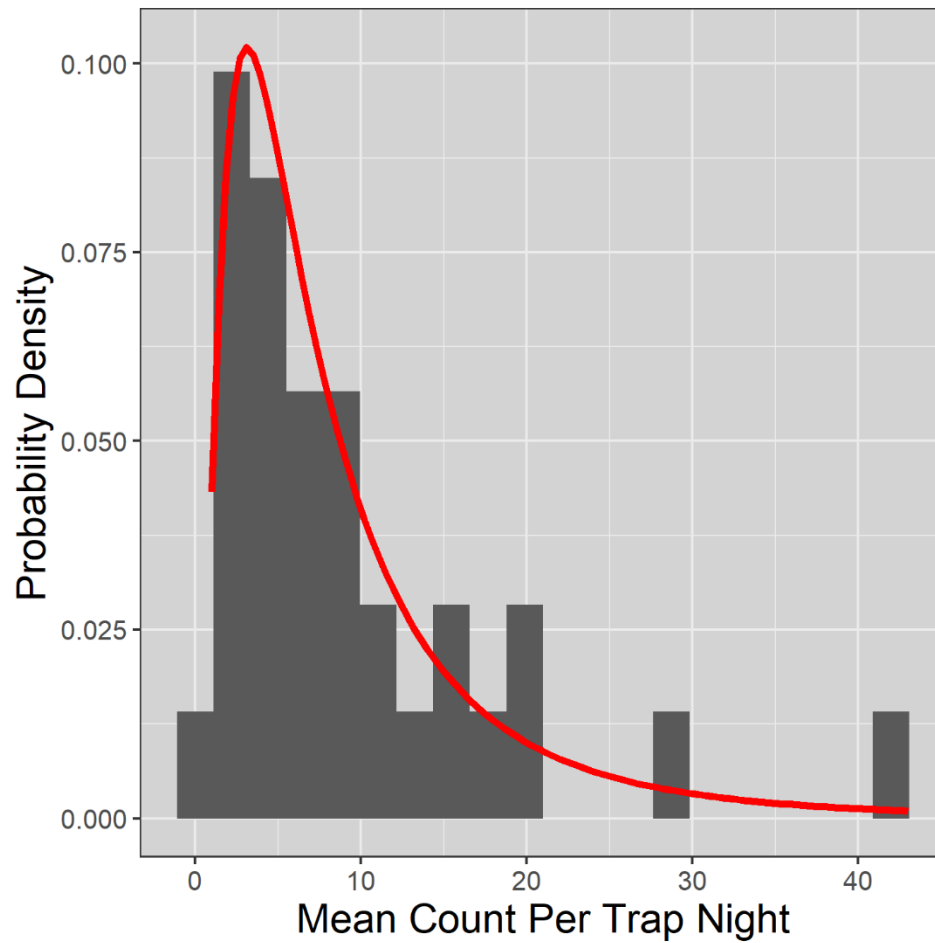
- Muzari, O. M., Adamczyk, R., Davis, J., Ritchie, S., & Devine, G. (2014). Residual Effectiveness of  $\lambda$ -Cyhalothrin Harbourage Sprays Against Foliage-Resting Mosquitoes in North Queensland. *Journal of Medical Entomology*, 51(2), 444-449.  
<https://doi.org/10.1603/ME13141>
- Oberhauser, K. S., Manweiler, S. A., Lelich, R., Blank, M., Batalden, R. v., & de Anda, A. (2009). Impacts of ultra-low volume resmethrin applications on non-target insects. *Journal of the American Mosquito Control Association*, 25(1), 83–93. <https://doi.org/10.2987/08-5788.1>
- Pokhrel, V., DeLisi, N. A., Danka, R. G., Walker, T. W., Ottea, J. A., & Healy, K. B. (2018). Effects of truck-mounted, ultra low volume mosquito adulticides on honey bees (*Apis mellifera*) in a suburban field setting. *PLoS ONE*, 13(3), e0193535.  
<https://doi.org/10.1371/journal.pone.0193535>
- R Development Core Team. (2019). R: A language and environment for statistical computing. In *R Foundation for Statistical Computing*. <https://doi.org/10.1017/CBO9781107415324.004>
- Reiskind, M. H., Griffin, R. H., Janairo, M. S., & Hopperstad, K. A. (2017). Mosquitoes of field and forest: the scale of habitat segregation in a diverse mosquito assemblage. *Medical and Veterinary Entomology*, 31(1), 44–54. <https://doi.org/10.1111/mve.12193>
- Richards, S. L., Volkan, J. K., Balanay, J. A. G., & Vandock, K. (2017). Evaluation of Bifenthrin and Deltamethrin Barrier Sprays for Mosquito Control in Eastern North Carolina. *Journal of Medical Entomology*, 54(6), 1659-1665. <https://doi.org/10.1093/jme/tjx152>
- Roiz, D., Wilson, A. L., Scott, T. W., Fonseca, D. M., Jourdain, F., Müller, P., ... & Corbel, V. (2018). Integrated *Aedes* management for the control of *Aedes*-borne diseases. *PLoS neglected tropical diseases*, 12(12), e0006845. <https://doi.org/10.1371/journal.pntd.0006845>

- Soetaert, K., & Petzoldt, T. (2010). Inverse modelling, sensitivity and monte carlo analysis in R using package FME. *Journal of Statistical Software*, 33(3), 1–28.  
<https://doi.org/10.18637/jss.v033.i03>
- Soetaert, K., Petzoldt, T., & Setzer, R. W. (2010). Solving differential equations in R: Package deSolve. *Journal of Statistical Software*, 33(9), 1–25. <https://doi.org/10.18637/jss.v033.i09>
- Sprenger, D., & Wuithiranyagool, T. (1986). The discovery and distribution of *Aedes albopictus* in Harris County, Texas. *Journal of the American Mosquito Control Association*, 2(2), 217.
- Stoops, C. A., Qualls, W. A., Nguyen, T.-V. T., & Richards, S. L. (2019). A Review of Studies Evaluating Insecticide Barrier Treatments for Mosquito Control From 1944 to 2018. *Environmental Health Insights*, 13, 1178630219859004.  
<https://doi.org/10.1177/1178630219859004>
- Tabashnik, B. E., Gould, F., & Carrière, Y. (2004). Delaying evolution of insect resistance to transgenic crops by decreasing dominance and heritability. *Journal of Evolutionary Biology*, 17(4), 904–912. <https://doi.org/10.1111/j.1420-9101.2004.00695.x>
- Tancredi, A., Papandrea, D., Marconcini, M., Carballar-Lejarazu, R., Casas-Martinez, M., Lo, E., Chen, X. G., Malacrida, A. R., & Bonizzoni, M. (2020). Tracing temporal and geographic distribution of resistance to pyrethroids in the arboviral vector *Aedes albopictus*. *PLoS Neglected Tropical Diseases*, 4(6), e0008350. <https://doi.org/10.1371/journal.pntd.0008350>
- Trout, R. T., Brown, G. C., Potter, M. F., & Hubbard, J. L. (2007). Efficacy of two pyrethroid insecticides applied as barrier treatments for managing mosquito (Diptera: Culicidae) populations in suburban residential properties. *Journal of medical entomology*, 44(3), 470-477. <https://doi.org/10.1093/jmedent/44.3.470>

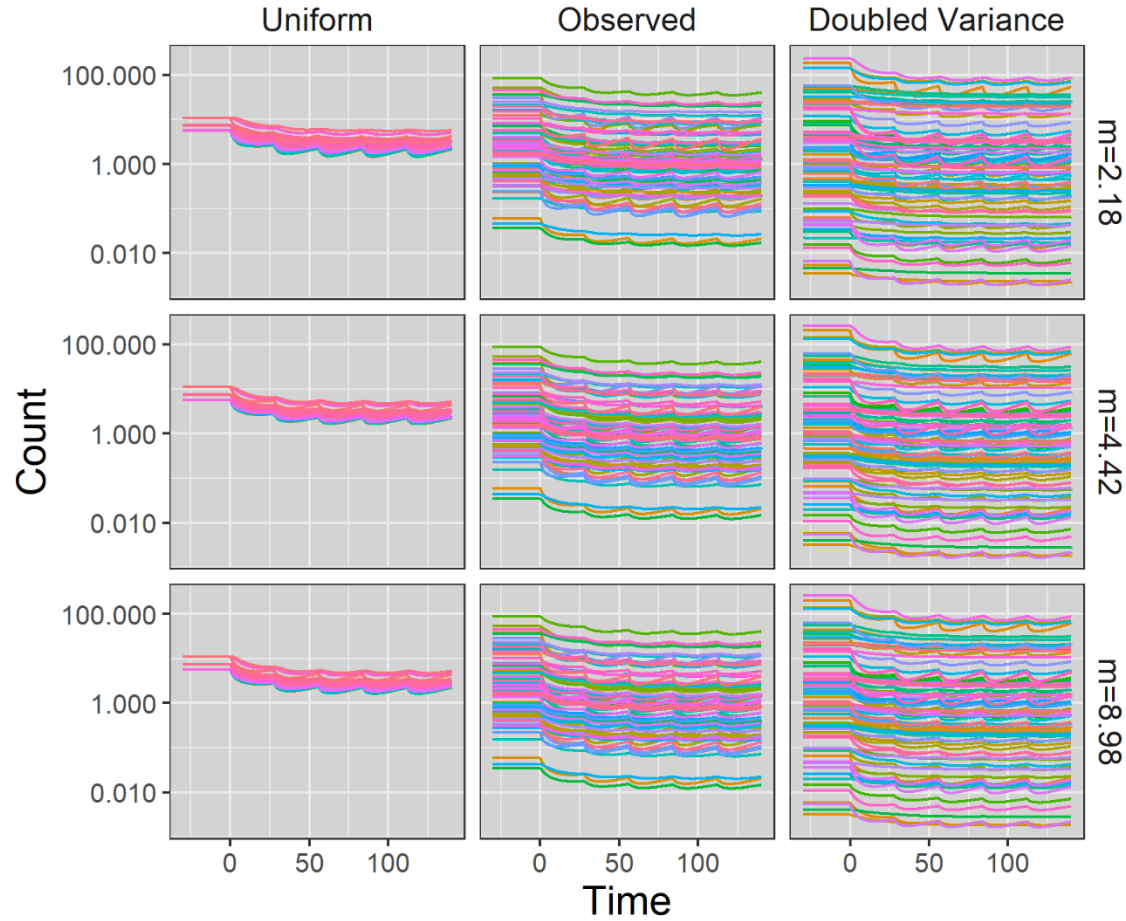
- Tun-Lin, W., Lenhart, A., Nam, V. S., Rebollar-Téllez, E., Morrison, A. C., Barbazan, P., Cote, M., Midega, J., Sanchez, F., Manrique-Saide, P., Kroeger, A., Nathan, M. B., Meheus, F., & Petzold, M. (2009). Reducing costs and operational constraints of dengue vector control by targeting productive breeding places: A multi-country non-inferiority cluster randomized trial. *Tropical Medicine and International Health*, 14(9), 1143–1153.  
<https://doi.org/10.1111/j.1365-3156.2009.02341.x>
- Unlu, I., Klingler, K., Indelicato, N., Faraji, A., & Strickman, D. (2016). Suppression of *Aedes albopictus*, the Asian tiger mosquito, using a “hot spot” approach. *Pest Management Science*, 72(7), 1427-1432. <https://doi.org/10.1002/ps.4174>
- Vandusen, A. E., Richards, S. L., & Balanay, J. A. G. (2016). Evaluation of bifenthrin barrier spray on foliage in a suburban eastern North Carolina neighborhood. *Pest Management Science*, 72(5), 1004-1012. <https://doi.org/10.1002/ps.4081>
- Walsh, R. K., Bradley, C., Apperson, C. S., & Gould, F. (2012). An experimental field study of delayed density dependence in natural populations of *Aedes albopictus*. *PLoS ONE*, 7(4), e35959. <https://doi.org/10.1371/journal.pone.0035959>
- Wickham, H. (2016). *ggplot2: Elegant Graphics for Data Analysis*. Springer-Verlag New York.  
<https://ggplot2.tidyverse.org>
- Williams, L. L. (1963). Malaria eradication in the United States. *American Journal of Public Health and the Nation's Health*, 53, 17–21. <https://doi.org/10.2105/ajph.53.1.17>
- Wilson, A. L., Boelaert, M., Kleinschmidt, I., Pinder, M., Scott, T. W., Tusting, L. S., & Lindsay, S. W. (2015). Evidence-based vector control? Improving the quality of vector control trials. *Trends in Parasitology*, 31(8), 380–390. <https://doi.org/10.1016/j.pt.2015.04.015>

Wilson, A. L., Courtenay, O., Kelly-Hope, L. A., Scott, T. W., Takken, W., Torr, S. J., & Lindsay, S. W. (2020). The importance of vector control for the control and elimination of vector-borne diseases. *PLoS Neglected Tropical Diseases*, *14*(1), e0007831.  
<https://doi.org/10.1371/journal.pntd.0007831>

## FIGURES

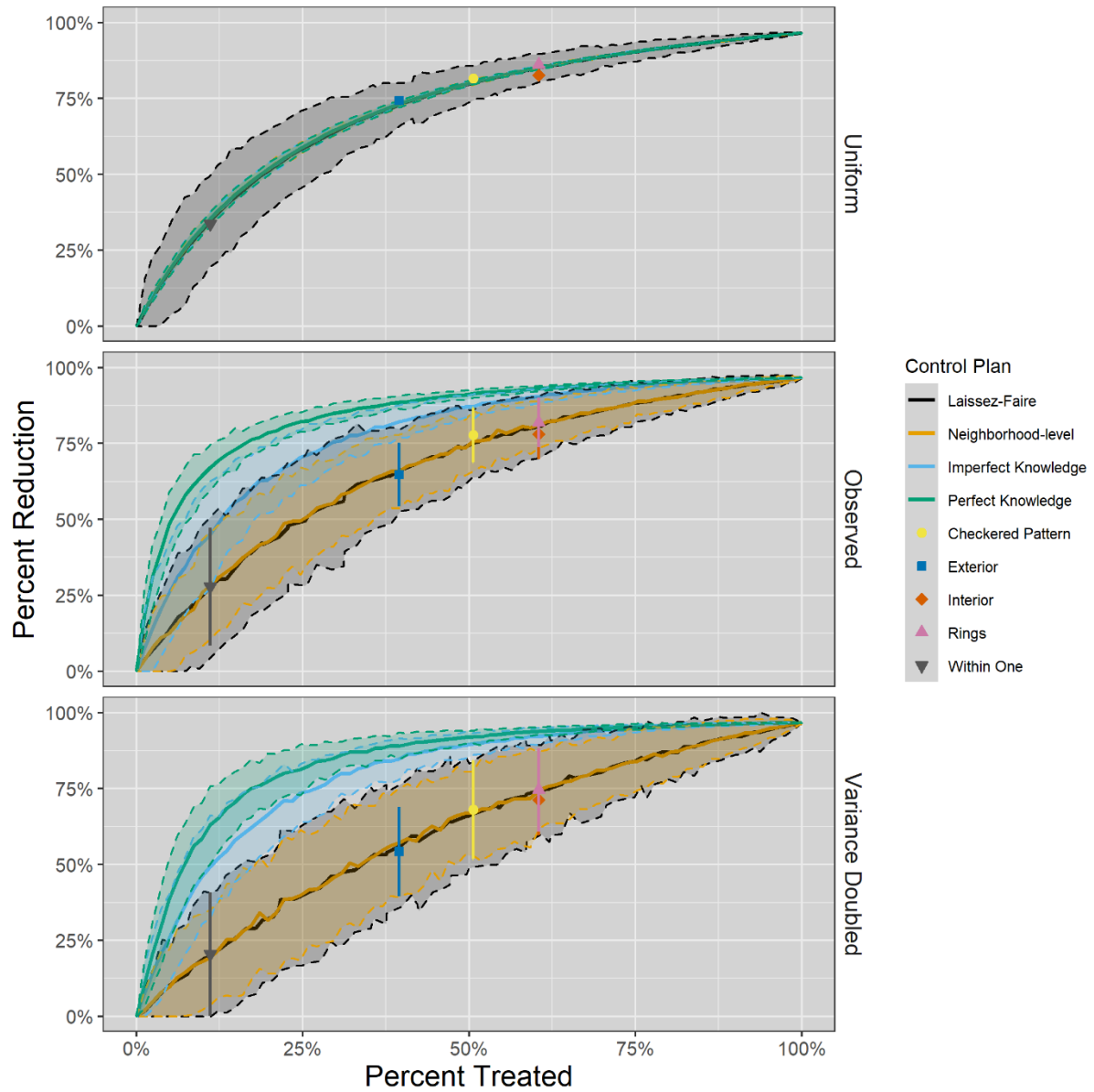


**Figure 4.1: Distribution of mean *Ae. albopictus* counts in yards during the study period.** Measurements taken after treatments were not included. Red curve is the best fit lognormal distribution that the yards were sampled from for the simulations.



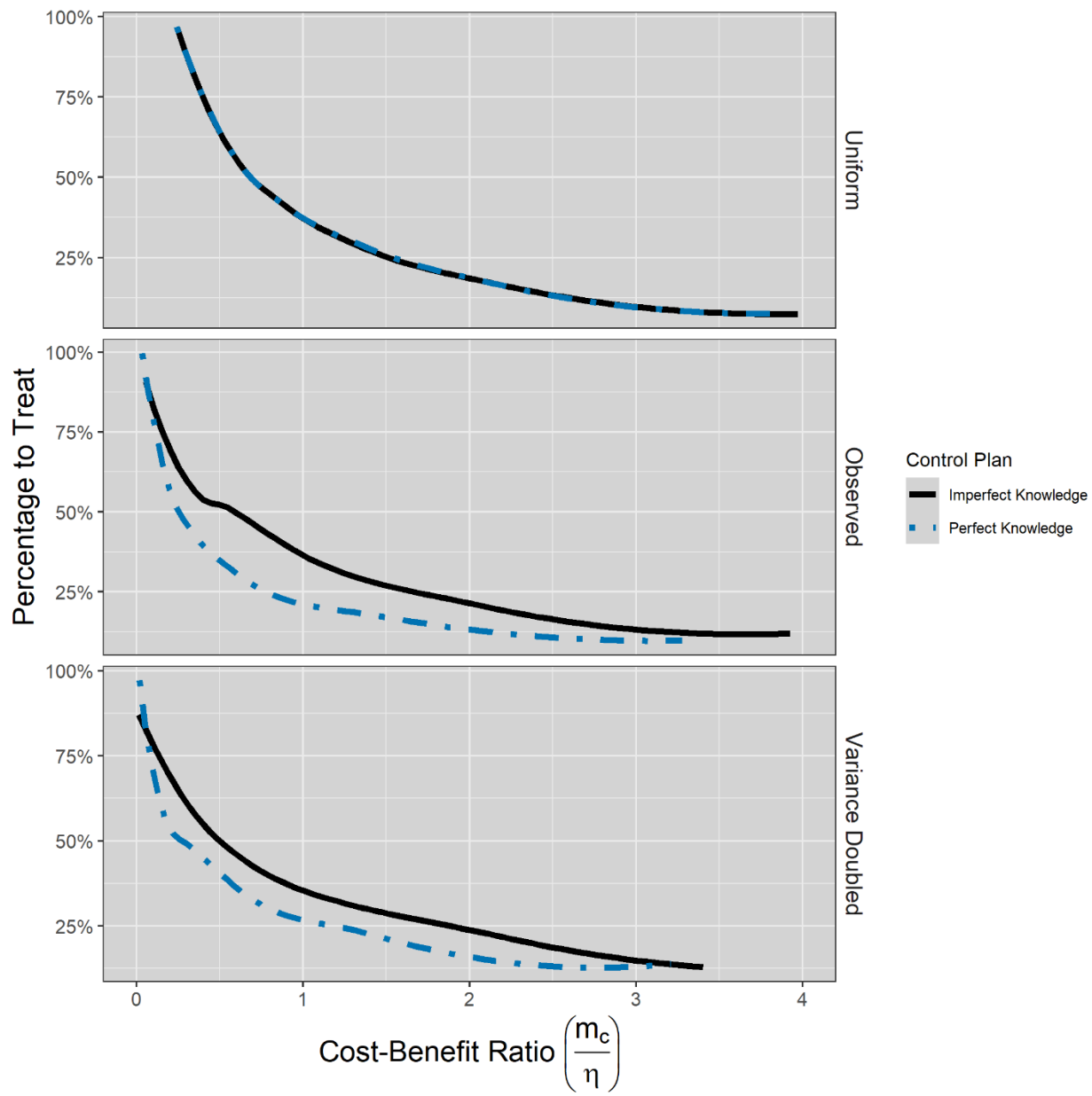
**Figure 4.2: Example simulation runs.** Number of adult female *Ae. albopictus* from simulations of a 9x9 neighborhood treated with 25% of the houses chosen randomly (neighborhood-level decision) for treatment. Fits from the observed data are in the center panel, with changes in the variation in larval habitat and movement rate increasing from left to right and top to bottom, respectively. Results are shown for a homogeneous population distribution, the observed population distribution, and a distribution with the observed variance doubled. The effect of the movement rate is also shown, using the estimated movement rate ( $m = 4.42$  /day, center row) and the bounds of its 95% confidence interval ( $m = 2.18$ , top row, and  $m = 8.98$ , bottom row). We see no difference in the simulation results due to uncertainty in the estimate of the movement parameter.

**Figure 4.3: Cost-benefit curves.** Mean and 95% confidence intervals for percent reduction in the mean neighborhood-wide *Ae. albopictus* population size (benefit) resulting from various levels of control (cost). Strategies relying on spatial patterns of treatments (shapes) are displayed based on the percentage of yards they treat in the 9x9 neighborhood, e.g. the checkered pattern results in treating 50% of yards. Results from the observed data are in the center panel, with variance increasing from top to bottom. Mean neighborhood-wide population size was found as the average across all yards over the entire post-treatment period (105 days). Simulations are conducted using the best-fit parameters for the three potential models with 100 simulations run per treatment level. Colors correspond to different treatment plans. When all yards are treated, the best fit model predicts a 97% reduction in the neighborhood wide population over the post treatment period. We see that under the assumption of a heterogenous distribution of larval habitat (top panel), all plans have a similar effect. However, as variance between yards increases, the plans using either perfect or imperfect knowledge outperform the naïve plans. Importantly, the plans that take advantage of knowledge of the population (either perfect or imperfect) reach high levels of control with a small percentage of yards being treated. Under the observed distribution (center panel), treating 25% of houses is predicted to result in a reduction of 71% and 82% for the plans using imperfect knowledge and perfect knowledge, respectively, as opposed to a 51% reduction under the laissez-faire system. As spatial heterogeneity increases, the added benefit of information is increased, while the benefits curves for the uninformed plans becomes more linear. With the variance in the availability of larval habitat doubled (bottom panel), we predict 74% and 83% reduction in population size for the plans using imperfect or perfect knowledge, respectively, compared with a 41% reduction under the laissez-faire system. None of the other naïve plans, either choosing a proportion at a neighborhood-level or spatial patterns (shapes), i.e. checkered pattern and with-in one, outperformed the laissez-faire system.



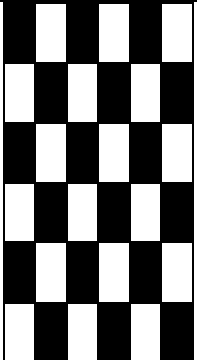
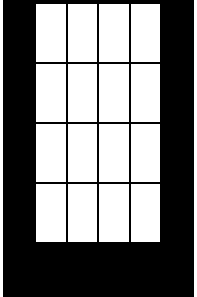
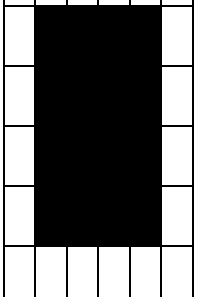


**Figure 4.4: Cost-benefit analysis.** Proportion of yards to treat for varying cost-benefit ratios, as suggested from our best model fit. Values are calculated as explained in the text, with a GAM used to estimate a smooth curve. Here,  $m_c$  is the cost of treating a single yard and  $\eta$  is the benefit, in monetary terms, of a reduction of 1% of the equilibrium population size in the neighborhood-wide mosquito population. Like previous results, there is no significant difference between plans under the assumption of the uniform distribution. For control programs using perfect knowledge, and to a lesser extent imperfect knowledge, the percentage of yards that should be treated falls rapidly for low cost-benefit ratios before leveling off. This suggests that a large benefit would be necessary to treat need to treat more than around 25% of the yards.

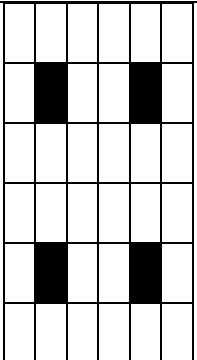
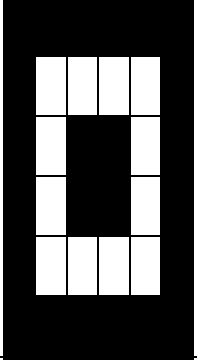
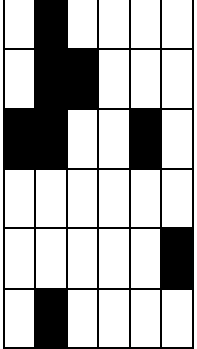


## TABLES

**Table 4.2: Treatment plans.** List of treatment plans, how yards are selected, the level of knowledge that is used, and example of treatment plans for a 36-yard neighborhood (6x6 grid).

Treatment Plan	How yards are selected	Information Needed	Example
Checkerboard	Spatial Pattern	None	
Perimeter	Spatial Pattern	None	
Interior	Spatial Pattern	None	

**Table 4.2: Treatment plans (Continued).** List of treatment plans, how yards are selected, the level of knowledge that is used, and example of treatment plans for a 36-yard neighborhood (6x6 grid).

Treatment Plan	How yards are selected	Information Needed	Example
Within-one	Spatial Pattern	None	
Rings	Spatial Pattern	None	
Laissez-faire	Homeowner Decision	None	 <p>(p=.2)</p>

**Table 4.2: Treatment plans (Continued).** List of treatment plans, how yards are selected, the level of knowledge that is used, and example of treatment plans for a 36-yard neighborhood (6x6 grid).

Treatment Plan	How yards are selected	Information Needed	Example
Neighborhood Level	Neighborhood Level Decision	None	<p>(p=.2)</p>
Imperfect Knowledge	Neighborhood Level Decision	Intermediate	<p>(p=.2)</p>
Perfect Knowledge	Neighborhood Level Decision	High	<p>(p=.2)</p>

**Table 4.3: Best fit parameter estimates for the three models.** Parameters that were not directly estimated are denoted with an asterisk (\*). 95% confidence intervals for all estimated parameters are given, along with the estimated amount of between subject variation (BSV) that was estimated by the fitting process

Parameter	Biological Interpretation (units)	Model 1			Model 2			Model 3		
		Estimate	Treated BSV (%CV)	Neighbor BSV (%CV)	Estimate	Treated BSV (%CV)	Neighbor BSV (%CV)	Estimate	Treated BSV (%CV)	Neighbor BSV (%CV)
$b$	Birth Rate ( $\backslash(\text{female} \cdot \text{day})$ )	6.92	---	---	6.92*	---	---	6.92*	---	---
$d_L$	Density-independent Larval Mortality Rate ( $\backslash \text{day}$ )	.0112*	---	---	.0112*	---	---	.0112*	---	---
$k_L$	Density-dependent Larval Mortality Rate	17.9 (10.4, 30.6)	2.55	1.95	---	---	---	143 (35.1, 586)	1.05	.951
$e$	Density-independent Emergence Rate ( $\backslash \text{day}$ )	5.16e-2*	---	---	5.16e-2*	---	---	5.16e-2*	---	---
$k_E$	Density-dependent Emergence Rate	---	---	---	1.97 (.785, 4.94)	1167	134.65	36.3**	---	---
$d_A$	Adult Mortality Rate ( $\backslash \text{day}$ )	1.45 (1.11, 1.90)	---	---	.0499 (.0458, .0545)	---	---	.0316 (.00891, .112)	---	---
$C(0)$	Initial Increase in Adult Mortality (%)	125% (105%, 148%)	---	---	2460% (1050%, 5740%)	---	---	1150% (232%, 5660%)	---	---
$r_C$	Rate of Loss of Effect of Barrier Spray ( $\backslash \text{day}$ )	.00803 (.000409, .158)	---	---	1.17 (.0487, 27.6)	---	---	.0802 (.0218, 8.98)	---	---
$R(0)$	Initial Reduction in Larval Habitat (%)	82.6% (57.1%, 94.4%)	---	---	53.7% (3.28%, 96.5%)	---	---	100% (91.3%, 100%)	---	---
$r_R$	Rate of Loss of Effect of LHM ( $\backslash \text{day}$ )	0*	---	---	0*	---	---	0*	---	---
$m$	Per Capita Movement Rate ( $\backslash \text{day}$ )	27.7 (.141, 5.47e3)	22.03	31.50	12.8 (.015, 1.09e4)	43.02	.0612	4.42 (2.18, 8.98)	5.05	21.6
AIC of Best Fit		4378			3378			5074		

**Table 4.4: AIC (and  $\Delta AIC$ ) values for each of the model fits.** Model 3 fitting the adult death rate ( $d_A$ ) and the rate of decay of the effectiveness of the barrier spray ( $r_c$ ), along with the carrying capacity term ( $k_L$ ), initial effect of the barrier spray ( $c$ ), proportion of larval habitat reduction ( $r$ ), movement rate ( $m$ ), and the between subject variation as described in the model description provided the best fit.

Fit parameters	Model 1	Model 2	Model 3
$b, d_A$ , and $r_c$	NA	3467	15619
$b$ and $d_A$	4751	10693	25684
$d_A$ and $r_c$	4378	3378	5074

## SUPPLEMENTAL INFORMATION

### Equilibria of Models

Model equilibria were found by setting the derivative to zero and solving for the state variables  $J$  and  $A$  for the single-patch model. Equilibria incorporating movement were not analytically solvable. I used the *Maple* software (*Maple 2016*, 2016) to solve for all equilibria. Non-trivial equilibria for the three models are given in Table S4.1. For brevity, the equilibrium values for adults,  $A^*$ , is given in terms of the equilibrium value of the juveniles,  $J^*$ .

### Initial Values for Parameters

Initial values for parameters are given in Table S4.2.

### PE model diagnostics

Diagnostic plots were used to determine overall model fit and to detect any violation of assumptions. I see that our best fit model had a slight tendency to underestimate the number of mosquitoes in the yard and shows signs of heteroskedasticity (Figure S4.1). The qq-plot of the conditional weighted residuals (CWRES) shows some deviation from the assumption of normality for observations in the furthest upper and lower quantiles, but the assumption seems to hold overall (Figure S4.2). The visual predictive check (VPC) suggests that the model vastly overpredicts the variation in the data. This is seen in the 95% confidence intervals for the data (Figure S4.3, dashed line) not falling within the 95% confidence interval predicted by simulation. However, VPC have been shown to be poor measures of fit when there is a significant variation in treatments and a small number of replicates per treatment, as seen here (Karlsson & Savic, 2007).

### Sensitivity to Neighborhood Size

To examine the assumption of no movement into or out of the neighborhood on our results, results were produced as described in the main text for neighborhoods of 49, 121, and



169 yards. As the neighborhood size is increased, the proportion of yards along the boundary decreases, and the effect of this assumption decreases. We see that as the number of patches increases, the mean reduction predicted by the model remains relatively unchanged, while the variation in the reduction is reduced (Figure S4.4). This suggests that our results are not significantly affected by our boundary condition.

### **Sensitivity to model parameters**

Sensitivity to model parameters was found by simulating the results using 100 random draws of the fitted parameters, i.e.  $d_A$ ,  $k_L$ ,  $C(0)$ ,  $r_C$ ,  $R(0)$ , and  $m$ , from their 95% confidence intervals using Latin hypercube sampling. A 95% confidence interval for the mean reduction in population size and the standard error of the predicted reduction were then calculated using the `sensRange()` function in the FME package (Soetaert & Petzoldt, 2010). Uncertainty in parameter estimates results in a significant amount of variation in the proportional reduction in the neighborhood-wide mosquito population. However, our main results still hold (Figure S4.5).

### **Identifiability of model parameters**

Identifiability of model parameter sets was determined using the collinearity of parameter estimates. Collinearity was calculated using the `collin()` function in the FME package (Soetaert & Petzoldt, 2010). Potential parameter sets were chosen based on the ability to estimate all control parameters ( $C(0)$ ,  $R(0)$ ,  $r_C$ ) while retaining a collinearity value less than 20. Collinearity of parameter sets used in the best fit for each model suggested that all parameters were identifiable from data.

## SUPPLEMENTAL FIGURES

### DV vs. IPRED | model.2patch.Both.ode.2

Ofv: 4663.4, Eps shrink: NA [1]

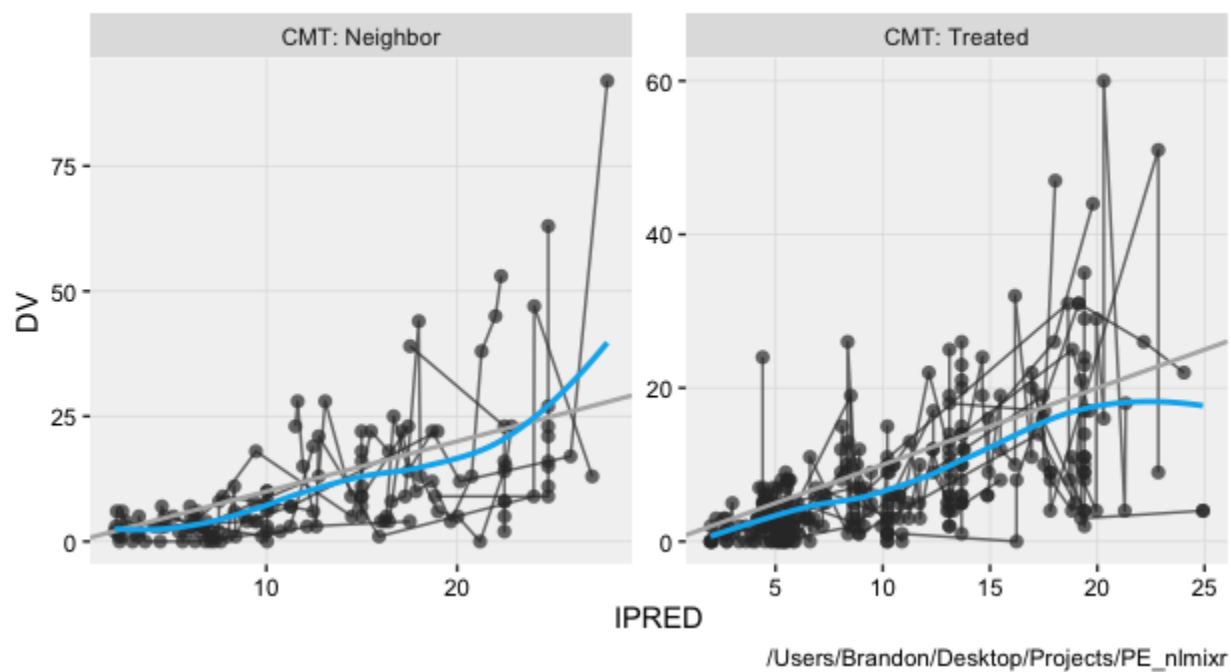
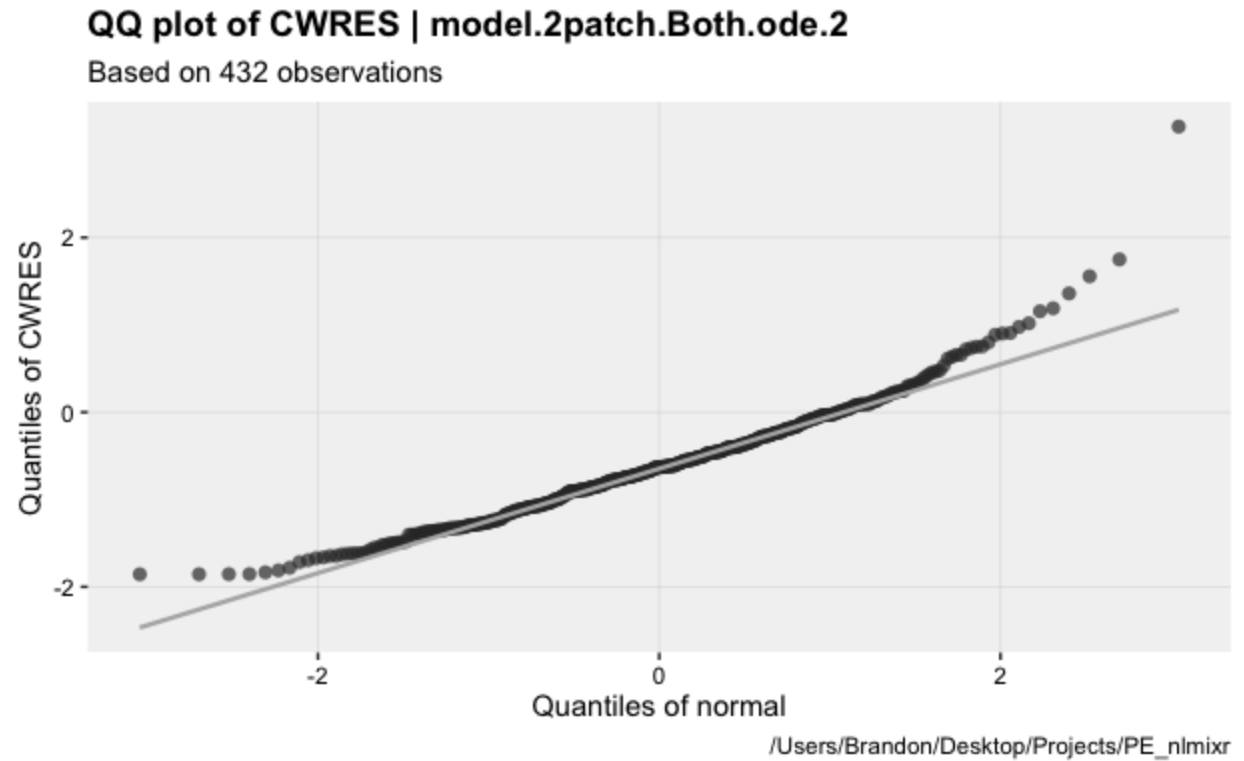
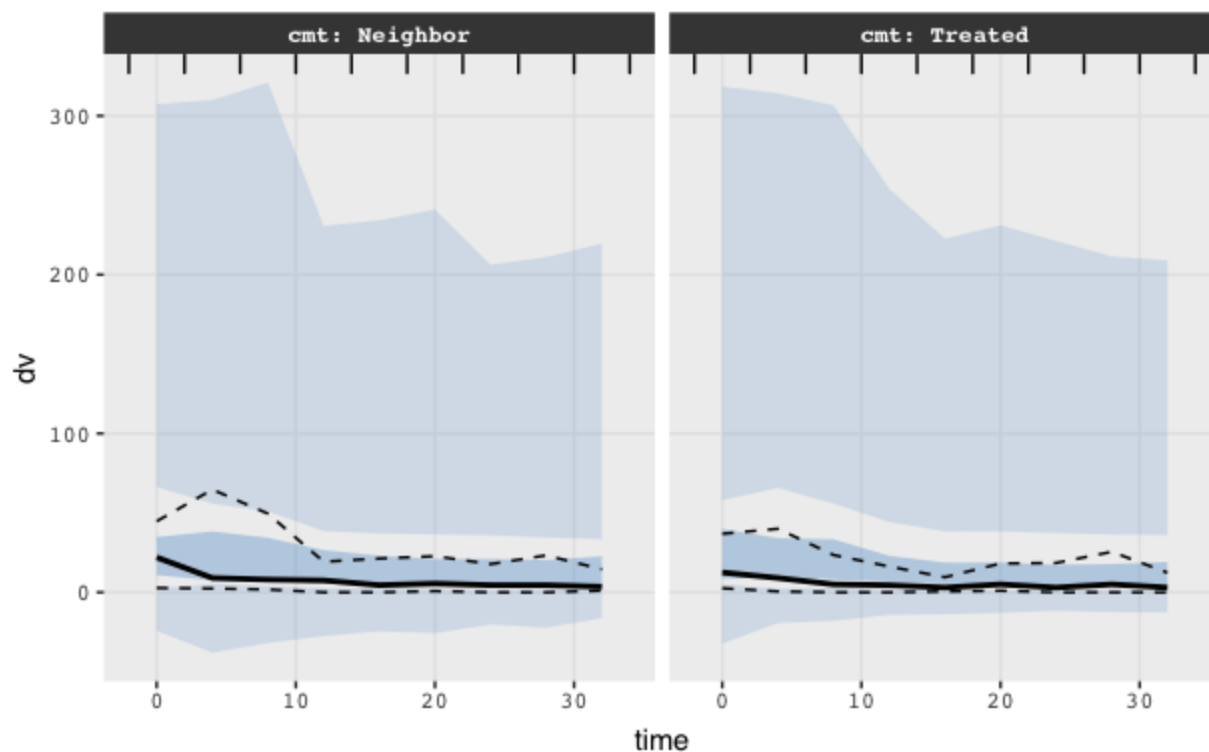


Figure S4.1: Observed data (DV) vs individual prediction (IPRED).



**Figure S4.2: QQ-plot for CWRES.** Figure shows some deviation of the residuals from normal for predictions in the highest and lowest quantile, but overall seems to fit the assumption well.



**Figure S4.3: VPC plot.** VPC suggests that the model drastically over predicts the variation in the data. Seen here as the bounds of the 95% confidence intervals for the observed data (dotted lines) not falling within the 95% confidence interval of their predicted values. However, VPC is known to be inconclusive when differences in treatment are high and replication for treatments is low as it is here.

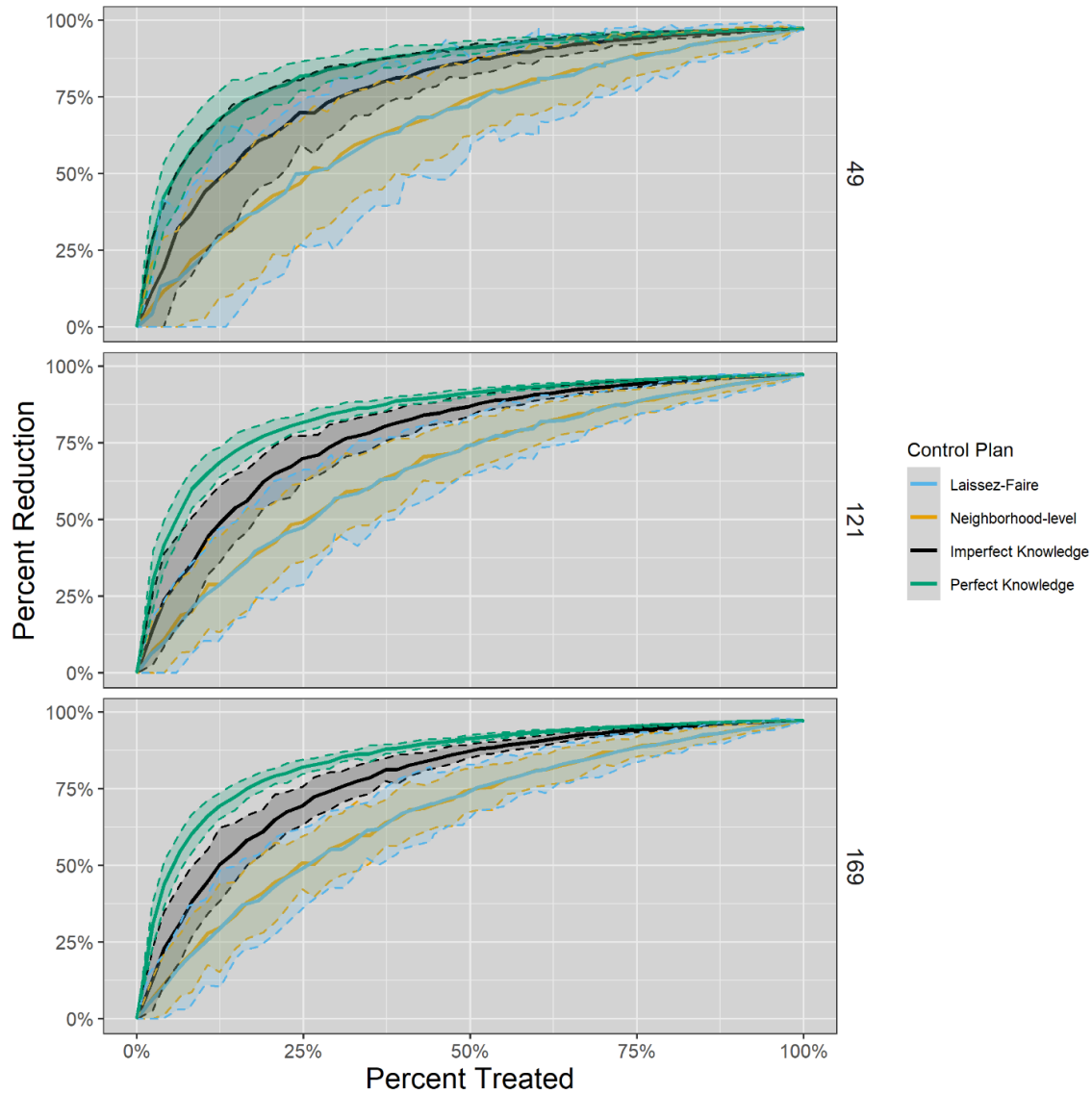


**Figure S4.4: Cost-benefit curves for differing neighborhood sizes.** Mean and 95% confidence intervals for percent reduction in the mean neighborhood-wide *Ae. albopictus* population size (benefit) resulting from various levels of control (cost). Mean neighborhood-wide population size was found as the average across all yards over the entire post-treatment period (105 days). Simulations are conducted using the best-fit parameters for the three potential models with 50 simulations run per treatment level. Colors correspond to different treatment plans. We see that as the neighborhood size increases (Panels), the mean reduction predicted does not change. However, the variation in the mean reduction decreases as the neighborhood size increases.

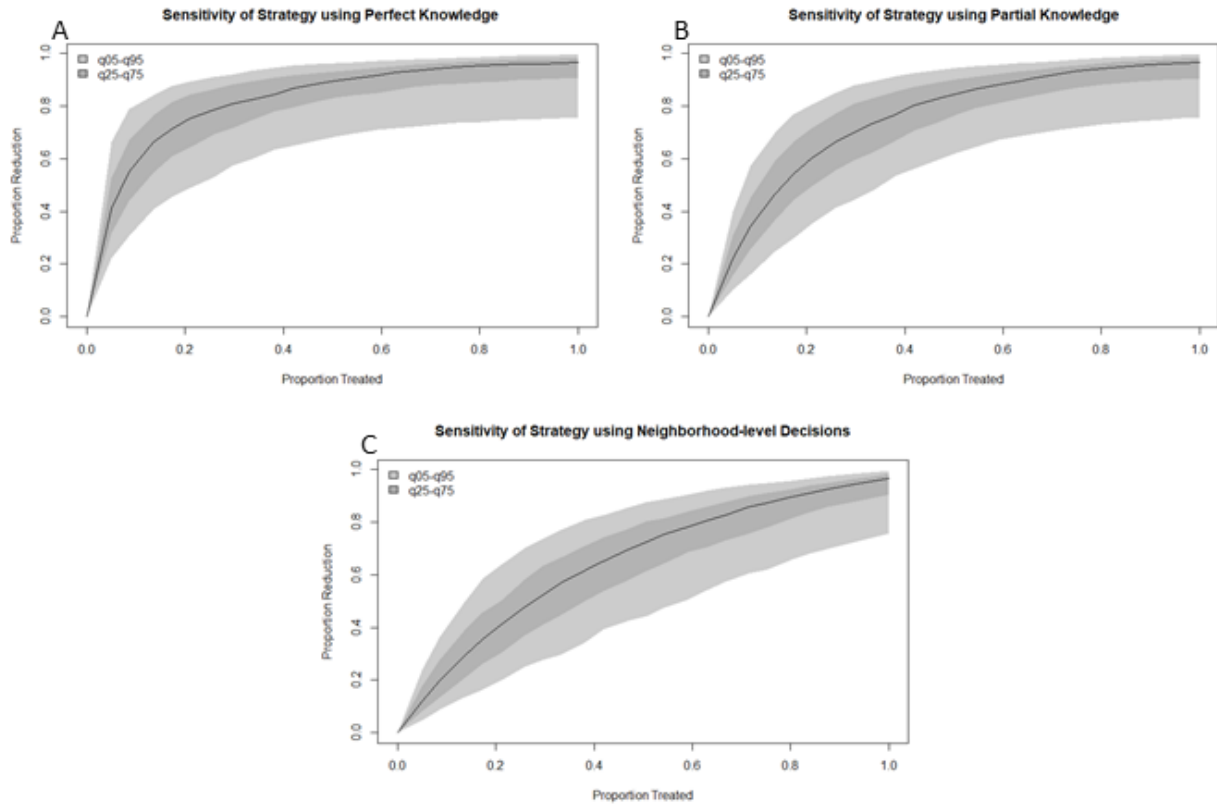


**Figure S4.5: Sensitivity of mean reduction to parameter values.** Mean (black line), 50% confidence interval (dark grey area), and 90% confidence interval (light grey area) of results using 100 random draws of parameter values from within their estimated 95% confidence intervals. (A) The strategy using perfect knowledge. (B) The strategy using partial knowledge. (C) The strategy using an uninformed neighborhood-level decision. There is significant variation in the mean reduction that is predicted due to uncertainty in the parameter values. However, this variation does not affect our main conclusions.

## SUPPLEMENTAL TABLES

**Table S4.1: Equilibrium values.** Equilibrium values for each model. For brevity, the equilibrium value of adults,  $A^*$ , is given in terms of the equilibrium value for juveniles,  $J^*$ .

Model	$(J^*, A^*)$
Model 1	$\left( \frac{k_L(be - d_A d_L - d_A e)}{d_A d_L}, \frac{eJ^*}{d_A} \right)$
Model 2	$\left( \frac{-k_E d_L d_A \pm \sqrt{(k_E d_L d_A)^2 - 4(d_A d_L)(k_E e)(d_A - b)}}{2d_A d_L}, \frac{ek_E L^*}{d_A(k_E + L^*)} \right)$
Model 3	$\left( \frac{-(d_A d_L)(k_E + k_L) \pm \sqrt{(k_E + k_L)^2 (d_A d_L)^2 - 4(d_A d_L)(k_E k_L)(-be + d_L d_A + ed_A)}}{2d_A d_L}, \frac{ek_E L^*}{d_A(k_E + L^*)} \right)$

**Table S4.2: Initial guesses for model parameterization and source, unless a best guess was used.**

Parameter	Initial Guess	Source
$b$	6.921	Mordecai et al. (2017)
$k_L$	10	
$k_E$	10	
$d_A$	.009601	Mordecai et al. (2017)
$C(0)$	5	
$r_C$	.06666	
$R(0)$	.1	
$m$	.1	
$g_T$ BSV	1	
$g_N$ BSV	1	
$k$ BSV: Treated	1	
$k$ BSV: Neighbor	1	
$\text{Cov}(g_T, g_N)$	.1	
$\text{Cov}(k_T, k_N)$	.1	



## **CHAPTER 5 – Conclusions**

Better understanding the impacts of mosquito control on *Aedes* population dynamics, both in the short- and long-term, are vital for the development of efficient control programs. Without this knowledge, control programs run the risk of being ineffective at reducing local population sizes or mitigating outbreaks of *Aedes*-vectored diseases. Without proper monitoring and an understanding of underlying population, genetics, and transmission dynamics, it is possible for poorly thought out, reactive controls to make the situation worse in the long-term, even when they appear to be successful in the short term. In this dissertation, I examined the dynamics resulting from the use of non-immunizing controls, most notably insecticide applications, against *Aedes* mosquitoes and the diseases they vector, with the hope of providing improved guidance for their use.

Chapter 2 of this the dissertation discussed the divorce effect. A phenomenon which occurs when outbreaks following the cessation of a control program were large enough to negate any benefit of the initial control program. I showed that during the time that incidence was suppressed by the control, from the time control is initiated until the infection reemerged, the population quickly lost herd immunity. This reduction in herd immunity puts populations at risk of a major outbreak upon reemergence, and the outbreak that occurs after reemergence almost always resulted in more infections than would have occurred if no control had been used. This represents a worst-case scenario for disease control in which it results in an increase in the number of infections. Importantly, I showed that this result was not unique to any disease system or control method and that, with very few exceptions, controls needed to be maintained for decades to avoid consequences related to the divorce effect.

In Chapter 3, I quantified the effect of two common mosquito control techniques, barrier sprays and larval habitat management (LHM), and how their effectiveness changes over time,

information that would be critical for deploying them in response to an *Aedes*-vectored disease outbreak. This was done using a field experiment conducted in 2018 in which I examined the temporal dynamics of *Aedes albopictus* populations in yards treated with barrier sprays or LHM, as well as in untreated neighboring yards. I was able to show that both the barrier spray and combined treatment were able to significantly reduce the *Ae. albopictus* populations within treated yards and found some evidence for a reduction in untreated neighboring yards. I also found that while LHM did not result in a significant reduction in the population over the entire post-treatment period, it did result in a significant reduction on the final days of sampling and evidence of a downward trajectory in the population sizes. This suggested that future studies of the effects of LHM should monitor yards for more than 25 days post-treatment.

In Chapter 4, I showed modeling results that suggest that treating 25% of yards using a combination of barrier sprays and LHM, deployed every three weeks, was sufficient to reduce the neighborhood-wide population by more than 50% if yards were chosen at random and more than 80% if the distribution of *Ae. albopictus* if yards with the highest densities were precisely targeted. These results were produced using a model I developed for the implementation of LHM and barrier sprays across a heterogeneous neighborhood. To do this, I used a nonlinear mixed effects model to estimate the parameters for control, density-dependence, and adult mortality from the data collected in Chapter 3. I then simulated the effects of 9 different strategies for deploying treatments in a heterogeneous neighborhood and examined the effect of using targeted controls compared to more naïve plans. These results suggested that the use of targeted controls may be useful for both the reduction of nuisance and disease risk caused by *Ae. albopictus*.

The work presented in this dissertation has added to the literature on the dynamics during and following mosquito control. The divorce effect, presented in Chapter 2, suggested that the use of insecticides to combat vector-borne diseases may be putting local populations at risk of major outbreaks. Outbreaks that could erase the benefits from years of successful suppression of disease like dengue. I then showed, using the data in Chapter 3 and the model in Chapter 4, that the use of targeted controls can suppress *Aedes* populations across a large area. If these methods prove as effective in field trials as the models suggest, they could provide a method to efficiently reduce the risk of outbreak due to the introduction, or reintroduction, of *Aedes*-vectored diseases.

## APPENDIX

## **Appendix A - Locally Fixed Alleles: A method to localize gene drive to island populations**

Sudweeks, J., Hollingsworth, B., Blondel, D. v., Campbell, K. J., Dhole, S., Eisemann, J. D., Edwards, O., Godwin, J., Howald, G. R., Oh, K. P., Piaggio, A. J., Prowse, T. A. A., Ross, J. v., Saah, J. R., Shiels, A. B., Thomas, P. Q., Threadgill, D. W., Vella, M. R., Gould, F., & Lloyd, A. L.

\*This appendix was published in Scientific Reports. Sudweeks, J., Hollingsworth, B., Blondel, D. v., Campbell, K. J., Dhole, S., Eisemann, J. D., Edwards, O., Godwin, J., Howald, G. R., Oh, K. P., Piaggio, A. J., Prowse, T. A. A., Ross, J. v., Saah, J. R., Shiels, A. B., Thomas, P. Q., Threadgill, D. W., Vella, M. R., Gould, F., & Lloyd, A. L. (2019). Locally Fixed Alleles: A method to localize gene drive to island populations. *Scientific Reports*, 9(1), 1–10.

## **CONTRIBUTION**

As second author on this paper, I was responsible for helping design and code the model, running simulations, analyzing the results, and writing the manuscript. I was also responsible for mentoring the first author as she worked on this project.

# OPEN Locally Fixed Alleles: A method to localize gene drive to island populations

Jaye Sudweeks<sup>1</sup>, Brandon Hollingsworth<sup>2</sup>, Dimitri V. Blondel<sup>3</sup>, Karl J. Campbell<sup>4</sup>, Sumit Dhole<sup>5</sup>, John D. Eisemann<sup>6</sup>, Owain Edwards<sup>7</sup>, John Godwin<sup>3,8</sup>, Gregg R. Howald<sup>4</sup>, Kevin P. Oh<sup>6,9</sup>, Antoinette J. Piaggio<sup>6</sup>, Thomas A. A. Prowse<sup>10</sup>, Joshua V. Ross<sup>10</sup>, J. Royden Saah<sup>4,8</sup>, Aaron B. Shiels<sup>6</sup>, Paul Q. Thomas<sup>11</sup>, David W. Threadgill<sup>12</sup>, Michael R. Vella<sup>2</sup>, Fred Gould<sup>5,8</sup> & Alun L. Lloyd<sup>1,2\*</sup>

Invasive species pose a major threat to biodiversity on islands. While successes have been achieved using traditional removal methods, such as toxicants aimed at rodents, these approaches have limitations and various off-target effects on island ecosystems. Gene drive technologies designed to eliminate a population provide an alternative approach, but the potential for drive-bearing individuals to escape from the target release area and impact populations elsewhere is a major concern. Here we propose the “Locally Fixed Alleles” approach as a novel means for localizing elimination by a drive to an island population that exhibits significant genetic isolation from neighboring populations. Our approach is based on the assumption that in small island populations of rodents, genetic drift will lead to alleles at multiple genomic loci becoming fixed. In contrast, multiple alleles are likely to be maintained in larger populations on mainlands. Utilizing the high degree of genetic specificity achievable using homing drives, for example based on the CRISPR/Cas9 system, our approach aims at employing one or more locally fixed alleles as the target for a gene drive on a particular island. Using mathematical modeling, we explore the feasibility of this approach and the degree of localization that can be achieved. We show that across a wide range of parameter values, escape of the drive to a neighboring population in which the target allele is not fixed will at most lead to modest transient suppression of the non-target population. While the main focus of this paper is on elimination of a rodent pest from an island, we also discuss the utility of the locally fixed allele approach for the goals of population suppression or population replacement. Our analysis also provides a threshold condition for the ability of a gene drive to invade a partially resistant population.

Genetic modification of pest species has been suggested as a means to address a wide variety of pest problems, including those impacting human health, pre- and post-harvest crop losses, and conservation of endangered species<sup>1–5</sup>. One approach to genetic pest management involves introducing a DNA sequence into the pest genome that causes its own over-representation in future generations by inducing super-Mendelian inheritance; generally referred to as gene drive. An engineered gene coding for a desirable trait, e.g. one that renders the pest species less troublesome (e.g. reduction of vector competence of a mosquito species) can be linked to the gene drive sequence in order to increase its frequency in the population. Alternatively, the gene drive sequence can be engineered

<sup>1</sup>Department of Mathematics, North Carolina State University, Raleigh, NC, 27695, USA. <sup>2</sup>Biomathematics Graduate Program, North Carolina State University, Raleigh, NC, 27695, USA. <sup>3</sup>Department of Biological Sciences, North Carolina State University, Raleigh, NC, 27695, USA. <sup>4</sup>Island Conservation, 2100 Delaware Ave., Suite 1, Santa Cruz, CA, 95060, USA. <sup>5</sup>Department of Entomology and Plant Pathology, North Carolina State University, Raleigh, NC, 27695, USA. <sup>6</sup>National Wildlife Research Center, US Department of Agriculture, Fort Collins, CO, 80521, USA. <sup>7</sup>CSIRO Land & Water, Centre for Environment and Life Sciences, Floreat, WA, Australia. <sup>8</sup>Genetic Engineering and Society Center, North Carolina State University, Raleigh, NC, 27695, USA. <sup>9</sup>Department of Microbiology, Immunology & Pathology, Colorado State University, Fort Collins, CO, 80523, USA. <sup>10</sup>School of Mathematical Sciences, The University of Adelaide, Adelaide, SA, 5005, Australia. <sup>11</sup>The Robinson Research Institute and School of Medicine, The University of Adelaide, Adelaide, SA, 5005, Australia. <sup>12</sup>Department of Molecular and Cellular Medicine, Texas A&M University, College Station, TX, 77843, USA. \*email: [alun\\_lloyd@ncsu.edu](mailto:alun_lloyd@ncsu.edu)



to disrupt a gene critical to fitness, or to deliver a payload that achieves this aim, and thereby suppress, or even eliminate, a population.

Ever since such drives were proposed, concerns have been raised in the peer-reviewed literature and in the popular media about unintended consequences of releases and ethical dimensions of the work. These include failure of the genetic construct being driven, but also the spread of gene drives beyond the region in which spread is intended and approved by the local population and governing authorities<sup>2–13</sup>. The nature and seriousness of these concerns differ between different gene drive technologies and applications (for instance, considerations would be quite different for an approach intended to replace a human disease-vectoring mosquito species by a variant that is refractory to the pathogen than for removal of an invasive species that causes ecological damage). These concerns are most acute in the case of drives that are designed to suppress and eliminate a population: spread of such a drive could have a risk of leading to global eradication of a species that is a pest in one area but a valuable component of an ecosystem in other areas (e.g. mice and rats). As a result, there is much interest in the ability to design gene drives that exhibit spatial localization, i.e. ones that have the ability to spread in a given region but will not spread globally.

Several approaches have been suggested to achieve localization of gene drives. Drives that exhibit an invasion threshold, such as the engineered underdominance (EU) approach, provide a natural means to achieve localization<sup>14,15</sup>. These drives exhibit frequency-dependent dynamics where the drive can only spread if its frequency exceeds a particular level—the invasion threshold. Below this level, the frequency of the drive will decrease, leading to its loss from the population. Spread of a threshold drive across a patchy environment is more difficult, and becomes highly unlikely or even impossible when the invasion threshold is 50% or higher<sup>16,17</sup>. Other approaches have been suggested to achieve localization, including killer-rescue<sup>18</sup>, multi-locus assortment<sup>19</sup>, sex-linked genome editors<sup>20</sup> and daisy-chain drive<sup>21</sup>. Theoretical analysis has suggested the ability of daisy-chain drive to simultaneously achieve spread and localization to a single area is only possible in a limited set of circumstances, and this concern also pertains to some other gene drives developed to be localized<sup>22</sup>. While all of these localized drives could change characteristics of pests in a population, their ability to locally suppress populations is questionable<sup>22,23</sup>, although see also<sup>24</sup>.

In this paper, we propose a localization method, the “Locally Fixed Alleles” (LFA) approach, that can be utilized for relatively small populations that exhibit a significant degree of genetic isolation from other populations. This method is particularly suited for elimination of pest species from small oceanic islands, where the target population has small effective population size and for which there is naturally limited gene flow with other populations. While multiple alleles are expected to be commonly maintained at loci in large populations, genetic drift in small island populations is predicted to result in fixation of alleles at some loci in the genome<sup>25,26</sup>.

Utilizing the high degree of genetic specificity of homing drives based on the CRISPR/Cas9 system<sup>4</sup>, our approach aims at employing one or more locally fixed alleles as the target for a gene drive on a particular island. Such a drive can spread to individuals carrying that allele, but individuals that do not have that specific allele are naturally resistant to the drive. For example, polymorphisms that occur in targeted Cas9 guide RNA binding sites or protospacer adjacent motifs (PAM) may effectively limit gene drive activity<sup>27</sup> such that a drive can spread to individuals carrying alleles that form functional sites, but individuals with alternate alleles are naturally resistant to the drive. By design, we would search for alleles that are fixed in the population on the target island but not fixed in populations beyond that island. Consequently, the drive could be expected to result in only limited transient suppression beyond the island. A special case of this approach, the “private allele” (PA) approach (dubbed “precision drive” by Esvelt *et al.*<sup>4</sup>; see also<sup>12</sup>), occurs when the target allele is specific to the target population, but absent from other populations. We emphasize that the LFA approach does not require the target allele be a private allele, simply that it not be fixed in non-target populations.

The LFA approach can be used with a variety of different gene drives (e.g. standard homing drives, sex-biasing drives, and so on). Here, for simplicity, we illustrate the method using a standard homing drive<sup>2,4</sup> aimed at population elimination. We describe this in the setting of removal of a rodent species, such as the house mouse, *Mus musculus*, from an island. Invasive mice, and other rodents, are a particular concern for species conservation<sup>28</sup>, having significantly impacted many island ecosystems, including causing extinctions of endemic island vertebrate, invertebrate and plant species<sup>29–31</sup>. Although an island release would involve procedures that attempt to confine the gene drive mice to the island, unintended escape of these mice must be considered a possibility. Here, we use mathematical modeling to explore the impact that escape of drive individuals would have on mainland populations.

While the focus of this study is on a drive that can eliminate a rodent pest species from an island, the LFA approach can be used more generally for drives aimed at population suppression or replacement provided that the drive bears some fitness cost. These more general settings are discussed in detail in the Supplementary Information, including some important differences in the dynamics from the elimination setting discussed in the main text.

This paper is organized as follows: we first introduce the mathematical model, then briefly describe the single-patch (island-only) dynamics before discussing those seen in a two-patch (island-mainland) setting. Supplementary information includes the derivation of an analytic threshold condition for the ability of drive to invade a partially susceptible population, an exploration of the sensitivity of results to various drive and ecological/demographic parameters, initial results of a stochastic model for the dynamics of LFA, and discussion of the use of LFA in more general population suppression and replacement settings.

## Methods

We employ a continuous-time non age-structured island-mainland model that describes the population dynamics and genetics of two populations. As our primary concern here is the impact of escape from the island, we assume unidirectional migration from the island to the mainland. (We recognize that migration from mainland to island would be an important consideration in the period following successful suppression or eradication from

the island, but this is not the topic of this study.) Throughout, we assume a 50:50 sex ratio and so track numbers of female individuals. For an  $n$ -genotype system, denoting genotypes with a subscript and denoting island population numbers with superscript  $I$  ( $N_i^I$ ) and mainland population numbers with a superscript  $M$  ( $N_i^M$ ), we have

$$\frac{dN_i^I}{dt} = f^I(N_1^I, \dots, N_n^I) - \mu N_i^I \quad (1)$$

$$\frac{dN_i^M}{dt} = f^M(N_1^M, \dots, N_n^M) + \mu N_i^I. \quad (2)$$

Here, the functions  $f^I$  and  $f^M$  describe the population dynamics and genetics that occur on island and mainland, respectively, and we assume unidirectional migration with per-capita migration rate equal to  $\mu$ .

We assume that island and mainland populations both undergo random mating (i.e. are well-mixed) and exhibit logistic-type population dynamics. Our description of population dynamics is based on an earlier model<sup>32</sup> for the population genetics and dynamics of gene drive in an island mouse population. Per-capita birth and death rates both change linearly with population size, with different coefficients on mainland and island (see<sup>32</sup> and references therein). Within either the island or mainland, and in the absence of migration, genotype dynamics are described by

$$\frac{dN_i}{dt} = b_i(t) \max(1 - q \sum_j N_j, 0) - \rho N_i - \alpha N_i \sum_j N_j. \quad (3)$$

Here, superscripts denoting the location have been suppressed for clarity on both state variables and parameters. The functions  $b_i(t)$ , described below, depict the genotype-specific birth rates in the absence of density dependence. For an entirely wild-type population,  $b(t)$  would equal  $\lambda N$ , where  $\lambda$  is the per-capita fecundity rate. The  $b_i(t)$  are multiplied by a function that describes the linear density-dependent decline in per-capita birth rates with total population size. (Note that the max function is required to ensure that birth rates remain non-negative.) Per-capita death rates are assumed to increase linearly with overall population size but be independent of genotype. The density-independent component of the per-capita death rate (i.e. the reciprocal of the average lifespan when the population is at low density) is written as  $\rho$ , while the coefficient  $\alpha$  describes the density-dependent linear increase in per-capita mortality. With these population dynamics, a single patch has a wild-type carrying capacity of  $N = \rho(R_0 - 1)/(\lambda q + \alpha)$ , where the basic reproductive number,  $R_0$ , (i.e. the average number of female offspring of a female over its lifetime, at low population density) is equal to  $\lambda/\rho$ .

Population genetics is determined by the functions  $b_i(t)$  which give the genotype-specific birth rates (c.f. the model of Robert *et al.*<sup>33</sup>) before accounting for the effects of density-dependence

$$b_i(t) = \lambda w_i \sum_j \sum_k \frac{P(i|j, k) N_j N_k}{\sum_l N_l}. \quad (4)$$

Here,  $\lambda$  is the baseline per-capita birth rate for females.  $P(i|j, k)$  gives the proportion of offspring from a mating involving individuals of types  $j$  and  $k$  that will have genotype  $i$ . The effects of the gene drive on biasing of inheritance are coded into these quantities. (The 216 entries of  $P(i|j, k)$ , together with a fully written out set of model equations, appear in the Maple worksheet in the Supplementary Information.) The  $w_i$  describe genotype-specific relative fitnesses, which we assume here to act at the embryonic stage and be equal in males and females of a given genotype.

As mentioned above, we use a simple homing-based elimination drive to illustrate the LFA method. We consider three alleles: the drive allele (D), the susceptible (S) allele, i.e. the target for the drive, and an allele that is resistant to the drive (R). All individuals in the target (island) population initially have the genotype SS, but those in the non-target (mainland) population can have SS, RS or RR genotypes. We assume only a single resistance allele in the mainland population. A large mainland population could have a number of different alleles that would be resistant to the drive, but they would all act similarly in being unaffected by the drive. Therefore our 3-allele model is sufficient for capturing dynamics of these cases. Note that here we are considering natural resistance to the drive, rather than drive-resistant alleles that are generated de novo as a result of the drive, e.g. by non-homologous end joining during homing. As a consequence, our model over-estimates the ability of the drive to spread and suppress populations<sup>34</sup>. Given that we are trying to evaluate the risk and implications of escape of drive, this assumption is conservative for our purposes. Homing is assumed to occur during gametogenesis, meaning that successful homing leads to an SD heterozygote individual giving rise to only D gametes. (Homing exclusively in the germline at any point during development would have the same consequences.) Successful homing occurs with probability  $e$ . The fitness,  $w_p$ , of SS, RR, or SR individuals is assumed to be 1. The fitness of DD individuals is  $(1-s)$ , and the fitness of SD and RD individuals is  $(1-hs)$ , where  $s$  is the fitness cost of the drive and  $h$  is the degree of dominance of the fitness cost. For instance, a recessive lethal drive has  $s=1$  and  $h=0$ . Notice that we assume there is no fitness cost for the RR individuals that occur naturally in the non-target population.

We employ parameters (see Table 1) that are appropriate for *Mus musculus* populations, largely based on those used by Backus & Gross<sup>32</sup> (see also<sup>35</sup>). For this set of parameters, the basic reproductive number of a wild-type population is 3.5. Assuming an island of area 6 hectares, these parameters lead to an equilibrium population size of 1000 females. We assume that the mainland has a population size that is 100 times larger than this.

	Parameter	Value	Source
$\lambda$	Female fecundity rate	$8.4 \text{ (year)}^{-1}$	Backus & Gross <sup>32</sup>
$q$	Coefficient quantifying density-dependent decline in birth rate	Island: $6.427 \times 10^{-3} \text{ (mouse)}^{-1}$ Mainland: $6.427 \times 10^{-3} \text{ (mouse)}^{-1}$	Backus & Gross <sup>32</sup>
$\rho$	Density independent per-capita death rate	$2.4 \text{ (year)}^{-1}$	Backus & Gross <sup>32</sup>
$\alpha$	Coefficient quantifying density-dependent increase in death rate	Island: $5.000 \times 10^{-5} \text{ (mouse)}^{-1} \text{ (year)}^{-1}$ Mainland: $5.000 \times 10^{-7} \text{ (mouse)}^{-1} \text{ (year)}^{-1}$	Backus & Gross <sup>32</sup>
$w_i$	Genotype specific fitness	Dependent on $s$ and $h$	
$\mu$	Per-capita migration rate from island to mainland	Varied ( $10^{-4}$ – $1.2 \times 10^{-1} \text{ (year)}^{-1}$ )	
$s$	Drive allele fitness cost	0.8	
$h$	Degree of dominance of fitness cost of drive allele	Non-threshold drive: 0.3 Threshold drive: 0.8	
$e$	Homing probability	0.95	

**Table 1.** List of Parameters and Their Values.

## Results

**Single patch model.** The single-patch behavior of the standard homing drive that we use here has been well-studied previously<sup>2,23,36,37</sup>. Depending on the drive parameters  $s$ ,  $h$  and  $e$ , several qualitatively different behaviors can occur following release of drive into an otherwise entirely susceptible population: guaranteed fixation of the drive, guaranteed loss of the drive, co-existence of drive and susceptible alleles at a stable polymorphic equilibrium or invasion threshold behavior (i.e. drive either goes to fixation or is lost, depending on its initial frequency) resulting from the existence of an unstable polymorphic equilibrium. Elimination of the population is possible when the drive remains in the population (going to a stable equilibrium with a positive frequency—either fixation or a polymorphic equilibrium) and imposes a cost that is sufficiently high to bring the reproductive number of the population below one.

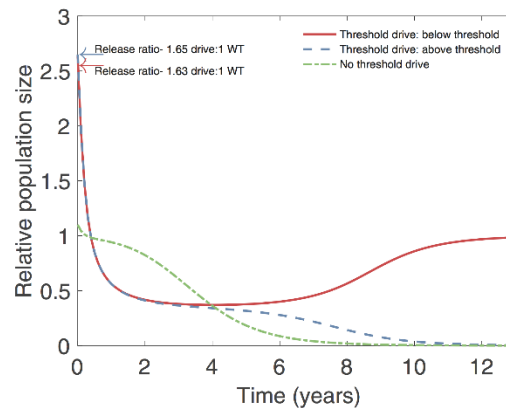
We illustrate these dynamics using two sets of parameters: one for which the drive can spread through a susceptible population regardless of its frequency (no invasion threshold scenario), and another for which the drive can only spread when its frequency exceeds an invasion threshold (invasion threshold scenario). In both cases we consider a fitness cost of  $s = 0.8$  and a homing probability of  $e = 0.95$ . The two scenarios differ only in the dominance,  $h$ , of the drive. For the no invasion threshold scenario we take  $h = 0.3$ , while for the invasion threshold scenario we take  $h = 0.8$ , which leads to an invasion threshold frequency of approximately 0.621 (corresponding to a ratio of approximately 1.64:1 drive:wild-type individuals). Releases occur into a population that is at carrying capacity, and population sizes are assessed relative to this carrying capacity.

Figure 1 shows the population dynamics that result from drive releases in these two scenarios. For the no invasion threshold scenario (green curve), even a small release of drive individuals, so that the initial relative population size is only just above one, leads to spread of the drive allele and hence reduction and eventual elimination of the population. For the invasion threshold scenario (blue and red curves), spread of the drive, and hence the fate of the population, depends on whether the release frequency of the drive is above (blue curve) or below (red curve) the invasion threshold. A sufficiently large release (blue curve) leads to fixation of the drive and elimination of the population, while an insufficient release (red curve) leads to loss of the drive and recovery of the population following a transient period of reduction.

**Island-mainland model.** We now turn to the main question of how migration from an island population on which drive individuals have been released will impact a mainland population that has a mix of susceptible and resistant individuals. To present something approaching a worst-case scenario, we first assume that the frequency of resistant individuals on the mainland is rather low, with a resistance allele frequency of 5% and susceptible allele frequency of 95%. We take our island population to be 1/100<sup>th</sup> the size of the mainland population, with unidirectional migration from the island to the mainland occurring at per-capita rate of 0.012 per year, corresponding to movement at the rate of one mouse per month at baseline.

For the invasion threshold drive scenario, we consider an island release that is above threshold, so that the drive approaches fixation in the long run (Fig. 2, upper panel, red curve) and the island population is successfully eliminated (Fig. 2, upper panel, blue curve). Even though drive individuals migrate from the island to the mainland, the large size of the mainland population means that the drive frequency remains small and never exceeds the invasion threshold. Thus, the drive cannot spread on the mainland, leaving the size and genetic composition of the mainland population largely unaffected.

The situation is different in the no invasion threshold scenario. The drive is able to spread on the mainland even when present at the low frequencies that arise due to migration of drive individuals from the island. Individuals with a resistance allele are unaffected by the drive, however, and so spread only occurs through the susceptible individuals. Again, the drive spreads on the island (Fig. 3, upper panel, red curve) causing successful elimination of the island population (Fig. 3, upper panel, blue curve). On the mainland, drive spreads through the susceptible portion of the population (Fig. 3, lower panel, red dashed curve) causing a reduction in the population size (Fig. 3, lower panel, blue curve) due to fitness costs incurred by drive-bearing individuals. Because they are unaffected by the drive, resistant individuals benefit from having a larger relative fitness in the presence of drive individuals and so their frequency increases (Fig. 3, lower panel, red dot dashed curve), while the drive frequency decreases. As the frequency of resistant individuals increases, the average fitness of the population returns to the level seen initially, and density-dependent dynamics returns the population to its original size. In this setting, we



**Figure 1.** Island population dynamics for the no invasion threshold and invasion threshold scenarios. In both scenarios the drive has an 80% fitness cost ( $s=0.8$ ) but have differing degrees of dominance: for the no invasion threshold scenario (green curve) we take  $h=0.3$ , while for the invasion threshold scenario we take  $h=0.8$ . Population sizes are plotted relative to pre-release equilibrium population numbers. In the no invasion threshold scenario, arbitrarily small releases of drive individuals lead to invasion and fixation of the drive allele, leading to suppression of the population (green curve; release of 100 homozygous drive individuals, 0.1:1 release ratio). In the invasion threshold scenario, invasion of the drive depends on whether the initial release exceeds the invasion threshold (for this choice of parameters, the invasion threshold frequency for drive is 0.621, corresponding to approximately 1.64 drive individuals for each wild-type individual). Red curve depicts a sub-threshold release (1630 homozygous drive females; 1.63:1 release ratio), leading to loss of the drive allele and only temporary suppression of the population before its return to carrying capacity. Blue curve depicts a successful release (1650 homozygous drive females; 1.65:1 release ratio), for which the drive invades and reaches fixation, leading to elimination of the population. Values of other parameters are given in Table 1.

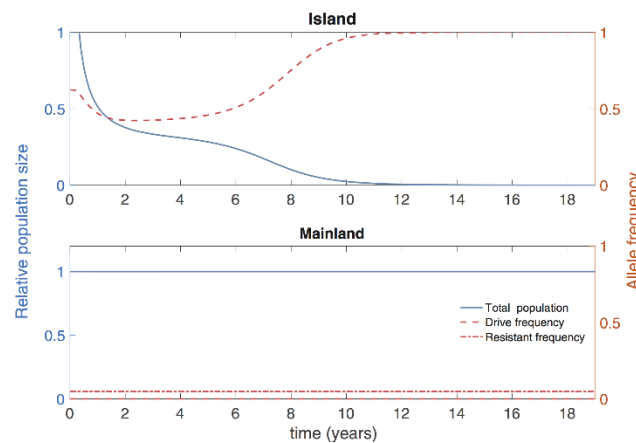


**Figure 2.** Island and mainland population dynamics (blue curves) and genetics (red curves) in the invasion threshold scenario ( $s=0.8$  and  $h=0.8$ ), following an above-threshold release of drive individuals on the island (1650 drive homozygotes released at  $t=0$ ; release ratio 1.65:1). Left axis (blue) denotes population size relative to pre-release equilibrium, right axis (red) denotes allele frequency. The drive spreads on the island (dashed red curve shows allele frequency for drive), suppressing its population (solid blue curve shows relative population size). Migration from the mainland to the island (at baseline, on average one island individual travels to the mainland a month) leads to a low drive frequency on the mainland that does not exceed the invasion threshold there. Consequently, the mainland population is largely unaffected. (Dot-dashed line denotes frequency of resistance allele. Note that the target allele being fixed means that the resistant allele is not present on the island).



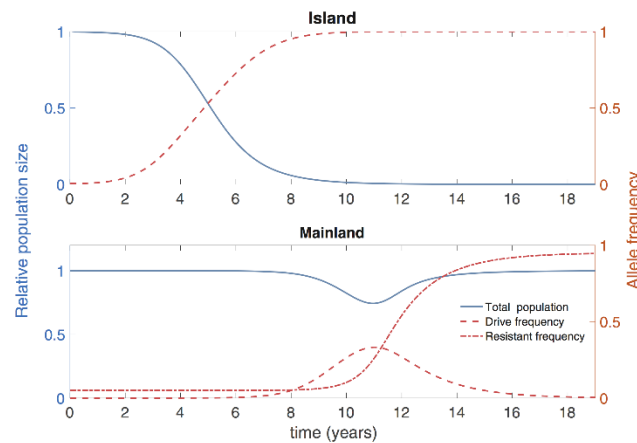


**Figure 3.** Island and mainland population dynamics and genetics in the no invasion threshold scenario ( $s = 0.8$  and  $h = 0.3$ ). As in Fig. 2, blue curves and axes denote population sizes, measured relative to pre-release equilibria, while red curves and axes denote allele frequencies. One hundred homozygous drive individuals (0.1:1 release ratio) are released at time  $t = 0$ . We assume that resistance is very low on the mainland (allele frequency of just 5%), representing a rather pessimistic scenario in terms of the susceptibility of the mainland population to the drive. The drive spreads to fixation and suppresses the island population. Migration to the mainland (at baseline, on average one island individual travels to the mainland a month) means that the drive is introduced to the mainland, where it can spread through the susceptible population, but not the resistant population. The total population undergoes a temporary suppression as the drive spreads through the susceptible population. The frequency of resistant alleles increases as a result of drive, and density dependent population regulation returns the mainland population to the pre-release equilibrium level.

see a transient reduction in the mainland population size before a recovery due to the presence of resistance. The genetic composition of the mainland undergoes a shift during this process, with a reduction in the frequency of susceptible alleles (although not their elimination) and a corresponding increase in the frequency of resistance (see Supplementary Information and Supplementary Fig. 3).

In the Supplementary Information we show that high levels of resistance prevent the spread of drive on the mainland. Using a linear invasion analysis, we show that drive cannot invade when the initial frequency of the resistant allele is above  $1 - hs/[e(1 - hs)]$ .

Figures 4 and 5 explore how the magnitude of population suppression and the maximum allele frequency of the gene drive observed on the mainland depend on the initial level of resistance on the mainland and the migration rate from the island to the mainland in the no invasion threshold scenario. Naturally, the level of transient suppression (fractional reduction below initial equilibrium) on the mainland depends strongly on the frequency of resistant and susceptible individuals there (Fig. 4), although an important observation is that the level of transient suppression is considerably lower than the initial frequency of susceptible individuals. The level of migration is seen to have little impact on the level of suppression. Similarly, the initial composition of the mainland population impacts the peak drive frequency reached on the mainland, while the level of migration again has little impact (Fig. 5). For the assumed demographic and drive parameters, 10% or higher levels of resistance on the mainland lead to a transient population suppression of at most 20% and peak drive frequency below 30%. Alternative choices for demographic and drive parameters would impact these numbers (see sensitivity analyses in the Supplementary Information). Obviously, in the PA setting, drive would be unable to spread on the mainland, but Figs 4 and 5 reveal that even in situations for which the susceptible allele is not absent, but only fairly uncommon on the mainland, the levels of suppression that would result would be small, and quite likely smaller than natural fluctuations in population size that might result from demographic or environmental stochasticity.

The peak level of suppression and the maximum drive frequency on the mainland occur at roughly similar times. The timing of these events is relatively insensitive to the initial frequency of resistance on the mainland and the migration rate over a wide range of conditions (see Supplementary Information and Supplementary Figs 1 and 2), with dynamics playing out over the course of 10 to 20 years. High initial levels of resistance, however, can lead to much slower spread of the drive on the mainland. As mentioned above, drive cannot invade when the initial frequency of the resistant allele is above  $1 - hs/[e(1 - hs)]$ . Invasion of drive will occur only slowly (and with a low peak level) when the frequency of resistance is not too far below this level. Supplementary Fig. 4 shows that the peak level of suppression on the mainland is almost independent of the size of the release on the island, while the time until this suppression occurs is only weakly dependent on the release size.

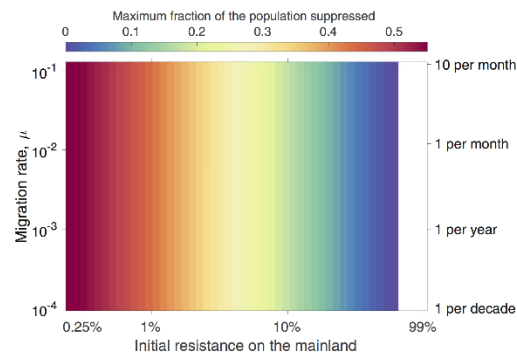


**Figure 4.** Maximum level of transient suppression seen on the mainland following an island release of 100 homozygous drive individuals in the no invasion threshold scenario ( $s = 0.8$  and  $h = 0.3$ ) across combinations of different migration rates and initial frequencies of resistant alleles on the mainland. Different levels of suppression are denoted by different colors (see color key on figure). Low initial resistance frequencies depict pessimistic scenarios (mainland is almost entirely susceptible to the drive), while high initial resistance frequencies approach the private allele scenario discussed in the text. The white region of the figure denotes initial levels of resistance that exceed the threshold level above which drive cannot invade the mainland.

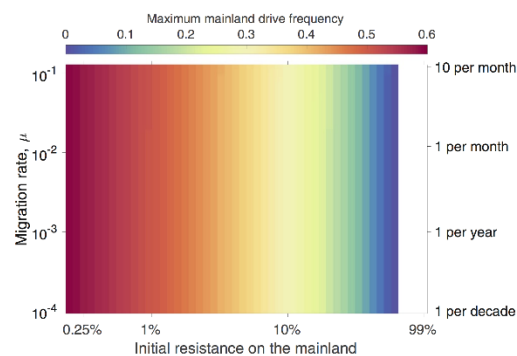


**Figure 5.** Maximum drive frequency observed on the mainland following an island release. Maximum drive frequency is indicated by color. All other details as in Fig. 4.

## Discussion

There is a fundamental tension between the ability of a gene drive to spread locally within a target area and its ability to invade populations beyond that area. For a non-threshold gene drive designed for suppression or elimination, the potential impact outside the targeted area can be of serious concern even if there is a likelihood that resistance to the drive will evolve before irreversible damage is done. Indeed, such concerns were strongly expressed in many of the seminal early papers on gene drive (e.g.<sup>2,3</sup>). Clearly, mechanisms that give some level of control over the spread of a gene drive are prerequisites for the deployment of a gene drive for suppression or elimination of a targeted population if other populations of the species contribute positively to biodiversity or economics. Utilizing the high degree of genetic specificity exhibited by homing drives, the LFA approach provides one option to limit the impact of unintended spread of a drive. In the fortunate, although perhaps rather unlikely special case of private alleles, where all individuals in non-target populations lack the susceptible allele and the susceptible allele is fixed on the island, the drive would be completely confined to the target population.

The LFA approach is related to two-step gene drive approaches that first spread a target allele into a population and then release a second drive that is specific to the target allele. For example, Esvelt *et al.*<sup>4</sup> suggested this approach for island populations, arguing that containment would happen provided that release of the second drive occurred before any individuals bearing the first drive escaped the island. The uncertainty involved in this scenario could be problematic for some stakeholders and regulatory authorities. In our approach, naturally occurring targeted alleles are expected to be fixed within small island populations due to genetic drift or founder effects

that have occurred in the past. These targeted alleles may be present in other locations, but as long as they are not fixed, impacts on populations in those locations should be transient.

As demonstrated by other mathematical models (e.g.<sup>22,38</sup>) some spatially limited gene drive mechanisms are unlikely to function well for strongly suppressing populations, because these require extremely large releases, which are neither feasible nor advisable for pest species on islands (but see<sup>39</sup> for an alternative approach for localized suppression of mainland populations). In this regard, the LFA approach stands out for its predicted ability to efficiently eliminate a small mostly isolated population without impacting other populations beyond a transient effect. The LFA approach could also be useful in the setting of a suppression or replacement drive that does not lead to elimination of the island population, although, as discussed in detail in the Supplementary Information (Section S.5), persistence of the drive on the island will mean continual reintroductions of drive to the mainland via migration, most likely leading to maintenance of drive on the mainland at a low frequency.

Our analysis employed a deterministic model, which allows for continuous migration from island to mainland. This model describes the average behavior of the system and so gives a good indication of expected dynamics in a large well-mixed mainland population. It describes the magnitude of suppression and its timing, but does not account for the discrete numbers of individuals in populations. Given that migration from the island to mainland is anticipated to occur as relatively infrequent events that involve small numbers of individuals, a stochastic model would be more realistic. Such a model would allow questions about the likelihood of the occurrence of migration events and of resulting transient spread of the drive, and distributions of the magnitude and timing of any transient suppression that results. However, we would not expect the qualitative results of such a model to predict a qualitatively different outcome from the current model in terms of impacts on the overall mainland population (see Supplementary Information for results from a stochastic model and some additional discussion of the impact of stochasticity).

For this proof-of-concept study of the LFA approach, we employed a highly simplified description of the population dynamics and genetics of the system. Many ecological and behavioral complexities, such as Allee effects<sup>40</sup>, the spatial and social structures of mouse populations, and mouse mating behavior, will impact the dynamics of population suppression and elimination under the action of gene drives. More refined models that include such features will have to be developed if the use of this approach is to be considered for a real-world release program.

It is important to recognize that one of the outcomes of mice arriving on the mainland that have a homing drive with no threshold is that the frequency of the resistant allele will increase. If after the mice are eliminated from the island a mouse or a few mice carrying the now more common resistant allele migrate to the island, it is likely that the new population on the island would no longer be a good target for the previously used construct. However, if recolonization was started by one or a few individuals, founder effects and drift would be likely to result in other fixed alleles that could be targeted.

There are a number of technical and societal challenges in moving the LFA from concept to application. While there is empirical evidence of lower polymorphism in small island populations (e.g.<sup>41–43</sup>), not every fixed allele in an island population will be a good target for a CRISPR-based gene drive. Appropriate targets will depend on the intended nature of the drive (e.g. if it is to be sex-specific, employ a split-drive design, etc), impacting the number of available loci. Furthermore, these alleles will optimally have at least two sites that can be targeted by the CRISPR-CAS nuclease complex to decrease the chance of drive failure due to resistant alleles arising through non-homologous end joining<sup>44</sup>. It will be critical that full genomes of individuals be scanned for the best possible targets and those targets will need to be scrutinized for potential problems. Also, because the LFA approach requires that the target allele is fixed, island populations will need to be sampled and evaluated extensively before moving ahead with any genetic engineering to ensure an acceptably high probability that the targeted allele is truly fixed on the island. This will require focused sequencing of the target loci in a large number of individuals, but it should be recognized that 100% assurance is not possible.

At a societal level, lack of an ecological impact of an LFA in a non-target location of the specific target species must be assured. Models that include details of the species biology, population structure and genetics will be critical in moving toward regulatory approval. But assurance of lack of an ecological impact of LFA constructs on the non-targeted populations may not be sufficient for some stakeholders who will have a concern with even one engineered individual arriving in their area.

Beyond direct impacts of an LFA, researchers must be cognizant of the fact that in developing the technology for LFA in a problematic species, they are also developing tools that could be used by others to construct unrestricted gene drives in that species. There will always be tradeoffs in developing new technologies and there are unlikely to be simple decisions. Vigilance and input from diverse stakeholders “early and often”<sup>45</sup> will be critical in coming to decisions.

Received: 1 April 2019; Accepted: 11 October 2019;

Published online: 01 November 2019

## References

1. Curtis, C. F. Possible use of translocations to fix desirable genes in insect pest populations. *Nature* **218**, 368–369 (1968).
2. Burt, A. Site-specific selfish genes as tools for the control and genetic engineering of natural populations. *Proc. R. Soc. Lond. B* **270**, 921–928 (2003).
3. Gould, F. Broadening the application of evolutionarily based genetic pest management. *Evolution* **62**, 500–510 (2008).
4. Esvelt, K., Smidler, A. L., Catteruccia, F. & Church, G. M. Concerning RNA-guided gene drives for the alteration of wild populations. *eLife* **3**, e03401 (2014).
5. Champer, J., Buchman, A. & Akbari, O. S. Cheating evolution: engineering gene drives to manipulate the fate of wild populations. *Nature Rev. Genet.* **17**, 146–159 (2016).
6. Spielman, A. Why entomological antimalaria research should not focus on transgenic mosquitoes. *Parasitol. Today* **10**, 374–376 (1994).
7. Alphey, L. *et al.* Malaria control with genetically manipulated insect vectors. *Science* **298**, 119–121 (2002).

8. Macer, D. Ethical, legal and social issues of genetically modifying insect vectors for public health. *Insect Biotech. Mol. Biol.* **35**, 649–660 (2005).
9. Marshall, J. M. The Cartagena Protocol and genetically modified mosquitoes. *Nature Biotech.* **28**, 896–897 (2010).
10. Akbari, O. S. *et al.* Safeguarding gene drive experiments in the laboratory. *Science* **349**, 927–929 (2015).
11. National Academies of Sciences, Engineering, and Medicine. Gene Drives on the Horizon: Advancing Science, Navigating Uncertainty, and Aligning Research with Public Values. (The National Academies Press, 2016).
12. Esvelt, K. M. & Gemmell, N. J. Conservation demands safe gene drive. *PLoS Biology* **15**, e2003850 (2017).
13. Marshall, J. M. & Akbari, O. S. Can CRISPR-based gene drive be confined in the wild? A question for molecular and population biology. *ACS Chem. Biol.* **13**, 424–430 (2018).
14. Davis, S., Bax, N. & Grewe, P. Engineered underdominance allows efficient and economical introgression of traits into pest populations. *J. Theor. Biol.* **212**, 83–98 (2001).
15. Altrock, P. M., Traulsen, A., Reeves, R. G. & Reed, F. A. Using underdominance to bi-stably transform local populations. *J. Theor. Biol.* **267**, 62–75 (2010).
16. Barton, N. H. The dynamics of hybrid zones. *Heredity* **43**, 341–359 (1979).
17. Barton, N. H. & Turelli, M. Spatial waves of advance with bistable dynamics: Cytoplasmic and genetic analogues of Allee effects. *Am. Nat.* **178**, E48–E75 (2011).
18. Gould, F., Huang, Y., Legros, M. & Lloyd, A. L. A Killer–Rescue system for self-limiting gene drive of anti-pathogen constructs. *Proc. R. Soc. Lond. B* **275**, 2823–2829 (2008).
19. Rasgon, J. L. Multi-locus assortment (MLA) for transgene dispersal and elimination in mosquito populations. *PLoS One* **4**, e5833 (2009).
20. Burt, A. & Deredec, A. Self-limiting population genetic control with sex-linked genome editors. *Proc. R. Soc. Lond. B* **285**, 20180776 (2018).
21. Noble, C. *et al.* Daisy-chain gene drives for the alteration of local populations. *Proc. Natl. Acad. Sci. USA* **116**, 8275–8282 (2019).
22. Dhole, S., Vella, M. R., Lloyd, A. L. & Gould, F. Invasion and migration of spatially self-limiting gene drives: A comparative analysis. *Evol. Applic.* **11**, 794–808 (2018).
23. Alphey, N. & Bonsall, M. B. Interplay of population genetics and dynamics in the genetic control of mosquitoes. *J. R. Soc. Interface* **11**, 20131071 (2014).
24. Khamis, D., El Mouden, C., Kura, K. & Bonsall, M. B. Ecological effects on underdominance threshold drives for vector control. *J. Theor. Biol.* **456**, 1–15 (2018).
25. Kimura, M. & Ohta, T. The average number of generations until fixation of a mutant gene in a finite population. *Genetics* **61**, 763–771 (1968).
26. Frankham, R. Do island populations have lower genetic variation than mainland populations? *Heredity* **78**, 311–327 (1997).
27. Hsu, P. D. *et al.* DNA targeting specificity of RNA-guided Cas9 nucleases. *Nature Biotech.* **31**, 827–832 (2013).
28. Howald, G. *et al.* Invasive rodent eradication on islands. *Conserv. Biol.* **21**, 1258–1268 (2007).
29. Cuthbert, R. & Hilton, G. Introduced house mice *Mus musculus*: A significant predator of threatened and endemic birds on Gough Island, South Atlantic Ocean? *Biol. Conserv.* **117**, 483–489 (2004).
30. Towns, D. R., Atkinson, I. A. E. & Daugherty, C. H. Have the harmful effects of introduced rats on islands been exaggerated? *Biol. Invasions* **8**, 863–891 (2006).
31. Campbell, K. J. *et al.* The next generation of rodent eradications: Innovative technologies and tools to improve species specificity and increase their feasibility on islands. *Biol. Conserv.* **185**, 47–58 (2015).
32. Backus, G. A. & Gross, K. Genetic engineering to eradicate invasive mice on islands: modeling the efficiency and ecological impacts. *Ecosphere* **7**, e01589 (2016).
33. Robert, M. A., Okamoto, K., Lloyd, A. L. & Gould, F. A reduce and replace strategy for suppressing vector-borne diseases: insights from a deterministic model. *PLoS One* **8**, e73233 (2013).
34. Prowse, T. A. A. *et al.* Dodging silver bullets: good CRISPR gene-drive design is critical for eradicating exotic vertebrates. *Proc. R. Soc. Lond. B* **284**, 20170799 (2017).
35. Nathan, H. W., Clout, M. N., MacKay, J. W., Murphy, E. C. & Russell, J. C. Experimental island invasion of house mice. *Popul. Ecol.* **57**, 363–371 (2015).
36. Deredec, A., Burt, A. & Godfray, C. The population genetics of using homing endonuclease genes (HEGs) in vector and pest management. *Genetics* **179**, 2013–2026 (2008).
37. Unckless, R. L., Messer, P. W., Connallon, T. & Clark, A. G. Modeling the manipulation of natural populations by the mutagenic chain reaction. *Genetics* **201**, 425–531 (2015).
38. Magori, K. & Gould, F. Genetically engineered underdominance for manipulation of pest populations: A deterministic model. *Genetics* **172**, 2613–2620 (2006).
39. Dhole, S., Lloyd, A. L. & Gould, F. Tethering homing gene drives: A new design for spatially restricted population replacement and suppression. *Evol. Applic.* **12**, 1688–1702 (2019).
40. Wilkins, K. E., Prowse, T. A. A., Cassey, P., Thomas, P. Q. & Ross, J. V. Pest demography critically determines the viability of synthetic gene drives for population control. *Math. Biosci.* **305**, 160–169 (2018).
41. Browne, R. A. Genetic variation in island and mainland populations of *Peromyscus leucops*. *Am. Midl. Nat.* **97**, 1–9 (1977).
42. White, T. A. & Searle, J. B. Genetic diversity and population size: island populations of the common shrew, *Sorex araneus*. *Mol. Ecol.* **16**, 2005–2016 (2007).
43. Harradine, E., How, R. A., Schmitt, L. H. & Spencer, P. B. S. Island size and remoteness have major conservation significance for how spatial diversity is partitioned in skinks. *Biodiv. Conserv.* **24**, 2011–2029 (2015).
44. Champer, J. *et al.* Reducing resistance allele formation in CRISPR gene drive. *Proc. Natl. Acad. Sci. USA* **115**, 5522–5527 (2018).
45. Piaggio, A. J. *et al.* Is it time for synthetic biodiversity conservation? *Trends Ecol. Evol.* **32**, 97–107 (2017).

## Acknowledgements

This work was funded by the DARPA Safe Genes Program (Grant DARPA-16-59-SAFE-FP-005), from which several of the authors (D.V.B., K.J.C., S.D., J.D.E., O.E., J.G., G.R.H., K.P.O., A.J.P., T.A.A.P., J.R.S., A.B.S., P.Q.T. and A.L.L.) receive support. Support was also received from the Research Training Group in Mathematical Biology, funded by NSF grant RTG/DMS-1246991 (JS, BH, MRV and ALL), NSF IGERT grant 1068676 (MRV, FG and ALL), NIH grant 1R01AI139085-01 (SD, FG and ALL) and the NC State Drexel Endowment (ALL). Contributions from other members of the Genetic Biocontrol of Invasive Rodents (GBIRD) consortium (<http://www.geneticbiocontrol.org/>) are acknowledged and greatly appreciated. We thank the referees for their constructive comments that helped improve this paper.

## Author contributions

J.S., B.H., F.G. and A.L.L. designed the model. J.S., B.H. and A.L.L. carried out model simulations and analysis. J.S., B.H., F.G. and A.L.L. wrote the first draft of the paper. All authors discussed model results and contributed to editing and revision of the manuscript.



### Competing interests

The authors declare no competing interests.

### Additional information

**Supplementary information** is available for this paper at <https://doi.org/10.1038/s41598-019-51994-0>.

**Correspondence** and requests for materials should be addressed to A.L.L.

**Reprints and permissions information** is available at [www.nature.com/reprints](http://www.nature.com/reprints).

**Publisher's note** Springer Nature remains neutral with regard to jurisdictional claims in published maps and institutional affiliations.



**Open Access** This article is licensed under a Creative Commons Attribution 4.0 International License, which permits use, sharing, adaptation, distribution and reproduction in any medium or format, as long as you give appropriate credit to the original author(s) and the source, provide a link to the Creative Commons license, and indicate if changes were made. The images or other third party material in this article are included in the article's Creative Commons license, unless indicated otherwise in a credit line to the material. If material is not included in the article's Creative Commons license and your intended use is not permitted by statutory regulation or exceeds the permitted use, you will need to obtain permission directly from the copyright holder. To view a copy of this license, visit <http://creativecommons.org/licenses/by/4.0/>.

© The Author(s) 2019

## Supplementary Information for

### Locally Fixed Alleles: A method to localize gene drive to island populations

Jaye Sudweeks <sup>a</sup>, Brandon Hollingsworth <sup>b</sup>, Dimitri V. Blondel <sup>c</sup>, Karl J. Campbell <sup>d</sup>, Sumit Dhole <sup>e</sup>, John D. Eisemann <sup>f</sup>, Owain Edwards <sup>g</sup>, John Godwin <sup>c,h</sup>, Gregg R. Howald <sup>d</sup>, Kevin P. Oh <sup>f,i</sup>, Antoinette J. Piaggio <sup>f</sup>, Thomas A. A. Prowse <sup>j</sup>, Joshua V. Ross <sup>j</sup>, J. Royden Saah <sup>d,h</sup>, Aaron B. Shiels <sup>f</sup>, Paul Q. Thomas <sup>k</sup>, David W. Threadgill <sup>l</sup>, Michael R. Vella <sup>b</sup>, Fred Gould <sup>e,h</sup> and Alun L. Lloyd <sup>a,b,\*</sup>

- (a) Department of Mathematics, North Carolina State University, Raleigh, NC 27695, USA
- (b) Biomathematics Graduate Program, North Carolina State University, Raleigh, NC 27695, USA
- (c) Department of Biological Sciences, North Carolina State University, Raleigh, NC 27695, USA
- (d) Island Conservation, 2100 Delaware Ave., Suite 1, Santa Cruz, CA 95060 USA
- (e) Department of Entomology and Plant Pathology, North Carolina State University, Raleigh, NC 27695, USA
- (f) National Wildlife Research Center, US Department of Agriculture, Fort Collins, CO 80521, USA
- (g) CSIRO Land & Water, Centre for Environment and Life Sciences, Floreat, WA, Australia
- (h) Genetic Engineering and Society Center, North Carolina State University, Raleigh, NC 27695, USA
- (i) Department of Microbiology, Immunology & Pathology, Colorado State University, Fort Collins, CO 80523, USA
- (j) School of Mathematical Sciences, The University of Adelaide, Adelaide, SA 5005, Australia
- (k) The Robinson Research Institute and School of Medicine, The University of Adelaide, Adelaide, SA 5005, Australia
- (l) Department of Molecular and Cellular Medicine, Texas A&M University, College Station, TX 77843, USA

\* Corresponding author, email: alun\_lloyd@ncsu.edu

## Contents:

### S.1. Threshold for Invasion of Drive into Partially Susceptible/Partially Resistant Mainland Population

### S.2. Additional Details of Dynamics on the Mainland: Timing of Suppression and Peak Drive Level; Long-Term Dynamics

### S.3. Sensitivity of Results to Parameter Values

#### S.3.1. Sensitivity to Drive Parameters

#### S.3.2. Sensitivity to Demographic and Density Dependence Parameters

##### S.3.2.1 Logistic Model

##### S.3.2.2. Generalized Logistic Model

### S.4. Stochastic Model

### S.5. Population Suppression and Population Replacement

### S.1. Threshold for Invasion of Drive into Partially Susceptible/Partially Resistant Mainland Population

It can be shown that there is a threshold level of resistance above which drive cannot invade the mainland. This threshold can be derived by examining the stability of a drive-free equilibrium state of the single patch model, using the standard approach of linearizing the model about the equilibrium (see, for example<sup>1</sup>). This process involves calculation of the eigenvalues of the Jacobian matrix (i.e. the matrix of the partial derivatives of the right-hand sides of the differential equations (eqns 3 in the main text) with respect to the state variables of the model) evaluated at the equilibrium of interest. The 6x6 Jacobian matrix and its eigenvalues are easily calculated with the assistance of a computer algebra package (e.g. Maple [Maplesoft, a division of Waterloo Maple, Inc., Waterloo, Ontario] or Mathematica [Wolfram Research, Inc., Champaign, IL]). A Maple worksheet providing details of the calculations is provided as a supplementary file.

Given that we assume equal fitness of susceptible and resistant types, in the absence of drive there is no selection between susceptible and resistant types and so we have non-unique drive-free equilibria:

$$N_{SS} = (1 - q_R)^2 N^*, \quad N_{SR} = 2q_R(1 - q_R)N^*, \quad N_{RR} = q_R^2 N^*, \quad N_{SD} = N_{RD} = N_{DD} = 0$$

Here  $q_R$  is the frequency of the resistant allele and  $N^*$  is the wild-type (i.e. drive-free) equilibrium population size (equal to  $(\lambda - \rho)/(\lambda q + \alpha)$ ). We note that these equilibria form a curve in phase space.

The linear stability analysis gives six eigenvalues, one of which is zero (corresponding to neutral stability along the curve of drive-free equilibria), one equal to  $\rho - \lambda$  and three equal to  $-\lambda(q\rho + \alpha)/(\lambda q + \alpha)$ . We see that these last four eigenvalues are negative (note that  $\lambda$  must be greater than  $\rho$  in order for  $N^*$  to be positive). The ability of drive to invade (from low initial frequency) is determined by the sign of the final eigenvalue, whose value is equal to  $\lambda[(1 - q_R)(1 - hs)e - hs](q\rho + \alpha)/(\lambda q + \alpha)$ . Invasion is only possible if this quantity is positive, and so consideration of the quantity in square brackets leads to the condition

$$q_R < 1 - hs/\{e(1 - hs)\}.$$

Another way to derive this threshold (and one that immediately applies to a number of previous studies in the literature) is by considering a discrete-time (discrete generations) description framed in terms of allele frequencies (see, for example<sup>2,3</sup>).

If the allele frequencies for Susceptible, Drive and Resistant alleles in the current generation are written as  $q_S$ ,  $q_D$  and  $q_R$ , it can be shown that the frequency of the drive allele in the next generation,  $q'_D$ , will be given by

$$q'_D = \frac{1}{\bar{w}} (\{1 - s\}q_D^2 + \{1 - hs\}q_S q_D \{1 + e\} + \{1 - hs\}q_R q_D),$$

where  $\bar{w}$  is the mean fitness, which equals

$$\bar{w} = 1 - sq_D^2 - 2hsq_D(q_S + q_R).$$

When thinking about invasion of drive into a population that initially consists of susceptible and resistant alleles,  $q_D$  will be small, and so the following linear equation can be derived for the change in the frequency of the drive allele from one generation to the next:

$$q'_D - q_D \approx q_D (\{1 - hs\}q_S \{1 + e\} + \{1 - hs\}q_R - 1).$$

(This equation is correct to first order in  $q_D$ .)

We see that the drive frequency can only increase if the term in parentheses is positive, meaning that

$$q_R < \frac{e(1-hs)-hs}{e(1-hs)},$$

which may be written as

$$q_R < 1 - hs/\{e(1 - hs)\}.$$

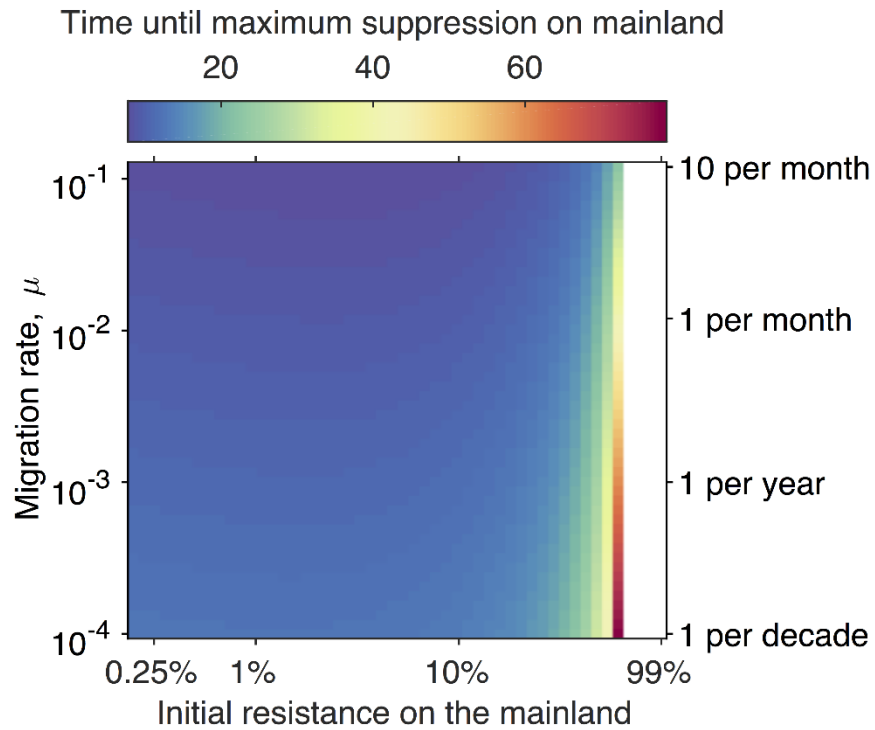
## S.2. Additional Details of Dynamics on the Mainland: Timing of Suppression and Peak Drive Level; Long-Term Dynamics

Supplemental Figures 1 and 2 explore the timing of (1) suppression on the mainland and (2) the peak level of drive seen on the mainland. These two events occur at similar times (but not at exactly the same time). We note that over a wide range of initial levels of resistance and migration rates, there is only weak dependence of either time on these quantities, and that these times increase substantially as the initial level of resistance approaches the non-invasion threshold.

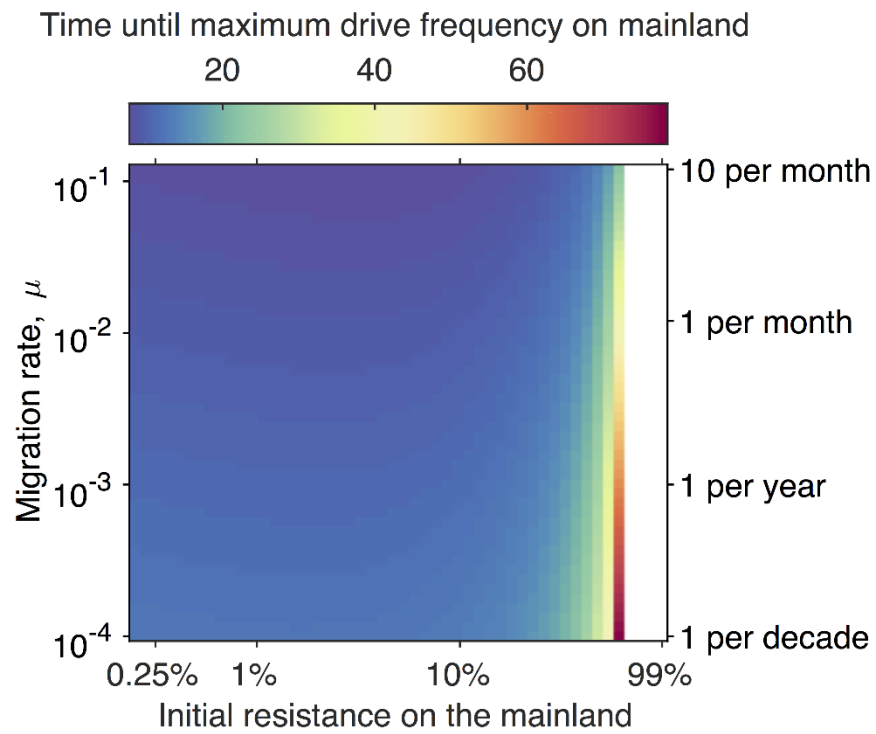
Supplemental Figure 3 explores the composition of the mainland population that remains after the transient spread of drive, showing the long-term (100 year) frequency of the susceptible allele. We note that, while the transient spread of drive leads to the reduction of susceptible alleles on the mainland, it does not lead to their elimination.

Supplemental Figure 4 shows that the peak level of suppression and the maximum drive frequency on the mainland are almost independent of the size of the release on the island (that they are not constant cannot be seen at the scale shown on this figure: both curves exhibit a very weak dependence on release size). The time until the peak suppression occurs is only weakly dependent on the release size for biologically plausible release sizes, varying only by about 3 years for release sizes between 1 and 1000 individuals, but continuing to increase in the limit as the release size approaches zero. In the deterministic model, invasion is possible from arbitrarily small releases, although it takes increasingly long for drive to increase to appreciable levels from extremely small release levels, hence the time to minimum continues to increase. Note that the model behaves qualitatively differently when the release size is zero from when the release size is non-zero.

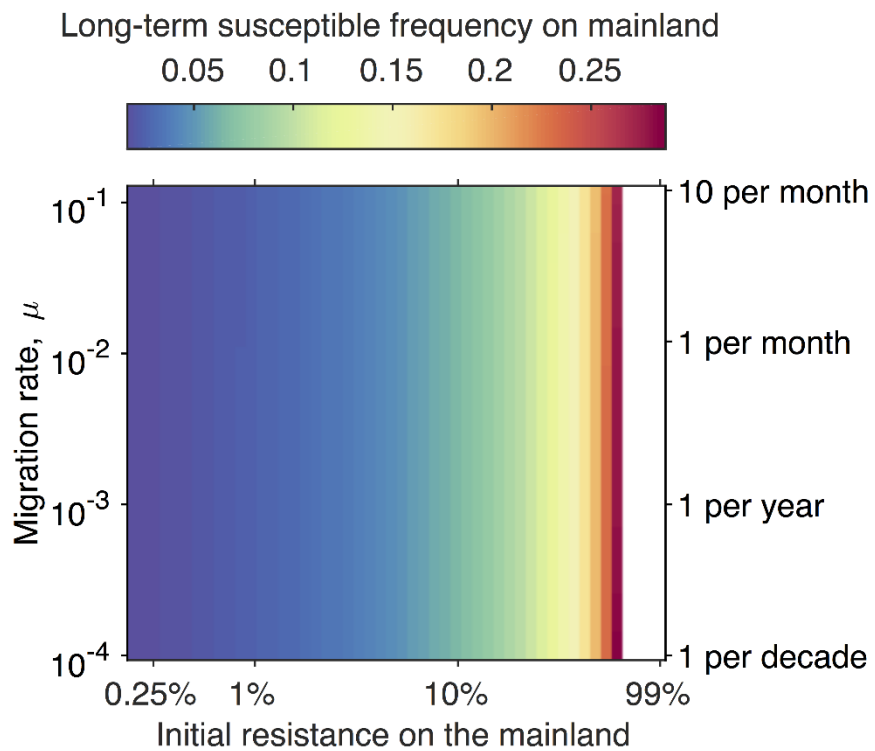
**Supplemental Figure 1.** Dependence of the time until the mainland population achieves its minimum on the initial level of resistance on the mainland and the migration rate from the island. All other details are as in Figure 4 of the main text. The white region of the figure denotes initial levels of resistance that exceed the threshold level above which drive cannot invade the mainland.



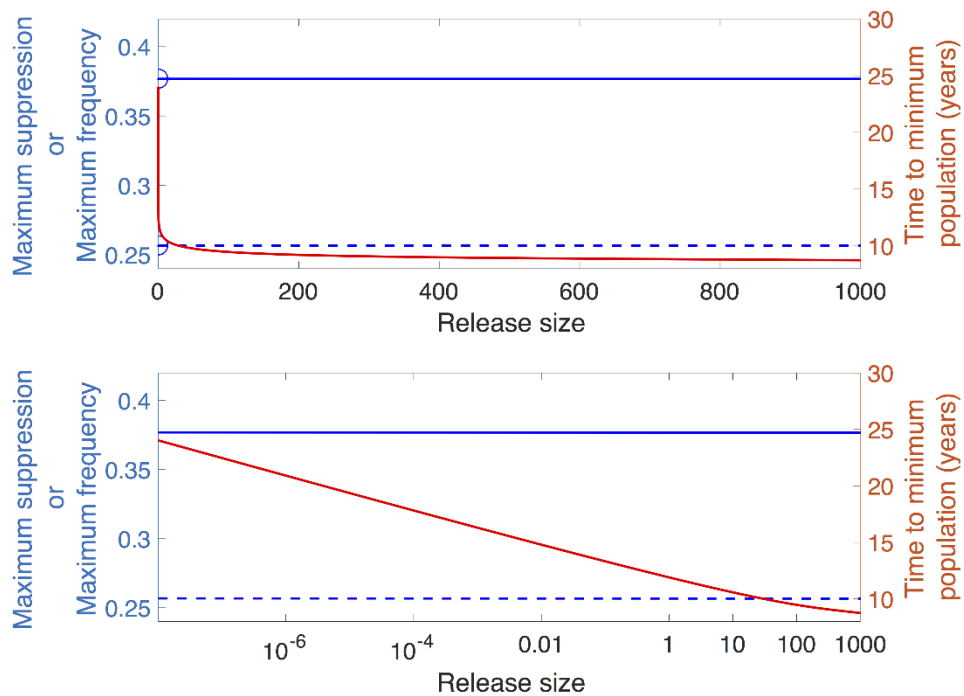
**Supplemental Figure 2.** Dependence of the time until the drive frequency achieves its maximum on the mainland on the initial level of resistance on the mainland and the migration rate from the island. All other details are as in Figure 4 of the main text.



**Supplemental Figure 3.** Frequency of the susceptible allele on the mainland 100 years after an island release in the no invasion threshold scenario ( $s = 0.8$  and  $h = 0.3$ ) across combinations of different migration rates and initial frequencies of resistant alleles on the mainland. All other details are as in Figure 4 of the main text. Note that susceptible alleles remain in the population after the transient spread and loss of drive on the mainland. The white region of the figure denotes initial levels of resistance that exceed the threshold level above which drive cannot invade the mainland.



**Supplemental Figure 4.** (Both panels) Maximum level of transient suppression (dashed blue curve; read scale on left axis), time taken for this level of suppression to occur (red curve, read scale on right axis) and maximum level of gene drive (solid blue curve; read scale on left axis) seen on mainland following releases of various sizes on the island under the no invasion threshold scenario. Initial frequency of resistance on the mainland is equal to 0.05 and migration occurs at a per-capita rate of 0.012 per year. All other parameters are as in Figure 3 of the main text. Circles on the vertical axis denote that the curves are not continuous when the release size is zero: the behavior of the model is qualitatively different between zero and positive release sizes. The bottom panel depicts the same results but using a logarithmic scale on the horizontal axis to emphasize the mathematical behavior as the release size approaches zero.





### S.3. Sensitivity of Results to Parameter Values

In this section we explore how model results, specifically the maximum level of suppression seen on the mainland and the peak level reached by drive on the mainland, depend on the drive and ecological parameters used. Such a sensitivity analysis provides increased confidence in the utility of the LFA approach.

Before exploring the impact of individual parameters in detail, we performed a global sensitivity analysis involving four parameters: the fitness cost of the drive,  $s$ , the dominance of this fitness cost,  $h$ , the homing probability,  $e$ , and the demographic parameter  $\lambda$ , the female fecundity parameter (i.e. the female per-capita birth rate of the population at low population densities, when density-dependent reductions in birth rate can be ignored). As discussed below (S.3.2.1), for the logistic model, if we choose to fix the equilibrium population size, there is only one demographic parameter, the net per-capita birth/death rate at low population densities, that can be independently varied. We choose to do this by varying the per-capita birth rate (female fecundity,  $\lambda$ ).

Given that we have little to no information on the uncertainties of these parameters about their baselines, we employed uniform distributions for their possible values (Table S.1), following the approach taken by Prowse et al.<sup>4</sup> in their sensitivity analysis of the Y-CHOPE Y chromosome shredding gene drive. We then used a sampling-based variation decomposition approach<sup>5</sup> (Fourier Analysis Sensitivity Test, FAST, implemented using the SAFE Toolbox<sup>6</sup>) to assess the contributions of the uncertainties in different parameters to the variation seen in model outputs across the parameter space. This approach is somewhat akin to more familiar analysis of variance statistical methods. 5000 simulation runs were carried out, each using a set of parameters sampled from the parameter space described in Table S.1.

**Supplemental Table 1:** Baseline values and assumed distributions for parametric sensitivity analysis.

Parameter	Baseline	Distribution
$s$	0.8	U(0.65,0.95)
$h$	0.3	U(0.1,0.5)
$e$	0.95	U(0.7,1.0)
$\lambda$	8.4	U(6,10)

Across the simulation runs based on 5000 sets of parameters, the range of observed maximum suppression values fall between less than 1% and 40.4%, with a mean of 20.8% and standard deviation of 0.08% (coefficient of variation of 38.8%). For the maximum drive frequency, the range of observed values was between less than 1% and 53.7%, with a mean of 31.8% and standard deviation of 12.2% (coefficient of variation of 38.2%).

For maximum suppression observed on the mainland, the first order effects of the four parameters explained 84% of the variation. Two of the drive parameters,  $h$  and  $e$ , and the demographic parameter  $\lambda$  explained fairly similar amounts of variation (26%, 22%, and 23%, respectively), while the fitness cost  $s$  explained just 12% of the variation. This analysis says that if we wished to predict the impact of LFA on

mainland population suppression, reducing the uncertainty in either  $h$ ,  $e$ , or  $\lambda$  has a bigger impact on the confidence in our predictions than reducing uncertainty in  $s$ .

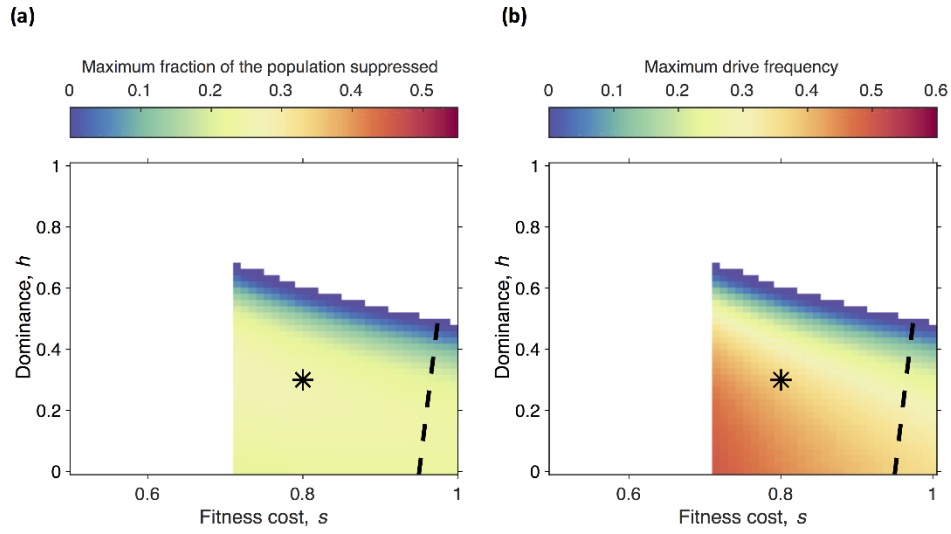
For maximum drive frequency observed on the mainland, the first order effects of the four parameters explained 94% of the variation. The drive fitness parameters  $s$  and  $h$  have the biggest impact, explaining 47% and 38% of variation, respectively. The homing probability  $h$  has a much smaller impact, explaining 8% of variation, while the demographic parameter  $\lambda$  has very little impact on the maximum drive frequency, explaining less than 0.1% of variation (see S.3.2.1 for more discussion on this).

### S.3.1. Sensitivity to Drive Parameters

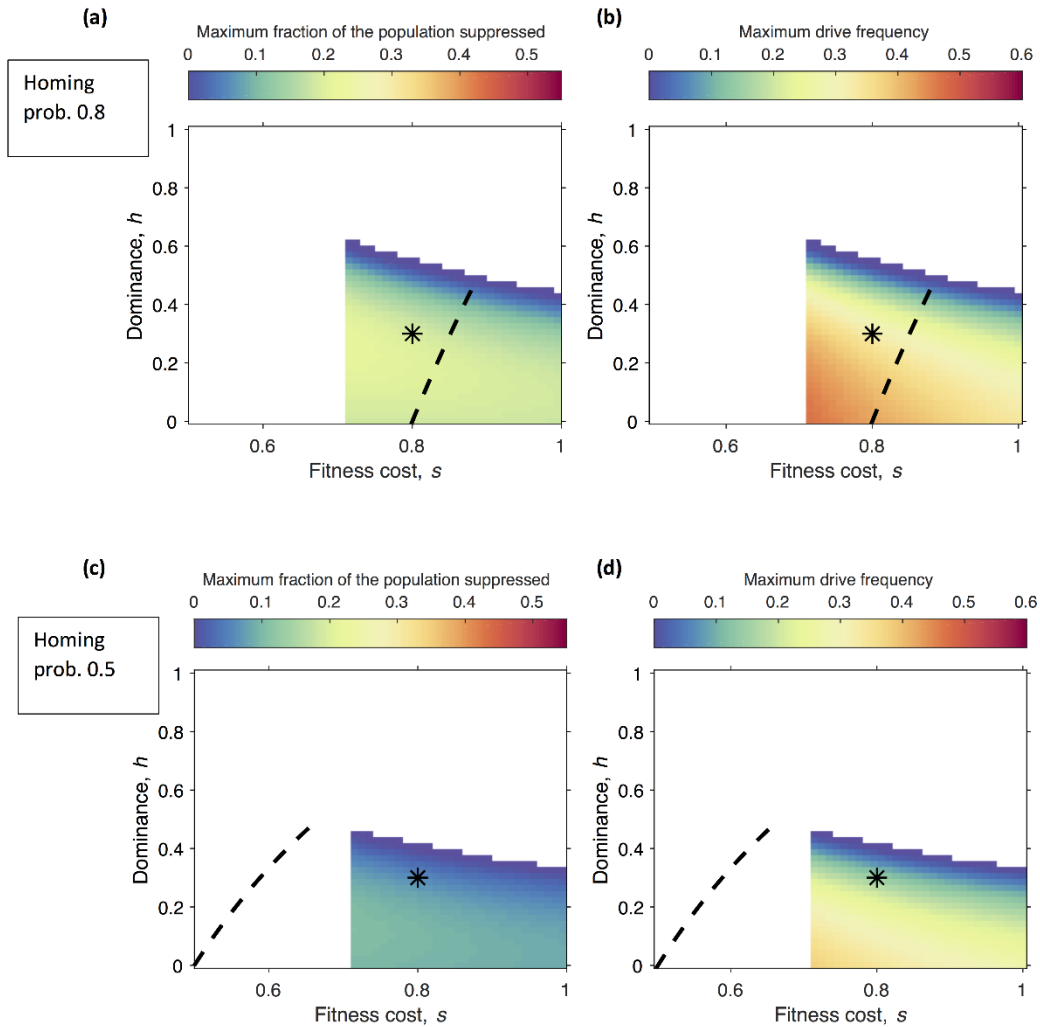
Figure S.5 shows the dependence of the maximum levels of suppression and drive seen on the mainland on the drive fitness cost and dominance of this fitness cost. Results are shown for the region of drive parameter space for which the island population is eliminated and for which no threshold behavior is observed (Deredec et al.<sup>2</sup> and Alphey and Bonsall<sup>7</sup> provide analytic expressions for the locations of these boundaries). The dashed line on the plot shows the boundary between the parameter regions for which drive becomes fixed or approaches a polymorphic equilibrium with wild-type<sup>2,7</sup>.

Figure S.6 shows sensitivity of outcomes over a region of drive parameter space assuming different values for the homing probability, and Figure S.7 shows dependence of outcomes on the initial level of resistance on the mainland assuming different values for the homing probability.

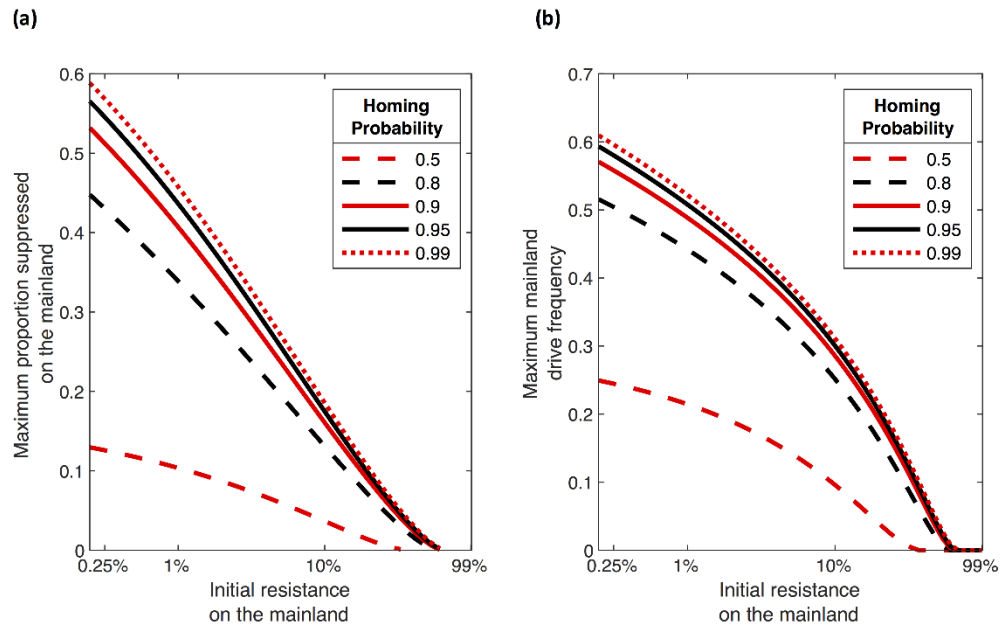
**Supplemental Figure 5:** Heatmaps showing the dependence of (panel a) the maximum suppression observed on the mainland and (panel b) the maximum level of drive seen on the mainland on the drive parameters  $s$  and  $h$ . The scales on the color bars are chosen to be the same as in Figures 4 and 5. White regions on this figure denote combinations of drive parameters that either lead to threshold behavior, loss of drive or for which the drive fails to lead to elimination of the island population. The initial frequency of the resistance allele on the mainland is 95%, and the migration rate is 0.012/year. All other parameters are as in Figures 4 and 5 of the main text. The black asterisk denotes the drive parameters used in Figures 4 and 5 of the main text. The dashed line denotes the boundary between the region of parameter space where drive approaches fixation (to the left of the line) and where drive approaches a polymorphic equilibrium with wild-type (to the right of the line).



**Supplemental Figure 6:** Heatmaps showing the dependence of (panels a and c) the maximum suppression observed on the mainland and (panels b and d) the maximum level of drive seen on the mainland on the drive parameters  $s$  and  $h$ , and for homing probabilities of (panels a and b) 0.8 and (panels c and d) 0.5. The scales on the color bars are chosen to be the same as in Figures 4 and 5 of the main text. White regions on this figure denote combinations of drive parameters that either lead to threshold behavior, loss of drive or for which the drive fails to lead to elimination of the island population. The initial frequency of the resistance allele on the mainland is 95%, and the migration rate is 0.012/year. All other parameters are as in Figures 4 and 5 of the main text. The black asterisk denotes the drive parameters used in Figures 4 and 5 of the main text. The dashed curve denotes the boundary between the region of parameter space where drive approaches fixation (to the left of the curve) and where drive approaches a polymorphic equilibrium with wild-type (to the right of the curve).



**Supplemental Figure 7.** (Panel a) Maximum population suppression seen on the mainland and (Panel b) maximum drive frequency seen on mainland for various levels of mainland initial resistant allele frequency, and for different values of the homing probability. In all cases, drive parameters are taken to equal  $s=0.8$  and  $h=0.3$ . All other parameters are as in Figure 3. of the main text.



### S.3.2. Sensitivity to Demographic and Density Dependence Parameters

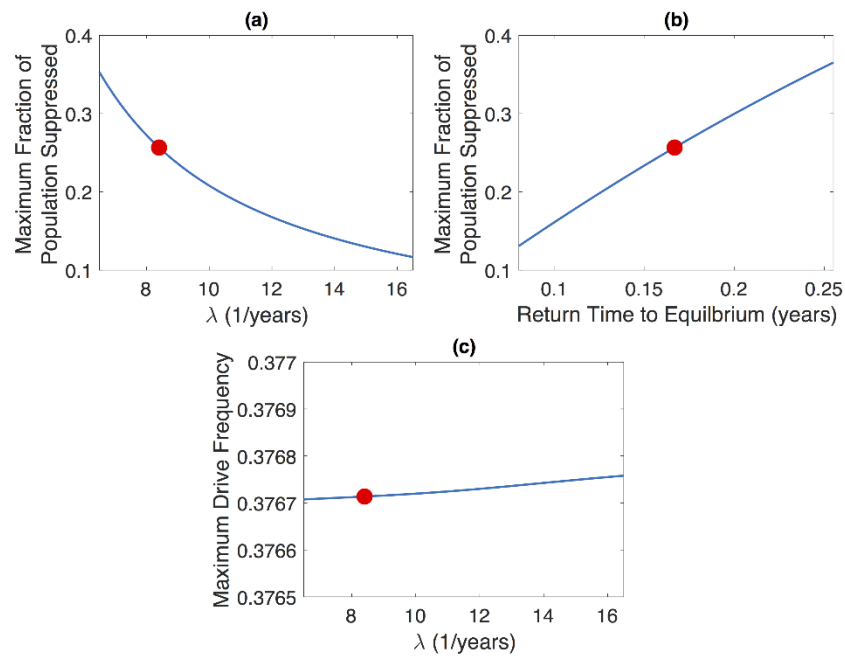
#### S.3.2.1 Logistic Model

We also explore the dependence of our results to demographic and density dependence parameters. The dynamics of the deterministic logistic model involves two parameter combinations: the per-capita growth rate of the population at low densities ( $\lambda - \rho$ ) and the per-capita rate of change of the population growth rate. In order to make comparisons across parameter values, we choose to keep the equilibrium population size fixed. This leaves us with the single parameter combination  $\lambda - \rho$  that can be varied in order to explore the impact of demographic parameters within this demographic model. Here, we choose to vary  $\lambda$  in order to achieve this. The primary impact of varying parameters in this way is to change the stability of the positive equilibrium of the logistic model. A natural way to characterize this is by calculating the *return time* of the equilibrium, a measure of the time taken for perturbations of the population about its equilibrium to decay that is commonly used in the theoretical ecology literature<sup>8</sup>. More precisely, the return time is calculated as the reciprocal of the absolute value of the largest eigenvalue of the Jacobian matrix of the model at its positive equilibrium,  $1/|f'(N^*)|$ , which for this model simply equals  $1/(\lambda - \rho)$ . Longer return times mean that the population responds more slowly to perturbations away from equilibrium (the equilibrium is “less stable” in this sense).

Figure S.8(a) shows how the maximum suppression seen on the mainland varies as  $\lambda$  is changed, and Figure S.8(b) reinterprets these results in terms of the resulting return time to equilibrium. We see that the maximum suppression seen on the mainland varies in an intuitive fashion as  $\lambda$  is changed. Longer equilibrium return times lead to higher levels of suppression: longer return times mean that the population responds more slowly to perturbations in its size and thus the fitness cost imposed by drive can push the population down to lower levels. The variation in the maximum suppression as  $\lambda$  changes can also be expressed in terms of the elasticity<sup>9</sup>, the ratio between the percentage change in maximum suppression and the percentage change in  $\lambda$ , calculated at the baseline parameter set and assuming that the percentage change in  $\lambda$  is small. This elasticity is equal to -1.22, which means that an  $X\%$  change in  $\lambda$  leads to an approximate change of -1.22 $X\%$  in the maximum suppression.

Figure S.8(c) shows that the maximum mainland drive frequency depends only weakly on the demographic parameter  $\lambda$ . This is not surprising: at the level of a single patch, population genetics and ecological dynamics are uncoupled (see<sup>7</sup>, for example). The weak dependence seen in the figure reflects the impact of migration between two populations whose sizes are varying. Changing the level of density dependence on the island leads to changing the timing of population reduction on the island, hence changing the numbers of drive individuals moving from the island to mainland over time. Similarly, changing the level of density dependence on the mainland changes the timing of population reduction on the mainland. This, in turn, changes the impact of arriving drive-bearing individuals: how they alter mainland drive frequency depends on the relative numbers of arriving and mainland individuals.

**Supplemental Figure 8:** Dependence of: (panel a) the maximum suppression observed on the mainland, and (panel c) the maximum drive frequency seen on the mainland as the intrinsic per-capita growth rate of the population ( $\lambda$ ) is varied. Panel (b) reinterprets the results of panel (a) in terms of the return time to equilibrium (see text for more details). All other parameters are kept fixed at the baseline values used in Figure 3, except for the parameters  $q$  that describe the linear decline in the per-capita birth rate with increasing population size. The  $q$  parameters are varied so as to keep island and mainland population sizes fixed as  $\lambda$  is changed. The red dot on each panel corresponds to the baseline set of demographic parameters used in Figure 3 of the main text.



### S.3.2.2. Generalized Logistic Model

In the previous section, the sensitivity of model results to the demographic assumptions of the logistic model was explored. As discussed, fixing the equilibrium population size leaves us with relatively little ability to impact demography within the confines of the logistic model framework. We can make a more general exploration of the impact of density dependence by employing a slightly more general population dynamics framework, the generalized logistic model<sup>10,11</sup>. Here we assume that the linearly increasing per-capita death rate of the logistic model is replaced by a nonlinear term that involves the exponent  $\beta-1$  :

$$\frac{dN}{dt} = \lambda N(1 - qN) - \rho N - \alpha N^\beta$$

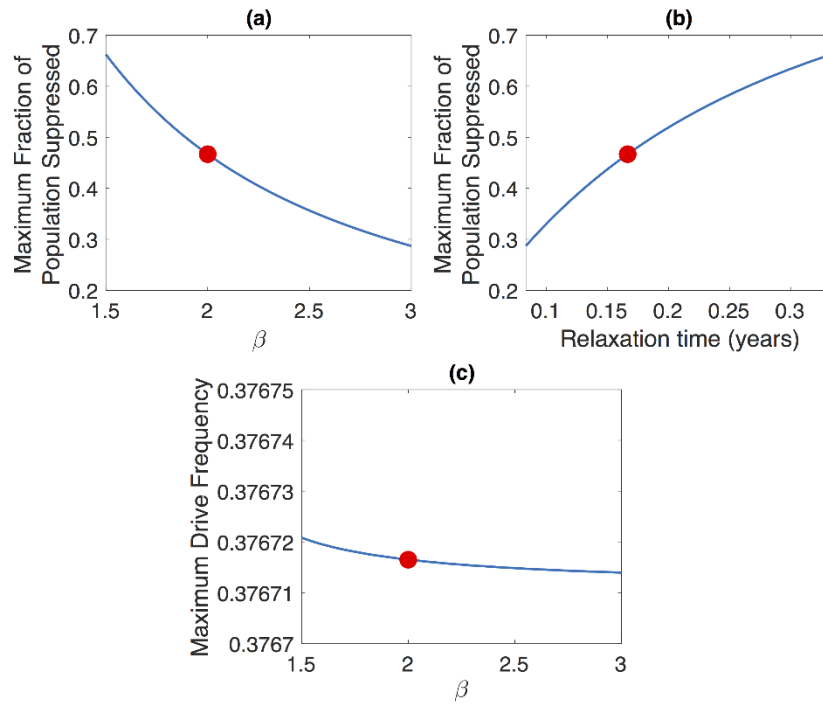
A  $\beta$  value of 2 corresponds to the logistic model employed in the main text and by Backus & Gross<sup>12</sup>. Values of  $\beta$  above 2 correspond to stronger density dependence, values below 2 to weaker density dependence.

As before, we keep the equilibrium population size constant when making comparisons. There are various ways to do this while varying  $\beta$ , but we employ the simplest choice: we keep the parameters  $\lambda$ ,  $q$  and  $\rho$  fixed, and choose an appropriate value of  $\alpha$ . To further simplify our exploration here, we only employ the generalized logistic model on the mainland, maintaining the baseline logistic dynamics on the island. (This means that the timeseries of numbers of migrants arriving on the mainland is kept the same as we vary  $\beta$ , and we explore how changing density dependence on the mainland alters the impact of these migrants on the mainland population.) Furthermore, we assume that density dependence only occurs in the death process on the mainland, i.e. we set the mainland value of  $q$  equal to zero.

As expected higher levels of suppression are seen for weaker density dependence ( $\beta < 2$ ) and lower levels for stronger density dependence ( $\beta > 2$ ), compared to the logistic model ( $\beta = 2$ ). The elasticity, calculated at the baseline level of the parameter, is -1.22.



**Supplemental Figure 9.** Dependence of: (panel a) the maximum suppression observed on the mainland, and (panel c) the maximum drive frequency seen on the mainland as the parameter  $\beta$  that determines the strength of density dependence is varied. Panel (b) reinterprets the results of panel (a) in terms of the return time to equilibrium (see text for more details). It is assumed that density dependence on the mainland only occurs via deaths (i.e. the mainland  $q$  parameter is set equal to zero). All other parameters are kept fixed at the baseline values used in Figure 3 of the main text, except for the coefficient  $\alpha$  of the density dependent (nonlinear) mortality term on the mainland. This parameter is varied so as to keep the baseline (pre-release equilibrium) mainland population size fixed as  $\beta$  is changed. The red dot on each panel corresponds to the baseline set of demographic parameters used in Figure 3 of the main text.



#### S.4. Stochastic Model

We formulate a stochastic model in the familiar way by reinterpreting the birth, death and migration rates of the deterministic model as rates at which discrete transitions occur in a continuous-time, discrete state Markov chain model (see, for example, Renshaw<sup>13</sup>). Numbers of individuals of each genotype are now integer-valued quantities and processes in the model occur discretely: for instance, migration events involve the movement of a single individual from the island to the mainland. Standard stochastic simulation methods can be used to produce a collection of realizations (simulation runs) of the model.

Because the model is stochastic, repeated simulation starting from the same initial condition leads to variation in observed dynamics. One way to summarize this variability is by a histogram that depicts the distribution of model outcomes across a collection of simulation runs.

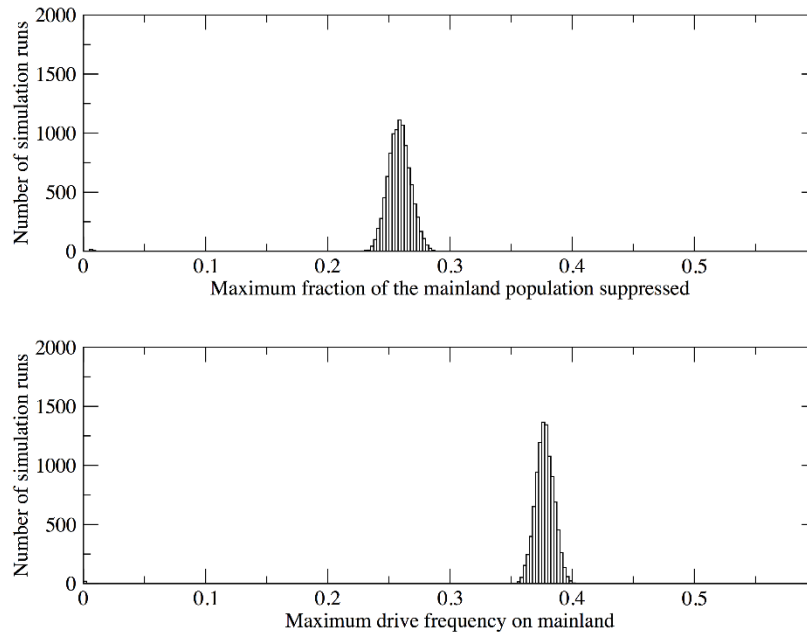
An important difference between stochastic and deterministic models is that invasion of drive is no longer guaranteed in the stochastic model, even for choices of parameters and initial conditions for which invasion is certain in the deterministic model. For instance, just by chance it could happen that a drive individual that arrives on the mainland dies before having any offspring there. In general, branching process theory can be used to calculate the probabilities that the arrival of a single drive individual will lead to successful invasion of drive or the failure of drive to spread<sup>14</sup>. These probabilities naturally depend on a number of drive-related parameters. Furthermore, repeated introduction of drive is more likely to lead to successful establishment of drive than a single introduction. For the baseline drive parameters used in the main text (and in this Appendix), numerical simulation shows that the probability of successful spread of drive following the arrival of a single drive individual is approximately 0.315.

For parameters corresponding to Figure 3. in the main text, with a mainland population of  $N = 100,000$ , a per-capita migration rate of 0.012/year and the rather pessimistic assumption that the frequency of the resistant allele on the mainland is only 5% (target allele frequency of 95%), we see that the stochastic model gives results that correspond closely to those obtained from the deterministic model. We see a relatively small variation in both the maximum level of suppression and maximum drive frequency seen on the mainland about the values predicted by the deterministic model (Figure S.10).

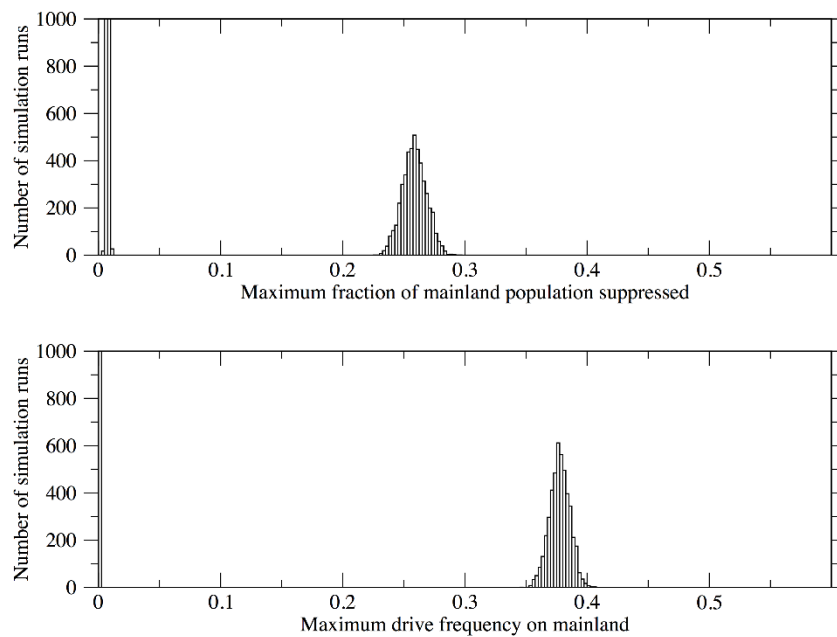
For a lower level of migration,  $\mu=0.0012$ /year, we see (Figure S.11) that drive fails to invade on the mainland in a large number of realizations (5,356 out of 10,000). This occurs because at this level of migration, no drive individuals migrated to the mainland before extinction happened on the island in about 14% of the realizations (1,440 out of 10,000). Even if drive-bearing individuals arrived on the mainland, invasion was not guaranteed to occur: drive failed to invade in 3,916 out of the 8,560 realizations in which drive arrived on the mainland (note that some realizations involved two or more arriving migrants). Neither of these two phenomena are captured by the deterministic model, in which migration is a continually-occurring process (minute fractions of individuals continually move from island to mainland) and in which drive can invade from arbitrarily low levels (so the arrival of a fraction of a drive-bearing individual will lead to invasion of drive). Consequently, the deterministic model is in one sense overly pessimistic about the impact of drive on the mainland, in that it predicts that drive is guaranteed to (transiently) invade the mainland. On the other hand, variation about the average behavior in the stochastic model means that the deterministic model can underestimate the impact of

drive when it does invade, although we see that this variation is not so large when the mainland population is large. We note that for the realizations in which drive fails to invade, we do see a non-zero maximum suppression: this reflects the variation that a stochastic wild-type population exhibits about its carrying capacity. (Note that these values would be larger if we observed the population over a longer time interval.)

**Supplemental Figure 10.** Histograms showing (a) maximum suppression seen on the mainland and (b) maximum frequency reached by drive on the mainland across 10,000 realizations of the stochastic model. Parameter values are as in Figure 3. of the main text, with a per-capita migration rate of 0.012/year and a mainland population size of 100,000.



**Supplemental Figure 11.** Histograms showing (a) maximum suppression seen on the mainland and (b) maximum frequency reached by drive on the mainland across 10,000 realizations of the stochastic model. Parameter values are as in Figure S.10, except that the per-capita migration rate is now lower, at 0.0012/year. Note that the observed results now exhibit bimodality: there are now a substantial number of simulation runs for which the maximum drive frequency is 0 (or low) and the maximum suppression is low. Note that the choice of scale on the vertical axis (chosen to allow the upper part of the bimodal distributions to be clearly visualized) truncates the lower parts of the bimodal distributions. 5,356 out of 10,000 simulation runs fall into the lower parts of the two distributions.



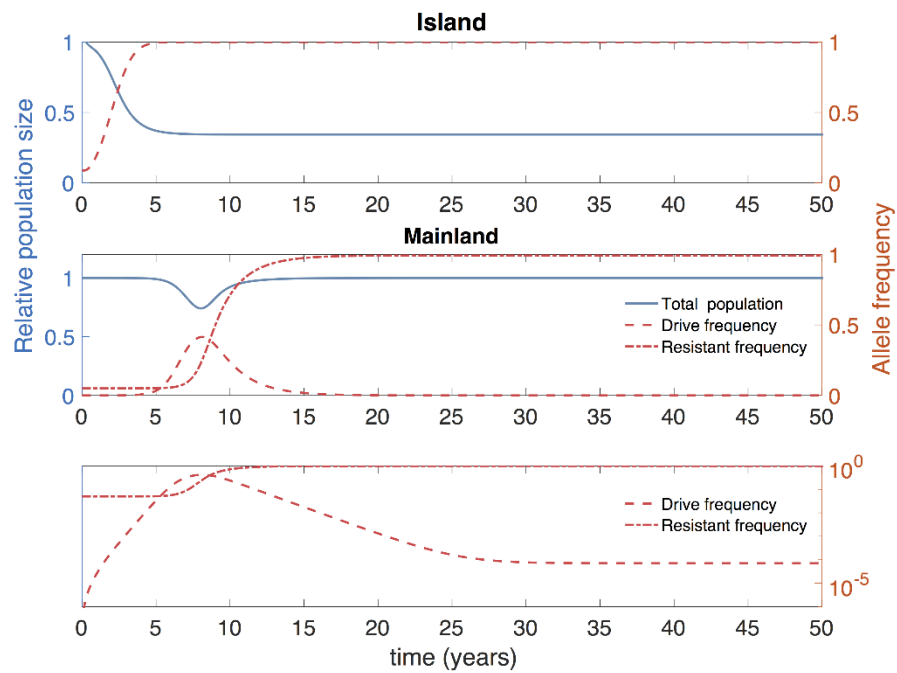
### S.5. Population Suppression and Population Replacement

We conclude with a brief description of the dynamics of the model in the case where the island population is suppressed but not eliminated. We assume that drive bears a positive fitness cost, but that the cost imposed (either at fixation or at the polymorphic equilibrium, depending on the outcome of the population genetics) is not sufficient to lead to elimination. This setting can either describe a drive that is intended to suppress the island population or one that is designed as a population replacement strategy. (Expressions for the threshold conditions governing the population genetic outcome are given in<sup>2,7</sup>, as are the allele frequencies at the polymorphic equilibrium (if it exists). Alphey and Bonsall<sup>7</sup> further provide threshold conditions for the elimination of a population given the population genetic outcome.)

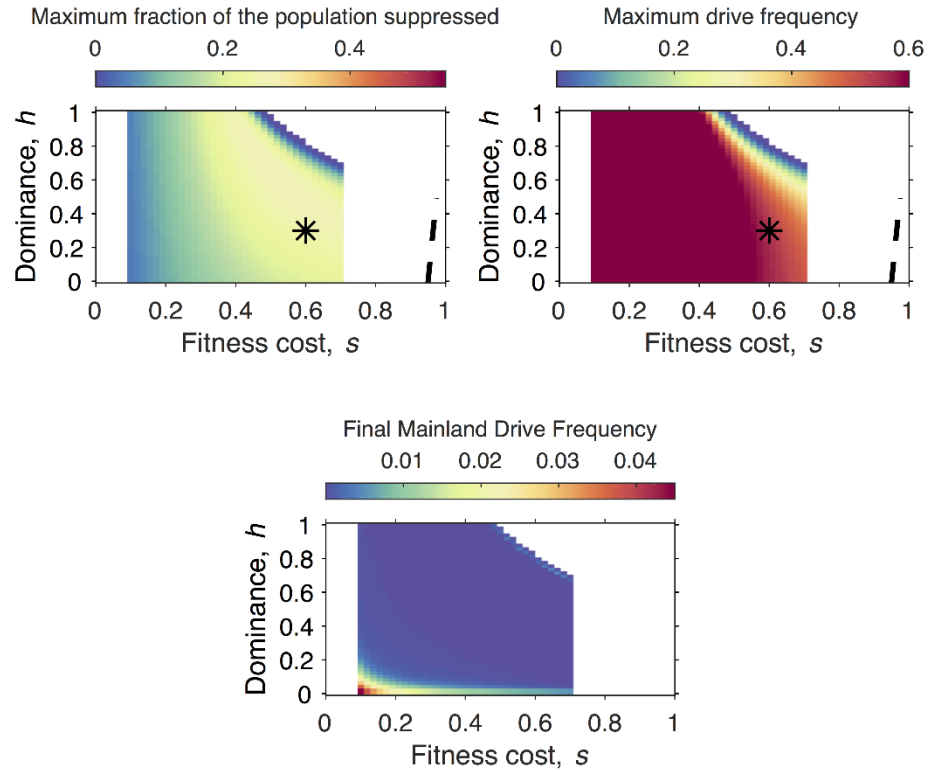
The primary difference in the dynamics here is that drive will remain in the island population, and hence there will be continual introduction of drive to the mainland by migration. Given that drive is outcompeted on the mainland, this leads to the establishment of a polymorphic equilibrium between drive, resistant and wild-types, with the level of drive typically low. We note that if the drive fitness cost is low, these dynamics, specifically the reduction in the level of drive that occurs following its initial transient rise, can take a long time to play out.

Figure S.12 shows typical time series of the dynamics of the LFA model with a suppression drive that does not achieve elimination. Figure S.13 shows variation in the maximum level of suppression seen on the mainland, maximum mainland drive frequency, and long-term mainland drive frequency (at  $t=100$  years) over a region of drive parameter space. (Note that we restrict the fitness cost  $s$  to be greater than 0.1 in order for our 100 year timescale to be appropriate to capture dynamics: as mentioned above, very low fitness costs lead to a very long timescale for the loss of drive on the mainland.) Figure S.14 explores the variation in the same quantities for the baseline suppression drive parameters, over a range of frequencies of resistance on the mainland and levels of migration. Results are also shown for a second set of drive parameters, with a lower fitness cost ( $s=0.3$ ,  $h=0.3$ ).

**Supplemental Figure 12.** Suppression/replacement dynamics. Top Panel: Island dynamics, showing relative population size (blue solid curve; left axis) and drive allele frequency (red dashed curve; right axis). Middle Panel: Mainland dynamics: relative population size (blue solid curve; left axis), and drive and resistant allele frequencies (red dashed and red dot-dashed curves, respectively; right axis). Bottom Panel: allele frequencies as in the previous panel, but depicted on a logarithmic scale. A drive that does not achieve elimination on the island is deployed ( $s=0.6$  and  $h=0.3$ ). For these parameters, the drive achieves fixation on the island but the resulting genetic load is not sufficient to cause elimination. This leads to a continual migration of drive-bearing individuals to the mainland. Initially, dynamics on the mainland play out much as seen for an elimination drive. However, the continual reintroduction of drive to the mainland by the migrants from the island leads to a polymorphic equilibrium for which drive is present at a low level (most visible on lower panel). Other parameters are as in Figure 3 of the main text, with homing probability of 0.95, initial resistance allele frequency of 95% on the mainland and per-capita migration rate of 0.012/year.



**Supplemental Figure 13.** Heatmaps showing the dependence of (panel a) the maximum suppression observed on the mainland, (panel b) the maximum level of drive seen on the mainland, and (panel c) the drive frequency on the mainland after 100 years, on drive fitness parameters  $s$  and  $h$  over regions of parameter space for which the drive does not have an invasion probability and suppresses the island population, but does not lead to extinction. The black asterisk denotes the drive parameters used in Figures S.12. All other parameters are as in Figure S.12. The scales on the color bars in panels (a) and (b) are chosen to be the same as in Figures 4 and 5 of the main text. White regions on this figure denote combinations of drive parameters that either lead to threshold behavior, loss of drive or for which the drive leads to elimination of the island population. The dashed curve denotes the boundary between the region of parameter space where drive approaches fixation (to the left of the curve) and where drive approaches a polymorphic equilibrium with wild-type (to the right of the curve). (Note that with the homing probability of 0.95 used here, the dashed curve lies in the region of drive space that leads to extinction of the island population.)



**Supplemental Figure 14.** Heatmaps showing the dependence of (panel a) the maximum suppression observed on the mainland, (panel b) the maximum level of drive seen on the mainland, and (panel c) the drive frequency on the mainland after 100 years, on initial level of resistance on the mainland and the migration rate, for drive parameters  $s=0.6$  and  $h=0.3$  that lead to threshold-free suppression but not extinction of the island population. Panels (d), (e), and (f) show the same information but for a drive with  $s=0.3$  and  $h=0.3$ . The scales on the color bars in panels (a) and (d), and (b) and (e) are chosen to be the same as in Figures 4 and 5 of the main text. All other parameters are as in Figure S.12.

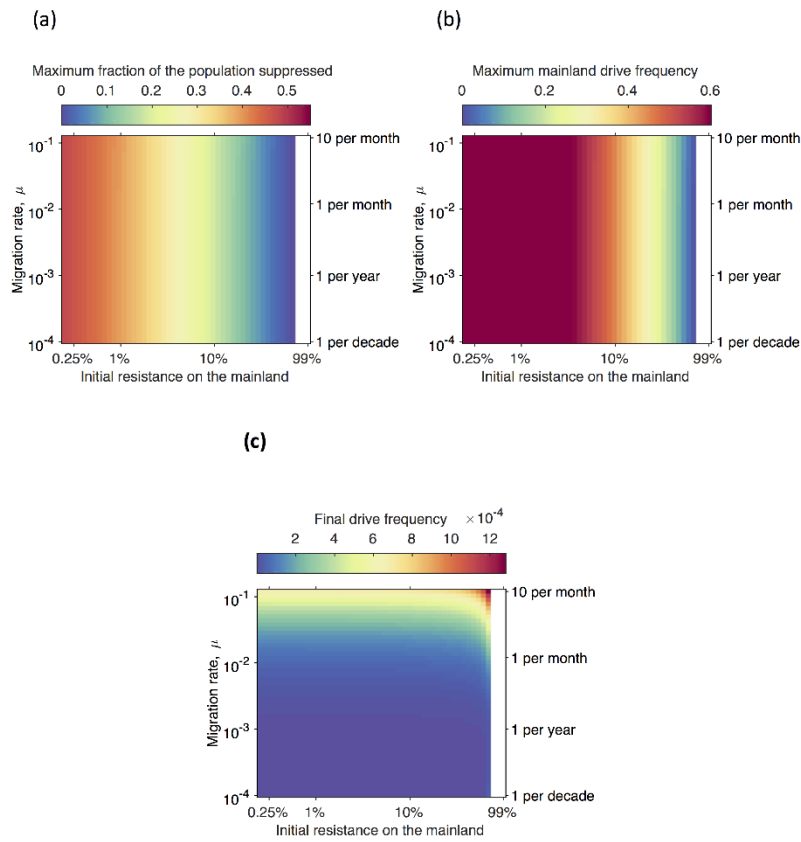
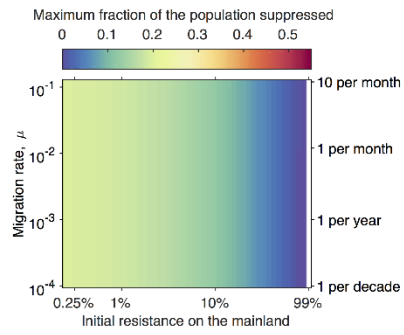


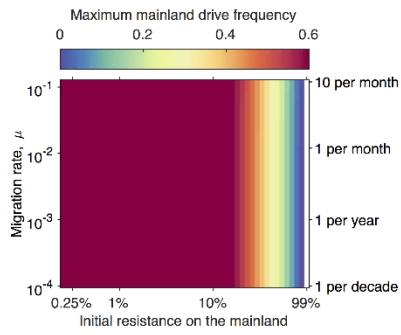
(Figure continues on next page)



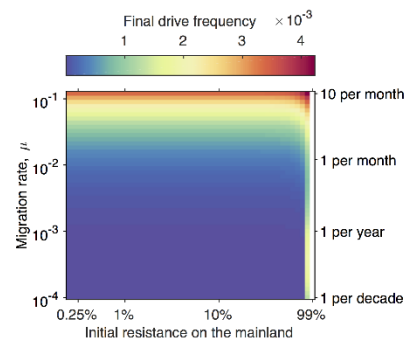
(d)



(e)



(f)



## References:

1. Strogatz, S. H. *Nonlinear Dynamics and Chaos*. (Westview Press, 2014).
2. Deredec, A., Burt, A. & Godfray, C. The population genetics of using homing endonuclease genes (HEGs) in vector and pest management. *Genetics* **179**, 2013-2026 (2008).
3. Vella, M. R., Gunning, C. E., Lloyd, A. L. & Gould, F. Evaluating strategies for reversing CRISPR-Cas9 gene drives. *Scientific Reports* **7**, 11038 (2017).
4. Prowse, T. A. A., Adikusuma, F., Cassey, P., Thomas, P. & Ross, J. V. A Y-chromosome shredding gene drive for controlling pest vertebrate populations. *eLife* **8**, e41873 (2019).
5. Saltelli, A. *et al. Global Sensitivity Analysis, the Primer*. (Wiley, 2008).
6. Pianosi, F., Sarrazin, F. & Wagener, T. A Matlab toolbox for global sensitivity analysis. *Environ. Model. Software* **70**, 80-85 (2015).
7. Alphey, N. & Bonsall, M. B. Interplay of population genetics and dynamics in the genetic control of mosquitoes. *J. R. Soc. Interface* **11**, 20131071 (2014).
8. DeAngelis, D. L. & Waterhouse, J. C. Equilibrium and Nonequilibrium Concepts in Ecological Models. *Ecol. Monogr.* **57**, 1-21 (1987).
9. Benton, T. G. & Grant, A. Elasticity analysis as an important tool in evolutionary and population ecology. *Trends Ecol. Evol.* **14**, 467-471 (1999).
10. Robert, M. A., Okamoto, K., Lloyd, A. L. & Gould, F. A reduce and replace strategy for suppressing vector-borne diseases: insights from a deterministic model. *PLoS One* **8**, e73233 (2013).
11. Prowse, T. A. A. *et al.* Dodging silver bullets: good CRISPR gene-drive design is critical for eradicating exotic vertebrates. *Proc. R. Soc. Lond. B* **284**, 20170799 (2017).
12. Backus, G. A., & Gross, K. Genetic engineering to eradicate invasive mice on islands: modeling the efficiency and ecological impacts. *Ecosphere* **7**, e01589 (2016).
13. Renshaw, E. *Modelling Biological Populations in Space and Time*. (Cambridge University Press, 1991).
14. Marshall, J. M. The effect of gene drive on containment of transgenic mosquitoes. *J. Theor. Biol.* **258**, 250-265 (2009).